ANAEROBIC REDUCTION OF MANGANESE OXIDES AND ITS EFFECT ON THE CARBON AND NITROGEN CYCLES

A Dissertation
Presented to
The Academic Faculty

by

Hui Lin

In Partial Fulfillment
of the Requirements for the Degree
Doctor of Philosophy in the
School of Earth and Atmospheric Sciences

Georgia Institute of Technology
May 2012

ANAEROBIC REDUCTION OF MANGANESE OXIDES AND ITS EFFECTS ON THE CARBON AND NITROGEN CYCLES

Approved by:

Dr. Martial Taillefert, Advisor
School of Earth and Atmospheric Sciences
Georgia Institute of Technology

Dr. Frank Stewart
School of Biology
Georgia Institute of Technology

Dr. Thomas J. DiChristina
School of Biology
Georgia Institute of Technology

Dr. Joel Kostka
School of Biology
Georgia Institute of Technology

Dr. Ellery Ingall
School of Earth and Atmospheric Sciences
Georgia Institute of Technology

Date Approved: March 30th, 2012

ACKNOWLEDGEMENTS

First and foremost I want to thank my advisor, Dr. Martial Taillefert, for his continuous support over the past years. I appreciate all his contributions of ideas, time, and funding to make my Ph.D. experience stimulating. His commitment and enthusiasm to science has been an inspiration and guide for me to pursue my academic goal.

Thanks to Dr. Thomas DiChristina for his support and help in all the microbiological works and thanks to Dr. Ellery Ingall and Dr. Joel Kostka for MIMS support.

I would like to thank my committee members, Dr. Thomas DiChristina, Dr. Frank Stewart, Dr. Ellery Ingall, and Dr. Joel Kostka for their time, interests, and helpful recommendations.

Thanks to all my past and present lab mates who have made life in the Taillefert Group a lot fun: Melanie, Stephanie, Morris, Jordon, Deidre, Nick, Kate, Anna, Keaton, Colin, Emily, and Beth. I also want to thank Justin and Nadia for all the collaboration and microbiological help.

A special thanks to all my friends in US and China and my past and present office mates. I am also grateful to the School of Earth & Atmospheric Sciences for providing me with a teaching assistantship.

And finally, I want to thank my family, my father Mr. Yuchun Lin, my mother Mrs. Xiaoqing Chen, my husband Dr. Xuejia Yan, and my coming baby girl, Yu Yan, for their love and support.

TABLE OF CONTENTS

LIST OF TABLES

Page

CHAPTER 5

APPENDIX A

APPENDIX C

LIST OF FIGURES

Page

CHAPTER 1

CHAPTER 2

CHAPTER 3

CHAPTER 4

LIST OF SYMBOLS AND ABBREVIATIONS

UV	Ultra Violet
IC	Ion Chromatography
AA	Atomic Asorption
MIMS	Membrane Inlet Mass Spectroscopy
DIC	Dissolved Inorganic Carbon
DOC	Dissolved Organic Carbon
HMDE	Hanging Mercury Drop Electrode
OM	Outer membrane
IM	Inner membrane
IC	Ion Chromatography
TDM	Total Dissolved Manganese
SLRS	St. Laurent's River Standard
DNRA	Dissmilaotry Nitrate Reduction to Ammonium
AOB	Ammonium oxidizing bacteria
NOB	Nitrite oxidizing bacteria
AMO	Ammonium monooxygenase
AOA	Ammonium oxidizing archeae
OMZ	Oxygen minimum zone

SUMMARY

The biogenic reduction of Mn(IV) oxides is one of the most favorable anaerobic electron transfer processes in aquatic systems and likely plays an important role in the redox cycle of both carbon and nitrogen in anaerobic environments; yet, the different pathways involved in the microbial transformation of Mn(IV) oxides remain unclear.

The coupling between the reduction of Mn(IV) to Mn(II) and the oxidation of organic carbon to CO_2 is largely catalyzed by microorganisms in various environments such as redox stratified water columns and sediments. The recent discovery that soluble Mn(III) exists in natural systems and is formed during biological oxidation of Mn(II) implies the possibility that Mn(III) is formed as an intermediate during the microbial reduction of Mn(IV). In this dissertation, mutagenesis studies and kinetic analysis were combined to study the mechanism of microbial reduction of Mn(IV) by *Shewanella oneidensis* MR-1, one of the most studied metal-respiring prokaryotes. We show for the first time that the microbial reduction of Mn(IV) proceeds step-wise via two successive one-electron transfer reactions with soluble Mn(III) as intermediate produced in solution. The point mutant strain *Mn3*, generated via random chemical mutagenesis, presents a unique phenotype that reduces solid Mn(IV) to Mn(III) but not to Mn(II), suggesting that these two reduction steps proceed via different electron transport pathways. Mutagenesis studies on various in-frame deletion mutant strains demonstrate that the reduction of both solid Mn(IV) and soluble Mn(III) occurs at the outer membrane of the cell and Mn(IV) respiration involves only one of the two potential terminal reductases (c-type cytochrome MtrC and OmcA) involved in Fe(III) respiration. Interestingly, only the second electron transfer step is coupled to the respiration of organic carbon, which opposes the long-

standing paradigm that microbial reduction of Mn(IV) proceeds via the single transfer of two electrons coupled to the mineralization of carbon substrates.

The coupling between anaerobic nitrification and Mn reduction has been demonstrated to be thermodynamically favorable. However, the existence of this process in natural system is still in debate. In this dissertation, characterization of coastal marine sediments was combined with laboratory incubations of the same sediments to investigate the effect of Mn oxides on the redox cycle of nitrogen. Our slurry incubations demonstrate that anaerobic nitrification is catalyzed by Mn oxides. In addition, mass balance calculations on NH_4^+ link the consumption of NH_4^+ to anaerobic ammonium oxidation in the presence of Mn oxides and confirm the occurrence of Mn(IV)-catalyzed anaerobic nitrification. The activity of anaerobic nitrification is greatly affected by the initial ratio of Mn(IV) to NH_4^+, the reactivity of Mn oxides, and the reducing potential of the system. Overall, Mn(IV)-catalyzed anaerobic nitrification may be an important source of nitrite/nitrate in anaerobic marine sediments and provide an alternative pathway for subsequent nitrogen losses in the marine nitrogen cycle.

CHAPTER 1 BACKGROUND AND INTRODUCTION

1.1 Manganese in natural systems

The element manganese (Mn), with an atomic number of 25 and electron configuration [Ar] $3d^5 4s^2$, is the fifth most abundant metal and the second most abundant transition metal on Earth (Nealson et al., 1988), contributes on average 0.072% by mass to surface rocks (Martin and Meybeck, 1979), and is ubiquitous in natural waters and sediments (Emelyanov, 2001, Aller, 1994, Davison, 1993). Due to its high abundance and redox reactivity, transformations of manganese influence the biogeochemical cycling of carbon, nitrogen, phosphate, and other toxic elements (Zhang et al., 2007, White et al., 2008, Neretin et al., 2003, Luther et al., 1997). Mn is also an essential trace element for life and plays an important role in catalyzing oxygen transformation in enzymatic photosynthesis (Dismukes, 1986). Therefore, understanding the properties and the biogeochemical cycle of manganese is of great environmental significance.

Theoretically, Mn may exist in any of the redox states ranging from 0 to +7, but it is primarily present under the three oxidation states +II, +III, and +IV in natural environments (Davison, 1993). Mn(II) is thermodynamically stable under anoxic conditions, usually as free hydrated cation in fresh waters, $MnCl^+$ in marine environments, or incorporated in insoluble phosphate and carbonate minerals (Tebo et al., 2004, Otero et al., 2009, Davison, 1993). The free hydrated Mn(II) cation is considered biologically available and required in trace amounts by organisms (Sunda and Huntsman, 1986); however, high concentrations of Mn(II) can be toxic (Millaleo et al., 2010). Mn^{2+} also displays a strong affinity for solid surfaces, including Mn oxides (Nealson et al., 1988, Tebo et al., 2004). The most common Mn(II) mineral in natural systems is the Mn(II)

carbonate, rhodochrosite, the formation of which is largely driven by microbial Mn(IV) reduction (Neumann et al., 2002).

Natural Mn(III) species are dominated by solid Mn(III) oxides, which are formed as meta-stable intermediates of birnessite due to kinetic limitations (Davison, 1993). Soluble Mn(III), although considered rare in natural environments, may be produced as the intermediate during the chemical and photochemical reduction of Mn(IV) (Perez-Benito, 2002, Ruppel et al., 2001) and during microbial oxidation of Mn(II) (Anderson et al., 2009, Webb et al., 2005, Learman et al., 2011). Generally, soluble Mn(III) is extremely unstable and rapidly disproportionates to yield Mn(II) and Mn(IV) under acidic conditions, or precipitates as Mn(III) oxides at pH >7 (Davison, 1993, Klewicki and Morgan, 1998). Soluble Mn(III), however, can be stabilized in soluble phases in the presence of several inorganic or organic ligands, such as pyrophosphate (Kostka et al., 1995), citrate (Klewicki and Morgan, 1998), hydroxycarboxylic acid (Heintze and Mann, 1947), and siderophores (Parker et al., 2004, Duckworth and Sposito, 2005a). Due to its extreme reactivity and the lack of appropriate analytical techniques, soluble Mn(III) was only recently discovered in low concentrations in the sub-oxic zone of natural systems (Trouwborst et al., 2006, Madison et al., 2011). The existence of soluble Mn(III) in these conditions motivates more research on the processes responsible for the production of Mn(III) under oxygen-limited conditions.

Due to the lack of ligands to complex Mn(IV) in aquatic systems at circum-neutral natural pH, soluble Mn(IV) has yet to been found, (Morgan, 2000a). Various oxides and oxyhydroxides of Mn(IV), sometimes incorporating Mn(III), form manganese nodules, which are important constituents of soils and sediments and serve as sources or

sinks for bioavailable Mn in natural environments (Murray, 1974). These Mn oxides are generally generated during diagenetic processes or the oxidation of Mn(II), which diffuses upward into the oxic zone (Mouret et al., 2009). In addition to their high reactivity, Mn oxides also show extremely high adsorption capacity for various heavy metals (such as Pb, Co, Cu, Ni, and Cd) and are considered to be the most important repositories for a wide variety of metals in soils and sediments (Stumm and Morgan, 1996, Tebo et al., 2004). Therefore, the formation and dissolution of manganese minerals play important roles in the oxic/anoxic transition zones of various natural waters and sediments.

1.2 Oxidation/reduction (redox) of Mn

The redox transformation of Mn in natural systems includes the oxidation of Mn(II) to Mn(IV) and the reduction of Mn(IV) to Mn(II), with Mn(III) as possible intermediates in either process, and is mediated via both chemical and microbial processes (Figure 1.1) (Luther, 2005). The redox cycle of manganese facilitates the transport of electrons across the oxic-anoxic transition zone and drives the redox cycles of many other elements in various sediments (Aller, 1990, Neretin et al., 2003, Aller, 1994, Van Cappellen et al., 1998).

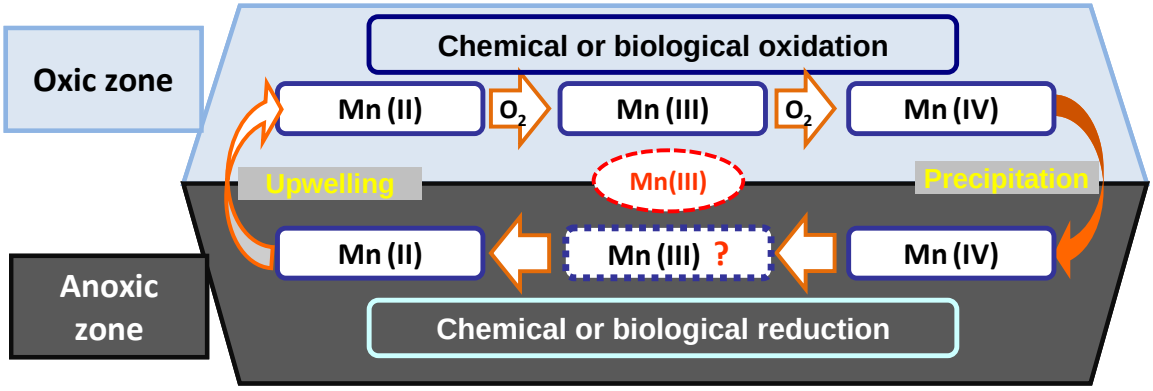

Figure 1.1. Conceptual model of the redox cycle of Mn at oxic-anoxic interfaces in aquatic systems. The upward flux of Mn(II) to the oxic zone is accompanied by the slow oxidation of Mn(II), while the downward flux of Mn oxides supplies a strong oxidant to the anoxic zone. Microorganisms are largely involved in both the reduction and oxidation of Mn.

1.2.1 Oxidation of Mn(II)

In natural systems, Mn(II) diffuses across oxic/anoxic interfaces and is oxidized to Mn(IV) either chemically or biologically by dissolved oxygen (Figure 1.1) (Thamdrup, 2000b). The chemical oxidation rate of Mn(II) by dissolved oxygen (Eq. 1.1) is slow at pH below or around 8 due to the large activation energy required for transferring electrons to oxygen (Morgan, 2005, Luther, 2005). Mn(II) usually exists in the form of 'free' hydrated ion $Mn(H_2O)_6^{2+}$ at low pH, and electrons have to be transferred from the Mn e_g* (σ) (HOMO) to the O_2 π* orbital (LUMO). The poor symmetry between these orbitals slows down the reaction at pH below 8 (Luther, 2005). In turn, the oxidation of Mn(II) is thermodynamically favorable at pH > 8 (Stumm and Morgan, 1996), as the hydrolysis of Mn(II) generates $Mn(OH)_x^{(2-x)}$ complexes that carry electron-donor type of ligands and facilitate the electron transfer even when the overlap between the orbitals is

not optimal (Luther, 2005). Mn(II) hydroxide species formed under basic conditions are readily transformed by aerobic oxidation processes to Mn(III/IV) species (Cotton et al., 1999). This process is autocatalytic, as the adsorption of Mn(II) to Mn(IV) oxides accelerates the rate of oxidation (Sun and Morgan, 1981), but too slow to be of environmental relevance at circumneutral pH (Stumm and Morgan, 1996). As a result, the oxidation of Mn(II) is proposed to be largely catalyzed by microorganisms in most natural environments (Tebo et al., 2005).

$$Mn^{2+} + \frac{1}{2} O_2 + H_2O \rightarrow MnO_2 + 2\ H^+ \quad \Delta G^{\circ\prime} = -80.8 \text{ kJ/mole Mn} \quad \text{(Equation 1.1)}$$

Indeed, microorganisms are able to increase the oxidation rate of Mn(II) by several orders of magnitude compared to the abiotic Mn(II) oxidation (Bargar et al., 2005). Among the physiologically diverse microorganisms involved in Mn(II) oxidation, three phylogenetically distinct types of bacteria have been well-studied, including: 1) the sheath-forming β-Proteobacterium, such as *Leptothrix discophora* strain SS-1 (Adams and Ghiorse, 1987), 2) the spores formed by the Gram-positive *Bacillus* sp. Strain SG-1 (Devrind et al., 1986), and 3) the γ-proteobacterium *Pseudomonas putida* strains MnB1 and GB-1 (Okazaki et al., 1997). Interestingly, the physiological reason for bacteria to oxidize Mn(II) remains unclear (Tebo et al., 2005, De Schamphelaire et al., 2007). Although chemolithoautotrophic growth on Mn(II) was proposed, no evidence has been reported to directly link Mn(II) oxidation to energy generation (Tebo et al., 2005). In addition, the biochemical pathways involved in the aerobic oxidation of Mn(II) have yet to be completely identified. Multi-copper oxidase (MCO) enzymes located on the cell

surface are considered to be essential in Mn(II) oxidation (Brouwers et al., 1999); however, it was recently demonstrated that *Roseobacter* sp. AzwK-3b indirectly oxidizes Mn(II) by first producing extracellular superoxide radicals to oxidize Mn(II) via a secondary abiotic reaction (Learman et al., 2011). Finally, production of Mn(III) during the aerobic oxidation of Mn(II) by spores of the marine *Bacillus* sp. Strain SG-1 or newly isolated Mn(II)-oxidizing strains *Aurantimonas manganoxydans*, sp. nov. and *Aurantimonaas litoralis*, sp. nov. or *Roseobacter* sp. AzwK-3b indicate that two consecutive one-electron-transfer reactions are taking place during bacterial oxidation of Mn(II) (Anderson et al., 2009, Webb et al., 2005, Learman et al., 2011). These findings suggest that the electron transfer pathway of Mn(IV) reduction to Mn(II) may proceed as the reverse process of that for Mn(II) oxidation, producing Mn(III) as intermediate.

1.2.2 Reduction of Mn(IV) oxides

In anaerobic conditions, Mn(IV) is reduced to Mn(II) either chemically by organic compounds, Fe(II), and sulfide (Stone and Morgan, 1984a, Villinski et al., 2003, Yao and Millero, 1993) or biologically by dissimilatory reducing microorganisms at circumneutral pH (Myers and Nealson, 1988, Lovley and Phillips, 1988, Lovley et al., 1993, Greene et al., 1997). The standard reduction potentials of the $Mn^{II}Mn^{III}{}_2O_4/Mn^{2+}$ and δ-$Mn^{IV}O_2/Mn^{2+}$ couples are slightly higher (618 mV) than those of the β-$Mn^{IV}O_2/Mn^{2+}$ and γ-$Mn^{III}OOH/Mn^{2+}$ couples (555 mV) (Thamdrup, 2000b). These reduction potentials, close to that of nitrate reduction, indicate that Mn(III) and Mn(IV) represent some of the strongest oxidants in anaerobic environments.

Chemical reduction of Mn(IV)

The chemical reduction of Mn(IV) occurs rapidly in the presence of a wide spectrum of organic and inorganic reductants (Stone and Morgan, 1984a, Stone and Morgan, 1984b). Ferrous ion and hydrogen sulfide are the most important reductants of Mn oxides in natural environments (Thamdrup, 2000b). The reduction of Mn oxides by Fe(II) is relatively fast at pH < 4; however, formation of Fe(III) precipitate may block the β-MnO_2 surface sites and in turn slow or even inhibit the reaction at pH > 4 (Postma, 1985). Reduction of Mn oxides by solid Fe(II) at higher pH, either FeS or FeS_2, was proposed to proceed via Fe(II)/Fe(III) cycling that transport electrons between two solids (Mn oxides and FeS/FeS_2) for further oxidation of S^{2-} and S_2^{2-} (Schippers and Jorgensen, 2001). The reduction of Mn(IV) by dissolved sulfide is much faster, however, as it involves the transfer of two paired electrons (Luther, 2010). This reaction follows a first order rate law with respect to both surface site and the H_2S concentration and forms inner-sphere surface complexes $>Mn^{IV}S^-$ and $>Mn^{IV}SH$ as intermediates (Yao and Millero, 1993). Sulfate is the main product of the oxidation of hydrogen sulfide by Mn(IV) oxides at low pH, and elemental sulfur is the main product at neutral pH (Herszage and Afonso, 2003). The rate of this reaction decreases as pH increases due to the repulsion of HS^- and the negatively charged solid Mn oxides (Yao and Millero, 1993, Luther, 2010). Colloidal MnO_2 can also be reduced by Mn^{2+} in acidic conditions to form Mn(III), according to Eq. 1.2 (Perez-Benito, 2002).

$$MnO_2 + Mn^{2+} + 4H^+ \rightarrow 2\ Mn^{3+} + H_2O \qquad \text{(Equation 1.2)}$$

Several organic compounds are able to reduce manganese oxides chemically but at a much lower rate (Stone and Morgan, 1984a). Natural organic compounds and microbial

metabolites, such as ascorbate, hydroquinone, or oxalate, may reductively dissolve Mn oxides by forming a surface complex prior to the electron transfer (Stone and Morgan, 1984b, Stone and Morgan, 1984a). In addition, desferrioxamine B, a trihydroxamate siderophore produced by microorganisms, reduces MnO_2 through a single electron transfer step to solid Mn(III) and solubilize Mn(III) by complexation (Duckworth and Sposito, 2007).

Biological reduction of Mn(IV) – Mn(IV) respiration

In addition to the uptake of manganese for assimilation, microorganisms can also gain energy during the dissimilatory reduction of Mn(IV) in anaerobic conditions (Lovley et al., 2004b). Anaerobic manganese respiration by prokaryotes, first demonstrated with *Alteromonas putrefaciens* MR-1 (Myers and Nealson, 1988). Dissimilatory Mn-reducing bacteria (DMRB) span a wide phylogenetic diversity of microorganisms residing in the redox-stratified aqueous and sedimentary environments (Lovley et al., 2004b, DiChristina et al., 2005). Some DMRB are fermenting bacteria, which channel only a small part of electrons from the organic matter to Mn oxides and do not conserve energy from the Mn reduction (Lovley, 1991); others (respiratory organisms), including most of DMRB, oxidize organic compounds with Mn oxides as terminal electron acceptor (Thamdrup, 2000b) and conserve energy from Mn reduction to support growth (Lovley et al., 1993, Nealson et al., 1988).

Due to the high abundance and reduction power of Mn(IV), Microbial Mn(IV) reduction contributes significantly to the global oxidation of organic matter in natural systems (De Schamphelaire et al., 2007, Davison, 1993). The respiration of organic carbon proceeds by a sequence of redox reactions according to the free energy yield of

the reactions with the different available electron acceptors (Froelich et al., 1979). In oxic zones, the oxidation of organic carbon is typically efficient, considering the high energy yield during aerobic respiration ($\Delta G^{\circ\prime}$ = -3190 kJ/mol) (Froelich et al., 1979, De Schamphelaire et al., 2007). Below the oxygen penetration zone, denitrification ($\Delta G^{\circ\prime}$ = -3030 kJ/mol), Mn-oxide reduction ($\Delta G^{\circ\prime}$ = -3090 ~ -2920 kJ/mol), Fe-oxide reduction ($\Delta G^{\circ\prime}$ = -1410 ~ -1330 kJ/mol), sulfate reduction ($\Delta G^{\circ\prime}$ = -380 kJ/mol), and methanogenesis ($\Delta G^{\circ\prime}$ = -350 kJ/mol) may contribute to the oxidation of organic carbon depending on the free energy yield of the reaction, bioavailablility of the electron acceptors, and environmental conditions (Schulz et al., 1994, De Schamphelaire et al., 2007). Direct oxidation of organic matter by Mn oxides in aquatic systems was demonstrated by the simultaneous production of alkalinity and Mn(II) in stoichiometric ratio (2:1) and the increasing amount of Mn and Fe reducing microorganisms in the oxic-anoxic transition zone of the Orca Basin (Van Cappellen et al., 1998). Reduction of Mn was found to account for up to 100% of organic carbon oxidation in the hemipelagic deposits of the Panama Basin (Aller, 1990) and the upper 10 cm-layer sediments of the Fjord, Skaggerak, Denmark (Canfield et al., 1993). In contrast, other studies argued that Mn oxides play a minor role in the oxidation of carbon with a maximum contribution of 6% of the total organic carbon oxidation in Galveston Bay on the Upper Gulf Coast of Texas (Warnken et al., 2008) and less than 2% in the Gotland Deep, Baltic Sea (Neretin et al., 2003). These differences in the contribution of Mn reduction to total carbon oxidation may depend on the total Mn content and the reactivity of different Mn species (i.e. Mn(II) carbonate v.s. Mn(IV) oxides in anoxic sediments) (Thamdrup, 2000b).

Compared to other respiratory processes, such as denitrification, sulfate reduction, and methanogenesis, the biochemistry of anaerobic manganese respiration remains poorly understood (Madigan et al., 2003). Furthermore, the mechanism by which electrons are transferred from the cells to solid Mn(IV) oxides has yet to be identified (DiChristina et al., 2005). The low solubility of Mn (IV) oxides at circumneutral pH prevents the inner membrane (IM)-localized electron transport systems to contact Mn(IV). Thus, bacteria must adopt specific strategies to transfer electrons from the inner membrane to solid terminal electron acceptors (TEAs) located on the outside of the cell (DiChristina et al., 2002) over a distance of at least 8 nm (Prescott et al., 1996).

Three main electron transfer strategies have been postulated for either Mn(IV) oxides or Fe(III) oxides or both (Myers and Myers, 2003a, Newman and Kolter, 2000, DiChristina et al., 2005) (Figure 1.2). First, bacteria are able to directly reduce metal oxides such as Mn(IV) by localizing the terminal reductase to the outer membrane (Myers and Myers, 2001) (Figure 1.2). The type II secretion system, which transports proteins from the periplasm to the outer membrane (Desvaux et al., 2004) is critical to the direct enzymatic reduction of Mn(IV) and Fe(III) oxides (DiChristina et al., 2002). Mutant strains of *S. putrefaciens* lacking the type II secretion gene ferE cannot respire on Fe(III) and Mn(IV) oxides but retain the ability to reduce soluble electron acceptors such as nitrate (DiChristina et al., 2002). Mutant strains of *S. oneidensis* lacking the type II secretion system genes *gspE* and *gspG* decrease the extracellular release of the *c*-type cytochromes MtrC and OmcA (Shi et al., 2008). These two outer membrane c-type cytochromes, are proposed to be involved in the terminal steps of electron transfer during

dissimilatory reduction of Mn oxides (Beliaev and Saffarini, 1998, Myers and Myers, 2002, Myers and Myers, 2003a, Heidelberg et al., 2002).

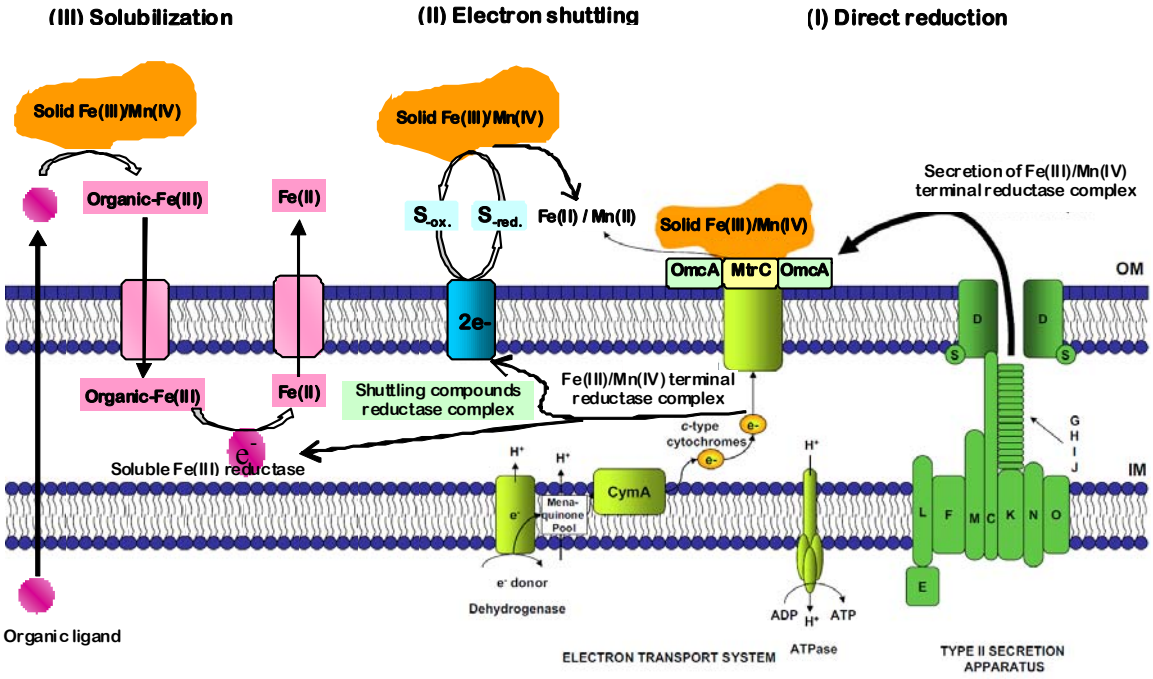

Figure 1.2. A working model for the three potential electron transfer strategies ((I) direct enzymatice reduction, (II) electron shuttling, and (III) solubilization) adopted by *Shewanella* to reduction Fe(III) or Mn(IV) oxides, modified from (DiChristina et al., 2005).

Second, some organic compounds such as AQDS (DiChristina et al., 2005), quinones (Newman and Kolter, 2000), and riboflavin (von Canstein et al., 2008) may act as electron shuttles by being first enzymatically reduced and chemically re-oxidized by solid Mn(IV) or Fe(III) oxides in a second (abiotic) electron transfer reaction (Figure 1.2). A mutant strain of *S. putrefaciens* MR-1 deficient in menaquinone production is unable to reduce solid Mn(IV) and Fe(III), suggesting that endogenous menaquinones or small

compounds related to menaquinones shuttle electrons to solid terminal electron acceptors (Newman and Kolter, 2000).

Third, microorganisms may reduce iron oxides by first dissolving Fe(III) with exogenous or endogenous organic ligands, then reducing the soluble Fe(III) species either on the outer membrane or inside the periplasm (Pitts et al., 2003, Taillefert et al., 2007a) (Figure 1.2). Recently, mutants of *S. oneidensis* deficient in the production of soluble organic-Fe(III) complexes have been found to be impaired in the respiration of Fe(III) oxides, supporting the hypothesis that soluble organic-Fe(III) complexes are produced as intermediates during anaerobic respiration of solid Fe(III) by endogenous organic ligands (Jones et al., 2010). These ligands are still elusive, but evidence suggests that the mechanism is distinct from assimilatory metal intake, as mutants of *S. oneidensis* lacking the genes involved either in the production of siderophores or the reduction of siderophore-Fe(III) complexes still retain wild-type production of soluble organic-Fe(III) complexes (Fennessey et al., 2010). In the case of Mn(IV), ligands promoting the non-reductive dissolution of Mn(IV) oxides have yet to be identified in natural environments at circumneutral pH (Morgan, 2000a, Duckworth et al., 2009). In turn, a variety of exogenous compounds including pyrophosphate and naturally-existing ligands such as citrate and siderophores can stabilize Mn(III) at a pH ranging between 5 and 8 (Kostka et al., 1995, Klewicki and Morgan, 1998, Parker et al., 2004). Mn(IV) oxides may be first reductively dissolved by microbial metabolites, such as pyruvate or siderophore (see previous section) (Stone, 1987b, Duckworth and Sposito, 2007), and form soluble Mn(III) complexes for dissimilatory reduction. In addition, Mn(III)-siderophore complexes are proposed to play a role in bacterial Mn(II) oxidation (Parker et al., 2007). Recently,

siderophores have also been suggested to be involved in microbial reduction of solid Mn(IV) oxides (Kouzuma et al., 2012). These findings imply that microorganisms may have to adopt a solubilization strategy that first reduces solid Mn(IV) oxides to soluble Mn(III) complexes as intermediates during the anaerobic respiration of Mn(IV). Yet direct evidence for the production of soluble Mn(III) complexes during microbial respiration of Mn(IV) oxides is still lacking.

One-electron transfer versus two-electron transfer reduction

Despite the fact that the physicochemical properties of Fe and Mn are different (Luther, 2010), similar electron transfer strategies have been proposed for the anaerobic respiration of solid Mn(IV) and Fe(III) by members of the *Shewanella* genus (Myers and Myers, 2000, Newman and Kolter, 2000, Bretschger et al., 2007, Shi et al., 2007). Indeed, the mechanism of bacterial Mn(IV) reduction may be more complex than that of Fe(III) considering that the electronic configuration of both elements is different and that Mn(IV) has to accept a total of two electrons. In addition, the fact that bacterial Mn(II) oxidation is proposed to proceed via two steps of one-electron transfer (Webb et al., 2005) raises the possibility the reduction of Mn(IV) involves two consecutive steps of one-electron transfer.

According to the molecular orbital theory, two steps of one-electron transfer during the reduction of Mn(IV) to Mn(II) may proceed by the addition of the first electron to one of the two empty e_g orbitals of Mn(IV) with a change of the orbital's geometry from purely octahedral Mn(IV) to octahedral Mn(III) and then to tetragonal Mn(III) (Figure 1.3 (A)) (Luther, 2005). For a two-electron transfer reaction with formation of octahedral Mn^{2+}, the two electrons are donated by the reductant either as a

lone pair to an empty orbital, followed by electron rearrangement to satisfy Hund's Law (Pathway A – C – B in Figure 1.3 (B)), or as two distinct electrons from separate orbitals (Figure 1.3 (B)). The later electron transfer pathway is thought to be less favorable because it requires a reductant with two orbitals filled with one electron (Luther, 2005). Indeed, chemical reduction of MnO_2 by Mn(II) under highly acidic conditions (Perez-Benito, 2002) or by organic reductants (e.g. oxalate and pyruvate) at neutral pH (Stone, 1987a), and the electrochemical reduction of MnO_2 (Ruppel et al., 2001) have been proposed to follow the one-electron transfer pathway with production of Mn(III) intermediates. Interestingly, Mn(III) has also been suggested to be produced as the intermediate during dissimilatory Mn(IV) reduction (Lovley, 1991), but evidence for the one-electron-transfer pathway has yet to be demonstrated during anaerobic Mn(IV) respiration.

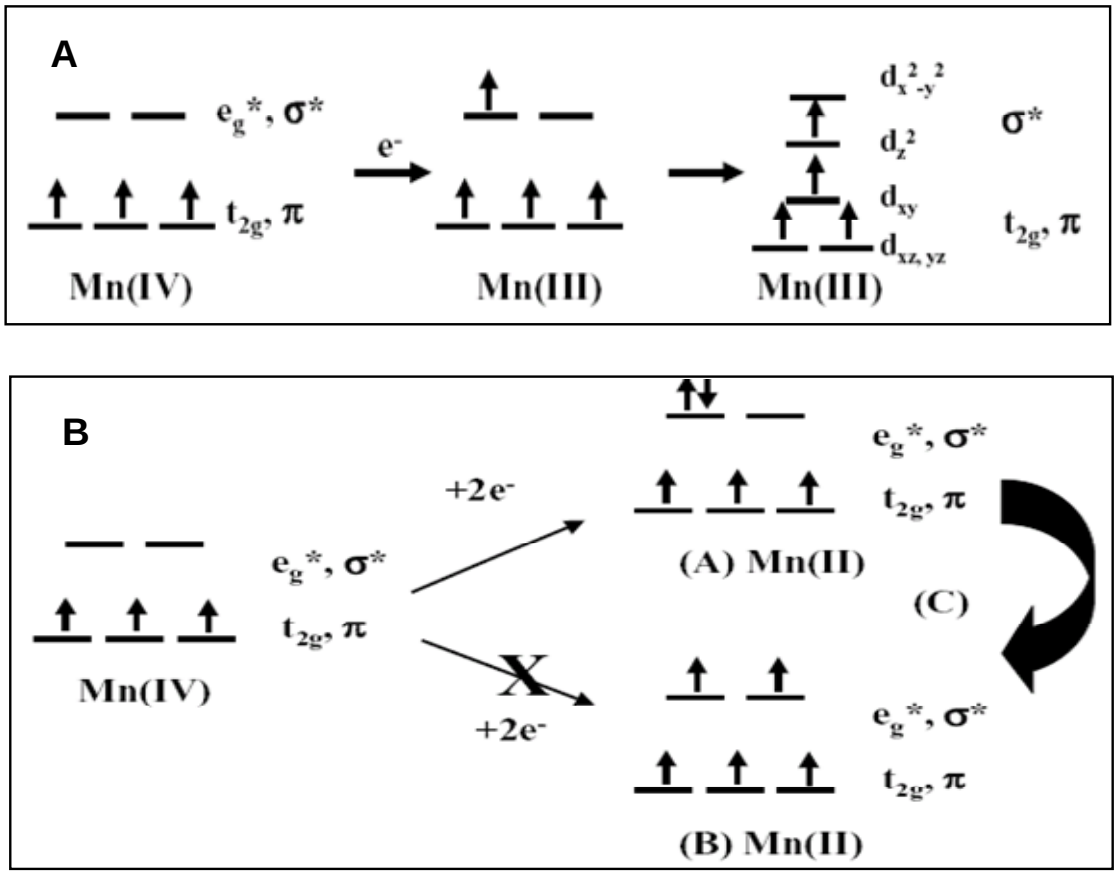

Figure 1.3.(A) Orbital energy diagrams showing the orbital structural change from Mn (IV) to octahedral Mn (III) then to tetragonally distorted Mn (III); (B): Orbital energy diagrams showing the possible ways that Mn (IV) can add two electrons to its eg* orbital set with electron rearrangement to satisfy Hund's Law. The second electron transfer pathway (B) is thought to be less favorable than the first one (A), because the second pathway requires a reductant with two orbitals filled with one electron (Luther, 2005).

1.4 Interactions of Mn and nitrogen cycles

1.4.1 The Role of Manganese in the Nitrogen Cycle

Nitrogen is one of the essential elements for life. It is a major constituent of nucleic acids and proteins, which determine both the genetic and metabolic properties of every living cell, and accounts for typically 6.25% of dry-cell mass (Galloway and Cowling, 2002, Bothe et al., 2007). Interestingly, the portion of nitrogen that is available to living organisms on Earth, the so-called 'fixed nitrogen', represents only 10% of the total nitrogen on Earth (Galloway et al., 1995), suggesting that the transformation of fixed nitrogen is relatively fast compared to the transformation of dinitrogen gas.

The balance of the marine nitrogen budget is still under debate. Some studies estimated that denitrification rates are higher than nitrogen fixation and suggested a significant unbalance between oceanic nitrogen inputs (nitrogen fixation) and outputs (denitrification) (Codispoti et al., 2001). Other studies, however, showed that nitrogen fixation may be underestimated in nitrogen budgets and that the oceanic nitrogen inputs and outputs should be in balance (Gruber and Sarmiento, 1997, Deutsch et al., 2007). These findings indicate limitations in our understanding of the nitrogen cycle (Ward et al., 2009) and that alternative N-transformation pathways that are presently not accounted for in the marine nitrogen budget may exist (Capone and Knapp, 2007).

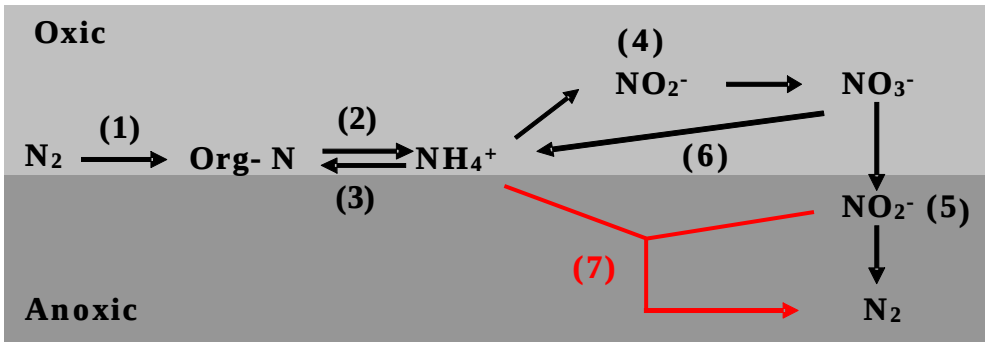

Figure 1.4. Simplified biogeochemical cycle of nitrogen, including processes of (1) nitrogen fixation, (2) mineralization of organic nitrogen (Org-N), (3) assimilation of nitrogen, (4) aerobic nitrification, (5) denitrification, (6) dissimilatory nitrate reduction to ammonium, and (7) anammox (modified from (Kuypers et al., 2003)).

The conventional biogeochemical cycle of nitrogen generally includes (1) nitrogen fixation, (2) mineralization of organic nitrogen, (3) assimilation of nitrogen, (4) aerobic nitrification, and (5) denitrification (Figure 1.4). Because of the triple bond that stabilizes both nitrogen atoms, dinitrogen gas (N_2) is the most dominant nitrogen species in natural environments and constitutes approximately 78% of the atmosphere. N_2 gas is unavailable to most organisms, leading to nitrogen limitations for photosynthesis in various environments (Galloway et al., 2004). Nitrogen fixation that converts di-nitrogen to reactive nitrogen therefore plays a crucial role in controlling global primary productivity (Borucki, 1984). While lightning may fix nitrogen (Borucki, 1984, Bothe et al., 2007), biological nitrogen fixation (BNF) by diazotrophs, which are able to produce reduced forms of nitrogen, such as ammonium, amines, and amino acids (Bothe et al., 2007, Galloway and Cowling, 2002), represents the main process of nitrogen fixation on Earth. Organic nitrogen produced via nitrogen fixation is converted to ammonium through mineralization ((2) in Figure 1.4) (Bothe et al., 2007). Aerobic nitrification ((4)

in Figure 1.4) is a two-step process, including the aerobic oxidation of ammonium to nitrite (Eq. 1.3) and nitrite to nitrate (Eq. 1.4) (Bothe et al., 2007, Mosier et al., 2002).

$$NH_4^+ + 3/2\ O_2 \rightarrow NO_2^- + H_2O + 2H^+ \qquad \text{(Equation 1.3)}$$

$$NO_2^- + 1/2\ O_2 \rightarrow NO_3^- \qquad \text{(Equation 1.4)}$$

These two oxidation steps are conducted by different groups of microorganisms, named ammonia-oxidizing bacteria (AOB) and nitrite-oxidizing bacteria (NOB) (Bothe et al., 2000). One of the essential steps during nitrification is the activation of ammonia to hydroxylamine (NH_2OH) by ammonium mono-oxygenase (AMO) (Bothe et al., 2007). Most of the microorganisms involved in aerobic nitrification are chemolithoautotrophs such as *Nitrosomonas* (AOB) and *Nitrobacter* (NOB), which use the energy released from nitrification for cell growth (Bothe et al., 2007). However, some heterotrophic microorganisms can also aerobically oxidize ammonia to nitrite and nitrate (Richardson et al., 1998). In fact, nitrifiers are suggested to display versatile metabolism, including other pathways that are not strictly lithotrophic and aerobic (Schmidt et al., 2002). For example, some AOB have been demonstrated to oxidize ammonium in the presence of pyruvate and nitrite under anaerobic conditions (Abeliovich and Vonshak, 1992), and ammonium oxidizing archaea (AOA) are also found to widely exist in marine waters and sediments including in oxygen-limited zones (Francis et al., 2005). So far, nitrification is considered one of the least understood steps of the nitrogen cycle (Bothe et al., 2007).

Denitrification ((5) in Figure 1.4) refers to the dissimilatory reduction of nitrate and nitrite to N_2 via a series of intermediates (nitric oxide, NO, and nitrous oxide, N_2O) (Knowles, 1982). A taxonomically diverse group of bacteria synthesizes a series of

enzymes, including a nitrate reductase, a nitrite reductase, or a NO reductase to successively reduce these different N species (Bothe et al., 2000). Denitrifiers are generally dominated by heterotrophs, which utilize organic carbon as terminal electron donor and produce reductase enzymes only under anaerobic conditions (Mosier et al., 2002). Denitrification is widely regarded as taking place under strict anaerobic conditions, such as in the oxygen minimum zones (OMZs) of the ocean (Mosier et al., 2002). Dissimilatory nitrate reduction to ammonium (DNRA) ((6) in Figure 1.4), which refers to the direct reduction of nitrate to ammonium, also exists in marine sediments and may be comparable to denitrification, especially under high sulfidic conditions (An and Gardner, 2002).

Anammox ((7) in Figure 1.4), a recent addition to the nitrogen cycle, refers to the anaerobic respiration of ammonium on nitrite or nitrate to produce N_2 as end product (Jetten et al., 2009). Although thermodynamic calculations suggest the possibility of ammonia oxidation by nitrite or nitrate (Broda, 1977), ammonium was considered an inert molecule under anaerobic conditions until the mid 1990's when the first evidence of anaerobic ammonium oxidation to N_2 (patented as the 'anammox' process) was found in a wastewater treatment plan (Mulder et al., 1995, deGraaf et al., 1996). In marine systems, the anammox process was first demonstrated in the anoxic zone of the Black Sea using ^{15}N tracer experiments (Kuypers et al., 2003). Since then, anammox bacteria have been proposed to play an important role in the removal of reactive nitrogen in various marine environments (Hamersley et al., 2007, Thamdrup et al., 2006). For example, the anammox process was suggested to contribute up to 50% of the global loss of fixed nitrogen from the oceans (Brandes et al., 2007), even though other studies suggested that

denitrification rather than anammox dominates the nitrogen loss in marine systems (Ward et al., 2009). Though in debate, anammox is generally considered to be an important process that significantly impacts the global nitrogen cycles and may improve wastewater treatment techniques (den Camp et al., 2006).

Although anammox has been intensively studied, the molecular pathway responsible for this reaction remains poorly understood (Jetten et al., 2009). In addition, the source of nitrite for anammox in oxygen-limited environments remains to be identified (Jetten et al., 2009, Mortimer et al., 2004). Most studies of anammox in marine environments have been based on anoxic incubations with addition of nitrate or nitrite (Dalsgaard et al., 2005, Engstrom et al., 2005, Kuypers et al., 2003). However, nitrate and nitrite are generally scarce in anoxic marine sediments and the pervasive distribution of anammox activity in sediment columns (Engstrom et al., 2005, Thamdrup and Dalsgaard, 2002) suggests that other processes supply these electron acceptors continuously. Aerobic ammonium oxidizers near oxic/anoxic interfaces may provide nitrite for anammox bacteria (Schmidt et al., 2002). However, the total production of NO_x^- by aerobic ammonium-oxidizing bacteria is not always able to sustain the loss of NH_4^+ through anammox, which requires an equivalent amount of moles of ammonium and nitrite (Lam et al., 2007). In addition, anammox is inhibited above 2 - 25 μM oxygen (Strous et al., 1997, Jensen et al., 2008, Kalvelage et al., 2011), implying that aerobic nitrification and anammox may be vertically separated in sediments. These findings indicate that sources other than aerobic nitrification may exist to supply nitrite or nitrate for anammox microorganisms. Several lines of evidence indeed suggest nitrite and nitrate may be formed anaerobically in marine sediments. First, nitrate was found to rebound below the

oxygen penetration depth in a variety of organic-rich sediments (Mortimer et al., 2004, Anschutz et al., 2000, Mortimer et al., 2002). Second, anaerobic nitrification, demonstrated by the production of nitrate, nitrite, and N_2 in anoxic NH_4^+ incubations, was proposed to represent a substantial source of nitrite for anammox (Lam et al., 2007). These studies did not identify the electron acceptor involved in anaerobic nitrification but proposed Mn oxides as potential candidate given their high abundance and oxidative power in sediments (Anschutz et al., 2005, Luther et al., 1997, Mortimer et al., 2004). Besides Mn oxides, other less thermodynamically favorable electron acceptors, such as Fe(III) (Park et al., 2009, Clement et al., 2005) and sulfate (Fdz-Polanco et al., 2001, Schrum et al., 2009), have also been suggested to be coupled to the anaerobic oxidation of ammonium.

1.4.2 Links between anaerobic ammonium oxidation and the Mn redox cycle

Interestingly, oxidation of organic-N or NH_4^+ to N_2 (but not NO_3^-) by MnO_2 in the presence of dissolved oxygen has been observed in both field and laboratory studies and this process was proposed to dominate the nitrogen cycle in Mn-rich continental margin sediments (Luther et al., 1997). The coupling between MnO_2 reduction and direct ammonium oxidation to N_2, however, has yet to be demonstrated under anaerobic conditions (Thamdrup and Dalsgaard, 2000, Thamdrup and Dalsgaard, 2002). While the oxidation of ammonium to N_2 by MnO_2 is thermodynamically favorable over a wide range of pH, the formation of nitrate is only favorable at pH < 7.8 (Luther et al., 1997, Hulth et al., 1999). Therefore, marine sediments may provide appropriate environments for Mn(IV)-promoted anaerobic oxidation of ammonium to nitrate. Indeed, several other laboratory and field studies suggested that Mn(IV) oxides promote anaerobic ammonium

oxidation to nitrate/nitrite (anaerobic nitrification) in marine sediments (Anschutz et al., 2000, Hulth et al., 1999, Mortimer et al., 2004). This conclusion was drawn from the good correlation between the production of dissolved Mn^{2+} and a second nitrate maximum found below the oxygen penetration zone in marine sediments (Anschutz et al., 2000). Nitrite/nitrate production was also stimulated by extra amendment of Mn oxides during anaerobic incubations of sediments from Long Island Sound (USA) (Hulth et al., 1999). In addition, the production of nitrate and nitrite during anaerobic incubations of sediments from Humber Estuary (UK) (Bartlett et al., 2008) and Arcachon Bay (France) (Javanaud et al., 2011) was accompanied by the simultaneous reduction of manganese oxides.

Unfortunately, the link between anaerobic nitrification and reduction of Mn oxides is difficult to make from field (in situ) observations alone (Bartlett et al., 2008, Bartlett et al., 2007), especially when considering the following: (1) Nitrate and nitrite act as transition species in anoxic environments and are consecutively consumed by several processes such as denitrification (Knowles, 1982), anammox (Kuypers et al., 2003), and dissimilatory nitrate reduction to ammonium (Bothe et al., 2007); (2) Ammonium may be consumed or produced by a variety of parallel processes, including assimilation (Bothe et al., 2007), adsorption/desorption (Mackin and Aller, 1984), and ammonification (Hulth et al., 1999, Bartlett et al., 2008), making it difficult to recognize the contribution from anaerobic ammonium oxidation; and (3) Other thermodynamically favorable electron acceptors, such as Fe(III) oxides (Park et al., 2009, Clement et al., 2005) and sulfate (Fdz-Polanco et al., 2001, Schrum et al., 2009), have also been proposed to be coupled to anaerobic ammonium oxidation.

The inconsistent observations of Mn-catalyzed anaerobic nitrification in different sediments (Thamdrup and Dalsgaard, 2000, Bartlett et al., 2008) imply that the onset of this process may be facilitated by specific geochemical conditions. For example, it has been proposed that the lack of evidence from extensive sediment incubations (Thamdrup and Dalsgaard, 2000) may have been caused by nitrogen-limitation in the sediments (Hulth et al., 2005). Similarly, the perturbation of sediments by microorganisms or burial events of freshly formed Mn oxides has also been proposed to affect the occurrence of Mn-catalyzed anaerobic nitrification in different sediments from Humber Estuary (UK) (Bartlett et al., 2008). Thus, laboratory incubations that manipulate the key factors involved in Mn-catalyzed anaerobic nitrification are needed to demonstrate the coupling between anaerobic nitrate/nitrite production and Mn-oxides reduction.

Besides the link between Mn reduction and anaerobic ammonium oxidation, another pathway that couples Mn(II) oxidation to nitrate reduction has also been found in anaerobic sediments and suboxic water column (Aller, 1990, Schulz et al., 1994, Murray et al., 1995). Significant oxidation of Mn(II) is observed in the surface layer of sediments below the oxygen penetration zone, suggesting the oxidation of Mn(II) by nitrate, the only thermodynamically favorable electron acceptor available in the absence of oxygen (Aller, 1990). This coupling, so-called chemo-denitrification process (Eq. 1.5) (Sorensen et al., 1987), may also be involved in the interaction between the redox cycles of Mn and N.

$$5\ Mn^{2+} + 2\ NO_3^- + 4\ H_2O \rightarrow 5\ MnO_2 + N_2 + 8\ H^+ \qquad \text{(Equation 1.5)}$$

1.5 Objectives of the Thesis

Anaerobic respiration of Mn oxides plays a significant role in the cycling of carbon, nitrogen, and other toxic elements (White et al., 2008, Neretin et al., 2003, Luther et al., 1997); however, the mechanism of electron transfer from the electron donor to the terminal acceptor (Mn oxides) remains poorly understood. The overall objective of the present research was to investigate the mechanism of microbial Mn(IV) reduction coupled to the oxidation of organic carbon and establish the link between Mn reduction and ammonium oxidation under anaerobic conditions. Two main hypotheses studied in this dissertation included that:

(1) The electron transfer pathway of microbial Mn(IV) reduction proceeds via two consecutive steps of one-electron transfer, similar to the reversal pathway of microbial Mn(II) oxidation.

(2) Mn(IV) acts as electron acceptor for anaerobic nitrification and provides an alternative source of nitrite/nitrate in anaerobic environments.

In this work, *Shewanella oneidensis* strain MR-1 was employed as a model Mn(IV)-reducing bacterium to test hypothesis (1) and study the mechanism of electron transfer to Mn(IV) oxides during anaerobic respiration of Mn(IV) oxides. The specific goals for this study include, 1) exploration of the electron transfer pathway during the anaerobic Mn(IV) respiration, 2) comparation of the anaerobic respiration of Mn(IV) oxides with the respiration of soluble Mn(III) to better understand the two electron transfer steps during Mn(IV) reduction, 3) demonstration that a new mutant strain of *S. oneidensis* MR-1 is deficient in one of the two electron-transfer steps involved in the

reduction of Mn(IV), and 4) understanding the coupling between Mn(IV) reduction and organic carbon oxidation during the anaerobic respiration of Mn(IV) oxides.

In the second part of this thesis, the surface layer of sediments from Skidaway salt marsh in Savannah, Georgia was sampled and incubated in the laboratory to test the hypothesis (2) that Mn reduction could be coupled to nitrification below the oxygen penetration zone. Sediment slurries amended with two different forms of Mn(IV) oxides in the presence of NH_4^+ were conducted under anaerobic conditions, and the chemical speciation of both Mn and N species was measured as a function of time to (1) determine evidence for Mn(IV)-mediated anaerobic nitrification and (2) investigate the key geochemical conditions that may affect the onset and activity of anaerobic ammonium oxidation in natural sediments.

The thesis is structured in six different sections. After the introduction (Chapter I), the different methods used in this dissertation are presented in Chapter II. In Chapter III, a suite of point mutant strains of *S. oneidensis* identified for their inability to reduce Mn(III) (strain Mn3) or solubilize Fe(III) oxides (strain *Sol* d29 and d64) were utilized to study the mechanism of Mn(IV) reduction. Chapter IV presents new findings on the mechanism of electron transfer during the anaerobic respiration of Mn(IV) oxides and its impact on carbon mineralization using known mutant strains of *S. oneidensis*. This chapter was recently submitted to Geochimica et Cosmochimica Acta and is under peer review. The role of Mn(IV) reduction in the anaerobic oxidation of ammonium to nitrite and nitrate in marine sediments is presented in Chapter V. Finally, Chapter VI summarizes the findings of this dissertation and provides recommendations for future studies.

CHAPTER 2 ANALYTICAL TECHNIQUES AND METHODS

2.1 Voltammetry

Oxygen and reduced species, such as Fe^{2+}, Mn^{2+}, and ΣH_2S, were analyzed voltammetrically by a computer-operated DLK-100A or DLK-60 potentiostat (Analytical Instrument Systems, Inc.) with microelectrodes or an Autolab instrument including a data-acquisition system and a potentiostat (ECO CHEMIE). The voltammetric measuremnt was performed with a three-electrode system: a hanging mercury drop electrode (HMDE) (Metrohm VA 663) or an Au/Hg solid-state microelectrode as working electrode, a 0.5 mm diameter glassy carbon (for HMDE) or a platinum wire as counter electrode, and a 0.5 mm diameter Ag/AgCl reference electrode. The Au/Hg solid-state microelectrode was fabricated following the procedure described previously (Brendel and Luther, 1995). The working microelectrodes consisted of a 100-μm-diameter Au wire held in epoxy into a 3-mm PEEK^{TM} tubing connected via a copper conducting wire to the potentiostat. The Au surface was polished sequentially with diamond pastes of 15, 6, 1, and 0.25 μm (Buehler) to generate a flat and smooth surface. The polished electrode was then plated with Hg for 4 min at -0.1V in a 0.1 M $Hg(NO_3)_2$ solution. The Hg-plated electrode was polarized at -9 V for 60 seconds in NaOH solution to form a good amalgam between the Au and Hg.

In voltammetry, a potential varying with time is applied between the working and reference electrodes to initiate the oxidation or reduction of different species at specific potentials, and the resulting currents from the redox reactions are read at the counter electrode. The specific reduction potentials of species of interest in the current studies are provided in Table 2.1 (Brendel and Luther, 1995). Voltammetry parameters used during

scans included: conditioning for 10 sec at -0.1 V, 200 mV/s scan rate from -0.1 to -1.8 V, and a pulse height of 0.05 V. Voltammograms were integrated using the semi-automatic integration program VOLTINT in Matlab (Bristow and Taillefert, 2008). The integrated peak heights were calibrated by calibration curves made daily with Mn^{2+} standards (Figure 2.1-A). At least three scans were obtained for each standard and sample. The Mn^{2+} calibration curve was also applied to quantify the concentrations of Fe^{2+} and ΣH_2S using the adjusting factors according to the Pilot Ion Technique (Brendel and Luther, 1995). The adjusting factors from the slope of Mn^{2+} calibration curve are 0.36 for Fe^{2+} calibration and 12.6 for ΣH_2S calibration. The matrix consisted either of 0.1M KNO_3 for HMDE or 50% seawater salt for the microelectrode at a pH around 7-8. O_2 was measured by linear sweep voltammetry with a 200 mV/s scan rate from -0.1 to -1.8 eV (Figure 2.1-B).

Table 2.1. Voltammetric half reactions of the species of interest in the current study and their reduction potentials at the Hg-plated gold wire surface of the microelectrode (Brendel and Luther, 1995).

Reactions	Reduction potentials
$O_2 + 2H^+ + 2e^- + Hg \rightarrow H_2O_2$ (Hg)	- 0.3
H_2O_2 (Hg) $+ 2H^+ + 2e^- \rightarrow 2H_2O$	-1.30
$HS^- + Hg \rightarrow HgS + H^+ + 2e^-$	< - 0.60
$HgS + H^+ + 2e^- \leftrightarrow HS^- + Hg$	-0.60
$Fe^{2+} + Hg + 2e^- \leftrightarrow Fe$ (Hg)	-1.43
$Mn^{2+} + Hg + 2e^- \leftrightarrow Mn$ (Hg)	-1.55

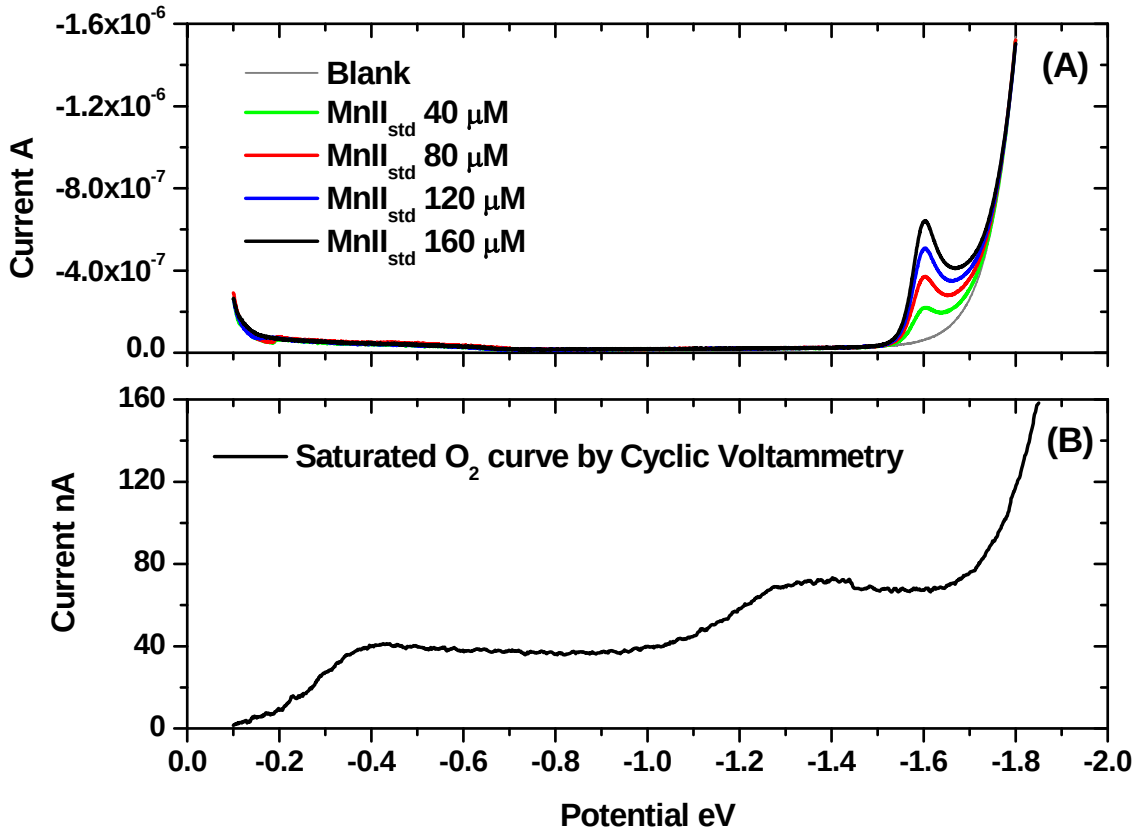

Figure 2.1. Examples of voltammogram scans (A) square wave scans of a Mn(II) calibration in a concentration ranging from 0 to 160 μM at pH 7 in diluted seawater. (B) the linear sweep scan of dissolved oxygen by microelectrodes with O_2 and H_2O_2 reduction waves at around -0.4 V and -1.3 V, respectively

2.2 Total Dissolved inorganic carbon (DIC)

Total dissolved inorganic carbon (Eq. 2.1) was measured by a flow injection analysis system with conductivity detection (Hall and Aller, 1992) coupled to an Analytical Instruments System (AIS, Inc.) LCC100 integrator. A small volume (~100 μl) of sample was inject into a flowing reagent stream (20 mM of HCl) to transform all carbonate species to gas phase CO_2. The carrier stream (10 mM of NaOH) was then passed over a gas-permeable hydrophobic membrane on the other side of the HCl stream to capture the CO_2 produced (Hall and Aller, 1992). The receiving carrier stream was then transferred to a conductivity detector (EC meter Model 1054, VWR Scientific) for quantification of the change in conductivity. A peristaltic pump (Model RP-1, Dynamax) was utilized to produce relatively low-pulse reagent streams (a flow rate of ~1.0 ml min^{-1} in both streams). A porous Teflon membrane strip was used as the gas exchange membrane to permeate only the gas phase CO_2.

A calibration curve to quantifiy DIC in a concentration range of 1 - 20 mM was generated every 20 measurements (Figure 2.2). The production of DIC in all incubations was subtracted from the background noise and normalized to the volume of the filtered sample.

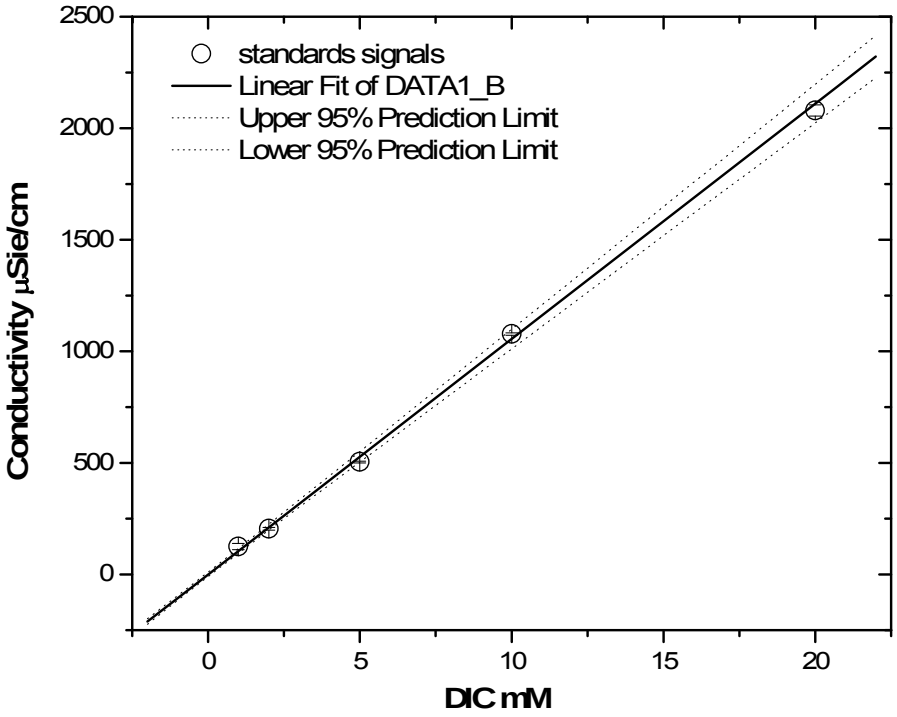

Figure 2.2. An example of the calibration curve for quantification of DIC in sample matrix solutions, using bicarbonate standards ranging from 1 mM to 20 mM. Circle symbols are measured standard signals and solid line is the linear fitted calibration curve. Standard deviations with upper and lower 95% prediction limit curves were shown as well.

2.3 pH

pH was measured with a pH/ISE meter (SB301 SympHony pH meter, VWR Scientific). The potential and temperature of the samples were recorded for the calculation of pH from the Nernst equation (Eq. 2.1):

$$pH_{sample} = pH_{std} - [F\times(E_{sample} - E_{std})]/(2.303\times R\times T) \quad \text{(Equation 2.1)}$$

where E is the measured potentials of the samples and standards (std), F is the Faraday's constant (96485.31 C/mol), R is the gas constant (8.3144 J/mol/K), and T is the temperature in K. The pH standards ranging from 5 to 9 were used for calibration with pH values.

2.4 Atomic Adsorption Spectrometer

Graphite Furnace Atomic Absorption Spectrometry (GFAAS) with atomizer pyrolytic coated partitioned graphite tube and Zeeman background corrections was used to determine the concentrations of total Mn and total dissolved Mn (TDM). The furnace operating conditions are listed in Table 2.2. Instrument parameters were as following: 5 mA lamp current, 0.2 nm spectral bandwidth, 279.5 nm wavelength, and 1.2 of maximum absorbance. Blanks and calibration curves were obtained every 20 samples, using Mn standards from 0 to 0.18 μM, and SLRS (St. Laurent's River Standard, Canada Certified Reference) samples were utilized for quality control.

Table 2.2. The graphite furnace operating conditions for the measurement of total Mn or TDM under Graphite Furnace Atomic Absorption Spectrometry (GFAAS).

Step No.	Temperature (°C)	Time (sec)	Gas Flow (L/min)	Gas Type	Read Command
1	85	5	3.0	Normal	NO
2	95	40	3.0	Normal	NO
3	120	10	3.0	Normal	NO
4	700	5	3.0	Normal	NO
5	700	1	3.0	Normal	NO
6	2400	2	0	Normal	NO
7	2400	1.1	0	Normal	YES
8	2400	5	0	Normal	YES
9	2400	2	3.0	Normal	NO

2.5 Colorimetry

2.5.1 Mn(III) pyrophosphate

Due to the high reactivity of Mn(III), stock solution of soluble Mn(III) must be stabilized by addition of ligands such as pyrophosphate (Kostka et al., 1995). Mn(III) pyrophosphate stocks were made by adding Mn(III) acetate dihydrate (97% Sigma Aldrich, ACS grade) to sodium pyrophosphate (Sigma Aldrich, ACS grade) solutions with a molar ratio of 1 Mn(III) : 5 pyrophosphate in N_2-purged de-ionized water (DI water). The Mn(III) standards made from the Mn(III) stock were then used to calibrate Mn(III) measurement by UV absorption spectrophotometry (Milton Roy spectronic 501) at a wavelength of 480 nm (Kostka et al., 1995).

2.5.2 NH_4^+

The concentration of ammonium was determined by colorimetric analysis described previously (Weatherb Mw, 1967). Measurements were conducted at a wavelength of 640 nm on a Milton Roy Spectronic 601 spectrophotometer with NH_4^+ standards of 0 to 20 μM made from a stock solution of NH_4Cl (Fisher) in DI water. The NH_4Cl was dried at 55°C overnight prior to preparation. Reagents used included phenol (8.5 mM; Sigma), nitroprusside (2.5 mM in 95% ethanol, Sigma Aldrich), and an alkaline solution containing 50 mM sodium citrate (Sigma Aldrich) and 20 mM NaOH (Fisher). A 2.5 mL of 4-6% sodium hypochlorite (NaOCl, Fisher) was added to 10 mL of the alkaline reagent immediately prior to analysis to create an oxidizing reagent. All the reagents were added in the following order to 1 mL of each sample and standard: phenol (500 μL),

nitroprusside (500 μL), and oxidizing reagent (1 mL). The samples with addition of all reagents were then heated at 45°C for 1 hour before analysis.

2.5.3 NO_2^-

Nitrite concentrations were determined by a colorimetric approach described previously (Grasshoff et al., 1983). Measurements were conducted at 540 nm on a Milton Roy Spectronic 601 spectrophotometer. Nitrite standards, ranging from 0 to 20 μM, were made from a stock solution of anhydrous $NaNO_2$ (Fisher) in DI water. The $NaNO_2$ was dried at 100°C for 1 hour prior to preparation. The reagents used included sulphanilamide (Fisher) and N-1-napthylethylenediamine dihydrochloride (NED) (Sigma). Sulphanilamide solution (5.8 mM) with 1 M of HCl and NED solution (0.97 mM) in a brown bottle were both stored in the refrigerator. The sulphanilamide solution (20 μL) was added to 1 mL of each standard and sample, and the mixture was well mixed and left to equilibrate for 1 minute to allow the reaction to proceed. The NED solution (20 μL) was then added and the sample was allowed to develop its color for at least 30 minutes before analysis at 540 nm. Minimum detection was 0.5 μM and analytical error on duplicate samples was < 5% RSD.

2.5.4 Fe(II)

The measurement of Fe(II) was also carried out via colorimetric analysis with ferrozine (Stookey, 1970). Fe(II) standards ranging between 5 and 20 μM were made from a 1 mM ferrous ammonium sulfate ($Fe(NH_4)_2(SO_4)_2 \cdot 6H_2O$, Fisher) stock solution (pH = 2 with trace metal grade HCl). A 5 mM ferrozine stock solution, composed of 5 mM ferrozine (3-(2-pyridyl)-5,6-diphenyl-1,2,4-triazine, Aldrich) and 0.5 M ammonium acetate, were added into each standard or sample containing to make a final concentration

of 2.5 mM of ferrozine solution. The purple color developed after addition of the ferrozine was quantified colorimetrically at 562 nm wavelength (Stookey, 1970).

2.6 Ion Chromatography (IC)

2.6.1 Nitrite and nitrate measurements

An anion chromatography technique coupled to ultraviolet detection was used to determine the concentration of nitrite (NO_2^-) and nitrate (NO_3^-) in high salinity solutions (Rozan and Luther, 2002). All measurements were conducted in an ion chromatograph (Dionex, DX-300 Series) with an Alltech Anion/R 10 μm (150 × 4.6 mm) chromatography column and Alltech All-Guard Anion/R 7.5 × 4.6 mm guard. A Waters 2487 Dual λ Absorbance Detector was used for ultraviolet detection at a wavelength of 220 nm with a sensitivity gain of 0.010 absorbance units to maximize the nitrite and nitrate signals. Filtered samples were pumped at a rate of 2 mL/min by a Waters 1525 Binary HPLC pump to the chromatography column to separate nitrite and nitrate before reaching the detector. A sodium perchlorate solution (2.5 mM $NaClO_4$, pH 10) was used as the eluent, due to its ability to rapidly elute anions and its low affinity for metal complexation and precipitation (Rozan and Luther, 2002). The pH of the eluent was maintained at 10 to ensure that all sulfide species are in the form of HS^-. The eluent solution was prepared freshly every 3 days due to the degradation of ClO_4^- and simultaneous decrease in pH. All samples were diluted in 1/5 or 1/10 proportions to reduce the interference of Cl^- to the sensitivity of nitrite (Beckler et al., 2012). Nitrate and nitrite species were separated based on charge affinity and size with retention times of 10.52 ± 0.19 mins for nitrite and 11.90 ± 0.08 mins for nitrate. Nitrite and nitrate standards ranging from 0 to 10 μM were used for calibration (Figure 2.3).

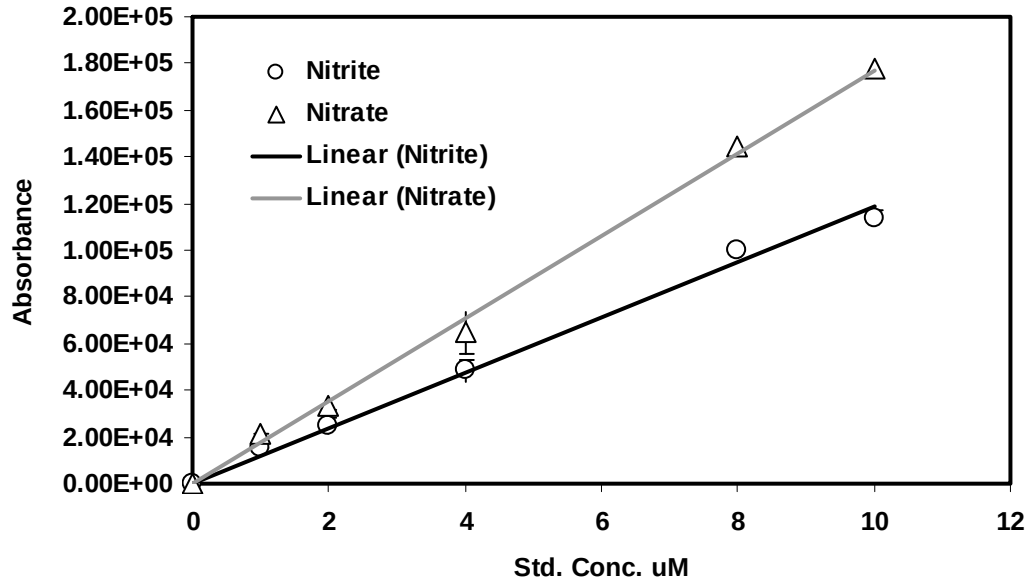

Figure 2.3. Calibration curves for nitrate (triangles) and nitrite (circles) in a seawater matrix (10 times of dilution) from the UV/Vis absorbance signals at 200 nm after separation by HPLC. The eluent contained 2.5 mM $NaClO_4$ at pH 10 and was purged with UHP N_2 gas.

2.6.2 Low-molecular-weight organic acid measurements

The consumption of lactate and production of acetate and other possible low molecular weight organic acids during the respiration of lactate by *Shewanella oneidensi*s MR-1 were measured by ion chromatography with conductometric detection. The ion chromatograph (Dionex, DX-300 series) was equipped with a Dionex IonPac® ICE-AS6 ion-exclusion column. The column, composed of a 8 μm cross-linked styrene/acrylate/divinylbenzene resin, is designed for efficient separation of low molecular weigh aliphatic organic acids based on an ion exclusion mechanism, which allows retention and separation of weakly ionized acids according to their different pKas.

The signal was detected by a CDM II detector with suppressed conductivity detection. Parameters for the measurement, such as eluent and regenerant solutions, flow rate, and background conductivity are listed in Table 2.3.

Table 2.3. Ion chromatograph parameters for the measurement of lactate, acetate and other low molecular weight organic acids.

Parameters	Read Command
Sample loop volume	50 µL
Analytical column	IonPac ICE-AS6
Eluent	0.4 mM Heptafluorobutyric acid
Pump	Dionex GP50 Gradient Pump
Eluent Flow rate	1.0 mL/min
Expected back pressure	< 500 psi
Temperature	21 °C
Suppressor	Anion-ICE MicroMembrane Suppressor II
Regenerant	5 mN Tetrabutylammonium hydroxide
Detector	Dionex Conductivity detector CDM-2
Background Conductivity	18 – 20 µS

As the retention times of different organic acids depend on the pKa values, lactic acid with a pKa of 3.66 shows a retention time of 9.67 min, pyruvic acid with a pKa of 2.26 shows a retention time of 5.00 min, and acetic acid with a pKa of 4.56 shows a retention time of 13.33 min (Figure 2.4-A). The standards ranging from 0 mM to 0.8 mM of pyruvate, lactate, and acetate were used for calibrations (Figure 2.4-B). Due to the high background lactate concentrations in the incubation samples (18 mM of initial lactate concentration), calibration of lactate was based on external standard addition method by adding extra lactate standard (0 to 0.8 mM) to diluted (a dilution factor of 10) background growth media (see section 2.10 for content of the media).

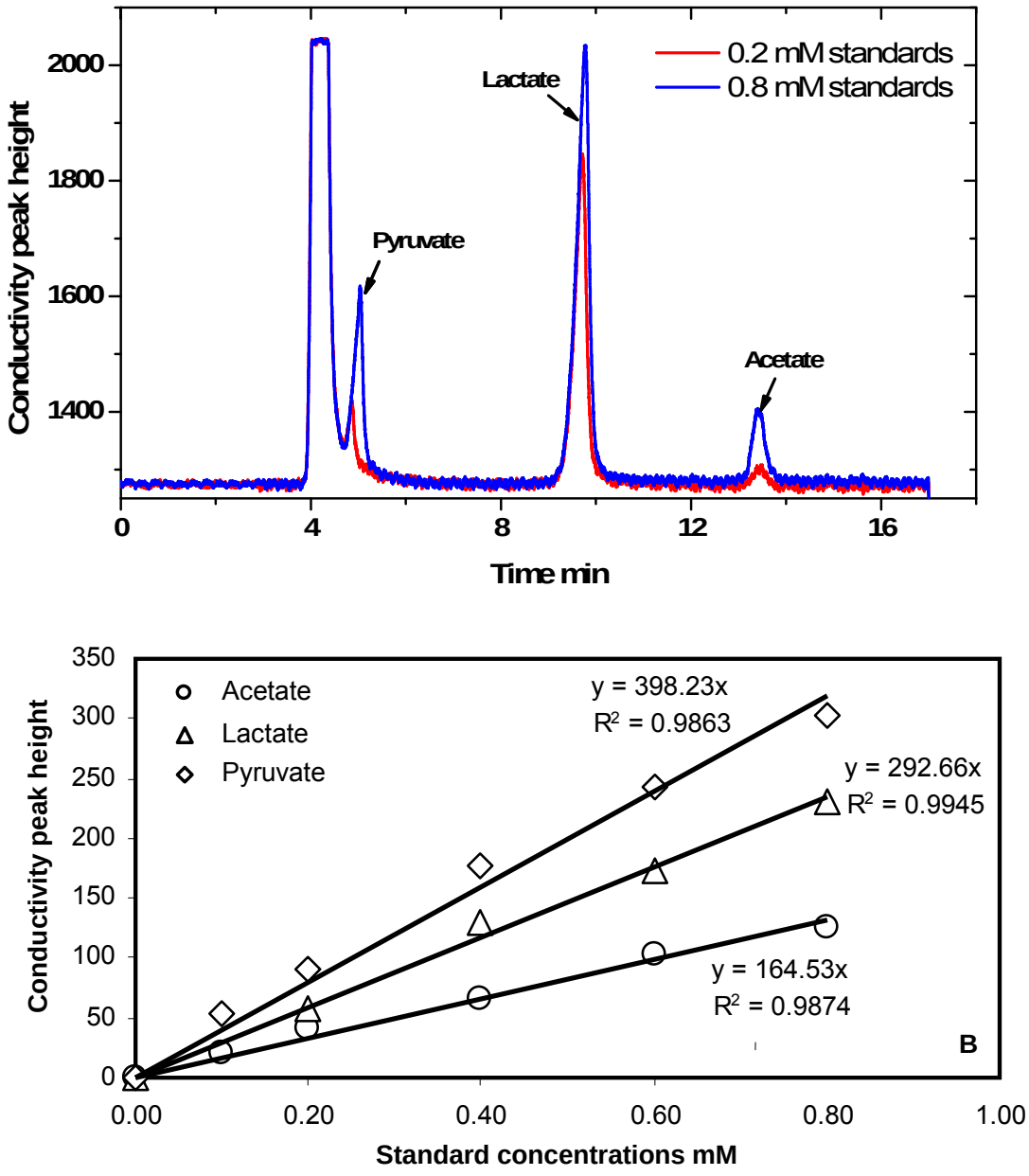

Figure 2.4. (A) Examples of chromatograms of standards containing 0.2 mM (blue) or 0.8 mM (red) acetate, lactate, and pyruvate in 10× diluted growth media (see section 2.10) as the bulk solution contained background lactate concentrations around 1.8 mM. (B) Calibration curves for acetate, lactate and pyruvate with standard concentrations ranging from 0 to 0.8 mM.

2.7 Membrane Inlet Mass Spectrometer (MIMS)

Concentrations of $^{29}N_2$ and $^{30}N_2$ were measured by MIMS following the approach described previously (Kana et al., 1994). MIMS requires no degassing step, a relatively small sample size (8-10 mL), and performs at relatively high efficiency and precision (Kana et al., 1994). The mechanism of MIMS has been reported previously (Kana et al., 1994) and is only briefly described here. A liquid or gas sample is put in contact with a semi-permeable membrane that separates the sample from the high vacuum of a mass spectrometer. Molecules that permeate the membrane follow a vacuum gradient and enter the mass spectrometer for detection. The mass spectrometer puts a charge on the gas molecules and filters out all masses except the one that has a stable path to the detector (Kana et al., 1994). A quadrupole mass spectrometer was used to (1) separate ions in an oscillating electrical field generated by 4 parallel rods and (2) rapidly sweep across masses from mass 1 to mass 45. In the current study, MIMS was used to differentiate N_2 with masses 28, 29, and 30, which were derived from various combinations of the stable isotopes of N (^{14}N and ^{15}N) in N_2. As mass 28 can also be attributed to carbon monoxide (CO) gas, produced during fragmentation of CO_2 gas, a liquid N_2 trap was used to remove water vapor and CO_2 to prevent interference of CO with $^{28}N_2$. All the samples were maintained under anaerobic conditions such that the interference of O_2 caused by the formation of NO with mass of 28 in the mass spectrometer was neglected. The liquid samples and standards were pumped by a peristaltic pump (IsmaTec, cole-Parmer Instrument Company) through a gas permeable silicone membrane located in a vacuum. The gases that are able to permeate the silicone membrane include water vapor, nitrogen, oxygen, argon, carbon dioxide, and any low molecular weight organic compounds, such

as methane. For nitrogen, oxygen and argon detection, liquid nitrogen was used to freeze out all of the other components. Gases were then transferred into the quadrupole mass spectrometer to separate them by mass before reaching the detector.

Five masses, including 28, 29, 30, 32, and 40, were detected in the mass spectrometer. All concentrations were calculated by normalizing the ratios of the N_2 species to Ar, as Ar, with high stability, can be used as an internal standard to correct the drift caused by the change of environment (salinity and temperature). The concentrations of gases in the standards were calculated based on the solubility of the species under saturated conditions at certain salinity and temperature (Weiss, 1970). Two water baths open to the atmosphere were used as the two temperature points (21°C and 30°C) for calibration.

The sampling process was conducted carefully to avoid contamination. Samples were generally stored in tall, narrow, and rubber-capped glass vials to limit air contamination. Prior to capping the container, a 0.1% volumetric addition of saturated $ZnCl_2$ solution was added as a preservative. The samples were then capped without entrapping any bubble and stored underwater at a temperature below the experimental temperature to avoid outgassing. The standards were run every four injections to monitor the instrument drift.

Conversion of the measured signal (AMU) to gas concentrations (μmol/L) was first based on the calculation of saturated gas concentrations of N_2, O_2, and Ar according to temperature and salinity (Eq.2.2) (Weiss, 1970) .

$$\ln C^* = A_1 + A_2 \times \frac{100}{T} + A_3 \times \ln\left(\frac{T}{100}\right) + A_4 \times \frac{T}{100} + S‰ \times \left[B_1 + B_2 \frac{T}{100} + B_3 \left(\frac{T}{100}\right)^2 \right] \qquad \text{(Equation 2.2)}$$

Where C is the gas concentration in solution (μmol/L), T is temperature (K), S is salinity, and A_i and B_i are constants as listed in Table 2.4.

Table 2.4. Constants for the calculation of the saturated gas concentrations (Weiss, 1970).

Gas	A_1	A_2	A_3	A_4	B_1	B_2	B_3
N_2	−172·4965	248·4262	143·0738	−21·7120	−0·049781	0·025018	−0·0034861
O_2	−173·4292	249·6339	143·3483	−21·8492	−0·033096	0·014259	−0·0017000
Ar	−173·5146	245·4510	141·8222	−21·8020	−0·034474	0·014934	−0·0017729

Saturated concentrations of N_2, O_2, and Ar at different temperatures (21°C and 30°C) and different salinities (0 and 18‰) are listed in Table 2.5.

Table 2.5. Saturated concentrations of N_2, O_2, and Ar at different temperature (21°C and 30°C) and different salinity (0 and 18‰).

T (°C)	S (‰)	[N_2] μmol/L	[O_2] μmol/L	[Ar] μmol/L	N_2/Ar	O_2/Ar
21.0	0.0	521.70	278.08	13.64	38.25	20.39
30.0	0.0	449.26	235.61	11.56	38.86	20.38
21.0	18.0	465.32	250.24	12.27	37.93	20.40
30.0	18.0	403.44	213.43	10.47	38.53	20.38

All the gas concentrations or ratios calculated according to Eq. 2.2 were used in the following conversions to obtain concentrations from AMU signals. A converting factor (CF, unitless) was calculated based on the ratio of calculated N_2/Ar value (μmol/L) to measured N_2/Ar value (atomic mass unit, AMU) (Eq. 2.3).

$$CF = \frac{\left(N_2 / Ar\right)_{measured}}{\left(N_2 / Ar\right)_{calculated}} \qquad \text{(Equation 2.3)}$$

Averaged CF value ($CF_{average}$) based on the CF values of all standards was used for calculation of $^{28}N_2$ concentrations in the samples, following Eq. 2.4

$$[^{28}N_2](\mu mol/L) = \left[CF_{average} \times N_2 delta + \left(\frac{N_2}{Ar} \right)_{calculated} \right] \times Ar_{calculated} \qquad \text{(Equation 2.4)}$$

Where N_2delta is determined by comparing the AMU28 signal of each sample to the standard signal (Hall, 2009).

The calculation of $^{29}N_2$ was based on the measured $^{29}N_2/^{28}N_2$ ratio in the samples. As the natural abundance of N-15 is 0.366%, a the theoretical $^{29}N_2/^{28}N_2$ ratio of 0.00723 can be calculated in natural samples (An et al., 2001). In this study, a $^{29}N_2/^{28}N_2$ ratio of 0.0072 was determined from the different standards (Figure 2.5), consistent to the theoretical ratio. The excess of AMU29 ($^{29}N_2$) signal was calculated as the deviation of $^{29}N_2/^{28}N_2$ ratio in the sample signal from the linear regression curve generated from the standards (Figure 2.5). Concentration of $^{29}N_2$ was then calculated according to Eq. 2.5.

$$\left[^{29}N_2 \right](\mu mol/L) = \frac{Excess^{29}N_2 \times N_{2,calculated}}{Average(N_{2,measured,standards})} \qquad \text{(Equation 25)}$$

$$\left[^{30}N_2 \right](\mu mol/L) = \frac{Excess^{30}N_2 \times N_{2,calculated}}{Average(N_{2,measured,standards})} \qquad \text{(Equation 2.6)}$$

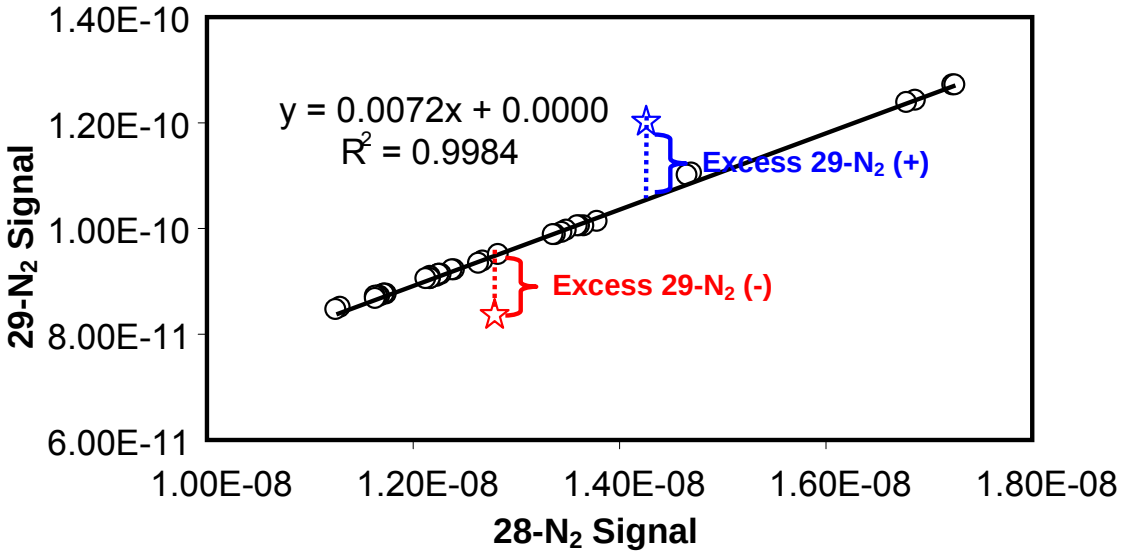

Figure 2.5. Linear correlation of 28-N_2 to 29-N_2 in seawater standards at 21 and 30°C. Star symbols (red and blue) are sample signals, below and above the linear regression curve (solid black line). Deviation of the sample signals the linear regression curve represents the Excess$^{29}N_2$, which can be either positive (blue) or negative (red).

The concentration of $^{30}N_2$ was derived from the excess AMU 30 signals, calculated following Eq. 2.6. The AMU30 signal in MIMS is complicated by reactions between N_2 and O_2 in the ion source of the mass spectrometer (Jensen et al., 1996, An et al., 2001). The NO^+ ions (AMU 30) formed from N_2 and O^+ inside the mass spectrometer generates a linear relationship between AMU and $(AMU28 \times AMU32)^{0.5}$(Jensen et al., 1996) (Figure 2.6). This relationship was used to determine the excess AMU 30 signal in the samples by comparing sample signals to the value of $(AMU28 \times AMU32)^{0.5}$ calculated from the standard signals, in a similar fashion to the calculation for the excess AMU 29.

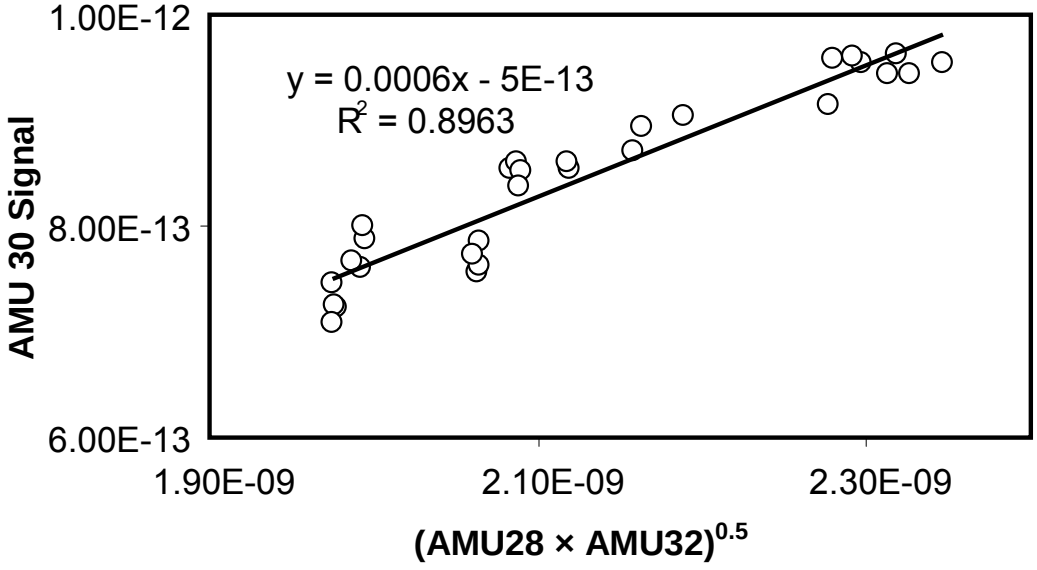

Figure 2.6. Linear correlation between AMU 30 signals and $(AMU28 \times AMU32)^{0.5}$ in seawater standards at 21 and 30°C.

2.8 AVS measurement

FeS/FeS_2 and acid volatile sulfide (AVS) were extracted by the distillation method described previously (Henneke et al., 1991). The operational definition of AVS includes amorphous forms of FeS, such as mackinawite ($(Fe, Ni)S_{0.9}$), greigite (Fe_2S_4), and pyrrhotite ($Fe_{(1-X)}S$, X=0 - 0.2) (Henneke et al., 1991).

The sediment in 1.5 ml of mixed slurry from the Mn and N reactors was centrifuged and transferred into a reaction vessel. Each vessel was connected to a 30 mL Hungate tubes containing 15 mL of 1 M NaOH, sealed and purged with UHP N_2 gas heated through a reduced copper trap at 350°C (Millero, 1986) to avoid oxygen

contaminations from the atmosphere. Concentrated HCl (3M) was added to each vessel through a nylon septum after the entire apparatus had been degassed with N_2 for at least one hour. The volatile H_2S gas produced due to the reaction between the concentrated HCl and the sediment was distilled at normal temperature with N_2 gas as the carrier and trapped in the 1M NaOH solution in the Hungate tubes (Henneke et al., 1991).

The sediment was reacted with concentrated HCl for four hours while stirring with a magnetic stir bar to ensure the completion of the reaction. After completion of the extraction, 100 µl of the NaOH solution was quickly transferred to 10 ml of N_2 purged 0.1 M NaCl solution and the concentration of sulfide was measured by voltammetry as described in the previous section (section 2.1).

2.9 Preparation of Mn oxides

2.9.1 Preparation of colloidal Mn oxides

Dark-brown colloidal Mn oxides solutions (10 mM) were prepared by reducing $KMnO_4$ with a stoichiometric amount of $Na_2S_2O_3$ according to Eq. 2.7 (Perezbenito et al., 1987):

$$8\ MnO_4^- + 3\ S_2O_3^{2-} + 2\ H^+ = 8\ MnO_2 + 6\ SO_4^{2-} + H_2O \qquad \text{(Equation 2.7)}$$

For incubations with *S. oneidensis*, a modified method was used as described below. Two 500 ml solutions, one containing 1 g/l yeast extract and 10 g/l gum arabic and the other containing 1 g/l yeast extract, 10 g/l gum arabic, and 7.5 mM of sodium thiosulfate, were prepared and autoclaved. After cooling the solutions to 55 °C, the first solution was amended with $KMnO_4$ to a 20 mM final conenration and slowly mixed with the second solution. Finally, 20 ml of Westlake media stock (50×) was added to the mixture, and the pH was adjusted to 8.0 with NaOH (10 N). This colloidal solution of

Mn oxides remained perfectly transparent during the entire incubation. For slurry incubations, the recipe was similar but without addition of yeast extract and Westlake media.

2.9.2 Preparation of amorphous Mn oxides

The amorphous Mn oxide was prepared by the oxidation of Mn^{2+} by permanganate, according to following the reaction (Eq. 2.8) (Murray, 1974).

$$3\ Mn^{2+} + 2\ MnO_4^- + 10\ H_2O = MnO_2 + 4\ H^+ \qquad \text{(Equation 2.8)}$$

The synthesis procedure was modified to maintain sterile conditions (Lovley and Phillips, 1988). Two separate 100 ml solutions, one with 0.30 M of $MnCl_2 \cdot 4H_2O$ and the other with 0.20 M of $KMnO_4$, were prepared in volumetric flasks. The Mn(II) solution was slowly dripped (≈ 2 drips/sec) into an autoclaved bottle containing a $KMnO_4$ solution to form black MnO_2 particles. The protons produced during the reaction were neutralized by NaOH (10 N) to maintain the pH around 10 throughout the reaction. After completion of the reaction, the synthesized particles were washed three times with $MgCl_2$ (0.1M) and DI water to remove the excess Mn^{2+}. The amorphous Mn oxide (20 mM) was stored in either Westlake media or 50% of artificial seawater (see the use of amorphous Mn oxides). As amorphous Mn oxide tends to aggregate after 2 to 3 weeks, fresh amorphous Mn oxide was synthesized for each batch of incubations.

2.9.3 Preparation of soluble Mn(III)-pyrophosphate

Mn(III) pyrophosphate stocks were made by adding Mn(III) acetate dihydrate (Sigma Aldrich, ACS grade) to sodium pyrophosphate (Sigma Aldrich, ACS grade) solution with a molar ratio of 1 Mn(III) : 5 pyrophosphate. The pH of the sodium pyrophosphate was adjusted to around 8.2 before addition of Mn(III) acetate dihydrate.

The final Mn(III) pyrophosphate stock was maintained at ph 7.8. Due to the high reactivity of Mn(III) (Luther et al., 1998), the actual concentration of the Mn(III) stock was analyzed by standard Winkler titration, first proposed by Winkler (Winkler, 1888) and modified by Strickland and Parsons (1968).

2.9.4 Modified Winkler titration

Based on the concentration of Mn(III) or Mn(IV), an excess amount of KI solution (10 mM) was added to reduce all Mn(III)/(IV) to Mn(II) in experimental solutions, following equations (Eq. 2.9 and 2.10).

$$2\ Mn(III) + 2\ I^- \rightarrow 2\ Mn(II) + I_2 \qquad \text{(Equation 2.9)}$$

$$Mn(IV) + 2\ I^- \rightarrow Mn(II) + I_2 \qquad \text{(Equation 2.10)}$$

HCl was added simultaneously to facilitate this reaction. Due to the formation of I_2, the solution turns blue in presence of several drops of 0.1% starch solution. Iodine was then titrated by 2 mM of $Na_2S_2O_3$ solution to form tetrathionate (Eq. 2.11), untill the disappearance of the blue color.

$$I_2 + 2\ S_2O_3^{2-} = 2\ I^- + S_4O_6^{2-} \qquad \text{(Equation 2.11)}$$

2.9.5 Determination of oxidation state of synthesized Mn oxides

The oxidation states of Mn in synthesized Mn oxides were determined according to a modified Winkler titration method used to calculate the oxidation states of metal oxides (Murray et al., 1984, Murray, 1974). Briefly, synthesized Mn oxides were dissolved in 10 M of nitric acid for detection of the concentration of total Mn via graphite furnace atomic adsorption spectrometry (GFAAS). The total amount of electrons transferred during the reduction of Mn oxides to Mn(II) was titrated through Winkler titration, as described previously. By using this method, the stoichiometry of the

synthesized Mn oxides was determined to be $MnO_{1.98}$. The stoichiometry of the synthesized Mn(III)-pyrophosphate complexes was quantified using the same method.

2.10 Preparation of *Shewanella oneidensis* MR-1 and mutant strains

2.10.1 Bacterial strains and growth media

Shewanella oneidensis strain MR-1 (ATCC No. 700550), provided by Dr. DiChristina's laboratory, was originally isolated from Oneida Lake, NY (Myers and Nealson, 1988). All strains, including the wild type MR-1 strain and mutant strains, were grown at 30˚C in a defined salt medium (SM) (Myers and Nealson, 1988) supplemented with 18 mM lactate as carbon/energy source. For SM solid medium, Bacto agar was added at 1.5% (w/v). The Westlake media, containing the following constituents: 2.87 mM K_2HPO_4, 14.1 mM Na_2SO_4, 18.7 mM NH_4Cl, 0.61 mM $MgSO_4 \cdot 7H_2O$, 1.36 mM $CaCl_2 \cdot 2H_2O$, 1.0 g/l yeast extract, 1.8 mg/l sodium lactate syrup, and 100 μM $FeCl_3$ solution, was used during all the batch incubations.

Mutant strains of *Shewanella oneidensis* MR-1 applied in the current studies included two groups, the in-frame deletion mutant strains (Chapter 4) and newly isolated mutant strains via random chemical mutagenesis (Chapter 3). The known in-frame deletion mutant strains utilized included (1) the mutant *ΔmtrB,* an *S. oneidensis* strain without the *mtrB* gene that encodes the outer membrane β-barrel protein MtrB postulated to anchor the decaheme *c*-type cytochromes MtrC and OmcA on the cell surface (Beliaev and Saffarini, 1998), (2) the mutant *ΔmtrC,* a *S. oneidensis* strain without the *mtrC* gene that encodes MtrC located on the surface of the outer membrane (Myers and Myers, 2001), (3) mutant *ΔomcA,* a *S. oneidensis* strain without the *omcA* gene that encodes OmcA (Myers and Myers, 2001), (4) mutant Δ*omcAmtrC,* a *S. oneidensis* strain without

both *mtrC* and *omcA* genes, (5) mutant *ΔgspD* is a *S. oneidensis* strain without the *gspD* gene, one of the key genes involved in the Type II secretion system (DiChristina et al., 2002), and (6) mutant T121, isolated via transposon mutagenesis of *S. putrefaciens* 200R (Saffarini et al., 1994), an anaerobic respiratory mutant strain, capable of aerobic growth only, that has been used as a negative control strain in a variety of studies (Burnes et al., 1998, DiChristina et al., 2002) (Table 2.6). Newly isolated mutant strains, generated via random chemical mutagenesis, were studied as well due to their specific phenotypes, including *Sol* mutant D29 and D64 deficient in producing soluble Fe(III) during reduction of solid Fe(III) (Jones et al., 2010) and a point mutant strain Mn3 deficient in reducing soluble Mn(III) (Table 2.6).

Table 2.6. Description of different *Shewanella oneidensis* strains used in the current studies, including wild-type *S. oneidensis* MR-1, Δ*mtrB*, Δ*mtrC*, Δ*omcA*, Δ*omcAmtrC*, Δ*gspD*, T121, *Sol* mutant strains d29 and d64, and point mutant strain Mn3.

Strain	Features	Source
Shewanella oneidensis		
MR-1	Wild-type strain	ATCC
Δ*mtrB*	in-frame *mtrB* gene deletion mutant	(Burns, 2010, Burns and Dichristina, 2011)
Δ*mtrC*	in-frame *mtrC* gene deletion mutant	(Burns, 2010, Wee et al., 2011)
Δ*omcA*	in-frame *omcA* deletion mutant	(Burns, 2010, Wee et al., 2011)
Δ*omcAmtrC*	in-frame *omcAmtrC* double deletion mutant	(Burns, 2010, Wee et al., 2011)
T121	Deficient in anaerobic respiration	(Burnes et al., 1998)
Sol mutant D29	Deficient in producing soluble Fe(III) and reducing solid Fe(III)	(Jones et al., 2010)
Sol mutant D64	Deficient in producing soluble Fe(III) and reducing solid Fe(III)	(Jones et al., 2010)
Mn3	Deficient in reduction of soluble Mn(III)	Current study

CHAPTER 3 USING POINT MUTANT STRAINS OF *SHEWANELLA ONEIDENSIS* MR-1 TO STUDY THE MECHANISM OF MICROBIAL MN(IV) REDUCTION

Abstract

The wild-type strain of *S. oneidensis* MR-1 and three novel mutant strains generated via chemical mutangenesis, *Mn3*, *Sol* d29, and *Sol* d64, were incubated anaerobically with either Mn(IV) or Mn(III) as terminal electron donor to study the mechanism of microbial Mn(IV) reduction. Reduction capabilities of these mutant strains on Mn(IV/III) were compared with each other and also to those on other electron acceptors, including Fe(III). The two *Sol* mutant strains d29 and d64, deficient in their ability to produce soluble Fe(III) and reduce solid Fe(III), did not reduce solid Mn(IV) oxides, suggesting that microbial Mn(IV) reduction may also require an initial solubilization step to facilitate the whole process. The mutant strain *Mn3*, deficient in its ability to reduce Mn(III), produced only 17% of the wild-type Mn(II) production, yet retained the ability to produce Mn(III) at wild-type levels during the incubations with Mn(IV) oxides as the electron acceptor. The phenotype of this newly found point mutant Mn3 suggests that the electron transport chain involved in the reduction of Mn(IV) and Mn(III) in *S. oneidensis* may not be identical. Components of the electron transport chain included in the reduction of Mn(III) but not Mn(IV) may be identified via genetic analysis of this point mutant strain.

3.1. Introduction

Shewanella oneidensis MR-1, a widely-distributed gram-negative γ-proteobacteria (Venkateswaran et al., 1999), is well-known for its ability to utilize a wide range of electron acceptors including insoluble manganese and iron oxides for anaerobic respiration (Lovley and Phillips, 1988, Myers and Nealson, 1988). Anaerobic respiration of manganese oxides significantly influences the biogeochemical cycling of carbon, nitrogen, phosphate, and toxic elements (Zhang et al., 2007, White et al., 2008, Neretin et al., 2003, Luther et al., 1997). Compared to other respiration processes such as aerobic respiration and anaerobic respiration on soluble electron acceptors, however, the mechanism of anaerobic respiration on solid Mn/Fe oxides remains poorly understood (Madigan et al., 2003, Borloo et al., 2007, DiChristina et al., 2005). To reduce insoluble Mn(IV)/Fe(III) oxides, bacteria have to transfer electrons from the conventional cytoplasmic membrane (CM)-localized electron transport systems via the periplasm and across the outer membrane (OM) to the extracellular face of the OM. The mechanism for this electron transfer pathway is of particular interest due to the potential applications in microbial fuel cells and bioremediation strategies (von Canstein et al., 2008). Generally, three electron transfer strategies have been postulated for either Mn(IV) oxides or Fe(III) oxides or both (Myers and Myers, 2003a, DiChristina et al., 2005, Newman and Kolter, 2000, Jones et al., 2010).

First, bacteria are proposed to directly reduce Mn oxides by localizing the terminal reductase to the outer membrane (Myers and Myers, 2001). Indeed, the type II secretion system, transporting protein from the periplasm to the outer membrane (Desvaux et al., 2004), appears to be critical to the direct enzymatic reduction of Mn and

Fe oxides (DiChristina et al., 2002). The OM *c*-type cytochromes MtrC and OmcA are proposed to be involved in the terminal steps of electron transfer during dissimilatory reduction of Mn oxides (Beliaev and Saffarini, 1998, Myers and Myers, 2002, Myers and Myers, 2003a). Interestingly, a mutant strain of *S. oneidensis* lacking a serine protease (SO3800) for bacterial adhesion to solid surfaces was shown to be incapable of adhering to Fe(III) oxides but reduce Fe(III) oxides at wild type rates, indicating that *S. oneidensis* may also be able to reduce Fe(III) oxides via alternative pathways than the direct contact mechanism (Burns et al., 2010).

Second, some organic compounds such as AQDS (DiChristina et al., 2005), quinones (Newman and Kolter, 2000), and riboflavin (von Canstein et al., 2008) may act as electron shuttles by being first enzymatically reduced and chemically re-oxidized by solid Mn(IV) or Fe(III) oxides in a second (abiotic) electron transfer reaction. A mutant strain of *S. putrefaciens* MR-1 deficient in menaquinone production is unable to reduce solid Mn(IV) and Fe(III), suggesting the possibility that endogenous menaquinones or small compounds related to menaquinones shuttle electrons to solid terminal electron acceptors (Newman and Kolter, 2000).

Third, microorganisms may reduce iron oxides by first dissolving Fe(III) with exogenous or endogenous organic ligands, then reducing the soluble Fe(III) species either on the outer membrane or inside the periplasm (Pitts et al., 2003, Taillefert et al., 2007a). Recently, mutants of *S. oneidensis* deficient in the production of soluble organic-Fe(III) complexes have been found to be impaired in the respiration of Fe(III) oxides, supporting the hypothesis that soluble organic-Fe(III) complexes are produced as intermediates during anaerobic respiration of solid Fe(III) by endogenous organic ligands (Jones et al.,

2010). The ligands for solubilizing Fe(III) are still elusive, but evidence suggests that siderophores are not involved in this process (Fennessey et al., 2010). Evidence for a similar solubilization strategy to reduce solid Mn(IV) has yet to be provided. In the case of solid Mn(IV), however, ligands that are able to complex Mn(IV) to facilitate the non-reductive dissolution of Mn(IV) oxides have yet to be identified in aqueous and sedimentary environments at circumneutral pH in aquatic systems (Morgan, 2000a, Duckworth et al., 2009). These findings suggest that if anaerobic respiration of solid Mn(IV) proceeds via a solubilization strategy, the process should be different than the anaerobic respiration of Fe(III) oxides.

A variety of exogenous compounds such as pyrophosphate and naturally-existing ligands such as citrate and siderophores are able to stabilize Mn(III) at a pH ranging between 5 and 8 (Kostka et al., 1995, Klewicki and Morgan, 1998, Parker et al., 2004). In addition, the reductive dissolution of Mn(IV) oxides by natural organic compounds and microbial metabolites such as oxalate and pyruvate is well known (Stone, 1987a, Stone and Morgan, 1984a). For example, desferrioxamine B, a trihydroxamate siderophore produced by microorganisms, is able to reduce MnO_2 through a single electron transfer step to solid Mn(III) and solubilize Mn(III) by complexation (Duckworth and Sposito, 2007). Recently, siderophore were proposed to be involved in both the bacterial Mn(II) oxidation (Parker et al., 2007) and microbial reduction of solid Mn(IV) oxides (Kouzuma et al., 2012). These findings imply that microorganisms may have to adopt a reductive solubilization strategy that reduces solid Mn(IV) oxides to soluble Mn(III) complexes as intermediates during the microbial reduction of Mn(IV).

Respiratory reduction of Mn(IV) should be more complicated than that of Fe(III), considering that a total of two electrons can be transferred through either two steps of one-electron transfer or one step of two-electron transfer. According to the molecular orbital theory, Mn(IV) is able to accept the first electron to one of the two empty e_g orbitals of Mn(IV) and rearrange the orbitals to form the Mn(III) intermediate which further accepts the other electron to form Mn(II) (Luther, 2005). Mn(III) has been demonstrated to be produced as intermediates during chemical or photochemical reduction of Mn(IV) (Perez-Benito, 2002, Ruppel et al., 2001) and during the aerobic oxidation of Mn(II) by spores of the marine *Bacillus* sp. Strain SG-1 (Webb et al., 2005).

In the present study, *Shewanella oneidensis* strains including the wild type strain MR-1 and a suite of mutant strains generated via chemical mutagenesis were incubated under anaerobic conditions with either solid Mn(IV) oxides, soluble (colloidal) Mn(IV) oxides, or soluble Mn(III)-pyrophosphate complexes as terminal electron acceptor to gain new insights into the mechanisms of anaerobic Mn(IV) respiration by *Shewanella oneidensis* MR-1. Phenotype of these novel mutant strains provided evidence that two steps of one-electron transfer are involved in the reduction of Mn(IV) oxides and suggested that microbial reduction of Mn(IV) may require an initial solubilization step to produce soluble Mn(III) for further reduction of Mn(III) to Mn(II).

3.2 Material and experimental Design

3.2.1. Materials

All glassware and plastic ware were soaked in 10% nitric acid overnight and washed with sterile DI water prior to use. All batch reactors were autoclaved before incubation. All solutions were prepared with ACS or trace metal grade chemicals in 18 MΩ-DI water

(Barnstedt). Preparation of colloidal and amorphous MnO_2 and soluble Mn(III)-pyrophosphate was described in Chapter 2.

3.2.2 Bacterial strains and growth media

Shewanella oneidensis strain MR-1 was originally isolated from Oneida Lake, NY (Myers and Nealson, 1988). The *S. oneidensis* strains used in the present study include the wild-type strain (displaying normal Mn(IV) and Mn(III) reduction activities), the anaerobic respiratory mutant strain T121 (incapable of growing in anaerobic conditions), and three mutants generated via random chemical mutagenesis, *Sol* d29, *Sol* d64, and Mn3 (Jones et al., 2010) (Table 3.1). All strains were grown at 30˚C in a defined salt medium (SM) (Myers and Nealson, 1988) supplemented with 18 mM lactate as carbon/energy source. For SM solid medium, Bacto agar was added at 1.5% (w/v).

Anaerobic respiratory mutant strain T121 (capable of aerobic growth only) was isolated via transposon mutagenesis of *S. putrefaciens* 200R (Saffarini et al., 1994) and was used as a negative control strain for anaerobic conditions (Burnes et al., 1998, DiChristina et al., 2002). Concentrations of Mn(II) remained at background levels in either the background solution or the two solid extracts in the T121 incubations, accounting for merely 4.5 ± 0.6% of the wild-type production (Table 3.2). This result confirmed that anaerobic conditions were maintained during all the incubations. *Sol* mutant strains d29 and d64 were identified for their growth deficiencies on 2L-ferrihydrite or soluble Fe(III)-citrate, yet retain the ability to respire all other alternative electron acceptors, such as O_2, NO_3^-, NO_2^-, DMSO, $S_2O_3^{2-}$, TMAO, fumarate) (Jones et al., 2010). At least one component of the soluble organic-Fe(III) production system, as a part of the electron transport strategy for the respiration of Fe(III) oxides by *Shewanella*

oneidensis MR-1, was impaired in the mutant strains *Sol* d29 and d64 (Jones et al., 2010). Details of the construction and isolation of d29 and d64 were described previously (Jones et al., 2010).

Table 3.1. Description of strains of *Shewanella oneidensis* MR-1 used in current incubations, including wild-type strain of *S. oneidensis* MR-1, *Sol* mutant D29 and D64, and Mn3 mutant.

Strain	Features	Source
Shewanella oneidensis		
MR-1	Wild-type strain	ATCC
T121	Deficient in anaerobic respiration	(Burnes et al., 1998)
Sol mutant d29	Deficient in producing soluble Fe(III) and reducing solid Fe(III)	(Jones et al., 2010)
Sol mutant d64	Deficient in producing soluble Fe(III) and reducing solid Fe(III)	(Jones et al., 2010)
Mn3	Deficient in reduction of soluble Mn(III)	Current study

Isolation of Mn(III) reduction-deficient mutant strains (Mn3) of *S. oneidensis*. Ethyl methane sulfonate (EMS) was used as a chemical mutagen following previously described procedures (Burnes et al., 1998, DiChristina et al., 2002). Liquid cultures of wild-type *S. oneidensis* were grown in SM medium to late exponential phase ($2x10^9$ cells mL^{-1}), harvested by centrifugation at 10,000 xg (4˚C), washed twice, and re-suspended in fresh SM medium. EMS was added (19 mg/mL) and the cell suspension was incubated 45 min to achieve 90% kill. The surviving EMS-treated cells were plated on SM agar and the colonies were subsequently subjected to a mutant screening technique to detect loss of Mn(III) reduction activity. Approximately 5,000 EMS-treated colonies were transferred to SM agar medium supplemented with 18 mM lactate as electron donor and 5

mM Mn(III)-pyrophosphate as electron acceptor (which imparts a distinctive pink color to the agar medium; Figure 4.1). After 48 hours of incubation in a Coy anaerobic chamber (atmosphere of 5% CO_2, 10% H_2, 85% N_2), wild-type colonies produced a distinctive clearing zone in their colony peripherey (an indication that pink-colored Mn(III)-pyrophosphate had been reduced to colorless Mn(II) end-products). Five putative Mn(III) reduction-deficient mutants were identified by their inability to produce a clearing zone (Figure 4.1), and one of them (designated strain Mn3) was selected to first study its phenotype on the overall respiratory capability and then investigate the kinetics of Mn(IV) and Mn(III) reduction. In the study of the overall anaerobic respiratory capability of strain Mn3, batch liquid cultures were grown in SM medium supplemented with 18 mM lactate under either aerobic or anaerobic conditions achieved through continuous flushing of nitrogen gas. The following compounds were tested as anaerobic electron acceptors at the indicated initial concentration: Mn(III)-pyrophosphate, 10 mM; NO_3^-, 15 mM; NO_2^-, 0.5 mM; colloidal MnO_2, 5 mM; TMAO, 25 mM; DMSO, 10 mM; fumarate, 10 mM; FeOOH 40 mM, Fe(III)-citrate, 50 mM; MnO_2, 10 mM; SO_3^{2-},10 mM; $S_2O_3^{2-}$,10 mM. In the kinetics study, the point mutant strain, Mn3, was incubated in anaerobic liquid cultures supplemented with 18 mM lactate and either 7 mM Mn(IV) oxide or 7 mM Mn(III)-pyrophosphate.

3.2.3. Anaerobic incubations of Mn(IV)/Mn(III) with the wild-type and point mutant strains

Incubations were conducted anaerobically in at least duplicates in 100 ml sealed reactors gently mixed with magnetic stirring bars. In each of the incubations, 1×10^7 cells/ml of *Shewanella oneidensis* MR-1 or its mutant strains (*Sol* d29, *Sol* d64, or Mn3)

were incubated in 50 ml of defined media, 18 mM of lactate as the electron donor, either solid Mn(IV) or colloidal Mn(IV) or soluble Mn(III) as the electron acceptor. Abiotic controls were conducted simultaneously with all incubations. Soluble Fe(III) deficient mutant strains *Sol* d29 and d64 were fed with 7 mM of either colloidal (soluble) or amorphous Mn(IV) oxides under identical conditions to test the reduction capability of these two Sol mutants on different types of Mn(IV) oxides. The point mutant Mn3 were incubated with 7 mM of either amorphous Mn(IV) oxides or soluble Mn(III) pyrophosphate as the sole terminal electron acceptor to study the phenotype of strain Mn3 on Mn reduction. Pyrophosphate (10 mM) was added in a few incubations with *S. oneidensis* MR-1 and mutant strain Mn3 to scavenge Mn(III) (Klewicki and Morgan, 1998) and investigate the production of Mn(III) as an intermediate during the anaerobic Mn(IV) respiration. The procedure of the sampling scheme during the incubations is described in Chapter 4.

3.3. Results and Discussion

3.3.1. Reduction of mutant strains *Sol* d29 and d64 on different types of Mn(IV) oxides

Amorphous Mn(IV) incubations

The microbial reduction of solid (amorphous) Mn(IV) by the wild-type strain of *S. oneidensis* was reproducible among different batches of incubations. In the incubations, reduction of solid Mn(IV) by the wild-type strain represented the normal reduction capacity (Figure 3.1-a). Concentrations of soluble Mn(II) produced in the wild-type incubations increased rapidly during the first 5 days and saturated at around 3.42 ± 0.27

mM, while production of soluble Mn(II) remained below 0.5 mM in the abiotic control (Figure 3.1-a). Concentrations of soluble Mn(II) in the incubations of the two point mutant strains (*Sol* d29 and d64) barely increased during the initial 72 hours, accounting for merely 10.9 ± 2.5% (*Sol* d29) and 7.9 ± 0.3% (*Sol* d64) of the wild-type production at 72 hour of the incubations (Table 3.2). The production of soluble Mn(II) in the two mutant incubations, however, increased significantly after a 72-hour phase lag (compared to the abiotic control), and reduced a maximum of 37.1 ± 8.1 % (*Sol* d29) and 24.3 ± 4.9% (*Sol* d64) of the wild-type Mn(II) production (Figure 3.1-a and Table 3.2). In addition, concentrations of soluble Mn(III) remained at background levels in the two *Sol* mutant incubations (Figure 3.1-a), compared to the significant production of soluble Mn(III) found in the wild-type production (see Chapter 4). These results suggest that the first reduction step of solid Mn(IV) was impaired in the two *Sol* mutant strains.

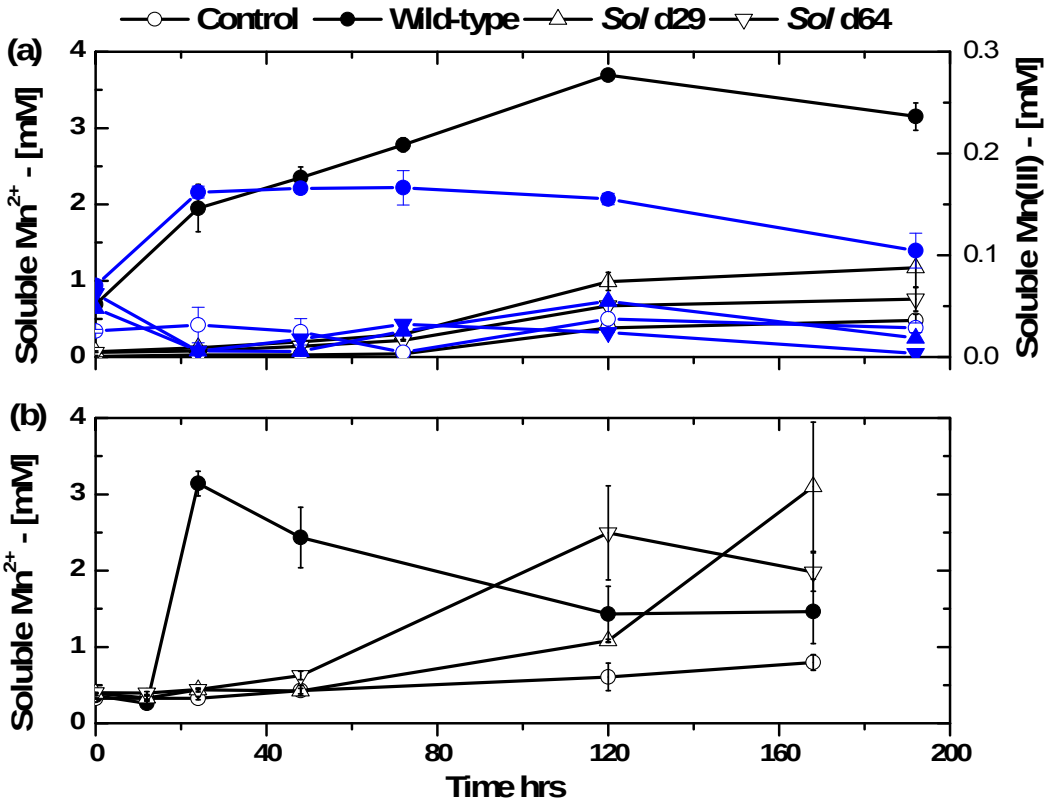

Figure 3.1. Concentration of soluble Mn(II) (black, left y-axis) and Mn(III) (blue, right y-axis) produced as a function of time during the anaerobic incubations of *S. oneidensis* MR-1 (solid circles), point mutant Sol d29 (solid upward triangles), point mutant Sol d64 (solid downward triangles), and the abiotic control (open circles) in the presence of (a) amorphous (solid) Mn(IV) oxides and (b) colloidal (soluble) Mn(IV) oxides as sole terminal electron acceptor. Error bars represent standard deviations from at least duplicates.

The *Sol* mutant strains d29 and d64 were isolated for their inability to produce soluble organic-Fe(III) complexes (Jones et al., 2010) which is proposed to be required for microbial reduction of solid Fe(III) (Jones et al., 2010, Taillefert et al., 2007a). *Sol* d29 presented 35% of the wild-type organic-Fe(III) production rate and 32% of the wild-type Fe(II) production rate during the anaerobic incubations with solid Fe(III) as the

terminal electron acceptor (Jones et al., 2010). Comparatively, the *Sol* mutant d64 was found to be more severely impaired in its ability to produce both organic-Fe(III) complexes (3% of the wild-type rate) and Fe(II) (9% of the wild-type rate) (Jones et al., 2010). These two *Sol* mutants display similar behavior when grown on solid Mn(IV) oxides, as both mutant strains were incapable of producing soluble Mn(III) and *Sol* d64 presented a relatively lower reduction capacity than strain d29 on either Mn(IV) or Fe(III) (Figure 3.1-a and Table 3.2). These findings suggest that the components deleted in these *Sol* mutants may also be required in the microbial reduction of solid Mn(IV). A solublization step may also be able to facilitate the reduction of solid Mn(IV) by either (1) lowering the activation energy of the formation of the intermediate or (2) preventing passivation of the binding sites on solid Mn(IV) surfaces by the strong adsorption of Mn(II) on Mn(IV) oxides (Tebo et al., 2004), or (3) providing a more bioavailable electron acceptor (i.e. soluble Mn(III)) than solid Mn(IV) as proposed for Fe(III) reduction (Taillefert et al., 2007a, Jones et al., 2010). The solubilization step for Mn(IV), however, should be different than the non-reductive Fe(III) dissolution involved in the reduction of solid Fe(III) (Jones et al., 2010) to account for the absence of Mn(IV)-complexing ligand in aqueous and sedimentary environments at circumneutral pH (Morgan, 2000a, Duckworth et al., 2009).

The Mn(IV) reduction capacities of these two *Sol* mutants were similar to those of the in-frame deletion mutant strains *ΔgspD* and *ΔmtrB* (described in Chapter 4), presenting 20.4 ± 3.5% and 37.4 ± 14.5% of the wild-type reduction capacity, respectively, but much lower than those of the OM *c*-type cytochrome mutant strains *Δmtrc*, *ΔomcA* and *ΔomcAmtrC* (Table 3.2). The findings suggest that the missing

components in these two *Sol* mutants may play more essential roles than MtrC and OmcA in the reduction of solid Mn(IV).

Table 3.2. Relative production of Mn(II) by different mutant strains of *S. oneidensis* MR-1, normalized to the corresponding wild-type production during incubations with either soluble (colloidal) Mn(IV) oxides, solid (amorphous) Mn(IV) oxides, or soluble Mn(III) as terminal electron acceptor. For the microbial reduction of solid Mn(IV), the extent of Mn(II) production was provided for both the initial 72 hrs of incubations and the entire incubations to account for the phase lag observed with some of the mutant strains. Errors represent standard deviations of at least duplicate culture incubations.

S.*oneidensis* strains	**soluble Mn(IV) reduction**	**solid Mn(IV) reduction**		**Mn(III) reduction**
		72 hrs	Final	
***Sol* d29**	98.7 ± 27.0 %	10.9 ± 2.5%	37.1 ± 8.1 %	-
***Sol* d64**	79.5 ± 19.6 %	7.9 ± 0.3%	24.3 ± 4.9%	-
Mn3	-	10.1 ± 2.2%	17.3 ± 2.9%	11.8 ± 1.4%
T121	-	3.5 ± 1.0%	4.5 ± 0.6%	-
Δ*mtrB*	-	30.0 ± 15.0%	37.4 ± 14.5%	44.3 ± 0.2%
Δ*gspD*	-	19.9 ± 10.4%	20.4 ± 3.5%	20.3 ± 4.4%
Δ*omcA*	-	100.1 ± 19.3%	88.3 ± 23.7%	99.0 ± 1.0%
Δ*mtrC*	-	85.7 ± 8.9%	92.6 ±9.1%	59.4 ± 0.9%
Δ*omcAmtrC*	-	35.1 ± 15.3%	74.5 ± 21.5%	74.1 ± 0.6%

Colloidal Mn(IV) incubations

Due to the lack of soluble Mn(IV) complexes in circumneutral environments (Morgan, 2000a), colloidal Mn(IV) oxides with particle diameters in the range of 89-193 nm (Perez-Benito et al., 1996) were generally considered to represent the stable soluble phases of Mn(IV) at neutral pH (Perezbenito and Arias, 1992). Otherwise identical incubations of the mutant strains *Sol* d29 and d64 fed with colloidal Mn(IV) oxides were conducted to compare the reduction behavior of these two mutant strains on different

types of Mn(IV) oxides (Figure 3.1-b). Reduction of colloidal Mn(IV) oxides by the wild-type was completed more rapidly (in 36 hrs) than that of solid MnO_2 while the production of Mn(II) in the abiotic control incubations was maintained at low levels (Supplementary Figure A.1). Concentration of soluble Mn(II) produced by the wild-type strain decreased after 36 hrs, which may be due to the secondary precipitation of Mn(II) with inorganic carbonate produced during the respiration of organic carbon (Chapter 4). In the two *Sol* incubations, the reduction of colloidal MnO_2 was initially blocked during the first 48 hours, as observed in the amorphous MnO_2 incubations (Figure 3.1-a), and this phase lag was shorter with strain *Sol* d64 than with strain *Sol* d29 (Figure 3.1-b). Reduction of colloidal MnO_2 by the two mutant strains, however, increased significantly after the phase lag and was completed in 172 hrs, with a maximum Mn(II) production as high as 98.7 ± 27.0 % (*Sol* d29) and 79.5 ± 19.6 % (*Sol* d64) of the wild-type level (Figure 3.1-b and Table 3.2), while the reduction rates of colloidal MnO_2 by these two *Sol* mutants remained low, accounting merely c.a. 40% (*Sol* d64) and 20% (*Sol* d29) of the wild-type reduction rate (Figure 3.1-b). These findings suggest that the reduction of colloidal MnO_2 may also require an initial solubilization step. Finally, the significant phase lags observed in the *Sol* incubations (Table 3.2) suggest that the mutant strains may either be able to repair themselves on the Mn(IV) reduction capability of Mn(IV) or to switch to an alternative electron transfer strategies (DiChristina et al., 2005).

Gene complementation of these two *Sol* strains has revealed that a single gene was missing in each of the *Sol* d29 and *Sol* d64 mutant strains and that *Sol* d29 lacks gene *gspG* while *Sol* d64 lacks gene *gspE* (Fennessey et al., in prep). Both of the genes encode one of the components of the Type II secretion system (protein GspG or GspE).

Therefore, the Type II secretion system may be involved in the extracellular translocation of not only the potential terminal reductases (OmcA or MtrC) (Shi et al., 2008) but also the protein components involved in the production of Fe(III)-solubilizing ligands and the reductase for reductive solubilization of Mn(IV).

3.3.2. The novel point mutant strain *Mn3* reduces Mn(IV) to Mn(III) only

Reduction of Mn(IV) may proceed either through a one-electron transfer via Mn(III) as the intermediate or through a direct two-electron transfer to Mn(II), depending on the availability of a single or two electrons from the reductant (Luther, 2005). Production of soluble Mn(III) as a transition intermediate during the incubations fed with Mn(IV) oxides demonstrated that Mn(IV) is reduced by two consecutive steps of one-electron transfer (Chapter 4 and Figure 3.1-a). To confirm these two consecutive steps of microbial Mn(IV) reduction, a point mutant strain Mn3 generated via chemical mutagenesis was identified for its deficiency in reducing soluble Mn(III) (Figure 4.1).

Overall anaerobic respiratory capability of Mn(III) reduction-deficient mutant strains Mn3.

Mutant strain Mn3 was able to reduce a wide range of soluble electron acceptors at wild-type rates, including O_2, NO_3^-, NO_2^-, colloidal MnO_2, TMAO, Fe(III)-citrate, SO_3^{2-}, and $S_2O_3^{2-}$, yet was unable to grow on soluble Mn(III), DMSO, fumarate, and FeOOH (Table 3.3). The phenotype of stain Mn3 was different than that of the *Sol* mutant strains d29 and d64, which were unable to reduce both soluble and solid Fe(III) (Jones et al., 2010) and both colloidal and amorphous Mn(IV) oxides (Figure 3.1 and Table 3.3). The different reduction capability of strain Mn3 with different electron

acceptors did not exactly follow the predictions based on the reduction potential of the different electron acceptors (Dale et al., 2007). For example, the reduction potentials of soluble Mn(III) and DMSO are higher than that of TMAO, while Mn3 retained its ability to reduce TMAO (Table 3.3). Interestingly, the reduction capabilities of strain Mn3 on different species of Mn and Fe were different: Mn3 was able to reduce soluble Fe(III) and solid Mn(IV) but not solid Fe(III) and soluble Mn(III) (Table 3.3). Although similar electron transfer strategies were proposed for the reduction of solid Mn(IV) and Fe(III) (Myers and Myers, 2000, Newman and Kolter, 2000, Bretschger et al., 2007, Shi et al., 2007), the phenotype of the mutant strain Mn3 suggests that the component deleted in Mn3 is involved in the reduction of soluble Mn(III) but not soluble Fe(III). These findings confirm that the electron transport pathway of *S. oneidensis* MR-1 during the anaerobic respiration of Mn(IV) and Fe(III) oxides are not identical.

Table 3.3. Overall anaerobic respiratory capability of Mn(III) reduction-deficient mutant strain *Mn3* compared with *S. oneidensis* MR-1. Concentrations of the electron acceptors are: Mn(III)-pyrophosphate, 10 mM; NO_3^-, 15 mM; NO_2^-, 0.5 mM; colloidal MnO_2, 5 mM; TMAO, 25 mM; DMSO, 10 mM; fumarate, 10 mM; FeOOH 40 mM, Fe(III)-citrate, 50 mM; SO_3^{2-},10 mM; and $S_2O_3^{2-}$,10 mM.

Strains	O_2	MnO_2	Mn(III)-pp	NO_3^-	Fe-cit	NO_2^-	DMSO	TMAO	Fumarate	SO_3^{2-}	FeOOH	$S_2O_3^{2-}$
MR-1	+	+	+	+	+	+	+	+	+	+	+	+
Mn3	+	+	-	+	+	+	-	+	-	+	-	+

Kinetic studies of the reduction of soluble Mn(III) complexes and solid Mn(IV) oxides by mutant strain *Mn3*.

In the incubations fed with soluble Mn(III)-pyrophosphate complexes, concentrations of Mn(III) decreased from 7.3 mM initially to approximately 0.2 mM in 48 hours due to the rapid respiration of Mn(III) complexes by *S. oneidensis* MR-1 (Kostka et al., 1995) (Figure 3.2), and the Mn(III)-pyrophosphate solution simultaneously turned from pink to colorless (Supplementary Figure A.2). In contrast, soluble Mn(III) concentrations remained relatively constant in the abiotic control reactors and during the incubations of mutant strain Mn3, accounting for merely 11.8 ± 1.4% of the wild-type reduction (Figure 3.2), indicating that pyrophosphate stabilizes Mn(III) without dismutation throughout the incubations and confirming the phenotype of strain *Mn3* (Table 3.3) as a Mn(III) reducing-deficient mutant strain.

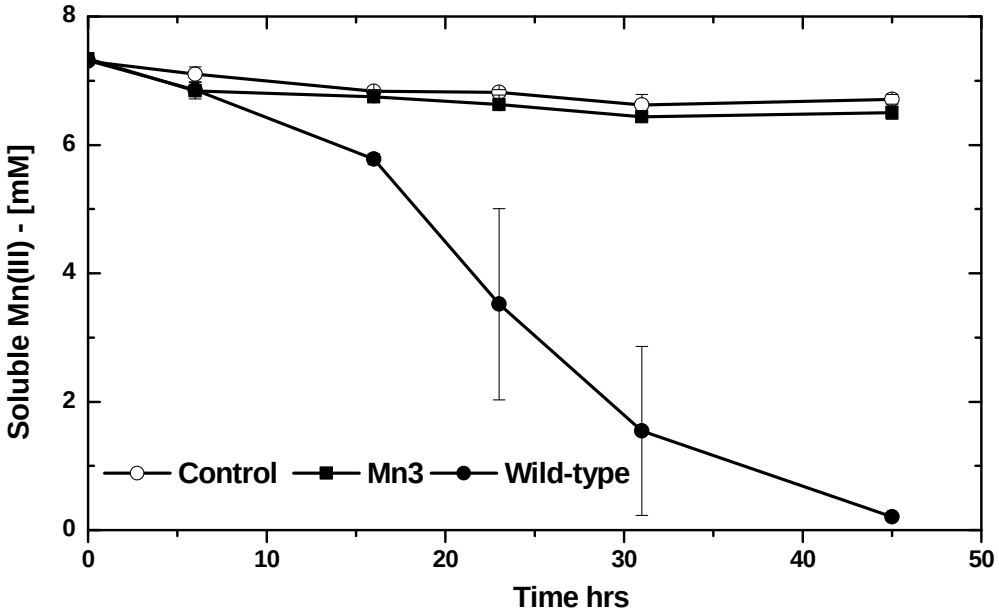

Figure 3.2. Anaerobic respiration of soluble Mn(III)-pyrophosphate by the wild-type strain (solid circles) and mutant strain Mn3 (solid) as a function of time, compared to the chemical control (open circles). Error bars represent standard deviations from at least duplicates.

In the incubations with solid Mn(IV) oxides, reduction of Mn(IV) oxides by the wild-type strain was evidenced by a gradual change from the black color of Mn(IV) oxides to white precipitates in the latter period of the incubation, while the black color remained during the incubations of mutant strain Mn3 (not shown). According to the speciation of Mn, Mn(II) generated during anaerobic respiration of Mn(IV) oxides existed in three phases, including soluble Mn(II), exchangeable Mn(II), and carbonate bound Mn(II) (Figure 3.3). Concentrations of soluble Mn(II) in the presence of the wild-type strain increased rapidly and saturated around 3.4 mM (ca. 45% of total Mn), while concentrations of soluble Mn(II) remained low (< 0.3 mM) in the abiotic controls (Figure 3.3-a). Similarly, little exchangeable Mn(II) was extracted in the control reactor

throughout the incubations (Figure 3.3-b), but concentrations of the exchangeable Mn(II) in the wild-type incubations increased as a function of time during the first 48 hrs and stabilized at relatively low concentrations (i.e., 0.3 mM), constituting approximately 4% of total Mn at the end of the incubations. In parallel to the production of soluble Mn(II), concentrations of Mn(II) bound to carbonate increased significantly in the presence of the wild-type strain and reached as much as 3 mM at the end of the incubation, compared to the abiotic control which formed negligible concentrations of $MnCO_3$ (Figure 3.3-c). Concentrations of both soluble Mn(II) and solid extracted Mn(II) in incubations with the point mutant strain Mn3 increased at much slower rate (compared to the wild-type incubations) (Figure 3.3). The maximum total Mn(II) production by strain Mn3 accounted for merely 17.3 ± 2.9% of the wild type production (Table 3.2), including 11.1% in solution, 1.3% adsorbed onto solid surface, and 3.6% precipitated as Mn(II) carbonate of the corresponding wild-type production (Figure 3.3-a, b, and c). The production of Mn(II) in both soluble and solid phase was severely impaired during the reduction of solid Mn(IV) by strain Mn3.

Although the deletion of genes involved in the reduction of Mn(III) significantly impaired the capability of mutant strain Mn3 to produce Mn(II) during the reduction of solid Mn(IV) (Figure 3.3), Mn3 retains the ability to produce Mn(III) at the same rate as the wild type (Figure 3.4-a), suggesting that the first step of Mn(IV) reduction to Mn(III) was not inhibited in this mutant strain (compared to the significant inhibition of Mn(II) production in Mn3).

As Mn(III) is able to dismutate rapidly (Davison, 1993), the ligand pyrophosphate, which forms stable complexes with Mn(III) (Kostka et al., 1995), was added to the

incubations fed with Mn(IV) oxides to investigate its effect on Mn(III) accumulation during microbial reduction of solid Mn(IV). Concentrations of Mn(III) remained at baseline level throughout the incubations with the wild-type in the presence 10 mM pyrophosphate (Figure 3.4-b), compared to significant Mn(III) accumulation in the wild-type incubations without pyrophosphate (Figure 3.4-a). In contrast, concentrations of Mn(III) increased to as much as 0.3 mM when incubating mutant strain *Mn3* on solid Mn(IV) in the presence of pyrophosphate (Figure 3.4-b), or approximately 50% higher than that in the Mn3 incubations without pyrophosphate (Figure 3.4-a and b). The increase in the rate of reduction of Mn(III) by the wild-type in the presence of pyrophosphate was shown previously (Kotska et al., 1995) and indicates that the complexation of Mn(III) by pyrophosphate does not empede electron transfer from the terminal reductase. These findings suggest that the terminal reductase is designed to handle stable Mn(III) complexes that could be produced by the enzymatic reductive dissolution of Mn(IV) in the presence of organic chelators. In turn, the increase production of Mn(III) by mutant strain Mn3 in the presence of high concentration of pyrophosphate is attributed to the impaired capability of Mn3 to reduce Mn(III) coupled with the ability of pyrophosphate to prevent dismutation of Mn(III) (Figure 3.4). Overall, these results demonstrate the unique phenotype of this point mutant strain Mn3 that reduces Mn(IV) half-way to Mn(III) but not to Mn(II). This phenotype confirms that the anaerobic respiration of Mn(IV) proceeds through two steps of one electron transfer and suggests that the two steps may be carried on via different electron transfer pathways.

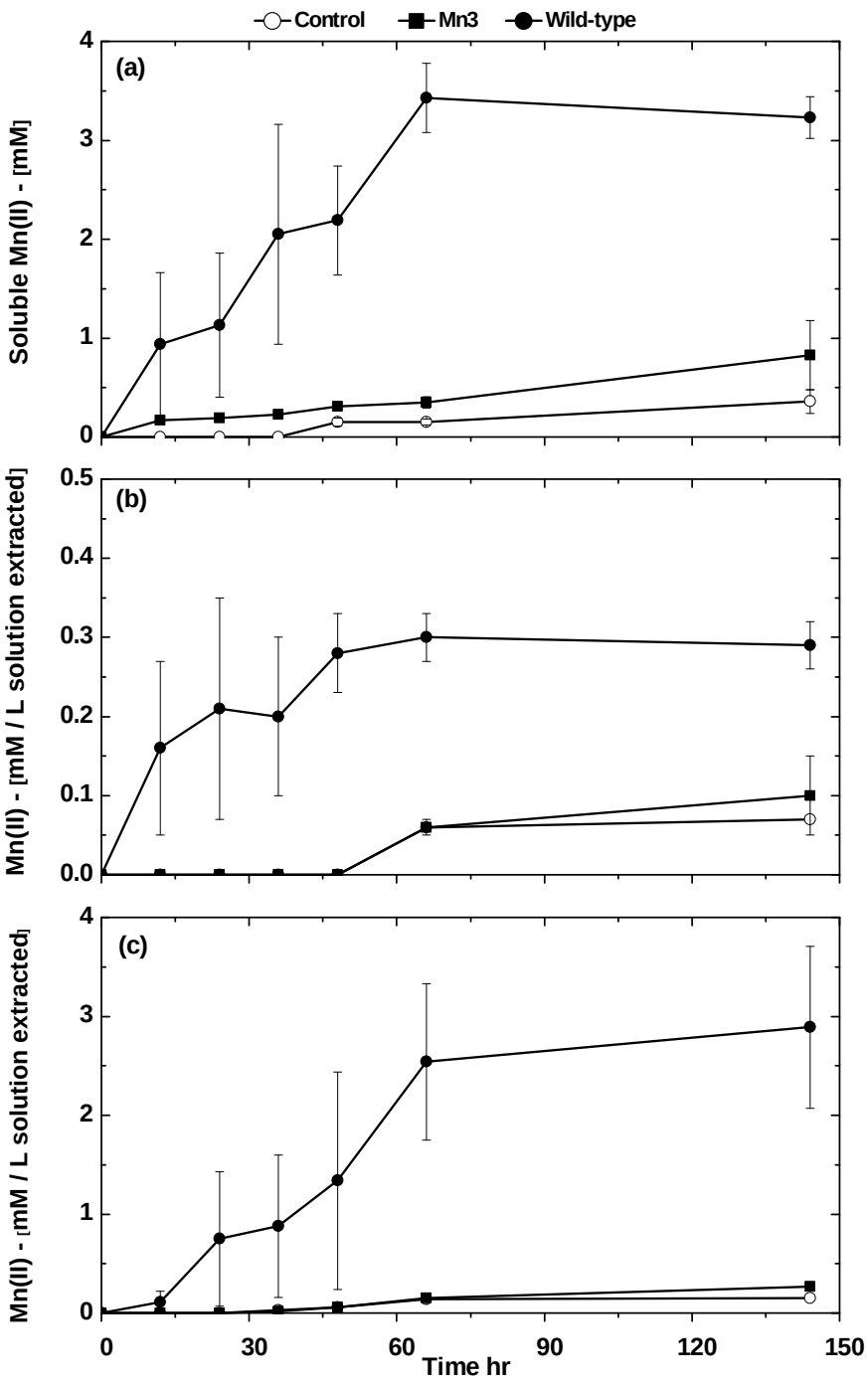

Figure 3.3. The concentration of Mn(II) produced as a function of time during anaerobic respiration of solid Mn(IV) by the wild-type strain of *S. oneidensis* MR-1 (solid circles) and point mutant strain Mn3 (solid squares), compared to the chemical control (open circles). (a) Soluble Mn(II) concentrations (mM) in different batch reactors. (b) Concentrations of exchangeable Mn(II) extracted with 0.5 M MgCl from the solid phase. (c) Concentrations of Mn(II) extracted from the residual solid with 0.1 M NaOAc. Error bars represent standard deviations from at least duplicates.

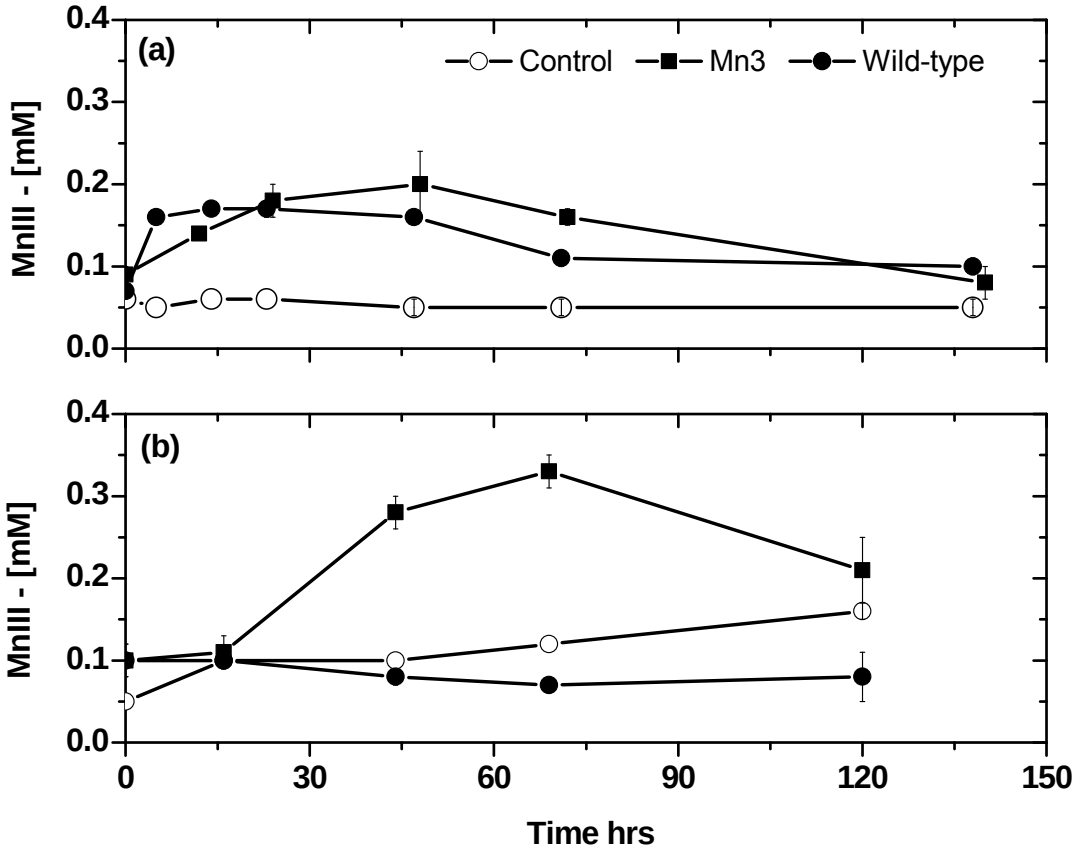

Figure 3.4. Concentrations of Mn(III) produced as a function of time during anaerobic respiration of solid Mn(IV) by the wild-type strain of *S. oneidensis* MR-1 (solid circles) and point mutant strain Mn3 (solid squares) compared to the chemical controls (open circles), in the presence (a) or without (b) 10 mM of pyrophosphate. Error bars represent standard deviations from at least duplicates.

3.4 Conclusions

In summary, a novel point mutant strain Mn3 generated via random chemical mutagenesis presents a unique phenotype that only reduces Mn(IV) to Mn(III) but not Mn(III) to Mn(II). These findings indicate that microbial reduction of Mn(IV) oxides by *Shewanella oneidensis* MR-1 proceeds via two consecutive steps of one-electron transfer with Mn(III) production as intermediate. Interestingly, the stabilization of Mn(III) by the addition of a redox inactive Mn(III)-complexing ligand in the presence of strain Mn3 and the accelerated Mn(III) reduction of the same complex by the wild-type strain suggest that a possible endogenic ligand is involved in the process to prevent dismutation of Mn(III). The mutant strains *Sol* d29 and d64, involved in the non-reductive solubilization of Fe(III) oxides by *Shewanella*, did not produce Mn(III) intermediates in the reduction of Mn(IV) oxides, suggesting that an enzymatic solubilization strategy requiring the Sol system may also be involved to respire Mn(IV) oxides. Due to the paucity of Mn(IV)-stabilizing ligands in natural environments, the anaerobic respiration of Mn(IV) oxides may require a reductive dissolution of Mn(IV) oxides to Mn(III) as alternative strategy to the non-reductive dissolution mechanism involved with solid Fe(III) oxides. We therefore propose that *S. oneidensis* may first reductively dissolve solid Mn(IV) to the more bioavailable soluble Mn(III), which can then be rapidly respired. The prevalent activity of microbial Mn(IV) reduction in oxygen depleted environments may provide an alternative natural source of Mn(III) in suboxic sediments. The genetic identification and nucleotide sequence analyses of the Mn(III) reduction-deficient mutant strain Mn3 are currently ongoing to characterize the biochemical mechanism involved in the reduction of Mn(III).

CHAPTER 4 MICROBIAL MN(IV) REDUCTION REQUIRES AN INITIAL ONE-ELECTRON REDUCTIVE DISSOLUTION STEP

Reproduced in part from Lin, H.; Szeinbaum, N.H.; DiChristina, T.J.; Taillefert, M. Microbial Mn(IV) reduction requires an initial one-electron reductive dissolution step. Submitted to Geochimica et Cosmochimica Acta.

Abstract

Mn(IV) and Mn(II) are the most stable and prevalent forms of manganese in natural environments. The occurrence of Mn(III) in minerals and the detection of soluble Mn(III) in natural waters, however, suggest that Mn(III) is an intermediate in both the oxidation of Mn(II) and the reduction of Mn(IV). Mn(III) has recently been proposed as an intermediate during the oxidation of Mn(II) by Mn-oxidizing bacteria but has never been considered as an intermediate during the bio-reduction of Mn(IV). Here we show for the first time that microbial Mn(IV) reduction proceeds step-wise via two successive one-electron transfer reactions with production of soluble Mn(III) as transient intermediate. Mutagenesis studies demonstrate that the reduction of both solid Mn(IV) and soluble Mn(III) occurs at the outer membrane of the cell. In addition, kinetic analysis indicates that Mn(IV) respiration involves only one of the two potential terminal reductases (c-type cytochrome MtrC and OmcA) involved in Fe(III) respiration. More importantly, only the second electron transfer step is coupled to production of dissolved inorganic carbon, suggesting that the first electron transfer reaction is a reductive solubilization step that increases Mn bioavailability. These findings oppose the long-standing paradigm that microbial Mn(IV) reduction proceeds via a single two-electron transfer reaction coupled to organic carbon oxidation, and suggest that diagenetic models should be revised to correctly account for the impact of manganese reduction in the global carbon cycle.

4.1 Introduction

Manganese is the third most abundant transition metal in the Earth's crust and plays an essential role in the biogeochemical cycling of carbon, nitrogen, phosphorus, and other metals (Neretin et al., 2003, Luther et al., 1997, White et al., 2008, Tebo et al., 2004). Manganese is primarily present under the three oxidation states +II, +III, and +IV in natural systems (Cotton et al., 1999). Manganese (IV) produced by Mn(II) oxidation generally exists as highly insoluble oxides at circum-neutral pH and constitutes a considerable fraction of soils and sediments (Davison, 1993). Soluble forms of Mn(IV), noted as colloidal Mn, are generally formed as products in permanganate reactions in aqueous solutions at circum-neutral pH (Perezbenito et al., 1987). Due to its larger specific surface than amorphous MnO_2 (water-insoluble forms), colloidal MnO_2 (or water-soluble form of Mn oxides) was thought to be more active in catalytic and oxidizing activities (Perezbenito et al., 1987, Perezbenito and Arias, 1992, Perez-Benito, 2002).

Mn(II) is thermodynamically more stable under anoxic conditions, usually as free hydrated cation (Mn^{2+}) or as insoluble phosphate or carbonate minerals (Tebo et al., 2004, Otero et al., 2009). Mn(IV) is reduced to Mn(II) in anaerobic conditions either chemically by Fe(II) and sulfide (Villinski et al., 2003, Yao and Millero, 1993) or biologically by dissimilatory reducing microorganisms at circumneutral pH (Myers and Nealson, 1988). Soluble Mn(III) is proposed to be produced as intermediate during the chemical and photochemical reduction of Mn(IV) (Perez-Benito, 2002, Ruppel et al., 2001) and during the aerobic oxidation of Mn(II) by spores of the marine *Bacillus* sp. Strain SG-1 and

newly isolated Mn(II)-oxidizing strains *Aurantimonas manganoxydans*, sp. nov. and *Aurantimonaas litoralis*, sp. nov. (Anderson et al., 2009, Webb et al., 2005).

Solid Mn(III) oxides (MnOOH or Mn_3O_4), produced as metastable products due to kinetic limitations, also exist as common forms of Mn oxides in natural aqueous environments (Davison, 1993). Soluble Mn(III) rapidly disproportionates to yield Mn(II) and Mn(IV) under acidic conditions or precipitates as Mn(III) oxides in basic environments (Davison, 1993). Soluble Mn(III), however, can be stabilized in soluble phases in the presence of certain inorganic or organic ligands, such as pyrophosphate (Kostka et al., 1995), citrate (Klewicki and Morgan, 1998), hydroxycarboxylic acid (Heintze and Mann, 1947), and siderophores (Parker et al., 2004, Duckworth and Sposito, 2005a). Due to its extreme reactivity and the lack of appropriate analytical techniques, soluble Mn(III) was only recently discovered in low concentrations in natural aquatic systems in the suboxic zone of the Black Sea (Trouwborst et al., 2006). The existence of soluble Mn(III) in these conditions suggests that microbial Mn(IV) reduction in oxygen-limited environments may be a candidate source of soluble Mn(III).

Microbial Mn(IV) reduction, first demonstrated with *Alteromonas putrefaciens* MR-1 (Myers and Nealson, 1988), is central to the biogeochemical cycling of manganese in aquifers (Coates et al., 1999), redox stratified water columns (Van Cappellen et al., 1998), and fresh water (Krishnan et al., 2009) and marine (Thamdrup, 2000b) sediments, yet the mechanism of dissimilatory Mn(IV) reduction by metal-reducing bacteria remains poorly understood. The ability to reduce Mn(IV) oxides is found in both domains of the prokaryotic world (Lovley et al., 2004b), including metal-reducing members of the genus *Shewanella* which reduce solid Mn(IV) (Myers and Nealson, 1988, Burnes et al., 1998),

soluble Mn(III) (Kostka et al., 1995), and a wide variety of alternate electron acceptors, such as solid and soluble forms of Fe(III) (DiChristina et al., 2005, Hau and Gralnick, 2007).

Fe(III)- and Mn(IV)-reducing gram-negative bacteria are presented with a unique physiological problem at circumneutral pH: they are required to reduce electron acceptors found largely as amorphous or crystalline (oxy)hydroxide particles (Morgan, 2000b) presumably unable to contact inner membrane (IM)-localized electron transport systems. To overcome this problem, metal-reducing bacteria employ a variety of novel electron transport strategies not found in other gram-negative bacteria that reduce soluble electron acceptors (DiChristina et al., 2005, Lovley et al., 2004b), including 1) direct enzymatic reduction of solid metal oxides via metal reductases localized on the outer membrane (OM) or on electro-active appendages (DiChristina et al., 2002, Myers and Myers, 2003a, Gorby et al., 2006, Reguera et al., 2005, Shi et al., 2008), 2) a two-step, solubilization and reduction pathway in which solid metal oxides are first dissolved by organic complexing ligands, followed by uptake and reduction of the soluble organic-metal complexes by periplasmic metal reductases (Jones et al., 2010, Fennessey et al., 2010, Taillefert et al., 2007a), and 3) a two-step, electron shuttling pathway in which exogenous or endogenous electron shuttling compounds are first enzymatically reduced and then chemically oxidized by the solid metal oxides in a second (abiotic) electron transfer reaction (Newman and Kolter, 2000, Lovley and Woodward, 1996, Marsili et al., 2008).

The mechanism of microbial Mn(IV) reduction is generally described as a single two-electron transfer reaction producing Mn(II) as end-product (Thamdrup, 2000a, Lovley et al., 2004a). According to the molecular orbital theory, two steps of one-

electron transfer during the reduction of Mn(IV) to Mn(II) may proceed by the addition of the first electron to one of the two empty e_g orbitals of Mn(IV) and the rearrangement of the orbitals to form Mn(III) intermediates (Luther, 2005). Indeed, chemical reduction of MnO_2 by Mn(II) under highly acidic conditions (Perez-Benito, 2002) or by some organic reductants (e.g. oxalate and pyruvate) at neutral pH (Stone, 1987a) and electrochemical reduction of MnO_2 (Ruppel et al., 2001) have been proposed to follow the one-electron transfer pathway with production of Mn(III) intermediates. In the present study, we demonstrate that the gram-negative, metal-reducing bacterium *S. oneidensis* MR-1 reduces Mn(IV) to Mn(II) step-wise via two successive one-electron transfer reactions with Mn(III) as transient intermediate. The Mn(IV) reduction pathway of *S. oneidensis* therefore appears to be a reversal of the Mn(II) oxidation pathways of a *Bacillus* species and two recently isolated alphaproteobacteria which oxidize Mn(II) to Mn(IV) step-wise via two successive one-electron transfer reactions also with Mn(III) as transient intermediate (Webb et al., 2005, Anderson et al., 2009).

4.2. Material and experimental Design

4.2.1. Materials

All glassware and plasticware were soaked in 10% nitric acid overnight and washed with sterile DI water prior to use. The reactors were autoclaved before incubations. All solutions were prepared with ACS or trace metal grade chemicals in 18 MΩ-de-DI (Barnstedt). Amorphous Mn(IV) oxides were synthesized using the permanganate oxidation method (Murray, 1974), modified to maintain sterile conditions (Lovley and Phillips, 1988). A 0.30 M of Mn(II) solution was slowly dripped (~ 2 drips/sec) into an autoclaved bottle containing a 0.2 M $KMnO_4$ solution to form black MnO_2 particles. The

protons produced during the reaction were neutralized by NaOH (10 N) to maintain a pH of 10. After completion of the reaction, the synthesized particles were washed three times with $MgCl_2$ (0.1M) and de-ionized water, to remove the excess Mn^{2+}, and dried at 40°C for 3-5 days. The synthesized Mn oxides contained 7.30 ± 0.06 mmol Mn g^{-1} solid, measured by graphite furnace atomic adsorption spectrometry (GFAAS). The stoichiometry of the synthesized Mn oxides was determined to be $MnO_{1.98}$, according to a modified Winkler titration method used to calculate the oxidation states of metal oxides (Murray et al., 1984, Murray, 1974). Soluble Mn(III) was prepared by dissolving Mn(III) acetate dihydrate (Alfa Aesar) in a defined medium with sodium pyrophosphate (Sigma Aldrich) in a molar ratio of one Mn(III) to four pyrophosphate. The solution was then filtered through a 0.2 μm polycarbonate filter.

4.2.2 Bacterial strains and growth media

Shewanella oneidensis strain MR-1 was originally isolated from Oneida Lake, NY (Myers and Nealson, 1988). The *S. oneidensis* strains used in the present study included the wild-type strain (displaying normal Mn(IV) and Mn(III) reduction activities), point mutant strain Mn3, and a set of in-frame deletion mutant strains (Δ*gspD*, Δ*mtrB*, Δ*mtrC*, *ΔomcA*, Δ*omcAmtrC* (Table 4.1). *S. oneidensis* Δ*gspD* and Δ*mtrB* mutants are severely impaired in the ability to reduce Mn(IV) oxides, Fe(III) oxides (Beliaev and Saffarini, 1998, DiChristina et al., 2002, Shi et al., 2008) and Mn(III) (from results of the present study). *gspD* encodes an outer membrane porin required for secretion of the decaheme *c*-type cytochromes MtrC and OmcA to the cell surface (DiChristina et al., 2002, Shi et al., 2008), while *mtrB* encodes an outer membrane β-barrel protein that is postulated to anchor MtrC and OmcA on the cell surface (Beliaev and Saffarini, 1998)

where they are involved in electron transfer to external Mn(IV) and Fe(III) oxides (Hartshorne et al., 2009). The Mn3 point mutant was recently identified in a genetic screen of chemically-mutagenized *S. oneidensis* strains selected for their inability to reduce Mn(III) (Figure 4.1).

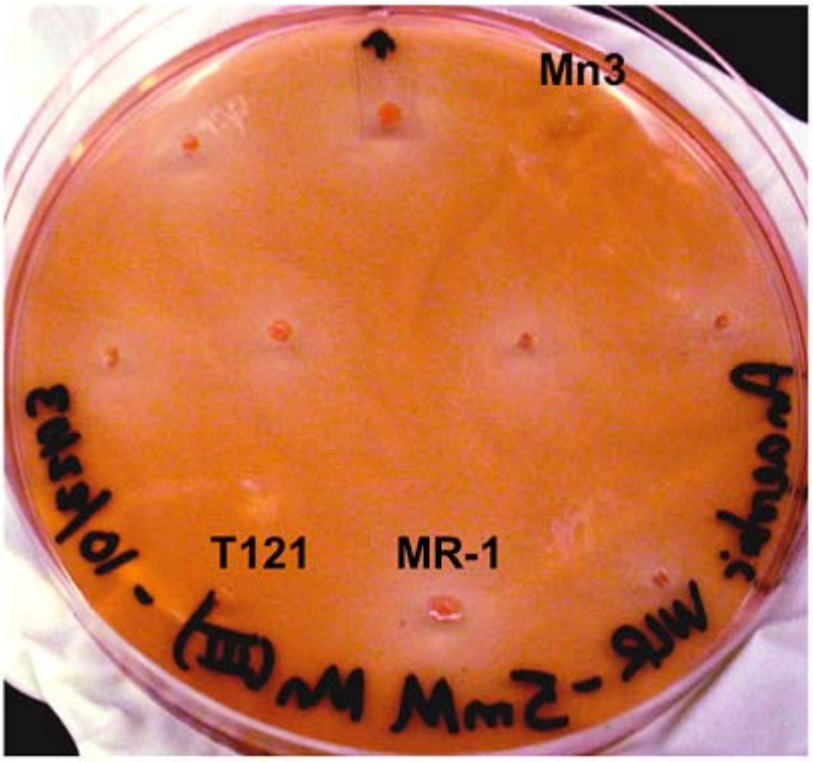

Figure 4.1. Identification of mutant strain Mn3 by Mn(III) reduction-deficient mutant screening (located at row 1, column 3). Wild-type strain MR-1 [row 3, column 2] and a previously isolated anaerobic respiratory mutant strain T121 (DiChristina et al., 2002, Burnes et al., 1998) [row 3, column 1] were included as Mn(III) reduction-positive and Mn(III) reduction-negative control strains, respectively. Note the clearing zone (indicative of wild-type Mn(III) reduction activity) in the colony periphery of all strains except Mn(III) reduction-deficient mutant strain Mn3 and anaerobic respiratory mutant strain T121.

All strains were grown at 30˚C in a defined salt medium (SM) (Myers and Nealson, 1988) supplemented with 18 mM lactate as carbon/energy source. For SM solid medium, Bacto agar was added at 1.5% (w/v).

Construction of markerless, in-frame gene deletion mutants of *S. oneidensis*. Targeted *S. oneidensis* genes (listed in Table 4.1) were deleted from the *S. oneidensis* genome via application of a newly constructed gene deletion system (Burns and DiChristina, 2009). Briefly, regions corresponding to ~750 bp upstream and downstream of each open reading frame (ORF) were independently PCR-amplified and subsequently joined using overlap-extension PCR. The resulting fragment was cloned into suicide vector pKO2.0 (which does not replicate in *S. oneidensis*) and the construct was mobilized into wild-type *S. oneidensis* via conjugal transfer from *E. coli* donor strain β2155 λ pir. *S. oneidensis* strains with the plasmid integrated into the genome were selected on solid LB medium containing gentamycin (15 μg mL^{-1}). Single integrations were verified via PCR with primers flanking the recombination region. Plasmids were resolved from the genomes of single integrants by plating on solid LB medium containing sucrose (10% w/v) with NaCl omitted. In-frame deletions were verified by PCR and direct DNA sequencing (University of Nevada, Reno Genomics Center). Details on primers used in mutant construction and DNA sequencing are found in the references listed in Table 4.1. Each gene deletion mutant was subsequently tested for Mn(IV) reduction, Mn(III) reduction, and DIC production activities in anaerobic liquid cultures supplemented with 18 mM lactate and either 7 mM Mn(IV) oxide or 7 mM Mn(III)-pyrophosphate.

Table 4.1. Description of strains of *Shewanella oneidensis* MR-1 used in current incubations, including wild-type *S. oneidensis* MR-1, Δ*mtrB*, Δ*mtrC*, Δ*omcA*, Δ*omcAmtrC*, Δ*gspD*, and Mn3 mutant.

Strain	Features	Source
Shewanella oneidensis		
MR-1	Wild-type strain	ATCC
Δ*mtrB*	in-frame *mtrB* gene deletion mutant	(Burns, 2010, Burns and Dichristina, 2011)
Δ*mtrC*	in-frame *mtrC* gene deletion mutant	(Burns, 2010, Wee et al., 2012)
Δ*omcA*	in-frame *omcA* deletion mutant	(Burns, 2010, Wee et al., 2012)
Δ*omcAmtrC*	in-frame *omcAmtrC* double deletion mutant	(Burns, 2010, Wee et al., 2012)
Mn3	Deficient in reduction of soluble Mn(III)	Current study

Isolation of Mn(III) reduction-deficient mutant strains (Mn3) of *S. oneidensis*.

Ethyl methane sulfonate (EMS) was used as a chemical mutagen following previously described procedures (Burnes et al., 1998, DiChristina et al., 2002). Liquid cultures of wild-type *S. oneidensis* were grown in SM medium to late exponential phase ($2x10^9$ cells mL^{-1}), harvested by centrifugation at 10,000 xg (4˚C), washed twice, and resuspended in fresh SM medium. EMS was added (19 mg/mL) and the cell suspension was incubated 45 min to achieve 90% kill. The surviving EMS-treated cells were plated on SM agar and the colonies were subsequently subjected to a mutant screening technique to detect loss of Mn(III) reduction activity. Approximately 5,000 EMS-treated colonies were transferred to SM agar medium supplemented with 18 mM lactate as electron donor and 5 mM Mn(III)-pyrophosphate as electron acceptor (which imparts a distinctive pink color to the agar medium; Figure 4.1). After 48 hours of incubation in a Coy anaerobic chamber (atmosphere of 5% CO_2, 10% H_2, 85% N_2), wild-type colonies produced a distinctive clearing zone in their colony peripherey (an indication that pink-

colored Mn(III)-pyrophosphate had been reduced to colorless Mn(II) end-products), while five putative Mn(III) reduction-deficient mutants were identified by their inability to produce a clearing zone (Figure 4.1). One of the five putative Mn(III) reduction-deficient mutants (desgnated strain Mn3) was selected and subsequently tested for Mn(IV) reduction, Mn(III) reduction, and DIC production activities in anaerobic liquid cultures supplemented with 18 mM lactate and either 7 mM Mn(IV) oxide or 7 mM Mn(III)-pyrophosphate.

4.2.3 Anaerobic incubations of *S. oneidensis* wild-type and mutant strains with Mn(IV) oxide or Mn(III)-pyrophosphate as electron acceptor.

Duplicate liquid cultures were incubated anaerobically in 100 ml sealed reactors gently mixed with magnetic stirring bars. Each incubation contained 1×10^7 cells/ml of *Shewanella oneidensis* wild-type or mutant strains incubated in 50 ml of SM medium with 18 mM lactate as electron donor and either 7 mM Mn(IV) oxide or 7 mM soluble Mn(III)-pyrophosphate as electron acceptor. Duplicate abiotic (purely chemical) control incubations were conducted simultaneously with all biotic incubations.

Duplicate liquid cultures were incubated anaerobically in sealed reactors gently mixed with magnetic stirring bars. Each incubation contained 1×10^7 cells/ml of *Shewanella oneidensis* wild-type or mutant strains incubated in 50 ml of SM medium with 18 mM lactate as electron donor. Either 7 mM Mn(IV) oxide (colloidal or amorphous) or 7 mM soluble Mn(III)-pyrophosphate was added into the reactor as sole terminal electron acceptor. Duplicate abiotic (purely chemical) control incubations were conducted simultaneously with all biotic incubations.

4.2.4. Sampling and chemical analyses

At each time point, a 2-ml aliquot was sampled with a sterile needle syringe from each batch reactor. 100 µl of unfiltered subsample was used to measure pH (MI-414 combination pH microelectrode, Microelectrodes, Inc. and SB301 SympHony pH meter, VWR Scientific). Another 1.5 ml subsample was filtered onto a 0.2 µm polyethersulfone membrane (Whatman) and divided into three aliquots to measure dissolved inorganic carbon (DIC), soluble Mn(II), and soluble Mn(III). In addition, concentrations of organic acids (lactate, pyruvate, and acetate) were measured in the wild-type incubations (lactate as the carbon source) to demonstrate the coupling of DIC production with carbon respiration. The precipitate on the filter membrane was digested sequentially, first by a 0.5 M $MgCl_2$ solution to extract exchangeable Mn^{2+} ions adsorbed onto the solid surfaces, then by a 0.1 M NaOAc-HOAc solution (pH 5) for Mn species bound to carbonate (Tessier et al., 1979). Each extraction was conducted in duplicate. Mn(II) concentrations in all sequential extractions were normalized to the volume of filtered solution to convert to concentration.

Total DIC was measured by a flow injection analysis system with conductivity detection (Hall and Aller, 1992) coupled to an Analytical Instruments System, Inc. (AIS, Inc.) LCC-100 integrator. Mn(II) concentrations in both the solution and solid extracts were determined by cathodic square wave voltammetry with a hanging mercury drop electrode (V663, Metrohm, Inc.) using an AIS, Inc. Model DLK-60 potentiostat. Square wave voltammetry parameters included a conditioning step for 10 sec at -0.1 V, a scan rate of 200 mV/s from -0.1 to -1.8 V, and a pulse height of 0.05 V. Voltammograms were integrated using the semi-automatic integration program VOLTINT in Matlab (Bristow

and Taillefert, 2008). Mn(III) concentrations were monitored spectrophotometrically at 480 nm (Milton Roy spectronic 501) in the presence of pyrophosphate (Kostka et al., 1995). Total Mn concentrations were measured by Graphite Furnace Atomic Absorption Spectrometry (GFAAS) with a pyrolytic-coated partitioned graphite tube (CPI international). Lactate, pyruvate, and acetate concentrations were measured by ion chromatography equipped with a Dionex IonPac® ICE-AS6 ion-exclusion column, Anion-ICE MicroMembrane Suppressor II, and CDM-2 conductivity detector. A solution of 0.4 mM heptafluorobutyric acid was used as the eluent at a flow rate of 1.0 ml/min; while the regenerant was made of a 5 mN tetrabutylammonium hydroxide solution at a flow rate of 3.0 ml/min.

4.2.5. Calculation of pseudo-first order reduction rate constants

Mn(IV) and Mn(III) reduction rates depend on pH, cell density, and concentrations of electron donor and acceptor (Dollhopf et al., 2000), and can be written as Eq. 4.1,

$$\frac{d[Mn_{IV/III}]}{dt} = -k[H^+]^a[lactate]^b[cell]^c[Mn_{IV/III}]^d \qquad \text{(Equation 4.1)}$$

As cell density, pH, and lactate concentration can be considered constant at the beginning of the incubations, they may be included in the apparent rate constant, k_{obs}, and the initial rate law can be simplified to:

$$\frac{d[Mn_{IV}]}{dt} = -k_{obs}[Mn_{IV}]^d \qquad \text{(Equation 4.2)}$$

$$\frac{d[Mn_{III}]}{dt} = -k_{obs}[Mn_{III}]^d \quad \text{(Equation 4.3)}$$

Mn(IV) concentrations used in Eq. 4.2 were determined using mass balance and the measured concentrations of Mn(III) and total Mn(II) as a function of time. Mn(III) concentrations used to solve Eq. 4.3 were measured directly. The linear representation of the integrated form of these rate laws (natural log of concentrations versus time, assuming first order with respect to Mn(IV) or Mn(III) reduction) confirms the initial pseudo-first order kinetics of both Mn(IV) and Mn(III) reduction, in agreement with previous studies conducted with Black Sea isolate *S. putrefaciens* MR-4 (Dollhopf et al., 2000). Values of k_{obs} were derived from the slopes of these representations.

4.3 Result and Discussion

4.3.1. Kinetics of Mn(IV) and Mn(III) reduction by *S. oneidensis* wild-type and mutant strains fed solid Mn(IV) as electron acceptor

Chemical speciation analysis of Mn showed no significant change of each species of Mn in both solid and soluble phases in the abiotic control. Mn(IV) reduction by the wild-type strain produced soluble Mn(III) as intermediate and Mn(II) as end-product in both soluble and solid phases (Figure 4.2). Concentrations of soluble Mn(II) in the presence of the wild-type strain increased rapidly and saturated around 3.0 mM (ca. 40% of total Mn) (Figure 4.2). Similarly, concentrations of exchangeable Mn(II) in the wild-type incubations increased as a function of time during the first 48 hrs but stabilized at relatively low concentrations (i.e., 0.3 mM), constituting approximately 9% of total Mn at the end of the incubations. In parallel to the production of soluble Mn(II), concentrations of Mn(II) bound to carbonate increased significantly in the presence of the wild-type

strain and reached as much as 3 mM at the end of the incubation (Figure 4.2). The accumulation of low concentrations of Mn(III) (3.4%) compared to total Mn(II) (9% surface-bound, 40% soluble, and 51% carbonate-bound) by the wild-type strain fed Mn(IV) oxides is consistent with the relatively low Mn(III) concentrations determined in natural waters (Trouwborst et al., 2006). The low Mn(III) concentrations may be due to either the rapid disproportionation of Mn(III) into Mn(II) and Mn(IV) (Davison, 1993) or the rate-limiting nature of the reduction step from solid Mn(IV) to soluble Mn(III).

To investigate the mechanism of Mn(IV) reduction, incubations of the *S. oneidensis* wild-type strain were compared to incubations of a suite of markerless, in-frame gene deletion mutants lacking *mtrB*, *omcA*, *mtrC* and both *omcA* and *mtrC* (Table 4.1) under identical Mn(IV)-reducing conditions (Figure 4.3). Mn(II) produced by different mutant strains partitioned in a similar fashion as the wild-type strain between the soluble and solid phases (Figure 4.3) and the majority of solid phase Mn(II) was precipitated under the form of $MnCO_3$ (e.g. Figure 4.2). Steady-state production of total Mn(II) by the Δ*omcA*, Δ*mtrC*, and Δ*omcAmtrC* mutants reached 88(± 23)%, 92(± 9)%, and 75(± 21)% of the wild-type Mn(II) levels (Figure 4.3). Pseudo-first order rate constants for Mn(IV) oxide reduction by Δ*omcA* were similar to that of the wild-type strain, while rate constants for Δ*mtrC* were only 43(±3)% of the wild-type strain (Figure 4.3 and Table 4.2). Pseudo-first order rate constants for Mn(IV) oxide reduction by Δ*omcA* were similar to that of the wild-type strain, while rate constants for Δ*mtrC* were only 43(±3)% of the wild-type strain (Table 4.2). In turn, the rate constant obtained with Δ*omcAmtrC* was similar to that of Δ*mtrC* (although Δ*omcAmtrC* displayed a 24-hr phase lag prior to onset of Mn(II) production (Table 4.2)). Results of previous studies have

indicated that the *c*-type cytochromes MtrC and OmcA display overlapping roles for reduction of both Mn(IV) (Myers and Myers, 2001, Myers and Myers, 2003b) and Fe(III) oxides (Borloo et al., 2007, Bretschger et al., 2007); however, the present results indicate that OmcA is not required for Mn(IV) reduction and MtrC is involved in the reduction of solid Mn(IV). MtrC and OmcA, therefore, appear to play different roles in the reduction of Fe(III) and Mn(IV) oxides, in contrast to the conventional view that *S. oneidensis* employs similar mechanisms to reduce these two electron acceptors (Myers and Myers, 2000, Newman and Kolter, 2000, Bretschger et al., 2007, Lovley et al., 2004b).

Production of both total Mn(II) and Mn(III) was significantly impaired during Mn(IV) oxide reduction by Δ*gspD* and Δ*mtrB* (Figure 4.4 and Figure 4.5). These findings suggest that GspD and MtrB are both required to reduce Mn(IV) oxides in a fashion similar to that found for Fe(III) oxide reduction (DiChristina et al., 2002, Beliaev and Saffarini, 1998, Shi et al., 2008). Rate constants for Mn(IV) oxide reduction by the Δ*omcA*, Δ*mtrC* or Δ*omcAmtrC* are significantly higher than rate constants for Mn(IV) oxide reduction by Δ*gspD* and Δ*mtrB* (Table 4.2), suggesting that *gspD*, the gene that encodes an outer membrane porin required for the secretion of decaheme *c*-type cytochromes MtrC and OmcA to the cell surface (DiChristina et al., 2002, Shi et al., 2008), and *mtrB*, the gene encoding an outer membrane β-barrel protein that is postulated to anchor MtrC and OmcA on the cell surface (Beliaev and Saffarini, 1998), are more central to Mn(IV) reduction than *omcA* and *mtrC* genes. These results also suggest that, in the absence of MtrC and OmcA, an alternative Mn(IV) reduction pathway requiring both GspD and MtrB is involved in Mn(IV) reduction. Mn(III) concentrations increased during the Mn(IV) reduction by strains *ΔmtrC* and *ΔomcA,* but remained at lower level

than those produced by MR-1 (Figure 4.5). The levels of soluble Mn(III) accumulated by the Δ*mtrC* during Mn(IV) reduction were approximately 2-fold higher than either Δ*omcA* or Δ*omcAmtrC* (Figure 4.5), implying that MtrC and OmcA also play different roles in Mn(III) reduction.

Production of soluble Mn(III) during reduction of Mn(IV) by the wild-type strain and some of the in-frame gene deletion mutants tested (*ΔmtrC* and *ΔomcA*, but not Δ*gspD* and Δ*mtrB*) indicated that microbial reduction of Mn(IV) by *S. oneidensis* proceeds via two consecutive steps of reduction 1) Mn(IV) to Mn(III) and 2) Mn(III) to Mn(II) and these two steps may be subjected to different electron transfer pathways. To verify these two successive one-electron transfer reactions, Mn(III) reduction-deficient point mutant Mn3 was tested for Mn(IV) reduction activity. Mn(III) reduction-deficient mutant strain Mn3 produced Mn(II) at levels only 17% of the wild-type strain (Figure 4.3 and Figure 4.4), yet retained the ability to produce Mn(III) at wild-type levels (Figure 4.5) when provided with Mn(IV) oxide as electron acceptor. The inability of *Mn3* to reduce Mn(III) was verified in anaerobic liquid incubations with soluble Mn(III) as electron acceptor (Figure 4.6). This newly found point mutant Mn3 suggests that *S. oneidensis* does not share all of the components of the electron transport chain for reduction of Mn(IV) and Mn(III). The point mutation in Mn(III) reduction-deficient mutant strain Mn3 is currently being identified via genetic and nucleotide sequence analyses.

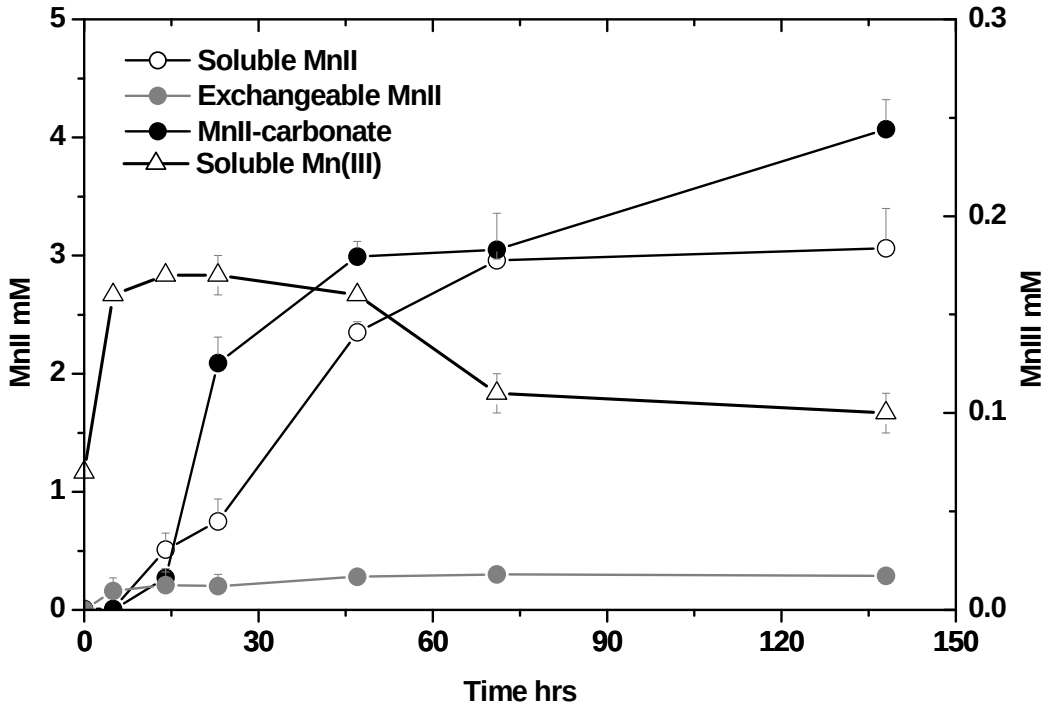

Figure 4.2. Concentrations of reduced Mn species produced as a function of time during anaerobic respiration of solid Mn(IV) by wild-type *Shewanella oneidensis* MR-1. The Mn species detected include soluble Mn(II) (open circles), soluble Mn(III) (open triangles), and sequentially exchangeable Mn(II) extracted from the solid phase with 0.5 M $MgCl_2$ (grey symbols) and $MnCO_{3(s)}$ extracted with 0.1 M NaOAc-AcOH (pH 5) from the residual solid (black symbols). Error bars represent correlations of at least duplicate culture incubations.

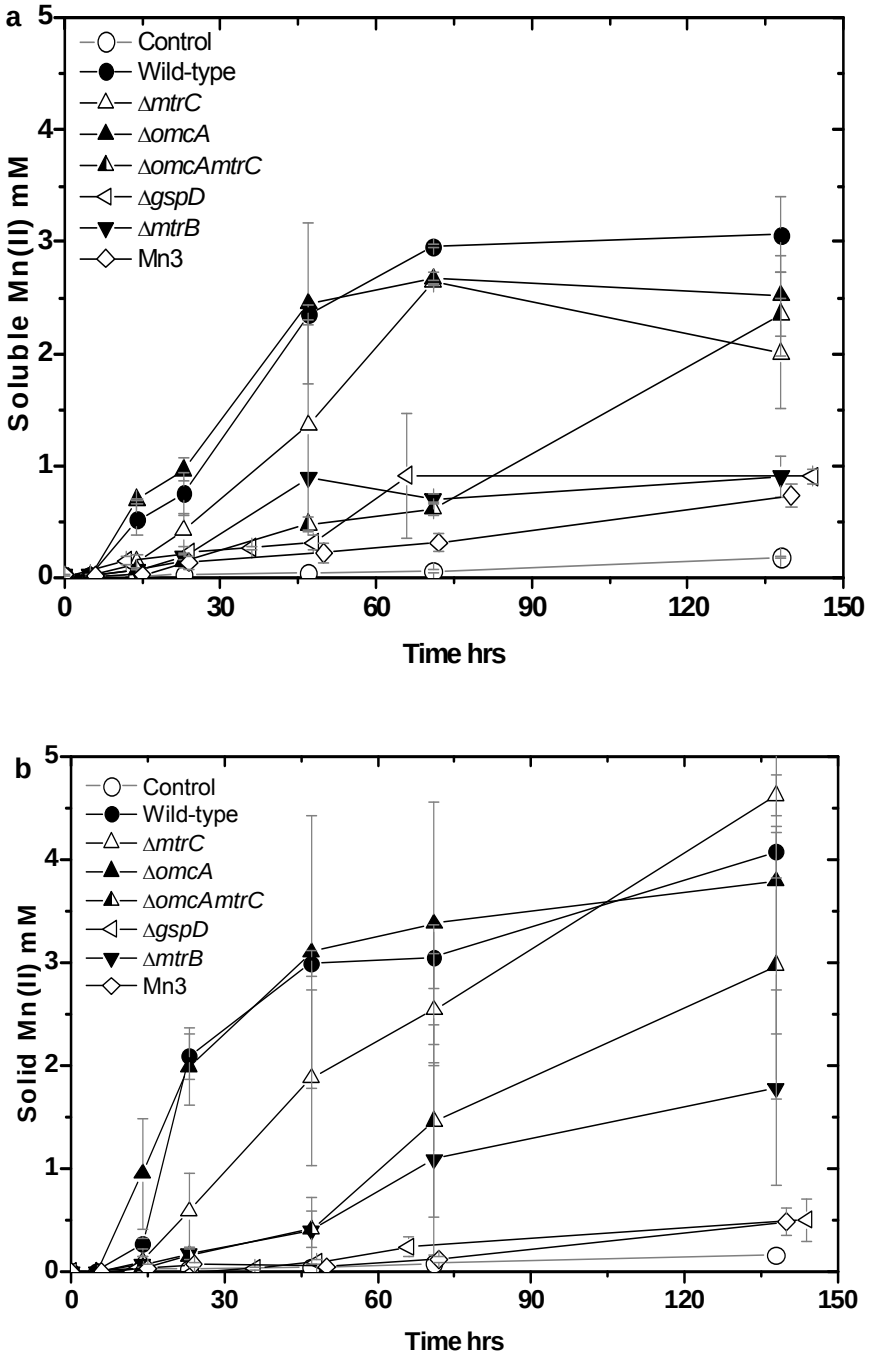

Figure 4.3 Concentration of Mn(II) produced as a function of time during anaerobic respiration of solid Mn(IV) by wild type *S. oneidensis* MR-1 (solid circles), Δ*mtrC* (open up-triangles), Δ*omcA* (solid up-triangles), Δ*omcAmtrC* (half-filled up-triangles), Δ*gspD* (left-triangles), Δ*mtrB* (solid down-triangles), Mn3 mutant (open diamonds), and abiotic controls (open circles). (A) Soluble Mn(II) concentrations (mM) in different batch reactors. (B) Concentrations of Mn(II) in solid phase extracted with 0.5 M $MgCl_2$ and 0.1 M NaOAc. Error bars represent standard deviations from duplicate culture incubations.

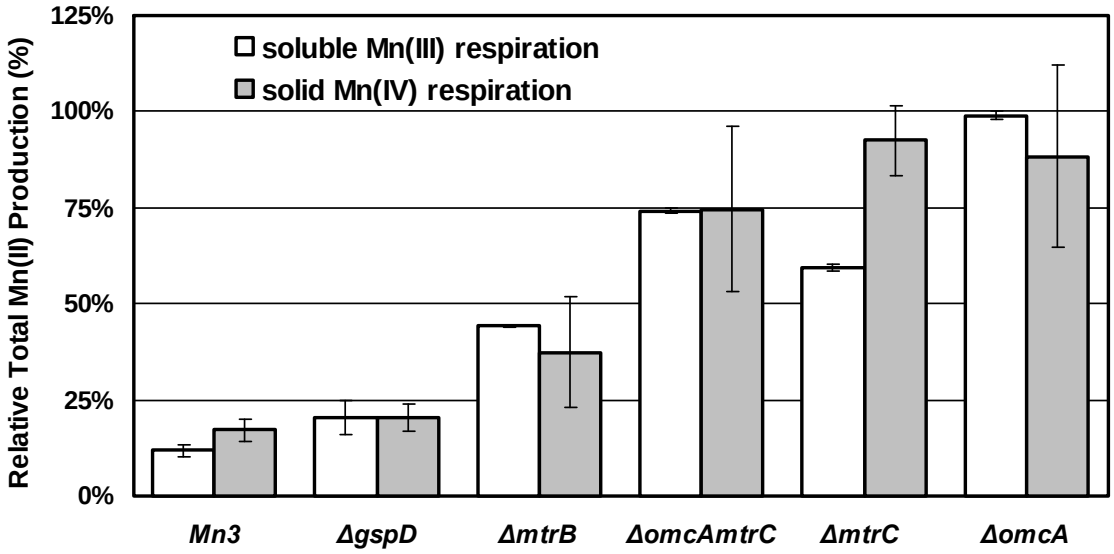

Figure 4.4. Total Mn(II) production at steady-state by different mutant strains of *S. oneidensis* MR-1 relative to the wild-type during incubations with either soluble Mn(III) (open bars) or solid Mn(IV) (filled bars) as terminal electron acceptor. Error bars represent standard deviations of at least duplicate culture incubations.

Table 4.2. Pseudo-first order rate constants for the reduction, in separated incubations, of solid Mn(IV) and soluble Mn(III)-pyrophosphate by *S. oneidensis* wild-type and mutant strains.

k_{obs} ($\times 10^{-2}$ hr^{-1})	Wild-type	Δ*omcA*	Δ*mtrC*	Δ*omcAmtrC*	Δ*mtrB*	Δ*gspD*
Mn(IV) reduction	**3.7±0.20**	**3.2±0.12**	**1.6±0.05**	**1.2±0.11**	**0.4±0.04**	**0.1±0.01**
Mn(III) reduction	**4.6±0.72**	**8.1±2.4**	**0.80±0.06**	**1.0±0.20**	**0.5±0.07**	**0.38±0.08**

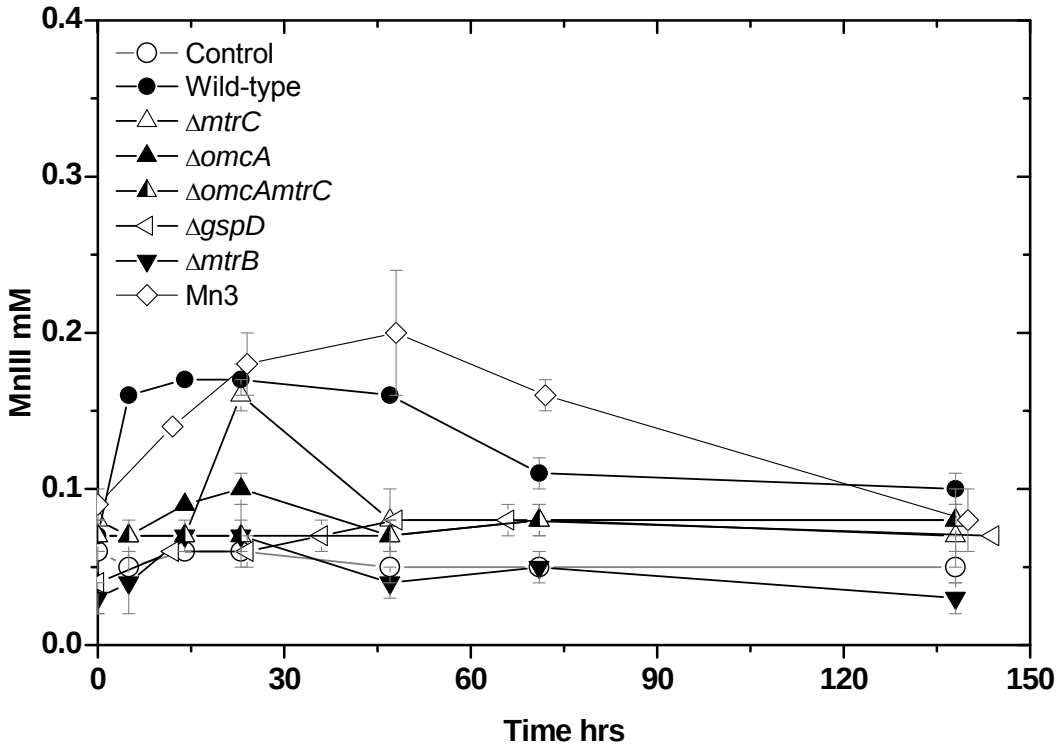

Figure 4.5. Production of soluble Mn(III) during anaerobic respiration of solid Mn(IV) by wild-type *S. oneidensis* MR-1 (solid circles), Δ*mtrC* (open up-triangles), the Δ*omcA* (solid up-triangles), Δ*omcAmtrC* (half-filled up-triangles), Δ*gspD* (left-triangles), Δ*mtrB* (solid down-triangles), Mn3 mutant (open diamonds), and abiotic controls (open circles). Error bars represent standard deviations from duplicate culture incubations.

4.3.3. Kinetics of Mn(III) reduction by *S. oneidensis* wild-type and mutant strains fed Mn(III) as electron acceptor

The *S. oneidensis* wild-type and mutant strains were incubated on soluble Mn(III)-pyrophosphate complexes (Kostka et al., 1995) as a model soluble Mn(III) compound (Figure 4.6). The concentrations of Mn(III) maintained at background level with less 7% change compared to the initial concentration of Mn(III) in the abiotic controls, compared to complete reduction of soluble Mn(III) in 110 hours of the

incubations with the wild-type strain (Figure 4.6). Soluble Mn(III) reduction activity is impaired in Δ*mtrB* and Δ*gspD* (20 (± 4)% and 44 (± 0.2)% of wild-type activity, respectively; Figure 4.4 and Figure 4.6). Involvement of MtrB and GspD in reduction of both solid Mn(IV) and soluble Mn(III) indicates that the reduction of both Mn(IV) and Mn(III) proceeds at the outer membrane of *S. oneidensis*. *S. oneidensis* most likely reduces soluble Mn(III) at the OM to avoid energetic costs associated with importing Mn(III) or exporting Mn(II) across the OM, or to avoid problems associated with intracellular Mn(II) toxicity after Mn(III) reduction (Gruzina et al., 1997, Davison, 1993).

Δ*mtrC* was severely impaired in Mn(III) reduction activity, while Δ*omcA* reduced Mn(III) at wild-type rates (Figure 4.4 and Figure 4.6). This finding confirms that MtrC is required for Mn(III) reduction while OmcA is not required. The pseudo-first order rate constant for Mn(III) reduction by the wild-type strain and Δ*omcA* was respectively, 25% and almost 3-fold higher than their corresponding constant for Mn(IV) reduction (Table 4.2). In contrast, the pseudo-first order rate constant for Mn(III) reduction by Δ*mtrC* was approximately 50% lower than that for Mn(IV) oxide reduction, suggesting that MtrC is central to Mn(III) but not Mn(IV) reduction. These results explain the accumulation of Mn(III) during anaerobic incubation of Δ*mtrC* with solid Mn(IV) oxides (Figure 4.5). The rate constant for Mn(III) reduction by Δ*omcA* was nearly two-fold higher than the wild-type strain (Table 4.2), indicating that the absence of OmcA may accelerate Mn(III) reduction rates (by an as yet unknown mechanism). The pseudo first order rate constant for Mn(III) reduction by the Δ*omcAmtrC* is slightly higher than Δ*mtrC* (Table 4.2), a finding attributed to the net effect of lacking both the *omcA* and *mtrC* genes. These

findings indicate that MtrC (but not OmcA) is a critical component of the Mn(III) reduction pathway of *S. oneidensis*.

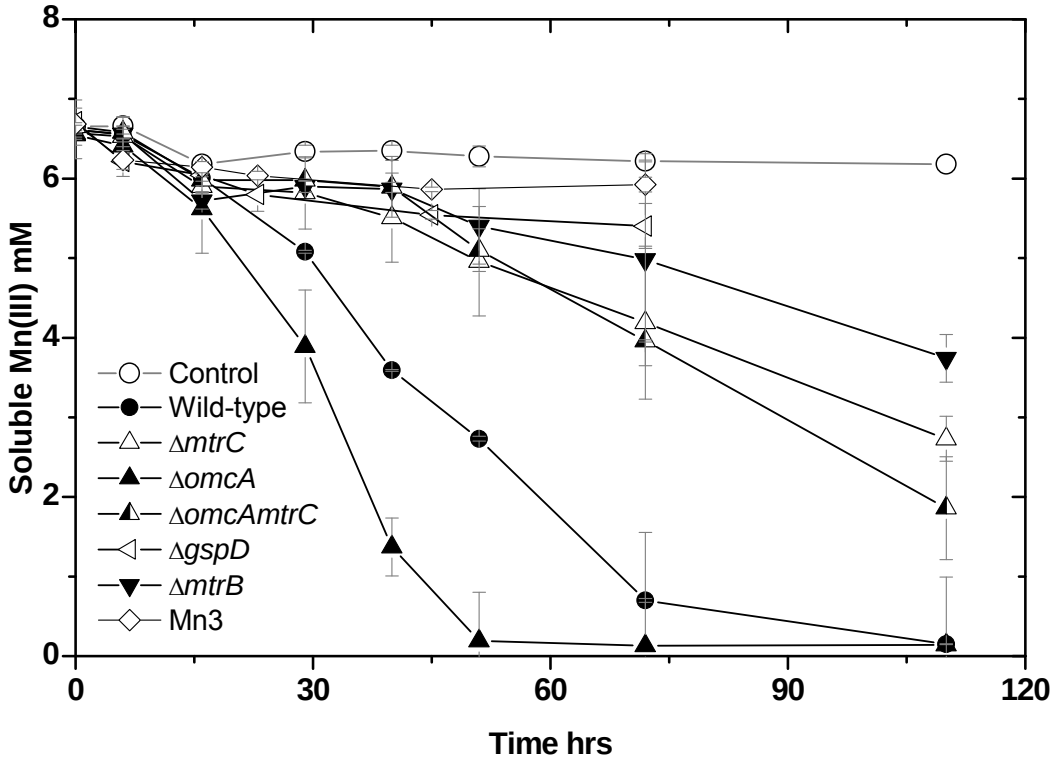

Figure 4.6. Consumption of soluble Mn(III) during anaerobic respiration of soluble Mn(III) by wild type *S. oneidensis* MR-1 (solid circles), Δ*mtrC* (open up-triangles), Δ*omcA* (solid up-triangles), Δ*omcAmtrC* (half-filled up-triangles), Δ*gspD* (left-triangles), Δ*mtrB* (solid down-triangles), Mn3 mutant (open diamonds), and abiotic controls (open circles). Error bars represent standard deviations from duplicate culture incubations.

4.3.4 DIC production by *S. oneidensis* wild-type and mutant strains fed Mn(IV) oxide or Mn(III) pyrophosphate as electron acceptor

Results of the present study indicate that Mn(IV) reduction by *S. oneidensis* proceeds via two successive one electron transfer reactions, with the possibility that

either one or both is coupled to DIC production (carbon mineralization). Previous studies have reported that lactate, the carbon-energy source supplied in the anaerobic incubations, is oxidized to acetate and CO_2 by *S. oneidensis* during Mn(IV) oxide respiration (Myers and Nealson, 1988), suggesting that production of dissolved inorganic carbon (DIC) may be used as a proxy for *S. oneidensis* Mn(IV) reduction activity. In the present study, production of DIC linearly correlated to the consumption of lactate and production of acetate during incubations with the wild-type strain under identical conditions, indicating that the production of DIC is coupled to respiration activities (Figure 4.7). DIC concentrations increased to approximately 10 mM during anaerobic incubations of *S. oneidensis* on 18 mM lactate and either solid Mn(IV) oxides or soluble Mn(III), while production of DIC in the chemical controls remained at low levels (Figure 4.8-a and b). The pH simultaneously increased by approximately 1.5 units (data not shown), reflecting lactate oxidation and proton consumption during Mn(IV) or Mn(III) reduction (Dollhopf et al., 2000). DIC concentrations correlated significantly with total Mn(II) produced during the reduction of either solid Mn(IV) oxide or soluble Mn(III)-pyrophosphate as electron donor (Figure 4.9-a and b), indicating that Mn(II) production is tightly coupled to lactate oxidation as previously reported for Mn(III) reduction by *S. oneidensis* (Kostka et al., 1995). In turn, DIC produced during Mn(IV) oxide reduction correlated poorly with Mn(III) produced (Figure 4.9-c), suggesting that the first reduction step of Mn(IV) to Mn(III) is not linked to DIC production. Assuming both electron-transfer steps are coupled to DIC production, Mn(IV) reduction is expected to produce twice as much CO_2 than that generated by Mn(III) reduction. However, similar concentrations of DIC were produced by *S. oneidensis* and its mutant strains incubated anaerobically with the same

concentration of either Mn(IV) oxides or dissolved Mn(III) (Figure 4.8-a and b). These results indicate that *S. oneidensis* couples only Mn(III) reduction to DIC production and that electron transfer to Mn(IV) is not coupled to DIC production. The electron transport pathway resulting in the reductive solubilization of Mn(IV) to Mn(III) is presently unknown but may originate with lactate oxidation to pyruvate (as opposed to direct oxidation to acetate and CO_2) by two recently discovered lactate oxidases (Pinchuk et al., 2009).

The present study demonstrates for the first time that the initial reduction step of Mn(IV) to Mn(III) is not coupled to DIC production by *S. oneidensis*. These findings imply that *S. oneidensis* first reductively solubilizes manganese prior to Mn(III) reduction (in a manner analogous to that recently proposed for the anaerobic reduction of Fe(III) oxides (Taillefert et al., 2007a, Jones et al., 2010). While *Shewanella* may reduce Fe(III) oxides by non-reductively dissolving Fe(III) with exogenous (Haas and Dichristina, 2002) or endogenous organic ligands (Pitts et al., 2003, Taillefert et al., 2007a, Jones et al., 2010), we propose that the paucity of ligands able to non-reductively solubilize Mn(IV) oxides at circumneutral pH in aquatic systems (Morgan, 2000a) has forced *S. oneidensis* to evolve a Mn(IV) reductive solubilization-based strategy that produces soluble Mn(III) intermediates whose subsequent reduction is linked to organic carbon oxidation. The Mn(IV) reduction pathway of *S. oneidensis* appears to involve the OM *c*-type cytochrome MtrC (Myers and Myers, 2003b, Shi et al., 2007), electron-shuttling compounds (Marsili et al., 2008), and potentially siderophores (Duckworth and Sposito, 2007). The siderophore desferrioxamine B (Def-B), for example, reduces Mn(IV) and stabilizes Mn(III) by complexation with the oxidized form of Def-B (Duckworth and Sposito,

2007). A random transposon-insertion mutant strain of *Shewanella oneidensis* MR-1, N22-7, identified as deficient in siderophore biosynthesis, was also deficient in MnO_2 reduction, suggesting the involvement of siderophore in microbial reduction of Mn((V) by *Shewanella oneidensis* (Kouzuma et al., 2012). In the present study, the pseudo first order rate constant for Mn(III) reduction by wild-type *S. oneidensis* is higher than the corresponding constant for Mn(IV) reduction (Table 4.2), an indication that the initial reductive solubilization step, which most likely depends on the bioavailability of the solid phase electron acceptor Mn(IV), is rate-limiting.

These findings have important implications for our understanding of the biogeochemical cycling of manganese in aquatic systems. First, Mn(III) production during Mn(IV) oxide reduction may explain the existence of soluble Mn(III) in suboxic or anoxic water columns (Trouwborst et al., 2006) and sediments (Madison et al., 2011). Second, Mn(IV) oxide is a readily available terminal electron acceptor for the mineralization of organic compounds in anaerobic environments (De Schamphelaire et al., 2007). If the first electron transfer reaction proceeds via a reductive solubilization step to activate Mn while the second step is coupled to CO_2 production, then diagenetic models which estimate the contribution of manganese reduction to carbon remineralization based on the transfer of two electrons (Neretin et al., 2003, Warnken et al., 2008, Bender et al., 1989) should be revised to more accurately quantify the global carbon cycle.

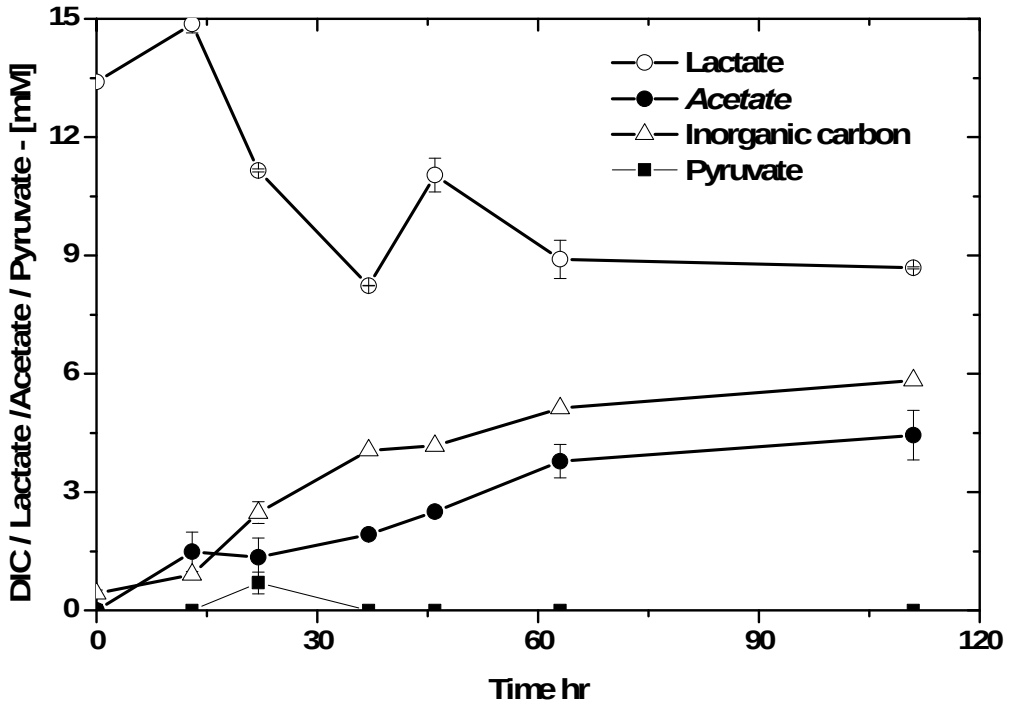

Figure 4.7. Evolution of carbon source, lactate (open circles), the by-product of lactate respiration, acetate (solid circles), pyruvate (solid squres) and total dissolved inorganic carbon (DIC, open triangles) as a function of time during anaerobic respiration of 3.5 mM of solid Mn(IV). Error bars represent standard deviations from duplicate culture incubations.

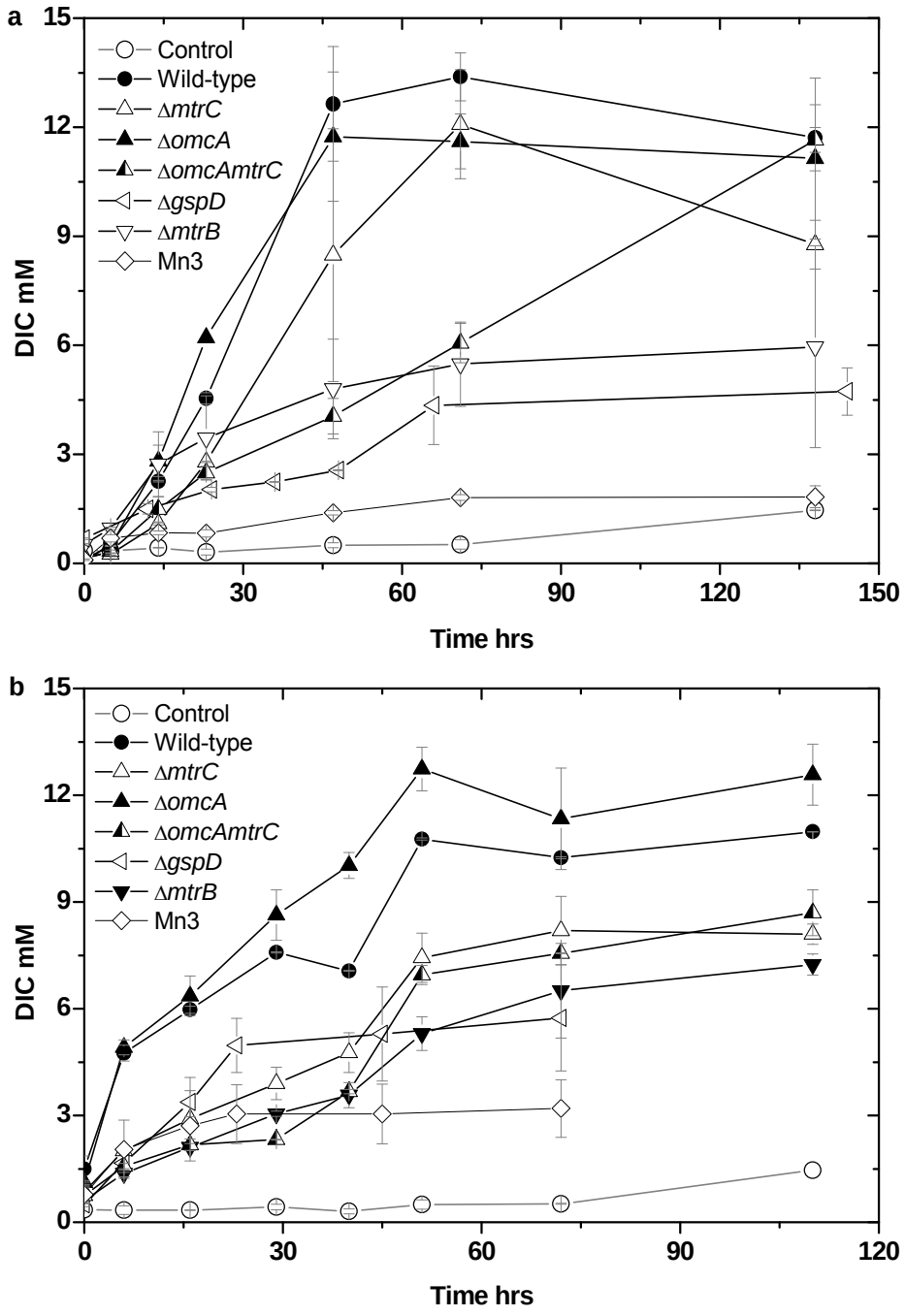

Figure 4.8. Production of total dissolved inorganic carbon (DIC) as a function of time during anaerobic respiration of solid Mn(IV) (A) and soluble Mn(III) (B) by wild-type *S. oneidensis* MR-1 (solid circles), Δ*mtrC* (open up-triangles), Δ*omcA* (solid up-triangles), Δ*omcAmtrC* (half-filled up-triangle), Δ*gspD* (left-triangles), Δ*mtrB* (solid down-triangles), Mn3 mutant (open diamonds), and abiotic controls (open circles). Error bars represent standard deviations from duplicate culture incubations.

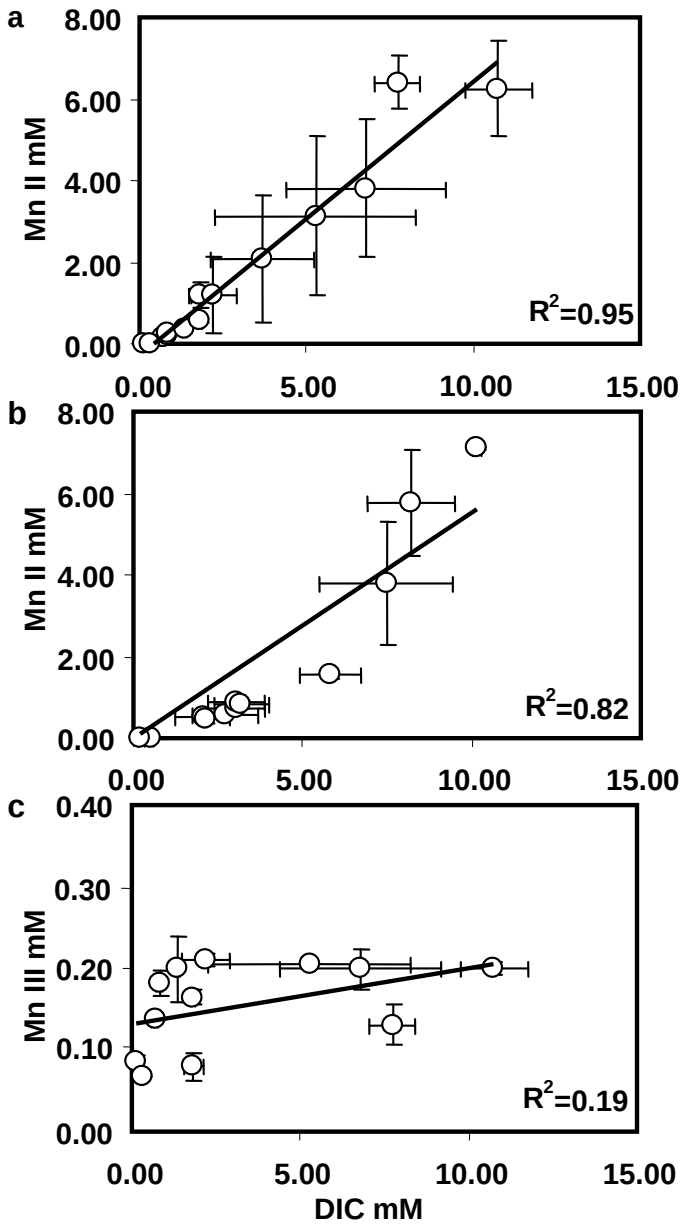

Figure 4.9. Total Mn(II) (**a** and **b**) and dissolved Mn(III) (**c**) versus dissolved inorganic carbon produced during anaerobic respiration of solid Mn(IV) oxides (**a** and **c**) and soluble Mn(III)-pyrophosphate (**b**) by wild-type *S. oneidensis* MR-1. Regression coefficients are provided in each case. Error bars represent standard deviations from duplicate culture incubations.

4.4. Conclusions

In contrast to the recent progress made on anaerobic Fe(III) respiration, the mechanism of electron transfer from bacterial cells to solid Mn(IV) oxides remains poorly defined. In this study, the mechanism of Mn(IV) reduction by *S. oneidensis* was investigated by comparing the kinetics of Mn(IV) and Mn(III) reduction by *S. oneidensis*, and a variety of markerless, in-frame gene deletion mutants fed either Mn(IV) or Mn(III) as electron acceptor. These experiments reveal for the first time that microbial Mn(IV) reduction proceeds step-wise via two successive one-electron transfer reactions with production of soluble Mn(III) as transient intermediate. Investigations with the in-frame gene deletion mutants show that MtrB (an outer membrane β-barrel protein) and GspD (an outer membrane porin) are required for the reduction of both solid Mn(IV) and soluble Mn(III) and indicate that the reduction of both Mn(IV) and Mn(III) proceeds at the outer membrane of *S. oneidensis*. Mn(IV) respiration, however, involves only one of the two potential terminal reductases (c-type cytochrome MtrC and OmcA) involved in Fe(III) respiration, as OmcA is not required to reduce either Mn(IV) or Mn(III). More importantly, production of dissolved inorganic carbon during the reduction of Mn(III) but not Mn(IV) indicates that the second electron transfer step only is coupled to energy generation in contrast to the long-standing paradigm that Mn(IV) reduction occurs via a single two-electron transfer reaction coupled to the mineralization of organic carbon. If applicable to all manganese-reducing microorganisms, these finding suggest that conventional diagenetic models should be revised to correctly account for the impact of manganese reduction in the global carbon cycle.

Acknowledgments

This work was funded by the National Science Foundation.

CHAPTER 5 EVIDENCE FOR MN(IV)-CATALYZED ANAEROBIC NITRIFICATION IN MARINE SEDIMENTS

Abstract

The recent debate on the marine nitrogen budget has motivated studies to investigate alternative pathways of nitrogen transformation. In this study, surface sediments from an intertidal salt marsh were incubated with colloidal and amorphous Mn oxides in the presence of elevated concentrations of NH_4^+ to test the hypothesis that anaerobic ammonium oxidation to nitrite and nitrate is coupled to the reduction of Mn(IV) oxides. The net production of nitrate was stimulated under anaerobic conditions with external addition of colloidal but not amorphous Mn oxides. Mass balance calculations indicate that the net consumption of NH_4^+ in the incubations amended with colloidal Mn oxides (compared to unamended controls) is partially caused by anaerobic ammonium oxidation and confirm the occurrence of Mn(IV)-catalyzed anaerobic nitrification. Factors such as the initial ratio of Mn(IV) to NH_4^+, the type of Mn oxides, and background levels of nitrate and sulfate, may also affect anaerobic nitrification. Anaerobic production of nitrate occurs in the incubations amended with colloidal MnO_2 but not in incubations amended with amorphous MnO_2. In addition, anaerobic nitrification was stimulated by the amendment of small concentrations of nitrate or by lowering initial sulfate levels, suggesting that suboxic conditions may facilitate the onset of anaerobic ammonium oxidation. Therefore, the occurrence and activity of anaerobic nitrification may not only depend on the abundance of Mn-oxides in sediments but also the redox potential of the sediment. These results suggest that Mn(IV)-catalyzed anaerobic nitrification may be an important source of nitrite and nitrate in anoxic

sediments and, in turn, provide an alternative pathway for subsequent marine nitrogen loss. Microbial communities responsible for anaerobic nitrification have to be isolated to demonstrate their importance in the nitrogen cycle.

5.1 Introduction

The balance of the marine nitrogen budget is still under debate. Some studies estimated that denitrification rates are higher than nitrogen fixation and suggested a significant unbalance between oceanic nitrogen inputs (nitrogen fixation) and outputs (denitrification) (Codispoti et al., 2001). Other studies, however, showed that nitrogen fixation may be underestimated in nitrogen budgets and that the oceanic nitrogen inputs and outputs are in balance (Gruber and Sarmiento, 1997, Deutsch et al., 2007). These findings suggest that alternative N-transformation pathways may exist that are presently not accounted for in the marine nitrogen budget (Capone and Knapp, 2007).

Most of the research on alternative pathways of N_2 formation (nitrogen loss) in natural environments focuses on the production of N_2 via anaerobic ammonium oxidation (anammox) using nitrite or nitrate as terminal electron acceptor (Dalsgaard et al., 2005, Jetten et al., 2009, Kuypers et al., 2003). Despite the fact that nitrate and nitrite are generally scarce in oxic marine sediments, anammox is found pervasively across sediment columns (Engstrom et al., 2005, Thamdrup and Dalsgaard, 2002), suggesting that other processes supply these electron acceptors continuously. Aerobic ammonium oxidizers near oxic/anoxic interfaces may provide nitrite for anammox bacteria (Schmidt et al., 2002). However, the total production of NO_x^- by aerobic ammonium-oxidizing bacteria is not always able to sustain the loss of NH_4^+ through anammox, which requires an equivalent moles of ammonium and nitrite (Lam et al., 2007). In addition, anammox is

inhibited above 2 - 25 μM oxygen (Strous et al., 1997, Jensen et al., 2008, Kalvelage et al., 2011), implying that aerobic nitrification and anammox may be vertically separated in sediments. These findings suggest that sources other than aerobic nitrification may exist to supply nitrite or nitrate for anammox microorganisms. Several lines of evidence indeed suggest nitrite and nitrate may be formed anaerobically in marine sediments. First, nitrate was found to rebound below the oxygen penetration depth in a variety of organic-rich sediments (Mortimer et al., 2004, Anschutz et al., 2000, Mortimer et al., 2002). Second, anaerobic nitrification, demonstrated by the production of nitrate, nitrite, and N_2 in anoxic NH_4^+ incubations, was proposed to represent a substantial source of nitrite for anammox (Lam et al., 2007). These latter studies did not identify the electron acceptor involved in anaerobic nitrification but proposed Mn oxides as potential candidate given their high abundance and oxidative power in sediments (Anschutz et al., 2005, Luther et al., 1997, Mortimer et al., 2004).

Interestingly, oxidation of organic-N or NH_4^+ to N_2 (but not NO_3^-) by MnO_2 in the presence of dissolved oxygen was evidenced in both field and laboratory studies, and this process was proposed to dominate the nitrogen cycle in Mn-rich continental margin sediments (Luther et al., 1997). The coupling between MnO_2 reduction and direct ammonium oxidation to N_2, however, has yet to be demonstrated under anaerobic conditions (Thamdrup and Dalsgaard, 2000, Thamdrup and Dalsgaard, 2002). While the oxidation of ammonium to N_2 by MnO_2 is thermodynamically favorable over a wide range of pH, the formation of nitrate is only favorable at pH < 7.8 (Luther et al., 1997, Hulth et al., 1999), suggesting that marine sediments may provide appropriate environments for Mn(IV)-promoted anaerobic oxidation of ammonium to nitrate. Thus,

instead of directly converting ammonium to N_2 (Luther et al., 1997), several other laboratory and field studies suggested that Mn(IV) oxides promote anaerobic ammonium oxidation to nitrate/nitrite (anaerobic nitrification) (Anschutz et al., 2000, Hulth et al., 1999, Mortimer et al., 2004). This conclusion was drawn from the good correlation between the production of dissolved Mn^{2+} and a second nitrate maximum found below the oxygen penetration zone in marine sediments (Anschutz et al., 2000). Nitrite/nitrate production was stimulated by extra amendment of Mn oxides during anaerobic incubations of sediments from Long Island Sound (USA) (Hulth et al., 1999). In addition, production of nitrate and nitrite accompanied with manganese reduction were also observed in anaerobic incubations of sediments from Humber Estuary (UK) (Bartlett et al., 2008) and Arcachon Bay (France) (Javanaud et al., 2011).

Unfortunately, the link between anaerobic nitrification and reduction of Mn oxides is difficult to make from field (in situ) observations alone (Bartlett et al., 2008, Bartlett et al., 2007), especially when considering the following: (1) Nitrate and nitrite act as transition species in anoxic environments and are consecutively consumed by several processes such as denitrification (Knowles, 1982), anammox (Kuypers et al., 2003), and dissimilatory nitrate reduction to ammonium (Bothe et al., 2007); (2) Ammonium may be consumed or produced by a variety of parallel processes, including assimilation (Bothe et al., 2007), adsorption/desorption (Mackin and Aller, 1984), and ammonification (Hulth et al., 1999, Bartlett et al., 2008), making it difficult to recognize the contribution from anaerobic ammonium oxidation; and (3) Other thermodynamically favorable electron acceptors, such as Fe(III) oxides (Park et al., 2009, Clement et al., 2005) and sulfate

(Fdz-Polanco et al., 2001, Schrum et al., 2009), have also been proposed to be coupled to anaerobic oxidation of ammonium.

The inconsistent observations of Mn-catalyzed anaerobic nitrification in different sediments (Thamdrup and Dalsgaard, 2000, Bartlett et al., 2008) imply that the onset of this process may be facilitated by specific geochemical conditions. For example, it has been proposed that the lack of evidence from extensive sediment incubations (Thamdrup and Dalsgaard, 2000) may have been caused by nitrogen limitations in the sediments (Hulth et al., 2005). It was suggested that Mn-catalyzed anaerobic nitrification is likely to occur in disturbed marine sediments via perturbations such as turbidity currents or burial events of Mn oxides (Bartlett et al., 2008). Thus, laboratory incubations that manipulate the key factors involved in Mn-catalyzed anaerobic nitrification are needed to demonstrate the coupling between anaerobic nitrate/nitrite production and Mn-oxides reduction.

In this study, sediment incubations amended with external Mn(IV) oxides, NH_4^+, or both were conducted under anaerobic conditions to investigate the appropriate geochemical conditions that stimulated anaerobic nitrification in marine sediments. Interactions between Mn(IV) reduction and ammonium consumption were investigated via analysis of the chemical speciation of both Mn and N species. Evidence for anaerobic nitrification was evaluated by comparing the net production or consumption of Mn(II), ammonium, and oxidized-forms of nitrogen species in the amended treatments to corresponding control incubations. Factors such as the ratio of Mn(IV) to NH_4^+, types of Mn oxides, and background levels of sulfate and nitrate on the anaerobic oxidation of ammonium were investigated.

5.2 Materials and methods

5.2.1 Study site and sediment sampling

All sediments used in the current study were collected from the Salt-marsh Ecosystem Research Facility (SERF) of Skidaway Institute of Oceanography on Skidaway Island, Georgia (USA) (Figure 5.1). This salt marsh is dominated by monospecific stands of the halophyte *Spartina alterniflora*. The interior platform of the marsh is dominated by low *Spartina*, while the levees adjacent to the creeks are vegetated by high *Spartina*. Fiddler crab *Uca pugnax* is abundant throughout the salt marsh (Gribsholt et al., 2003). Semidiurnal tides (a maximum range of about 2m) and the geomorphology of the marsh significantly affect the redox geochemistry of the site (Taillefert et al., 2007b). High hydrostatic pressure gradients during tidal cycles maintain creek bank sediments at generally suboxic conditions. Iron and manganese reduction provide most of the oxidative power for carbon re-mineralization in creek bank sediments of the marsh. In contrast, mud flat sediments which are not exposed to significant hydrostatic pressures are dominated by sulfate reduction (Taillefert et al., 2007b).

Triplicate sediment cores were collected within 1 meter from each other at a creek bank site (CB) (Figure 5.1) (Newton, 2006, Taillefert et al., 2007b) in both March and October, 2010 (Core-M and Core-O) using a home-made corer (50 cm long and 7.5 cm diameter) with a long handle to sample submerged sediments without disturbing the nearby sediment. The creek bank site (CB) is located in a perennial creek (2.5 m wide at high tide and 1.5 m deep) next to the main creek (Figure 5.1). All sediment cores were collected with a large volume of overlying salt mash water to avoid disturbing the sediment-water interface (SWI). Salinity and temperature of the overlying water captured

by the sediment corer were measured immediately after sampling. Vertical pore-water profiles of the main redox species involved in diagenesis (O_2, Fe^{2+}, Mn^{2+}, ΣH_2S, and other complexes) were obtained voltammetrically (Taillefert et al., 2000b). After profiling, the sediment cores were sectioned in slices of ~0.8-1 cm thickness in a N_2 gas-filled polypropylene glove bag (Aldrich), and pore waters of the different layers extracted by centrifugation and filtration (0.2 μm filters, Puradisc, Whatman). The remaining sediment layers were stored at -20^{o}C for further laboratory incubations. Extracted pore waters were analyzed for the nitrogen species (NH_4^+, NO_2^-, and NO_3^-).

5.2.2 Sediment slurry incubations

As burial events of Mn oxides into sediments were proposed to trigger anaerobic oxidation of ammonium (Anschutz et al., 2000, Mortimer et al., 2004), sediments amended with Mn oxides were incubated in slurries in closed batch reactors (~ 30 ml) to promote Mn-mediated anaerobic nitrification (Hulth et al., 1999). Mn(IV) oxides and ammonium were amended to the original sediment in different combinations, including (1) unamended reactors with original sediment only (control), (2) reactors amended with NH_4^+ only, (3) reactors amended with Mn oxides only, and (4) reactors amended with both NH_4^+ and Mn oxides (Table 5.1). Each reactor contained approximately 8 g of wet homogenized sediment and 30 ml of artificial sea water (ASW) diluted with DI water to simulate the *in situ* salinity of 18. The ASW was composed of NaCl (0.43 M), Na_2SO_4 (29 mM), KCl (11 mM), $MgCl_2 \cdot 6H_2O$ (55 mM), $CaCl_2 \cdot 2H_2O$ (11 mM), and $NaHCO_3$ (2.3 mM). Batch reactors were flushed with Ar gas after all amendments and sealed with rubber stopper and aluminum crimps (National Scientific. 20 mm). The slurry in each

sealed reactor was maintained well-mixed on a rotary shaker in the dark and at room temperature.

According to previous studies, an initial ratio of NH_4^+ : Mn(IV) of 2 - 4 was optimal to induce the apparent coupling between Mn(IV) and anaerobic ammonium oxidation (Newton, 2006). Both colloidal (smaller particle size, with particle diameters in the range of 89-193 nm (Perez-Benito et al., 1996)) and amorphous (larger particle size, c.a. 1 μm (Murray, 1974)) Mn oxides were utilized to investigate the effect of different types of Mn oxides on the nitrogen cycle under anaerobic conditions. As redox conditions may significantly affect Mn-mediated anaerobic nitrification, modifications in the composition of ASW (increase of nitrate or decrease of sulfate levels) were also considered to inhibit or delay the onset of sulfate reduction during the incubations (Javanaud et al., 2011, van de Vossenberg et al., 2008) or to maintain the redox potential relatively high during the incubations. Two independent sets of incubations with modified medium containing either higher nitrate (50 μM) or lower sulfate concentrations (1 mM) were conducted to investigate the effect of nitrate and sulfate on anaerobic ammonium oxidation. Each set of incubations were performed with both the modified medium and the original 50% ASW incubations. Both the modified an the 50% ASW incubations included four treatments, including an unamended control with sediment only (T1), a treatment amended with NH_4^+ only (T2), a treatment amended with colloidal MnO_2 only (T3), and a treatment amended with both colloidal MnO_2 and NH_4^+ (T4). In addition, the isotope pairing technique (Nielsen, 1992) with N-15 ammonium or nitrate was used to trace the formation of N_2 under the form of $^{29}N_2$ or $^{30}N_2$ in some of the reactors. The evolution of Mn^{2+}, NH_4^+, NO_3^-, NO_2^-, pH, $^{29}N_2$, $^{30}N_2$, and dissolved inorganic carbon (DIC) was

monitored as a function of time throughout the incubations. All treatments were replicated independently at least three times.

Thermodynamic calculations were conducted to determine which reaction could be coupled to the anaerobic oxidation of ammonium in the conditions of the experiments (Table 5.2). According to these calculations, the anaerobic oxidation of NH_4^+ is thermodynamically favorable with several alternative electron acceptors such as MnO_2, FeOOH, or SO_4^{2-} (Table 5.2). The oxidation of NH_4^+ by MnO_2 presented the most negative ΔG_r values, compared to those with Fe(III) or sulfate as the electron acceptor.

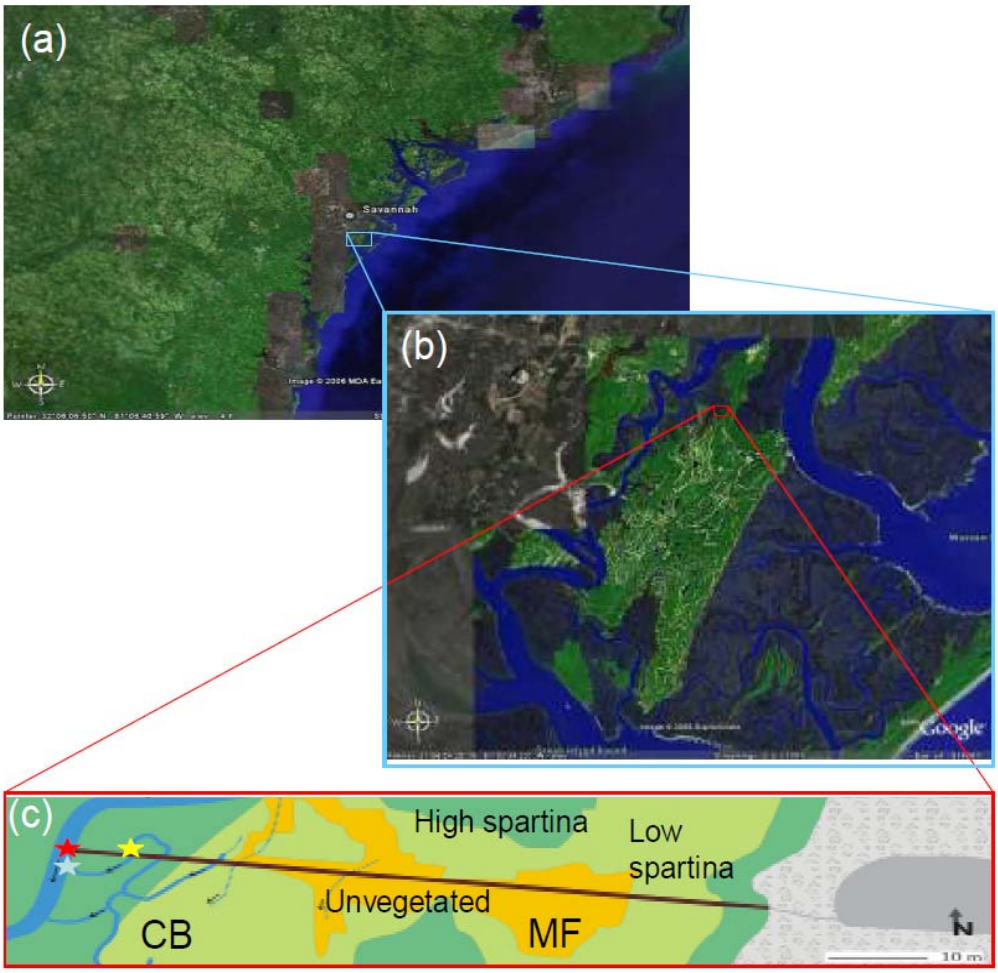

Figure 5.1. (a) Map of Skidaway Island (blue box) in Savannah, Georgia. (b) Zoom-in view of Skidaway Island. (c) Zoom-in view of the salt marsh study area with locations of the sediment sampled in the current study (stars). The dark green regions indicate dense Spartina grass, the light green regions indicate low Spartina grass, and the yellow regions indicate areas without vegetation. CB represents the creek bank and MF represents the mud flat. All sediments used in the current study were sampled from the creek bank (CB), where metal reduction dominated anaerobic respiration processes. (Newton, 2006, Taillefert et al., 2007b).

Table 5.1. Different treatments conducted to investigate the MnO_2-mediated anaerobic oxidation of ammonium, including (1) an unamended control containing sediments and 50% of diluted ASW only; (2) a sediment amended with 800 μM NH_4^+ only; (3) a sediment amended with approximately 300 μM of Mn(IV) oxides only; and (4) a sediment amended with both NH_4^+ and Mn(IV) oxides.

Treatments	Control	NH_4^+	Mn(IV) oxides	NH_4^+ + Mn(IV)
Sediments (~2.5 ml)	+	+	+	+
50% ASW in DI water	+	+	+	+
NH_4^+ (800 μM)	-	+	-	+
Mn(IV) oxides (300 μM)	-	-	+	+

Table 5.2. Gibbs free energy of the reactions R (ΔG_R; kJ mol^{-1}) that could be involved in the current incubations. Organic material is for simplicity represented as carbohydrate, CH_2O. Conditions used for calculations: $[CO_2]$ = 50 μM, $[HCO_3^-]$ = 1000 μM, pN_2 = 0.781 atm, $[NH_4^+]$ = 800 μM, $[Mn^{2+}]$ = 10 μM, $[Fe^{2+}]$ = 5 μM, $[SO_4^{2-}]$ = 15 mM, $[H_2S]$ = 25 μM, $[HS^-]$ = 5 μM, $[NO_3^-]$ = 5 μM, $[NO_2^-]$ = 5 μM, and pH = 7. * ΔG_R /e^- refers to the Gibbs free energy per moles of electron transferred.

Reactions	ΔG_R	ΔG_R /e^- *
$5/4\ CH_2O + NO_3^- + H^+ \rightarrow 5/4\ CO_2 + ½\ N_2 + 7/4\ H_2O$	-596	-119
$5/3\ NH_4^+ + NO_3^- \rightarrow 4/3\ N_2 + 3\ H_2O + 2/3\ H^+$	-435	-87
$CH_2O + 3\ CO_2 + H_2O + 2\ MnO_2 \rightarrow 2\ Mn^{2+} + 4\ HCO_3^-$	-391	-98
$4\ MnO_2 + NH_4^+ + 6\ H^+ \rightarrow 4\ Mn^{2+} + NO_3^- + 5\ H_2O$	-206	-26
$3\ MnO_2 + NH_4^+ + 4\ H^+ \rightarrow 3\ Mn^{2+} + NO_2^- + 4\ H_2O$	-181	-30
$3/2\ MnO_2 + NH_4^+ + 2\ H^+ \rightarrow 3/2\ Mn^{2+} + 1/2\ N_2 + 3\ H_2O$	-241	-80
$NH_4^+ + 6FeOOH + 10H^+ \rightarrow NO_2^- + 6Fe^{2+} + 10H_2O$	-39.5	-6.6
$NH_4^+ + 8FeOOH + 12H^+ \rightarrow NO_3^- + 8Fe^{2+} + 13H_2O$	68.5	8.6
$CH_2O + ½\ SO_4^{2-} \rightarrow ½\ H_2S + HCO_3^-$	-121	-30
$4/3\ NH_4^+ + ½\ SO_4^{2-} \rightarrow 2/3\ N_2 + 2\ H_2O + 1/3\ H^+ + 1/2\ H_2S$	-6.7	-1.7

5.2.3 Methods

All glass and plastic wares were soaked in 10% nitric acid overnight and washed with sterile DI water prior to use. The glass batch reactors were autoclaved before incubations. All solutions were prepared with ACS or trace metal grade chemicals in 18 – Ohm de-ionized water (Barnstedt). Colloidal Mn oxides (diameter range of 89-193 nm) solutions were prepared by reducing $KMnO_4$ with a stoichiometric amount of $Na_2S_2O_3$ (Perez-Benito et al., 1996, Perezbenito et al., 1987). Amorphous Mn oxides (particle diameter range of 0.2-1.0 μm) were generated by the oxidation of Mn^{2+} by permanganate (Murray, 1974).

Salinity and temperature of the overlying water in each salt marsh sediment core were measured with a RHS-10ATC portable refractometer. Oxygen, soluble organic-Fe(III) (Taillefert et al., 2000a), Fe^{2+}, Mn^{2+}, and ΣH_2S (= H_2S + HS^- + S(0) + S_x^{2-}) (Brendel and Luther, 1995) were analyzed voltammetrically by a computer-operated DLK-100A or DLK-60 potentiostat (Analytical Instrument Systems, Inc.) using a three-electrode system that included a Hg/Au microelectrode as working electrode, an Ag/AgCl reference electrode, and a Pt counter electrode. Linear sweep (for O_2) and square wave (for soluble organic-Fe(III) complexes, Fe^{2+}, Mn^{2+}, and ΣH_2S) voltammetry were used from -0.1 to -1.8 V at a rate of 200 mV/s with a conditioning step at -0.1 V for 10 sec before each scan. When soluble organic-Fe(III) complexes or dissolved sulfide signals were detected, an additional conditioning step was applied at -0.9 for 10 s to clean the electrode surface prior to the next measurement. Voltammograms were integrated using the semi-automatic integration program VOLTINT in Matlab (Bristow and Taillefert, 2008). A computer-operated DLK MAN-1 micromanipulator (AIS, Inc.) coupled to the

DLK-100 potentiostat was used to obtain depth profiles of these redox species in intact sediment cores.

Nitrate concentrations in pore waters were analyzed by high pressure liquid chromatography (HPLC) with ultraviolet detection (Rozan and Luther, 2002). Measurements were conducted with a 10 μm Anion/R (150 × 4.6 mm) anion exchange column and an All-Guard Anion/R (7.5 × 4.6 mm) guard column (Altech) coupled to a DG50 pump (Dionex) and a dual λ Absorbance UV Detector (Waters 2487) at a wavelength of 220 nm. A sodium perchlorate solution (2.5 mM $NaClO_4$, pH 10) pumped at a rate of 2 mL/min was used as the eluent. All slurry incubation samples were diluted in 1:5 proportions to reduce the interference of Cl^- to the sensitivity of the detector. Concentrations of NH_4^+ and NO_2^- were determined by colorimetric analysis as described previously (Grasshoff et al., 1983, Weatherb Mw, 1967). Total dissolved inorganic carbon (DIC) was measured by a flow injection analysis system with conductivity detection (Hall and Aller, 1992) coupled to an AIS, Inc. LCC-100 integrator. Concentrations of $^{29}N_2$ and $^{30}N_2$ were obtained based on the excess atomic mass unit (AMU) of the 29 and 30 signal measured on a membrane inlet mass spectrometer (MIMS) (Kana et al., 1994, An et al., 2001). The concentration of gases in the standards diluted in ASW were calculated according to the solubility of the species under saturated conditions at certain salinity and temperature (Weiss, 1970). Two water baths open to the atmosphere at two different temperatures (21°C and 30°C) for calibration were used. Acid volatile sulfide (AVS) in the solid phase of the incubation slurries was extracted by 3 M HCl under a N_2 gas at room temperature using a distillation procedure with voltammetric detection (Henneke et al., 1991).

5.2.4 Estimates of NH_4^+ production and consumption processes in the slurry incubations.

To determine the proportion of NH_4^+ consumption attributed to the Mn-catalyzed anaerobic oxidation of NH_4^+ ($\Delta[NH_4^+]_{an.\text{-}oxid.}$), a mass balance approach that accounts for the change of ammonium in solution during the incubations was used. Three major non-redox sinks and sources of ammonium: (1) adsorption/desorption ($\Delta[NH_4^+]_{adsorption}$, sink), (2) NH_4^+ assimilation ($\Delta[NH_4^+]_{assimilation}$, sink), and (3) ammonification ($\Delta[NH_4^+]_{ammonification}$) were considered to balance the anaerobic oxidation of ammonium ($\Delta[NH_4^+]_{an.\text{-}oxid.}$) (Eq. 5.1):

$$\Delta[NH_4^+]_{solution} = \Delta[NH_4^+]_{ammonification} - \Delta[NH_4^+]_{adsorption} - \Delta[NH_4^+]_{assimilation} - \Delta[NH_4^+]_{an.\text{-}oxid} \quad \text{(Eq. 5.1)}$$

(1) Adsorption/desorption (exchange between solid/soluble phase)

Reversible adsorption on sediment solids is one of the most important processes that affect the distribution of dissolved ammonium in marine sediments. The Freundlich Asorption Isotherm reproduces this process efficiently (Eq. 5.2) (Mackin and Aller, 1984)

$$\acute{\Gamma} = K_F * C^{1/n} \quad (n \geq 1) \quad \text{(Eq. 5.2)}$$

where K_F is the adsorption constant (unitless); $\acute{\Gamma}$ is the concentration of adsorbed NH_4^+ ions (mol/L); and C is the concentration of NH_4^+ in solution (mol/L).

As NH_4^+ is a minor cation in marine sediments, its ion-exchange behavior can be simplified to a linear adsorption isotherm, in which $n \approx 1$ (Mackin and Aller, 1984). The adsorption equation is then written as:

$$\acute{\Gamma} = K_F * C \quad \text{(Eq. 5.3)}$$

In the current incubations, the concentration of DIC measured (as a proxy of respiration activity) remained constant during the initial 5 days in the control treatment (T1, natural sediment only) and the treatment amended with ammonium only (800 μM) (T2) (Fig. 5.3). Therefore, the activity of assimilation and ammonification are negligible in these two treatments (T1 and T2) and the distribution of ammonium was assumed to be dominated by adsorption/desorption processes in these two treatments. The adsorption equilibrium constant (K_F) was calculated from the slope of the adsorption density as a function of the concentration in solution.

The concentration of total NH_4^+ (C_{total}) is equal to the sum of NH_4^+ in the solid phase ($\acute{\Gamma}$) and in solution (C) (Eq. 5.4).

$$C_{total} = \acute{\Gamma} + C = K_F * C + C \quad \text{(Eq. 5.4)}$$

Therefore, total NH_4^+ (C_{total}) in treatment T1 and T2 can be written as,

$$C_{total\text{-}T1} = \acute{\Gamma}_{T1} + C_{T1} = K_F * C_{T1} + C_{T1} \quad \text{(Eq. 5.5)}$$

$$C_{total\text{-}T2} = \acute{\Gamma}_{T2} + C_{T2} = K_F * C_{T2} + C_{T2} \quad \text{(Eq. 5.6)}$$

As additional 800 μmol/L of NH_4^+ was added into T2 (Table 5.1),

$$C_{total\text{-}T2} = C_{total\text{-}T1} + 800\ (\mu mol / L) \quad \text{(Eq. 5.7)}$$

Therefore, K_F can be solved by combining Eq. 5.5-5.7,

$$K_F = (800+C_{T1}-C_{T2})/(C_{T2}-C_{T1}) \quad \text{(Eq. 5.8)}$$

Using this approach, a K_F value of 0.27 ± 0.08 was determined, which was consistent with previous studies (Mackin and Aller, 1984). The consumption of NH_4^+ via adsorption was correlated to the change of soluble NH_4^+ measured in solution (Eq. 5.9), and this equation was used to estimate the change in NH_4^+ concentration due to the

adsorption onto the sediment in the other incubations (T3 – T6), as the same sediment was used in each treatment.

$$\Delta[NH_4^+]_{adsorption}\ (\Delta\ \acute{I}) = \Delta[NH_4^+]_{solution} * K_F \quad \text{(Eq. 5.9)}$$

(2) Ammonification ($R\text{-}NH_2 \rightarrow NH_4^+$)

During respiration, organic carbon is oxidized to produce inorganic carbonate species, ammonium, and orthophosphates according to Eq.5.10.

$$(CH_2O)_a(NH_3)_b(H_3PO_4)_c \rightarrow a\ HCO_3^- + b\ NH_4^+ + c\ HPO_4^{2-} \quad \text{(Eq. 5.10)}$$

Therefore, rates of ammonification depend on rates of DIC production and the C:N ratio of organic matter (a:b coefficients in Eq. 5.10). In this study, the production of NH_4^+ via ammonification (Eq. 5.11) was calculated based on the production of DIC measured (ΔDIC) and a C/N ratio (R) of 12.4 ± 0.04 reported for the creek banks of SERF (Gribsholt et al., 2003).

$$\Delta[NH_4^+]_{ammonification} = \Delta DIC/R \quad \text{(Eq. 5.11)}$$

(3) NH_4^+ assimilation

Assimilation of NH_4^+ by microorganisms during growth is another non-redox process of ammonium consumption, and rates of NH_4^+ assimilation depend on the C/N ratio in the biomass synthesized and the yield coefficient (Y_{XD}) during respiration (Fdz-Polanco et al., 2001). The yield coefficient (Y_{XD}) represents the number of moles of carbon assimilated into biomass per mole of carbon oxidized during respiration (i.e. ΔDIC) (Pavlostathis and Giraldogomez, 1991, Heijnen and Vandijken, 1992). Therefore, the amount of carbon assimilated into biomass ($\Delta[Carbon]_{assimilation}$) can be calculated as (Eq. 5.12).

$$\Delta[Carbon]_{assimilation} = \Delta DIC * Y_{XD} \quad \text{(Eq. 5.12).}$$

In general, the C/N ratio in biomass is considered to be 5 according to an average biomass composition of $C_5H_7O_2N$ (Madigan et al., 2003). Therefore, the concentration of NH_4^+ assimilated by microorganisms can be calculated as,

$$\Delta[NH_4^+]_{assimilation} = \Delta DIC * Y_{XD}/5 \quad \text{(Eq. 5.13)}$$

Thus, the fraction of ammonium consumed via anaerobic oxidation ($\Delta[NH_4^+]_{an.-oxid.}$, Eq. 5.1) can be explicitly written by the difference between the change in ammonium concentration in solution and the three major non-redox sinks/sources of ammonium, according to Eq.5.9, Eq. 5.11, and Eq. 5.13. (Eq. 5.14):

$$\Delta[NH_4^+]_{an.-oxid.} = \Delta DIC/R - \Delta[NH_4^+]_{solution} * K_F - \Delta DIC * Y_{XD}/5 - \Delta[NH_4^+]_{solution} \quad \text{(Eq. 5.14)}$$

where $\Delta[NH_4^+]_{solution}$ and ΔDIC are the change of soluble NH_4^+ and DIC measured during the incubations (μmol/L), K_F is the adsorption equilibrium constant of NH_4^+ onto the sediment calculated from control experiments, 0.27 ± 0.08, R is the C/N ratio of natural organic matter measured at the site, 12.4 ± 0.04 (Gribsholt et al., 2003), and Y_{XD} (mol C biomass/mol C respired) is the yield coefficient of NH_4^+ assimilation by microbial communities.

The yield coefficient is the only constant from Eq. 5.14 that is not well characterized, as it may vary significantly depending on different carbon sources (Heijnen and Vandijken, 1992) and different respiration processes (sulfate reduction, Mn(IV) reduction, or aerobic respiration) (Lensing et al., 1994, Pradeep and Jinno, 2010). In the current incubations, the composition of organic carbon was likely to be similar in the different treatments, as the same homogenized sediment was used in all experiments,

suggesting that Y_{XD} could only vary if changes in respiration process occurred. The six incubations were then divided into three sets according to the composition of the main terminal electron accepting processes involved: (1) unamended with MnO_2 (T1 and T2), (2) amended with colloidal MnO_2 (T3 and T4), and (3) amended with amorphous MnO_2 (T5 or T6) (Table 5.1), and Y_{XD} was assumed to be the same for each set. Apparent values of Y_{XD} ($Y_{XD\text{-}0}$ for T1 and T2, $Y_{XD\text{-}c}$ for T3 and T4, and $Y_{XD\text{-}a}$ for T5 and T6) were obtained by assuming that the consumption of NH_4^+ via anaerobic oxidation was negligible in the treatments without NH_4^+ amendment ($\Delta[NH_4^+]_{an\text{-}oxid.} = 0$ in T1, T3, and T5). These Y_{XD} values ($Y_{XD\text{-}0}$, $Y_{XD\text{-}c}$, and $Y_{XD\text{-}a}$), calculated from T1, T3, and T5 according to Eq. 5.14, were then applied correspondingly to the treatments amended with NH_4^+ (T2, T4, and T6) to calculate the amount of NH_4^+ consumed via anaerobic oxidation (Table 5.5).

5.3 Results

5.3.1 Pore water profiles

Pore water profiles sampled in the Spring (Core M) and Fall (Core O) of 2010 generally displayed similar geochemical characteristics over the top 15 cm of sediment (Figure 5.2-a and b). The Depths of oxygen penetration into the sediment reached 3 mm in both sediment cores. After the disappearance of O_2, soluble Mn^{2+} and Fe^{2+} were generated in sequence, which was consistent with the predictions based on the free energy yields of oxidation of natural organic matter by different terminal electron acceptors (Froelich et al., 1979) (Figure 5.2). In both sediment cores, Mn^{2+} was found well below the maximum depth of O_2 penetration. Concentrations of Mn^{2+} reached a maximum of ca. 300 μM around 20 to 30 mm depth and decreased in the deeper layers, suggesting the dominance of Mn(IV) reduction in the 10 to 40 mm depth interval. The onset of iron reduction, measured by the production of Fe^{2+} in the pore waters, was always below the zone of Mn^{2+} production and the concentration of Fe^{2+} was much less in Core O than Core M sediments (Figure 5.2). Voltammetric signals for soluble organic-Fe(III) complexes coincided with the production of Fe^{2+} in the deep layers of both sediment cores, and the intensities of the signals reflected the concentrations of Fe^{2+} produced at each season (Figure 5.2-a and b). These organic-Fe(III) complexes may be produced as intermediates during microbial Fe(III) reduction (Jones et al., 2010), and the two profiles suggested that microbial iron reduction was much more intense in the fall season (Core O). According to thermodynamic considerations (Froelich et al., 1979), dissolved sulfides should be produced below the zone of microbial iron reduction. Concentrations of dissolved sulfides and their oxidized intermediates, however, were

below minimum detection limit in the top 100 mm of both sediment cores (Figure 5.2-a and b).

NH_4^+ concentrations in the pore waters of both cores increased from 5 μM at the sediment water interface (SWI) to a maximum of ca. 100 μM at a depth of 50 mm below the SWI, and stabilized around this value in the deeper zone (Figure 5.2). Concentrations of nitrite and nitrate were maintained at around 10 and 25 μM throughout both sediment cores (Figure 5.2) and comparable with those found in other sediments (Mortimer et al., 2004, Luther et al., 1997). Interestingly, two small subsurface peaks of nitrate (as indicated by the arrows) were found around 20-40 mm and 80-100 mm depth in both cores (Figure 5.2-a and b), with a more dramatic change in concentration in Core O, suggesting the possibility of anaerobic nitrification in these sediments.

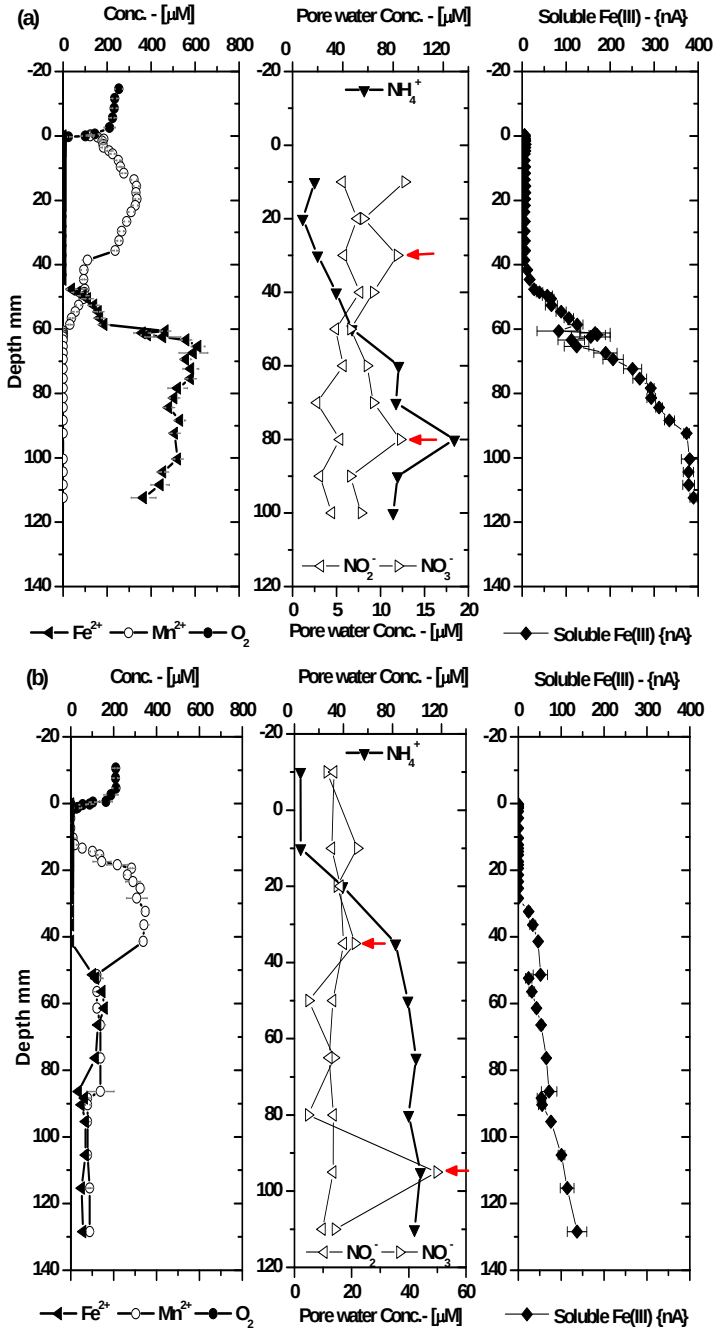

Figure 5.2. Pore water geochemistry of two sediment cores sampled from the tidal creek bank (CB) of SERF in the Skidaway salt marsh in March 2010 (Core M) (a) and October 2010 (Core O) (b). Concentrations of $O_{2(aq)}$, Mn^{2+}, and Fe^{2+}, as well as the current intensities of soluble organic-Fe(III) complexes were determined by *ex situ* voltammetry with Au/Hg microelectrodes. Concentrations of NO_2^-, NO_3^-, and NH_4^+ were determined in extracted pore waters using conventional techniques. No significant sulfide species were detected in the top 14 cm layer of the sediment cores. Arrows showed the peaks of nitrate below the oxygen penetration zone.

5.3.2 Batch sediment incubations amended with colloidal or amorphous Mn oxides

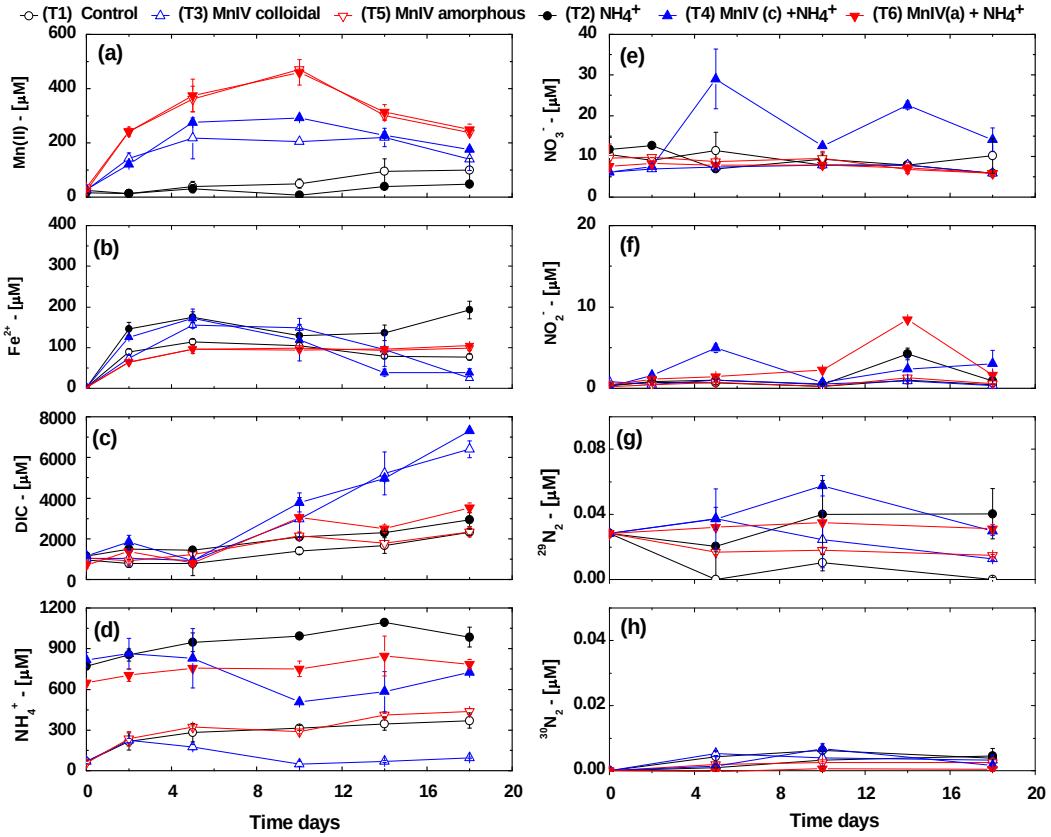

Figure 5.3. Evolution of (a) Mn^{2+}, (b) Fe^{2+}, (c) dissolved inorganic carbon (DIC), (d) NH_4^+, (e) NO_3^-, (f) NO_2^-, (g) $^{29}N_2$, and (h) $^{30}N_2$ in solution as a function of time in anaerobic slurry incubations conducted without any amendment (T1, control, open circles) or in the presence of 800 µM $^{15}NH_4^+$ (T2, solid circles), 300 µM colloidal MnO_2 (T3, open blue upward triangles), 800 µM $^{15}NH_4^+$ and 300 µM colloidal MnO_2 (T4, solid blue upward triangles), 400 µM amorphous MnO_2 (T5, open red downward triangles), and 800 µM $^{15}NH_4^+$ and 400 µM amorphous MnO_2 (T6, solid red downward triangles). The error bars represent the standard deviations of duplicate incubations.

The sediment layers between 20 and 40 mm depth of each sediment core were incubated under anaerobic conditions in diluted artificial sea water to reflect the salinity of the marsh pore waters. The pH was generally maintained around 7.5 but slightly

increased (approximately 0.1-0.2 pH unit) during the later part of the incubations (Supplementary Figure C.1) due to the consumption of protons and production of DIC during respiration in the treatment amended with Mn oxides. Respiration activities were evidenced by the simultaneous production of Mn(II), Fe(II), and DIC and the consumption of DOC in solution (Figure 5.3-a,b,c and Table 5.3). Reduction of MnO_2 was completed within the first 10 days (Figure 5.3-a), and production rates of Mn(II) in incubations amended with either colloidal or amorphous MnO_2 (T3 and T6) were significantly higher than in the control treatments without MnO_2 (T1 and T2) (Table 5.3). Simultaneously, production rates of DIC were also higher in the MnO_2 treatments (T3 and T6) than in the controls (T1 and T2) (Table 5.3 and Figure 5.3-c), suggesting a link between Mn(IV) reduction and DIC production. Interestingly, higher rates of Mn(II) production were observed in incubations amended with both colloidal MnO_2 and NH_4^+ (T4) compared to the incubations with colloidal MnO_2 only (T3). In contrast, similar Mn(II) production rates were obtained in the amorphous MnO_2 incubations either amended or not with NH_4^+ (T5 and T6) (Table 5.3). Mn(II) production rates were approximately 50% higher in the amorphous MnO_2 treatments (T5 and T6) than the colloidal treatments (T3 and T4). In turn, carbon mineralization, evidenced by DIC production and DOC consumption, was generally slower in the treatments amended with amorphous MnO_2 (T5 and T6) than the treatments amended with colloidal MnO_2 (T3 and T4) (Table 5.3). Rates of DIC production were higher in the incubations amended with both NH_4^+ and MnO_2 (T4 and T6), compared to those treatments amended with MnO_2 only (T3 and T5) (Table 5.3), indicating that respiration is increased by external addition of NH_4^+. Due to the high content of solid Fe(III) oxides of the sediments at this site

(Taillefert et al., 2007b), reduction of Fe(III) oxides was also observed during the first 10 days of the incubations (Figure 5.3-b). The rates of Fe^{2+} production were similar among all treatments, except for the slightly lower rates in the amorphous MnO_2 treatments (T5 and T6) (Table 5.3), which may be due to the adsorption of Fe(II) to solid MnO_2 (Tebo et al., 2004).

Table 5.3. Net rates ($\mu M\ day^{-1}$) of change in dissolved concentration of Mn^{2+}, NH_4^+, NO_3^-, and inorganic (DIC) and organic (DOC) carbon during the first 10 days of the anaerobic slurry incubations conducted with colloidal (T3 and T4) and amorphous (T5 and T6) MnO_2 in the presence (T4 and T6) or absence (T3 and T5) of NH_4^+ compared to their respective unamended controls (T1 and T2).

Treatments	Mn^{2+}	Fe^{2+}	NH_4^+	NO_3^-	DIC	DOC
(T1) Control	2.4 ± 1.5	10 ± 1.7	25 ± 4.2	-0.14 ± 0.16	41 ± 5	-8.9 ± 2.3
(T2) NH_4^+	1.5 ± 0.7	13 ± 1.2	22 ± 0.7	-0.23 ± 0.11	109 ± 18	-6.5 ± 1.6
(T3) MnO_2 colloidal	18 ± 1.0	15 ± 0.7	-2.0 ± 0.8	0.17 ± 0.03	198 ± 70	-43 ± 12
(T4) NH_4^+ + MnO_2 (c)	26 ± 1.3	12 ± 3.7	-31 ± 2.1	4.6 ± 0.52	279 ± 34	-41 ± 11
(T5) MnO_2 amorphous	43 ± 1.7	9.8 ± 0.5	23 ± 5.0	-0.01 ± 0.06	115 ± 11	-17 ± 8.9
(T6) NH_4^+ + MnO_2 (a)	44 ± 4.5	9.4 ± 0.1	20 ± 1.6	0.03 ± 0.10	205 ± 44	-18 ± 9.8

Net production of NH_4^+ was observed in all the incubations except the ones amended with colloidal MnO_2 (T3 and T4) (Figure 5.3-d and Table 5.3). Production of NH_4^+ was also observed in previous incubations of anaerobic NH_4^+ oxidation and was attributed to carbon mineralization (Dalsgaard and Thamdrup, 2002, Bartlett et al., 2008), suggesting that similar processes may be responsible for the production of NH_4^+ in these incubations (T1, T2, T5, and T6). In contrast, the consumption rate of NH_4^+ in the colloidal MnO_2 treatments (T3 and T4) during the first 10 days was approximately 15 fold higher in the presence of NH_4^+ (T4) than that without NH_4^+ (T3) (Table 5.3). In the later period of the incubations (after 10 days), however, concentrations of NH_4^+ recovered in both T3 and T4 and the production rate of NH_4^+ was higher in T4 than T3

(Figure 5.3-d). Simultaneously, the production of nitrate and nitrite were significantly higher in the incubations amended with colloidal MnO_2 and NH_4^+ (T4) than those in the controls without either colloidal MnO_2 or NH_4^+ or both (T1, T2, and T3) (Figure 5.3 e and f). A maximum of 30 μM nitrate was detected during the first 5 days of the incubations in T4, followed by a slight decrease and subsequent rebound after 12 days (Figure 5.3-e), and the production rate of nitrate during the first 10 days was higher in the colloidal (T3 and T4) than the amorphous (T5 and T6) treatments (Table 5.3). The temporal evolution of nitrite mirrored that of nitrate in the same incubation (T4) (Figure 5.3 e and f). Nitrite was produced around 5 days, though with a maximum of 5 μM only, and consumed in the latter part of the incubations (Figure 5.3-f). Production of nitrite, but not nitrate, was also detected in the incubations amended with both amorphous MnO_2 and NH_4^+ (T6), compared to its corresponding controls (T1, T2, and T5), albeit after a longer phase lag than for the colloidal MnO_2 incubations. As N_2 is also proposed as an alternative product of Mn(IV)-catalyzed anaerobic NH_4^+ oxidation (Luther et al., 1997), production of $^{29}N_2$ and $^{30}N_2$ due to the oxidation of $^{15}NH_4^+$ was also measured in all the treatments (Figure 5.3-f and g). Although slightly higher concentrations of $^{29}N_2$ and $^{30}N_2$ were detected in the treatment amended with both colloidal MnO_2 and NH_4^+ (T4), compared to other treatments, concentrations of $^{29}N_2$ and $^{30}N_2$ in the incubations were generally maintained at background levels (less than 0.1 μM) (Figure 5.3).

Production of DIC increased dramatically after 10 days (Figure 5.3-c), which may be due to sulfate reduction observed in the later period of the incubations. Significant decrease of soluble Fe^{2+} (Figure 5.3-b) was accompanied by the formation of black precipitates after 10 days in both treatments amended with colloidal MnO_2 (T3 and T4)

(Figure 5.4), suggesting that FeS precipitated during the incubations despite the fact that dissolved sulfide was not detected in these incubations (not shown). Acid volatile sulfide (AVS) extraction of the solid phase detected 3.0 ± 0.1 mmol sulfide /L in these two treatments (T3 and T4) at the end of the incubations, while less than 0.1 mmol sulfide /L was extracted from the other treatments. These results confirmed the production of sulfide via sulfate reduction and suggested a significant change of electron accepting processes at around 10 days. This transition at around 10 days may also be observed from the temporal evolution patterns of Mn and N species in the colloidal treatments (T3 and T4) (Figure 5.3).

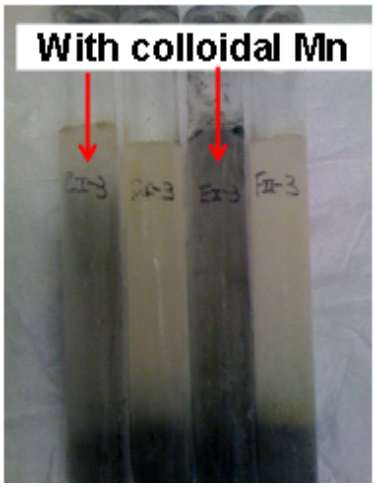

Figure 5.4. Formation of black precipitates in the colloidal treatments (red arrows) after 10 days of incubation compared to the amorphous treatments.

To determine whether amorphous MnO_2 is able to catalyze anaerobic nitrification over longer periods of time, the amorphous MnO_2 incubations (T5 and T6) along with their control treatments (T1 and T2) were incubated up to 100 days with periodic

replenishment of each reactant (NH_4^+, amorphous MnO_2, or both) (Figure 5.5). The evolutions of all species (DIC, Mn^{2+}, NH_4^+, NO_2^-) during these extended incubations, however, yielded similar patterns as observed in the 18 day long incubations and showed insignificant levels of anaerobic nitrification (T5 and T6 in Figure 5.3). Concentrations of NH_4^+ generally remained slightly higher in the incubations amended with amorphous MnO_2 (T5 and T6) compared to their corresponding controls (T1 and T2) (Figure 5.5-a). Simultaneously, the reduction of amorphous MnO_2 and the production of DIC were continuously observed after each replenishment in T5 and T6 (Figure 5.5-b and d), while the production of nitrite was maintained at low levels (< 2 μM) except for a couple of time points after each replenishment (Figure 5.5-c). Nitrite production was slightly higher in T6 than other treatments during the first 50 days; however, this difference diminished after the second replenishment at around 50 days (Figure 5.5-c). Finally, nitrate concentrations were close to the detection limit in all the treatments (T1, T2, T5, and T6) (data not shown), as already demonstrated during the 18-day incubations.

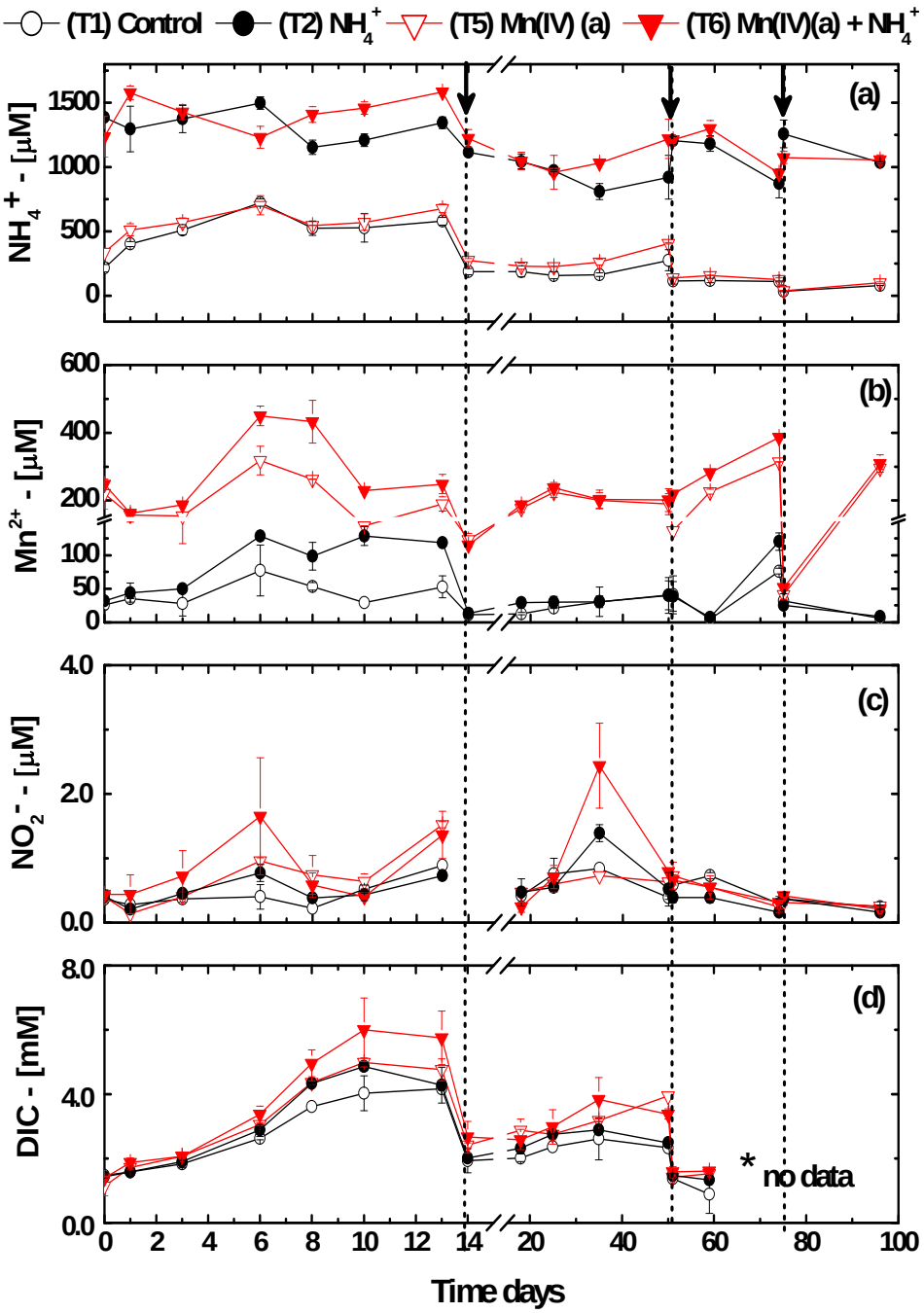

Figure 5.5. Evolution of (a) Mn^{2+}, (b) NH_4^+, (c) NO_2^-, and (d) dissolved inorganic carbon (DIC) as a function of time in extended anaerobic slurry incubations conducted without any amendment (T1, control, open circles) or in the presence of 800 µM NH_4^+ (T2, solid circles), 300 µM amorphous MnO_2 (T5, open red downward triangles), and 800 µM NH_4^+ and 300 µM amorphous MnO_2 (T6, solid red downward triangles). Black arrows indicate the days (14, 51, and 75) at which each treatment was replenished with their corresponding reactants. The error bars represent the standard deviations of duplicate incubations.

5.3.3 Batch incubations under different initial conditions of sulfate and nitrate

The effect of nitrate and sulfate on Mn-mediated anaerobic nitrification was investigated by two independent sets of incubations, including (1) incubations amended with excess nitrate (50 μM) and the control incubations without nitrate (Figure 5.6) and (2) incubations depleted in sulfate (1 mM compared to 15 mM) as well as their original control incubations (15 mM sulfate) (Figure 5.7). In these control incubations, the consumption of NH_4^+, accompanied by an increase in Mn(II) and nitrate concentrations, was only observed in the incubations amended with colloidal MnO_2 and NH_4^+ (T4) (Figure 5.6-(a_0 and d_0) and Figure 5.7-(a_0 and d_0)). In the incubations with low sulfate concentrations (1 mM), the concentrations of Mn(II) and NH_4^+ in all the different treatments (i.e. unamended control (T1), NH_4^+-only (T2), $MnO_{2(c)}$-only (T3), and NH_4^+ and $MnO_{2(c)}$ (T4)) were similar to those of the original incubations conducted in the presence of 15 mM of sulfate (Figure 5.6-a and b), but concentrations of nitrate increased in the treatment amended with both NH_4^+ and $MnO_{2(c)}$ (T4) compared to their respective controls (T1, T2, and T3) (Figure 5.6-d). In addition, concentrations of DIC and nitrite were generally lower in all low-sulfate incubations than their respective treatments in the high-sulfate incubations (original control) (Figure 5.6-c and e). In the incubations amended with 50 μM nitrate, the concentrations of nitrite and DIC in all treatments (T1 – T4) were similar to their respective treatments conducted in the original incubations without initial nitrate amendment (Figure 5.7-c and e). At the end of these nitrate-amended incubations, however, concentrations of Mn(II) were higher and NH_4^+ concentrations lower in the treatments amended with both NH_4^+ and $MnO_{2(c)}$ (T4), compared to the nitrate-unamended incubations (Figure 5.7-a and b). In addition, while

the initial concentrations of nitrate were much higher in the nitrate-amended incubations, the least decrease in nitrate during these 10-day long incubations was detected in the presence of NH_4^+ and $MnO_{2(c)}$ (T4) (Figure 5.7-d).

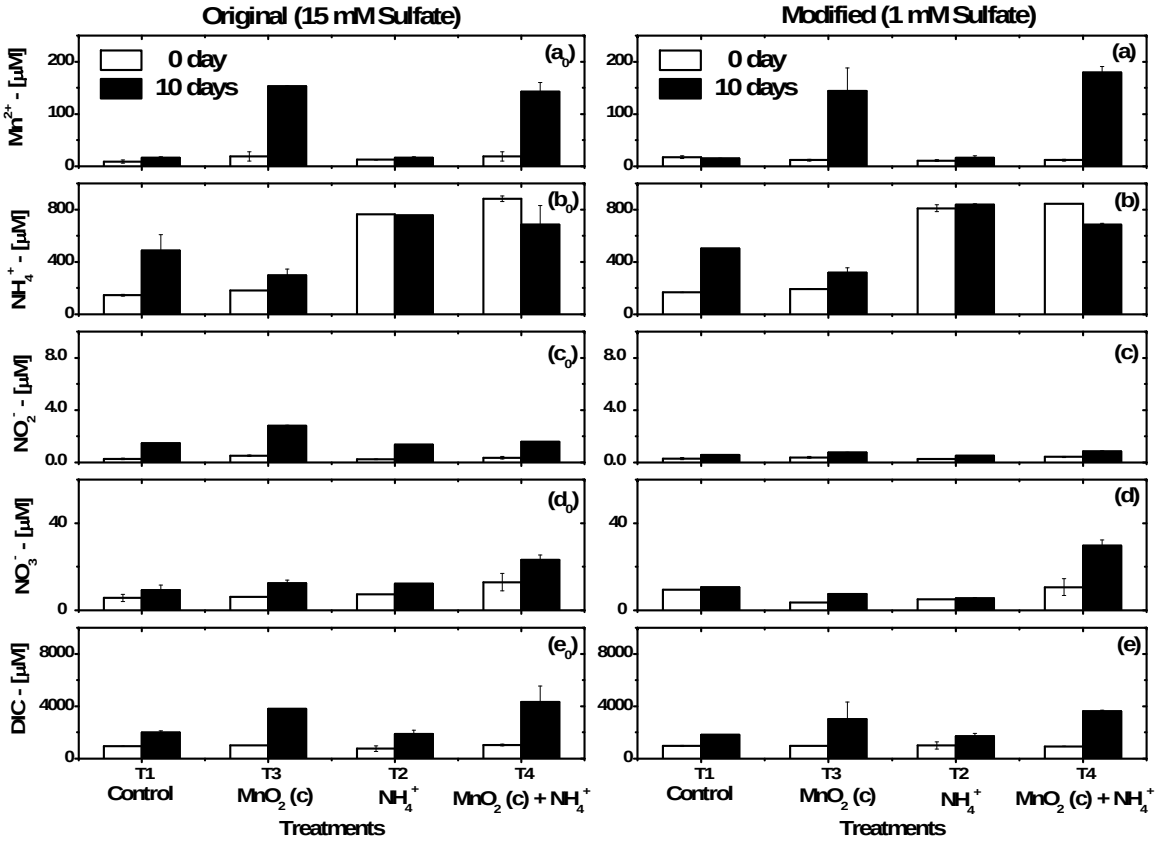

Figure 5.6. Concentrations of dissolved Mn^{2+}, NH_4^+, NO_3^-, NO_2^-, and inorganic carbon (DIC) initially (open columns) and after 10 days (closed columns) in anaerobic slurry incubations conducted in high (original sulfate level, 15mM, left column, (a_0) – (e_0)) and low (modified sulfate level, 1mM, right column, (a) – (e)) sulfate concentrations. The x-axis represents different treatments, including the no amendment control (T1) and the treatments amended with 600 μM NH_4^+ (T2), 200 μM colloidal MnO_2 (T3), and 600 μM NH_4^+ and 200 μM colloidal MnO_2 (T4). The error bars represent the standard deviations of duplicate incubations.

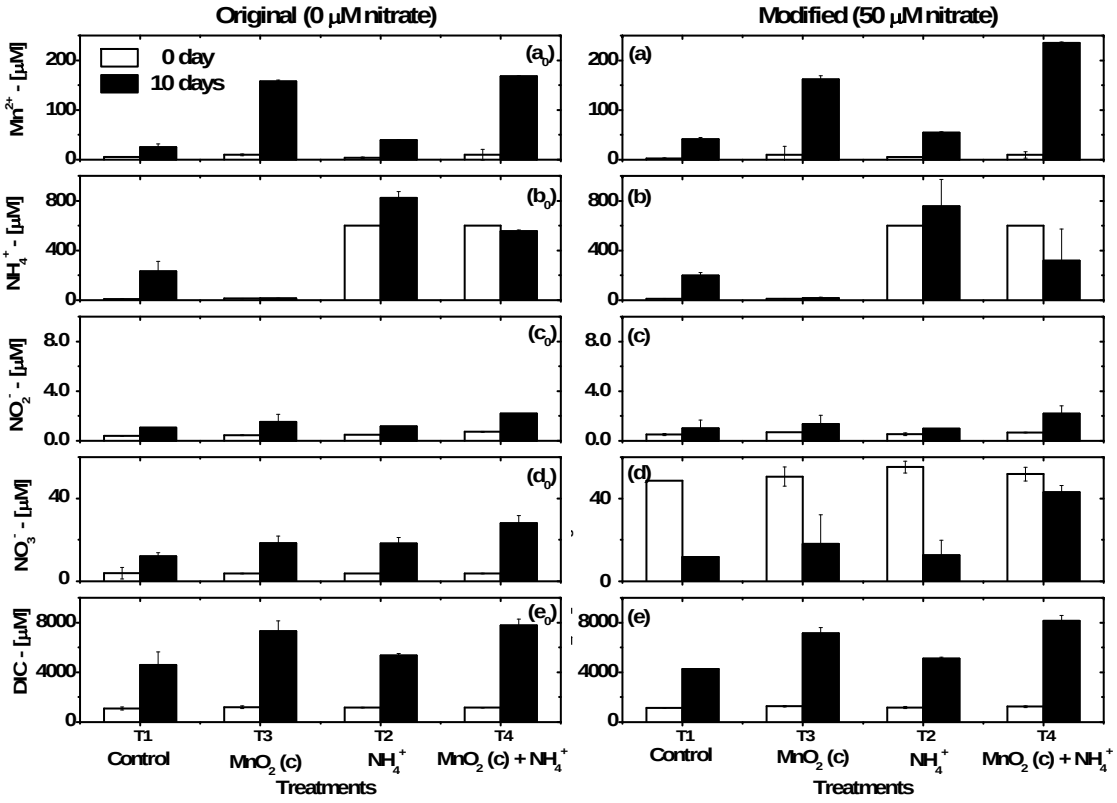

Figure 5.7. Concentrations of dissolved Mn^{2+}, NH_4^+, NO_3^-, NO_2^-, and inorganic carbon (DIC) initially (open columns) and after 10 days (closed columns) in anaerobic slurry incubations conducted in without (original, left column, (a_0) – (e_0)) and with (modified, right column, (a) – (e)) 50 μM of initial nitrate addition. The x-axis represents different treatments, including the no amendment control (T1) and the treatments amended with 600 μM NH_4^+ (T2), 200 μM colloidal MnO_2 (T3), and 600 μM NH_4^+ and 200 μM colloidal MnO_2 (T4). The error bars represent the standard deviations of duplicate incubations.

The changes in concentration (ΔC) of each species in the different treatments were obtained from the difference in concentrations between the end (10 days) and the beginning (0 day) of the incubations. Considering the high background noise in the slurry incubations, a differentiated change ($[\Delta C]_D$) for the colloidal MnO_2 incubations (T3 and T4) was calculated by subtracting the change in concentration of each species in their corresponding controls (T1 or T2) from their change in the amended incubations (T3 or

T4). (Eq. 5.15 and 5.16). The differentiated change of each species, representing the production or consumption caused by the amendment of colloidal MnO_2 in the presence (T4) or without NH_4^+ (T3), was then used to evaluate the effect of the two modifications of the medium (i.e. decrease in sulfate and increase in nitrate) on the Mn-mediated anaerobic nitrification (Figure 5.8).

$$[\Delta C_{T3}]_D = \Delta C_{T3} - \Delta C_{T1} \quad \text{(Eq. 5.15)}$$

$$[\Delta C_{T4}]_D = \Delta C_{T4} - \Delta C_{T2} \quad \text{(Eq. 5.16)}$$

While the production of Mn(II) and nitrite and the consumption of NH_4^+ in the treatment amended with colloidal MnO_2 only (T3) and both $MnO_{2(c)}$ and NH_4^+ (T4) were similar between the original (15 mM) and low-sulfate (1 mM) incubations, the production of DIC in these two colloidal treatments (T3 and T4) decreased approximately 33% (T3) and 8% (T4) in the low sulfate incubations (Figure 5.8-a and b), likely due to the inhibition of sulfate reduction. More importantly, a slight increase in the nitrate production was observed in the low-sulfate incubations amended with $MnO_{2(c)}$ only (T3) compared to the high sulfate incubations (Figure 5.8-a), and this increase was much more pronounced in the presence of both colloidal MnO_2 and NH_4^+ (T4) (Figure 5.8-b).

When nitrate was initially added to the incubations, the changes in the production or consumption of each species in the incubations amended with colloidal MnO_2 only (T3) were trivial (Figure 5.8-c). In contrast, the effect of nitrate addition on the incubations amended with both colloidal MnO_2 and NH_4^+ (T4) was more pronounced (Figure 5.8-d). The production of Mn(II) and the consumption of NH_4^+ were significantly increased when the incubations were spiked with 50 μM nitrate initially, while the production of DIC was much less significant (Figure 5.8-d). More importantly, the initial addition of

small concentrations of nitrate also enhanced the final production of nitrate in the incubations amended with colloidal MnO_2 and NH_4^+ (T4) (Figure 5.8-d).

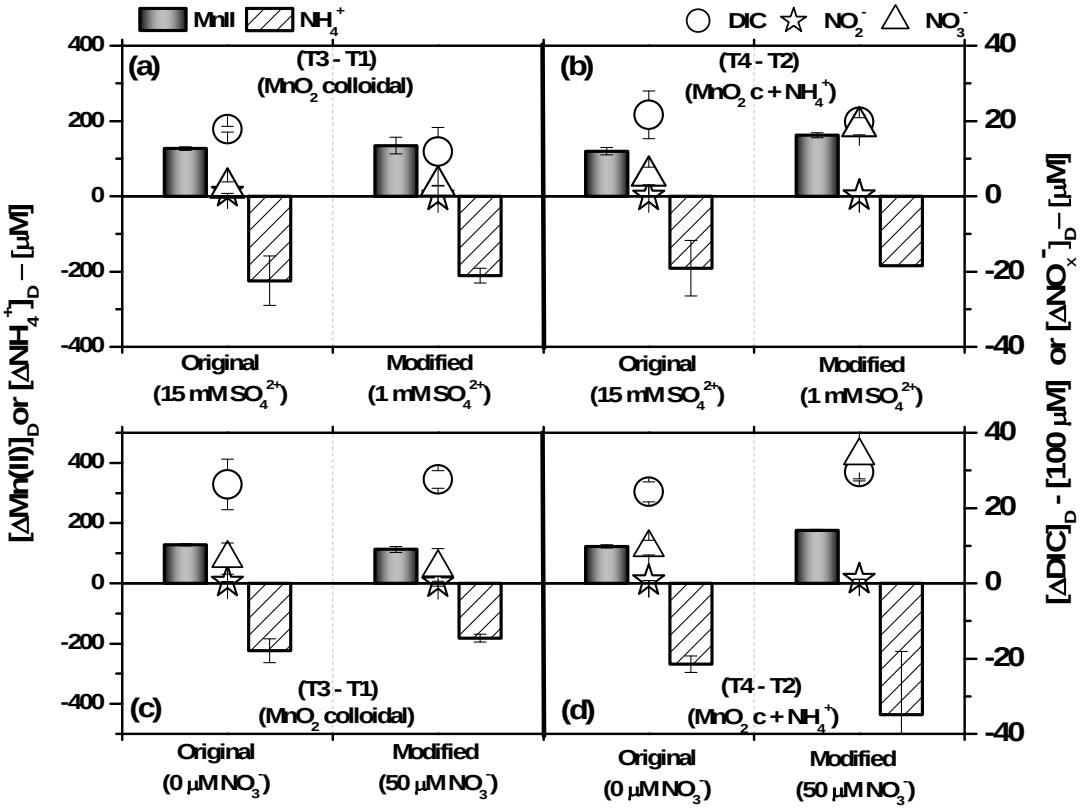

Figure 5.8. Differentiated changes (production or consumption) ($[\Delta C]_D$) of Mn^{2+} (left y-axis), NH_4^+ (left y-axis), NO_3^- (right y-axis), NO_2^- (right y-axis), and dissolved inorganic carbon (DIC) (right y-axis) during two separate sets of independent incubations modified or not with (1) less sulfate (a and b) and (2) more nitrate (c and d) in the incubation medium. (a) and (c) showed $[\Delta C]_D$ of each species in both the original and modified incubations amended with colloidal MnO_2 (T3). (b) and (d) showed $[\Delta C]_D$ of each species in both the original and modified incubations amended with colloidal MnO_2 and NH_4^+ (T4). The calculation of $[\Delta C]_D$ was shown in the text. The error bars represent the standard deviations of duplicate incubations and the calculations.

5.3.4 Batch incubations amended with $^{15}NO_3^-$ only

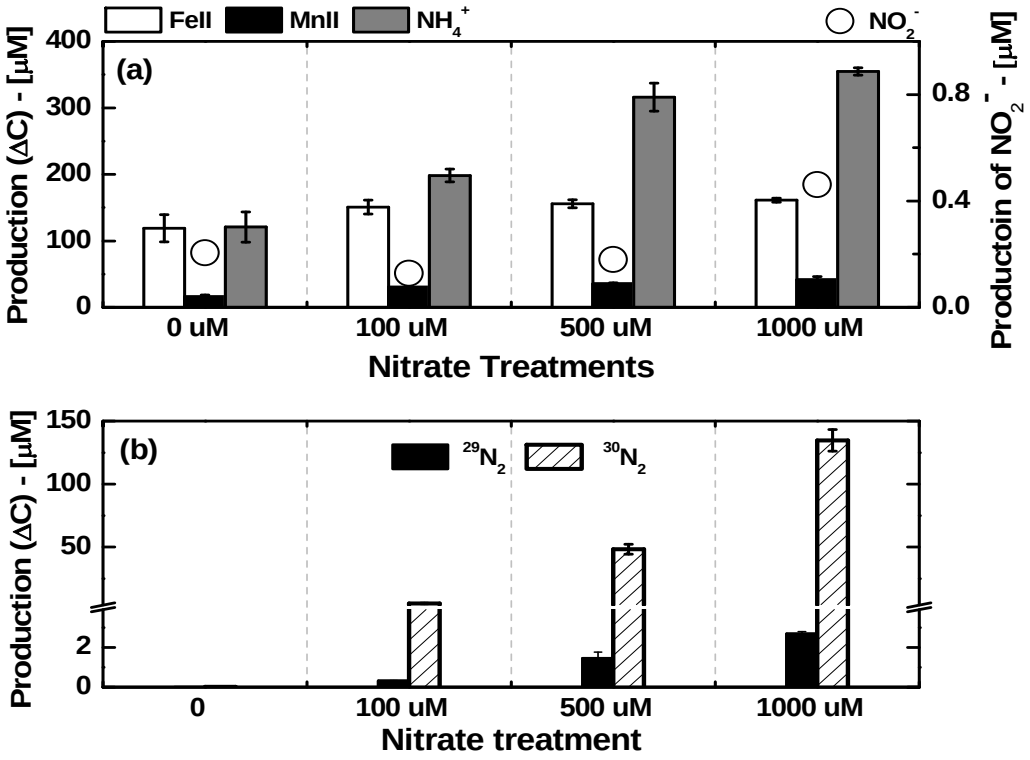

Figure 5.9. Production (ΔC) of Mn^{2+}, NH_4^+, Fe^{2+} (a, left y-axis), NO_2^- (a, right y-axis), and $^{29}N_2$ and $^{30}N_2$ (b) during separate sets of independent incubations amended with increasing initial concentrations of $^{15}NO_3^-$. ΔC represents the change in each species between the beginning and end of these 20-day incubations. The error bars include error propagation of the different incubations conducted in duplicate.

Different levels of nitrate (but no MnO_2, nor NH_4^+) were initially amended in independent incubations to determine whether denitrification plays an important role in these sediments (Figure 5.9). At the end of these 20-day long incubations, the consumption of nitrate was complete in all incubations, regardless of the initial concentration of nitrate (0, 100, 500, or 1000 μM). Simultaneously, the production of NH_4^+ was significantly enhanced as nitrate levels were increased in the different treatments, while the production of Fe(II) and Mn(II) remained similar and the

concentration of nitrite was maintained at low levels (< 0.5 μM) (Figure 5.9-a). As $^{15}NO_3^-$ was amended into the current incubations, $^{29}N_2$ and $^{30}N_2$ were produced as a result of anammox and denitrification (Thamdrup et al., 2006) (Figure 5.9-b). The production of $^{29}N_2$ was much less than that of $^{30}N_2$, suggesting denitrification but not anammox as the main N_2 formation pathway in these incubations. The differentiated change ($[\Delta C]_D$), or the control-subtracted change of each species in the nitrate amended incubations, was also used to evaluate the effect of nitrate addition on nitrate reduction and denitrification (Table 5.4). Only 10-25% of total $^{15}NO_3^-$ was converted to $^{30}N_2$, which represented the denitrification activity in the current incubations (Table 5.4). In turn, the differentiated production of NH_4^+ was positively correlated to the initial concentration of nitrate in each treatment (Table 5.4), which implied the possibility of ammonium production via dissimilatory nitrate reduction to ammonium (DNRA) in these incubations (An and Gardner, 2002). DNRA may account for as much as 80% of nitrate consumption in the treatment amended with 100 μM of $^{15}NO_3^-$ (Table 5.4). These results suggested that DNRA may be more significant than denitrification in the current sediment incubations, especially in low initial nitrate conditions (100 μM).

Table 5.4. Differentiated change ($[\Delta C]_D$, μM) of $^{29}N_2$, $^{30}N_2$, and NH_4^+ in the incubations amended with different levels of $^{15}NO_3^-$ (100, 500, or 1000 μM). The differentiated change ($[\Delta C]_D$) was obtained by subtracting the change in the control without nitrate from the change in each of the $^{15}NO_3^-$ amended incubations. Error bars represent the error propagation from duplicate incubations.

$^{15}NO_3^-$ amended (μM)	**$([\Delta C]_D)$ - $^{29}N_2$ (μM)**	**$([\Delta C]_D)$ - $^{30}N_2$ (μM)**	**$([\Delta C]_D)$ - NH_4^+ (μM)**
100	0.3 ± 0.01	5.3 ± 0.2	78 ± 28
500	1.5 ± 0.3	48 ± 4	195 ± 14
1000	2.7 ± 0.1	135 ± 9	234 ± 32

5.4 Discussion

The anaerobic oxidation of ammonium coupled to MnO_2 reduction has been proposed more than a decade ago (Hulth et al., 1999, Mortimer et al., 2004, Bartlett et al., 2008, Javanaud et al., 2011, Luther et al., 1997), yet direct evidence of this process from both field and laboratory studies is still lacking (Thamdrup and Dalsgaard, 2000, Bartlett et al., 2007). To investigate the effect of Mn(IV) oxides on the redox cycle of nitrogen, laboratory incubations were conducted with sediments selected for their ability to reduce manganese oxides and produce nitrite and nitrate well below the oxygen penetration depth. Factors that may affect the interaction between Mn and N species were also considered to investigate the existence of anaerobic nitrification by MnO_2 in marine sediments.

5.4.1 Evidence for Mn-mediated anaerobic nitrification

Production of nitrite and nitrate via aerobic nitrification was likely negligible in the current incubations, considering the following: (1) all the incubations were conducted in sealed serum bottles initially purged with Ar gas and stored under a N_2:H_2:CO_2 atmosphere, (2) concentrations of dissolved O_2 were consistently below the detection limit of electrochemical measurements (~ 4 μM) (Taillefert et al., 2007b) and such levels of dissolved oxygen should not produce more than 2.5 μM nitrite or nitrate according to the stoichiometry of aerobic nitrification, and (3) soluble Fe^{2+}, the most reactive reductant of dissolved oxygen, was present in significant concentrations (> 100 μM) during the incubations (Figure 5.3 - b). Therefore, the increase in nitrite or nitrate concentrations in the current incubations can be attributed to anaerobic production of nitrite or nitrate.

Evidence of anaerobic nitrification was observed in the incubations amended with colloidal MnO_2 (Figure 5.3 and Figure 5.10). The significant production of Mn^{2+}, NO_2^-, and NO_3^- and the removal of NH_4^+ over the first 10 days (Figure 5.3) suggest that anaerobic nitrification occurs in the first part of the incubations amended with colloidal MnO_2 and NH_4^+ (T4). The production of $FeS_{(s)}$ at the end of incubations, along with the large increase in dissolved inorganic carbon suggest that the dominant electron accepting processes may shift from Mn(IV) reduction to sulfate reduction after 10 days. Therefore, the results of the current slurry incubations appear to represent two distinct biological processes, and only the first 10 days were considered to investigate the effect of Mn oxides on the cycle of nitrogen species (Figure 5.10-a and b). The differentiated change ($[\Delta C]_D$, net production or consumption) of each species during the incubations was used to compare the effect of the different MnO_2 treatments (T3, T4, T5, and T6) (Figure 5.10).

During the first 10 days of the incubations, addition of colloidal MnO_2 resulted in significant consumption of NH_4^+ and production of nitrate (Figure 5.10-a), indicating that anaerobic nitrification is catalyzed by addition of colloidal MnO_2. Incubations amended with colloidal MnO_2 and high initial concentration of NH_4^+ (T4) displayed more NH_4^+ consumption, more production of nitrate and Mn(II), but similar DIC production, compared to the incubations amended with colloidal MnO_2 only (T3, Figure 5.10-a). A previous study, that investigated the effect of the initial ratio of NH_4^+ and MnO_2 on the correlation of MnO_2 reduction and NH_4^+ consumption proposed that a N:Mn ratio between 2 and 10 was optimal to promote anaerobic nitrification (Newton, 2006). Thus, the enhanced formation of nitrate and the higher consumption of NH_4^+ when ammonium was added to the incubations (T4 compared to T3) may be due to the different initial

N:Mn ratio in these two treatments. Although production of Mn(II) was higher in the sediment amended with amorphous MnO_2 (T5 and T6) than colloidal MnO_2 (T3 and T4) irrespective of the presence or absence of NH_4^+, the consumption of NH_4^+ and production of nitrate were much lower in the presence of amorphous MnO_2 (T6, Figure 5.10-a). In addition, 274 ± 11 μM of Mn(II) was produced in treatment amended with colloidal MnO_2 and ammonium (T4), which should have accounted for approximately 60 μM of nitrate production if Mn(IV) reduction was entirely linked to anaerobic nitrification. As only 10 μM of nitrate was produced in these incubations (Figure 5.10-a) and the initial rates of Mn(II) and nitrate production also present similar disparities (Table 5.3), these results demonstrate that Mn(IV) reduction is partly heterotrophic. The higher rate of initial DIC production during the first 10 days in all MnO_2-amended incubations (T3 to T6) compared to their unamended counterparts (T1 and T2) corroborates these findings (Table 5.3). Although heterotrophic Mn(IV) reduction coupled to DIC production was proposed to compete with Mn(IV)-catalyzed anaerobic nitrification (Bartlett et al., 2007), the current results imply no competition between these two Mn(IV) reduction processes.

In the second period of the incubations (10 - 18 days), reduction of Mn(IV) stopped due to the depletion of MnO_2 and concentrations of Mn(II) decreased (Figure 5.10-b), which may be caused by a secondary precipitation of soluble Mn(II) under conditions of increasing carbonate production (Van Cappellen et al., 1998). Loss of NH_4^+ and production of nitrate were repressed during this period in the treatments amended with colloidal MnO_2 (Figure 5.10-b). Indeed, after depletion of colloidal MnO_2 around 10 days, anaerobic nitrification became insignificant in both incubations amended with colloidal MnO_2 (T3 and T4) (Figure 5.10-b). Simultaneously, the net balance of NH_4^+

turned positive during this period, which may be attributed to the increase in ammonification during the mineralization of organic matter as evidenced by the increase in DIC production during the latter part of these incubations (Figure 5.10-b). The Mn-mediated denitrification of ammonium (Javanaud et al., 2011) was not observed in the current incubations as the production of both $^{29}N_2$ and $^{30}N_2$ remained trivial throughout the incubations (Figure 5.3). These results suggest that denitrification and anammox may be insignificant in the current incubations, as a result of either (1) competitive nitrate consumption via dissimilatory nitrate reduction to ammonium (DNRA) (Table 5.4) (An and Gardner, 2002), (2) a switch in the dominant terminal electron accepting process from Mn(IV) reduction to sulfate reduction (Bartlett et al., 2008), or (3) the inhibitory effects of sulfide on denitrification (Brunet and GarciaGil, 1996) or anammox (Jetten et al., 2009).

In summary, production of nitrate and consumption of NH_4^+ were stimulated by the addition of colloidal MnO_2, suggesting the occurrence of Mn-catalyzed anaerobic nitrification. However, due to the complexity of sediment incubations, consumption of NH_4^+ may be affected by several other processes, such as adsorption on solid surface or assimilation of NH_4^+ by microorganisms, which are not directly related to the oxidation of ammonium. In the next section, the fate of NH_4^+ was investigated to demonstrate that consumption of NH_4^+ in the colloidal treatments (T4) is at least partially caused by anaerobic oxidation of NH_4^+.

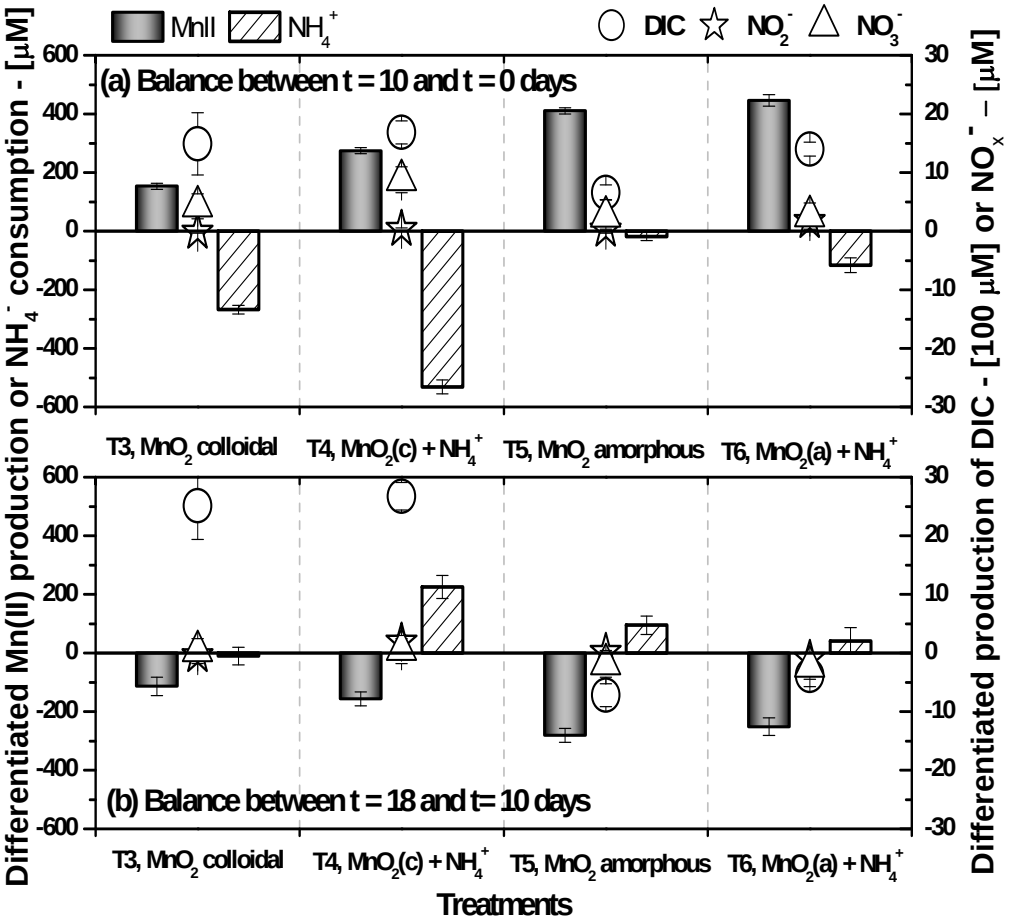

Figure 5.10. Differentiated changes ($[\Delta C]_D$, production or consumption) of Mn^{2+} (μM, left y-axis, grey bars), NH_4^+ (μM, left y-axis, shaded bars), NO_3^- (μM, right y-axis, triangles), NO_2^- (μM, right y-axis, stars), and dissolved inorganic carbon (DIC) (mM, right y-axis, circles) during the incubations amended with either colloidal (T3 and T4) or amorphous (T5 and T6) MnO_2, including (A) the first 10 days and (B) the second part of the incubations. A negative value represents a decrease in production compared to the control. The error bars represent the error propagation calculated from duplicate incubations.

5.4.2 Fate of NH_4^+ in the incubations

Processes that may affect the distribution of NH_4^+ in each treatment were divided into two categories, (1) redox processes, including denitrification, nitrification, nitrogen

fixation, anammox, dissimilatory nitrate reduction to ammonium (DNRA), and anaerobic oxidation of NH_4^+ and (2) non-redox processes, including adsorption/desorption, ammonification, and assimilation of NH_4^+ during growth of microorganisms. As all the incubations were conducted under strict anaerobic conditions in the dark with initial concentrations of nitrate or nitrite less than 5 μM, denitrification, DNRA, aerobic nitrification, nitrogen fixation, and anammox can be considered minor processes initially. Therefore, during the first part of the incubations, the major sources of NH_4^+ in the slurry solutions were likely non-redox processes, including the release from solid phase sediments (Mackin and Aller, 1984) and ammonification (mineralization) (Dalsgaard and Thamdrup, 2002), while the sinks of NH_4^+ included either anaerobic oxidation of NH_4^+ or non-redox processes (i.e. adsorption and assimilation of NH_4^+). A mass balance approach (described in method section 5.2) that accounts for the consumption of ammonium via anaerobic NH_4^+ oxidation ($\Delta[NH_4^+]_{an.\text{-}oxid}$) and three major non-redox sinks and sources of ammonium was employed to estimate the possible NH_4^+ consumption attributed to the Mn-catalyzed anaerobic oxidation of NH_4^+ (Eq. 5.1 and Eq. 5.14). According to the mass balance equation (Eq. 5.1), any positive value of $\Delta[NH_4^+]_{an.\text{-}oxid.}$ indicates an alternative NH_4^+ consumption process that can be attributed to the anaerobic oxidation of NH_4^+. The mass balance calculation for NH_4^+ was considered only during the first 10 days of the incubations to assess the effect of Mn(IV) reduction on the balance of NH_4^+ (Table 5.5).

Changes in the different sink and source terms in the different incubations are reported in Table 5.5, along with the contribution of anaerobic oxidation to the removal of NH_4^+. These calculations reveal that the incubations amended with NH_4^+ only (T2) and with both amorphous MnO_2 and NH_4^+ (T6) are approximately balanced with respect to

NH_4^+, suggesting that anaerobic nitrification was not significant in these incubations. In turn, a significant consumption of NH_4^+ ($\Delta[NH_4^+]_{anaerobic}$ = 157 ± 60 μM) is evident in the incubations amended with both colloidal Mn(IV) and NH_4^+ (T4), indicating that anaerobic ammonium oxidation accounts for a significant fraction of NH_4^+ consumption in this incubation (Table 5.5).

Table 5.5. Changes in NH_4^+ concentrations in solution ($\Delta[NH_4^+]_{solution}$, μM) measured during the first 10 days of incubations in each treatment along with the changes in NH_4^+ concentrations due to non-redox processes (i.e. adsorption, ammonification, and assimilation) estimated from theoretical considerations, and anaerobic nitrification ($\Delta[NH_4^+]_{an.-oxid.}$, μM) estimated from mass balance (Eq. 5.13). Positive values represent alternative consumption of NH_4^+ while negative values represent alternative production of NH_4^+ in the slurries. *Y_{XD} (apparent yield coefficient) for NH_4^+ assimilation was calculated based on the assumption that it was not affected by the addition of NH_4^+ and that no other processes were involved in the removal/production of NH_4^+ in treatments without addition of NH_4^+ (T1, T3, and T5). Errors associated with the different calculations are shown in parenthesis.

Treatments	$\Delta[NH_4^+]$ solution	$\Delta[NH_4^+]$ adsorption	$\Delta[NH_4^+]$ ammonification	$\Delta[NH_4^+]$ assimilation	Y_{XD}*	$\Delta[NH_4^+]_{an.-oxid.}$ μM/L
(T1) Control	33 (± 11)	9 (± 3)	33 (± 9)	-9 (± 3)	-0.11	0 (± 15)
(T2) NH_4^+	83 (± 13)	22 (± 3)	88 (± 1)	-24 (± 0.3)	-0.11	8 (± 14)
(T3) MnIV c	-176 (± 11)	-47 (± 3)	159 (± 30)	382 (± 51)	0.97	0 (± 57)
(T4) MnIV c + NH_4^+	-372 (± 28)	-99 (± 7)	225 (± 27)	539 (± 45)	0.97	**157 (± 60)**
(T5) MnIV a	41 (± 9)	11 (± 2)	93 (± 11)	41 (± 4)	0.18	0 (± 14)
(T6) MnIV a + NH_4^+	79 (± 8)	21 (± 2)	165 (± 2)	72 (± 1)	0.18	-8 (± 8)

5.4.3 Factors that affect Mn(IV)-catalyzed anaerobic nitrification

Direct field observation of Mn-catalyzed anaerobic nitrification is difficult, considering the complexity of the redox cycles of N and Mn and the high reactivity of nitrite and nitrate in anaerobic environments. As a result, sediment manipulations in the laboratory have been used extensively to investigate the coupling between Mn reduction and anaerobic ammonium oxidation (Bartlett et al., 2008, Hulth et al., 2005). The current

laboratory incubations provided clear evidence that addition of colloidal Mn oxides results in the consumption of NH_4^+ and production of nitrate and nitrite, suggesting that the reduction of colloidal MnO_2 is coupled to the anaerobic nitrification of ammonium. Interestingly, a similar effect was not observed in the incubations amended with amorphous Mn oxides (Figure 5.10). Previous studies have suggested that the perturbation of sediments, such as slumping or fresh burial events of Mn oxides, may stimulate anaerobic nitrification (Mortimer et al., 2004, Anschutz et al., 2000). The results of the present study reveal that the reactivity of Mn oxides may also play an important role in triggering the Mn(IV)-catalyzed anaerobic nitrification process. Indeed, soluble forms of Mn oxides (colloidal MnO_2), with their large specific surface area, may enhance the reactivity and oxidizing capacity of Mn oxides compared to amorphous MnO_2 (Perezbenito et al., 1987, Perezbenito and Arias, 1992, Perez-Benito, 2002). Similarly, fresh Mn(III) oxyhydroxides have been shown to display higher reactivity in catalyzing anaerobic nitrification than Mn(IV) oxides (Anschutz et al., 2005). Results from the present study indicate that the reactivity of Mn oxides, which may also be affected by physical perturbations in natural sediments (Mortimer et al., 2004), may be the most important constraint on the Mn(IV)-catalyzed anaerobic nitrification process.

Besides the property of Mn oxides, anaerobic nitrification may also be affected by the occurrence of sulfate reduction and the presence of nitrate. Sulfate reduction during Mn(IV)-catalyzed anaerobic nitrification was already observed in previous slurry incubations (Hulth et al., 1999, Bartlett et al., 2008) but its effect never discussed. Other incubations that demonstrated Mn(IV)-mediated anaerobic nitrification were conducted in sulfate-free artificial seawater or in the presence of high concentrations of molybdate

to inhibit sulfate reduction (Javanaud et al., 2011). In the present study, anaerobic nitrification in the presence of colloidal MnO_2 and NH_4^+ in low sulfate conditions was more significant compared to identical incubations in high sulfate conditions (Figure 5.8-b). Low sulfate environments may either lead to (1) a delay of sulfate reduction or (2) an increase in the reduction potential of the sediment, which may in turn facilitate the coupling of Mn(IV) reduction to anaerobic nitrification. Indeed, slurry incubations amended with small concentrations of nitrate have been found to promoted Mn-catalyzed anaerobic nitrification (Newton, 2006, Javanaud et al., 2011), despite the fact that such incubations were not compared to unamended controls. In the current study, anaerobic nitrification was significantly higher in the presence of ammonium and colloidal Mn oxides (T3 and T4) when 50 μM of nitrate were initially added to the incubations, compared to identical incubations performed without nitrate addition (Figure 5.8-d). These findings suggest that addition of nitrate increases the initial redox potential in the slurry system (Froelich et al., 1979) and may favor the anaerobic oxidation of ammonium. Simultaneously, addition of nitrate stimulated dissimilatory nitrate reduction to ammonium (DNRA) in these sediments (Figure 5.9), which may also enhance anaerobic nitrification catalyzed by Mn(IV) oxides.

Overall, the anaerobic nitrification catalyzed by Mn(IV) oxides is likely to be of great importance in anaerobic sediments with high ammonium concentrations, active recycling of Mn(IV) oxides and NH_4^+, and a moderate redox potential. This alternative pathway may be able to provide nitrite/nitrate for anammox bacteria and, in turn, promote anammox activity in these sediments. The nitrite/nitrate supply for anammox bacteria in anaerobic sediments may play an important role in regulating the significance of

anammox versus denitrification as the main nitrogen loss pathway in the marine nitrogen budget, a controversial topic in the literature (Lam et al., 2009, Ward et al., 2009). The maximum anaerobic production rate of nitrate was estimated as 4.6 ± 0.5 μM/day based on the current incubations (Table 5.3). Therefore, considering a sediment dilution factor of 12 used in these experiments (2.5 ml of salt marsh sediments into 30 ml of slurry) and depth of the sediments tested in the current incubations (2 cm), Mn(IV)-catalyzed anaerobic nitrification may account for $(1.1 \pm 0.1) \times 10^{-7}$ mol nitrate/cm^2/day of the nitrate flux in these sediments. If applicable to global scale, anaerobic nitrification may contribute 5.0 ± 0.57 Tg N/yr of nitrate input for subsequence nitrogen loss in the marine nitrogen budget. This number only balances 2% of total benthic denitrification in the oceans. In coastal sediments, however, the contribution of anaerobic nitrification to the nitrogen budget should be much more significant as the upward flux of ammonium to the sediment surface is much higher than in the average ocean.

5.5 Conclusions

The uncertainty in current understanding of marine nitrogen budget suggests that alternative N-transformation pathways may exist in marine environments. Among these processes, the reduction of Mn(IV) oxides coupled to anaerobic ammonium oxidation has been proposed for more than a decade to contribute to the fixed nitrogen pool in marine sediments, yet the existence of this process is still under debate. Results from the present study demonstrate the existence of anaerobic nitrification in sediments (from Skidaway salt marsh) with elevated concentrations of Mn-oxides. Anaerobic nitrification was enhanced in the presence of high initial concentrations of NH_4^+, suggesting that the initial ratio of MnO_2 and NH_4^+ has a significant effect on this process. In addition, anaerobic

nitrification was only observed when Mn oxides with larger specific surface area (colloidal MnO_2) were used in the incubations, suggesting that freshly formed Mn(IV) oxides with smaller particle size may be needed to catalyze this reaction in natural sediments. Finally, moderately reducing environments, as revealed by incubations performed in the presence of small nitrate concentrations or low sulfate concentrations, may favor the onset of anaerobic nitrification and dissimilatory nitrate reduction to ammonium may play an important role on this process in nitrate-rich environments. These findings provide possible explanations to the inconsistent observations of anaerobic nitrification in different Mn-rich sediments and should be considered in future experiments. More importantly, the Mn(IV)-catalyzed anaerobic nitrification of ammonium may act as a source of nitrite and nitrate for anammox microorganisms in anoxic environments, and, in turn, contribute to the marine nitrogen loss in the global nitrogen cycle. The enrichment of a pure culture is now required to identify the microorganisms involved in this process.

Acknowledgments

This work was supported by NSF geobiology and low temperature geochemistry programs.

CHAPTER 6 CONCLUSIONS AND RECOMMENDATIONS

6.1 Conclusions

As a result of their high abundance and reactivity, Mn oxides constitute one of the most powerful electron acceptors in anaerobic natural systems. The reduction of Mn oxides plays an essential role in the biogeochemical cycling of many other elements, including carbon and nitrogen. This dissertation investigates the processes that couple Mn reduction to the redox cycle of both carbon and nitrogen. Microbial Mn reduction is one of the main processes that link Mn reduction to carbon mineralization and has been demonstrated for decades. Compared to the recent progress made on microbial Fe(III) reduction, the mechanism of microbial reduction of solid Mn(IV) oxides remains unclear. Recently, Mn oxides have also been proposed to act as the electron acceptor for anaerobic nitrification, which provides an alternative source of nitrite or nitrate in anoxic systems. The oxidation of ammonium to nitrate by MnO_2 is thermodynamically favorable under environmentally realistic conditions; however, its existence in natural system is still in debate. Therefore, the main hypotheses tested in this dissertation included:

(1) The electron transfer pathway of microbial Mn(IV) reduction proceeds via two consecutive steps of one-electron transfer, similar to the reversal pathway of microbial Mn(II) oxidation and,

(2) Mn(IV) acts as electron acceptor for anaerobic nitrification and provides an alternative source of nitrite/nitrate in anaerobic environments.

The current study reveals for the first time that microbial Mn(IV) reduction proceeds step-wise via two successive one-electron transfer reactions by demonstrating

the production of soluble Mn(III) as intermediate compound during the respiration of Mn(IV). Phenotype studies of a novel point mutant strain Mn3 showed that strain Mn3 reduces Mn(IV) to Mn(III) but not Mn(III) to Mn(II) and thus confirmed that there are two independent steps of one electron transfer during Mn(IV) reduction. The accumulation of low concentrations of Mn(III), compared to total Mn(II) production during the microbial reduction of amorphous MnO_2, is consistent with the relatively low Mn(III) concentrations determined in natural waters and sediments and suggests that the first reduction step from Mn(IV) to Mn(III) may be the rate-limiting step in the reduction of Mn(IV) oxides. Mn(III) produced by strain Mn3 was stabilized by the addition of a non-redox Mn(III)-complexing ligand, while the reduction of Mn(III) by the wild-type strain was promoted under identical conditions. These results imply that a possible endogenic ligand that stablizes the Mn(III) intermediates is involved in the reduction process.

Incubations of the in-frame gene deletion mutants with either solid Mn(IV) or soluble Mn(III) revealed that the OM β-barrel protein MtrB and the OM porin GspD involved in the type II protein secretion system are required for the reduction of both solid Mn(IV) and soluble Mn(III). These findings indicate that the reduction of both Mn(IV) and Mn(III) proceeds at the outer membrane of *S. oneidensis*. Microbial Mn(IV) reduction, however, involves only one of the two potential terminal reductases (*c*-type cytochrome MtrC and OmcA) involved in Fe(III) respiration, as OmcA is not required to reduce either Mn(IV) or Mn(III). The OM cytochrome MtrC also appears to play a more important role in the reduction of Mn(III) than in the reduction of Mn(IV).

More importantly, dissolved inorganic carbon is produced during the reduction of Mn(III) to Mn(II) but not during the reduction of Mn(IV) to Mn(III), indicating that only the second electron transfer step is coupled to the mineralization of organic carbon. These results are in contrast to the long-standing paradigm that Mn(IV) reduction occurs via a single two-electron transfer reaction coupled to organic carbon oxidation. If applicable to all manganese-reducing microorganisms in natural systems, conventional diagenetic models that couple both electrons transferred to Mn(IV) to carbon mineralization should be revised to correctly account for the impact of manganese reduction in the global carbon cycle.

In a parallel study, the link between Mn reduction and anaerobic ammonium oxidation was studied in laboratory slurry incubations amended with either MnO_2, ammonium, or both to (1) test the hypothesis that anaerobic ammonium oxidation to nitrite and nitrate is coupled to the reduction of Mn(IV) oxides and (2) investigate the factors that affect the coupling of anaerobic ammonium oxidation and reduction of Mn oxides.

Results from this study show the net production of nitrate was stimulated under anaerobic conditions with external addition of Mn oxides, suggesting the existence of anaerobic nitrification in the sediments from the Skidaway salt marsh. Mass balance calculations on NH_4^+ concentrations indicate that anaerobic ammonium oxidation contributes to the net consumption of NH_4^+ observed in the incubations amended with Mn oxides, which confirms the occurrence of Mn(IV)-catalyzed anaerobic nitrification. Interestingly, anaerobic nitrification was only found in the incubations amended with colloidal Mn oxides (smaller particle size) but not amorphous Mn oxides (larger particle

size), suggesting that the activity and aging of the Mn(IV) oxides may control this process in natural sediments. In addition, anaerobic nitrification was enhanced in the presence of high initial concentrations of NH_4^+, indicating that the initial ratio of MnO_2 and NH_4^+ may greatly affect this process. Finally, moderately reducing environments, maintained either by a decrease of sulfate levels or a slight increase of initial nitrate level, may facilitate the onset of anaerobic nitrification. These findings therefore suggest the occurrence and activity of anaerobic nitrification may not only depend on the abundance of Mn-oxides in sediments but also the type of Mn oxides, the background level of ammonium, and the redox potential of the sediment, which should be considered in future studies. More importantly, these results suggest that Mn(IV)-catalyzed anaerobic nitrification may provide nitrite and nitrate for anammox microorganisms in anoxic sediments and could enhance the contribution of anammox in sediments to the nitrogen loss in the marine nitrogen cycle.

6.2 Recommendations for future research

Microbial Mn(IV) reduction coupled to carbon oxidation has been demonstrated to proceed via two steps of one-electron transfer process in the current study and future research in this area is required to characterize the mechanism of these two electron transfer step.

(1) Point mutant strain Mn3 presents a unique phenotype that reduces Mn(IV) to Mn(III), but not to Mn(II). Therefor, genetic identification and nucleotide sequence analyses of strain Mn3 should be conducted to confirm the phenotype and provide information on the genes and proteins required in the reduction of Mn(III).

(2) In the current study, we propose that the paucity of ligands that non-reductively solubilize Mn(IV) oxides at circumneutral pH in aquatic systems has forced *S. oneidensis* to evolve a Mn(IV) reductive solubilization-based strategy that produces soluble Mn(III) intermediates. The ligands eventually produced by the microorganism to reductively dissolve solid Mn(IV) should be identified. Siderophores have been suggested to be involved in microbial reduction of Mn(IV) (Kouzuma et al., 2012) but not Fe(III) (Fennessey et al., 2010). Studies on the Mn(IV/III) reduction activity of mutant strains of *S. oneidensis* deficient in producing siderophores could be used to study the role of siderophores in the reductive dissolution of solid Mn(IV).

(3) Although the existence of colloidal MnO_2 is limited in natural systems, studies on the microbial reduction of colloidal Mn(IV) may be employed to understand the effect of reactivity or bioavailability of Mn(IV) on the two electron transfer steps involved in Mn(IV) reduction (Appendix A). Unfortunately, difficulties in quantifying Mn(III) by colorimetry when using colloids limit the scope of these studies. In addition, efforts to develop electrochemical approaches for Mn(III) measurement (Trouwborst et al., 2006) have been unsuccessful in this study. The calibration of Mn(III) has been confounded by bad reproducibility, ligand competition problems, and unpredictable peak shifts (Appendix B). Development of alternative approaches for Mn(III) measurements (Madison et al., 2011) should facilitate these investigations.

(4) Speciation of Mn in solid phase could be further explored. A XPS technique has been utilized to detect the oxidation states of Mn at the solid surface (Appendix A). However, XPS only provides information on the speciation of Mn in the top 10 nm from the surface. Other techniques such as X-ray absorption spectroscopy should then be

employed in future to study the composition of Mn(II), Mn(III), and Mn(IV) in the solid phase.

In the study on the coupling of Mn and N redox cycles, Mn-catalyzed anaerobic nitrification was demonstrated via laboratory incubations. Several questions have arisen from the findings of the slurry incubations. Processes in the slurry incuabtions that may interfere the anaerobic ammonium oxidation include (1) the coupling of Mn reduction to carbon mineralization, (2) alternative ammonium production/consumption processes, such as ammonium assimilation, ammonification, and ammonium adsorption on solid phase, and (3) alternative processes of anaerobic ammonium oxidation that are coupled to other electron acceptors (Fe(III) or sulfate). In the future, enrichments of the microbial community involved in the Mn(IV)-coupled anaerobic nitrification should be conducted to definetely demonstrate that this process exists in marine sediments and to study the mechanism of this process. One of the essential questions for this process, which has yet been addressed, is the origin of the oxygen atom for the first step of enzymatic ammonium oxidation, during which ammonium is oxidized to hydroxylamine (NH_2OH) by ammonia mono-oxygenase (AMO) (Bothe et al., 2007). Recently, a novel pathway has been proposed to couple the anaerobic oxidation of methane to a modified nitrite reduction pathway, during which nitric oxide as the intermediate is converted to dinitrogen and oxygen (Ettwig et al., 2010). This finding may cast a fresh insight into the study for the origin of oxygen during the pathway coupling Mn(IV) reduction and anaerobic ammonium oxidation.

In collaboration with Dr. DiChristina's group, serial dilutions in batch reactors were conducted to enrich the microbial communitites involved in the Mn-catalyzed

ammonium oxidation. Salt marsh sediments were independently incubated in artificial sea water amended with Mn(IV), Mn(III), ammonium, or both since May 2010. After 400 days of incubation, the enrichment fed with 1 mM ammonium and 0.2 mM soluble Mn(III) retained its Mn(III) reduction capability in the absence of organic carbon sources (Appendix C). The behavior of these enrichment cultures is currently under investigation, and molecular analyses coupled to these culture experiments should help characterize the microbial community and provide more information on the process that links Mn reduction to anaerobic ammonium oxidation.

APPENDIX A SUPPLEMENTAL INFORMATION FOR CHAPTER 3

A.1 Kinetics of Mn reduction by *S. oneidensis* MR-1 fed with colloidal Mn(IV)

Shewanella oneidensis MR-1 was fed with colloidal Mn oxides as terminal electron acceptor under anaerobic conditions to study the mechanism of Mn(IV) respiration. The initial addition of colloidal Mn(IV) in each reactor was approximately 10 mM, with concentrations of total Mn maintaining at 9.92 ± 0.67 mM in both the abiotic control and the wild-type incubations (Figure A.1-A). The pH was consistent around 7.30 ± 0.11 in the abiotic control, while a significant increase in pH was observed in the wild-type incubations (Figure A.1-A). The pH in the wild-type incubations increased approximately 0.5 pH unit after 18 hours of incubation, and then decreased back to the background level at the end of the incubation. Simultaneously, significant amounts of Mn^{2+} were produced in the wild-type incubations, suggesting that the increase in pH may be caused by the proton consumption during the reduction of colloidal MnO_2 (Figure A.1-B) (Van Cappellen et al., 1998).

Concentration of soluble free Mn^{2+} in the wild-type incuabtions increased significantly compared to those in the abiotic control (Figure A.1-B), suggesting the reduction of colloidal Mn oxides to Mn(II). Concentrations of Mn^{2+} reached a maximum (971.59 ± 19.01 μM) during the first 24 hours, and slightly decreased to 470.5 ± 130 μM after 24 hours (Figure A.1-B). In turn, no significant production of Mn^{2+} was found in the abiotic control, which maintained a background level of soluble Mn^{2+} at 183.71 ± 44.97 (Figure A.1-B).

As colloidal Mn oxide, with a particle diameter generally less than 0.2 μm, stays in the soluble phase after filtration with 0.2 μm filter (Perez-Benito et al., 1996), total dissolved Mn (TDM) in the incubations with colloidal Mn oxides included soluble Mn(II), soluble Mn(III) and Mn(IV) colloids. In turn, the concentrations of TDM were not expected to change significantly during the incubation, which was confirmed by the consistent concentrations of TDM in the abiotic controls at around 8.90 ± 0.43 mM (Figure A.1-B). Interestingly, concentrations of total dissolved Mn (TDM) changed remarkably in the wild-type incubations, especially after 18 hours, from the initial value of 8.91 ± 1.15 mM to 1.44 ± 0.12 mM at the end of the incubation (Figure A.1-B). This decrease of TDM indicated the removal of Mn species from solutions, which may be due to either aggregation/precipitation, or diffusion into the cells, or adsorption on cell surfaces, or secondary precipitation of Mn(II) produced. Porins, as channel proteins at outer membranes of cells, form small pores of about 1 nm in diameter (Madigan et al., 2003); therefore, colloidal Mn oxides, with a diameter about 100 nm (Perez-Benito et al., 1996) should not be able to diffuse into the cells. In addition, no significant change in the TDM concentrations in the abiotic control (Figure A.1-B) indicated that precipitation or aggregation of colloidal Mn(IV) during the incubations is negligible. As the incubations on solid Mn(IV) oxides have demonstrated significant secondary precipitation of Mn carbonate during the respiration of the wild-type strain, the significant decrease in TDM observed in the current incubations with colloidal MnO_2 may be caused by secondary precipitation of Mn(II), which was evidenced by the change of the brown color of colloidal Mn oxides to cloudy white precipitate during the wild-type incubations.

Unfortunately, quantification of Mn^{3+} concentrations by spectrophotometry during the colloidal incubations was impossible due to the scattering of light by colloids. Instead, pyrophosphate, which can form stable Mn(III)-$P_2O_7^{4-}$ complexes with a pink color (Kostka et al., 1995), was used to visually determine whether Mn(III) was produced during the incubations. The color of the samples from the abiotic control remained dark brown (colloidal Mn oxides) over time (Figure A.2). The color of the live reactor samples with pyrophosphate changed from dark brown at time zero to slightly pink (but not clear) at 12 hours, then to clear pink color after 18 hours, indicating the formation of Mn(III)-$P_2O_7^{4-}$ complexes (Figure A.2). After 24 hours, samples of the two live reactors turned from pink to transparent (Figure A.2) and remained transparent until the end of the incubation. These results suggested the formation of soluble Mn(III) between 12 to 18 hours and disappeared after 24 hours (Figure A.2), when concentrations of Mn(II) reach a plateau (Figure A.1-B). This initial production and ultimate consumption of Mn(III) indicated that soluble Mn(III) is produced as an intermediate during the reduction of colloidal Mn(IV) by MR-1, suggesting the dissimilatory reduction of colloidal Mn oxides may proceed in two consecutive steps of one-electron transfer with Mn(III) as the intermediate.

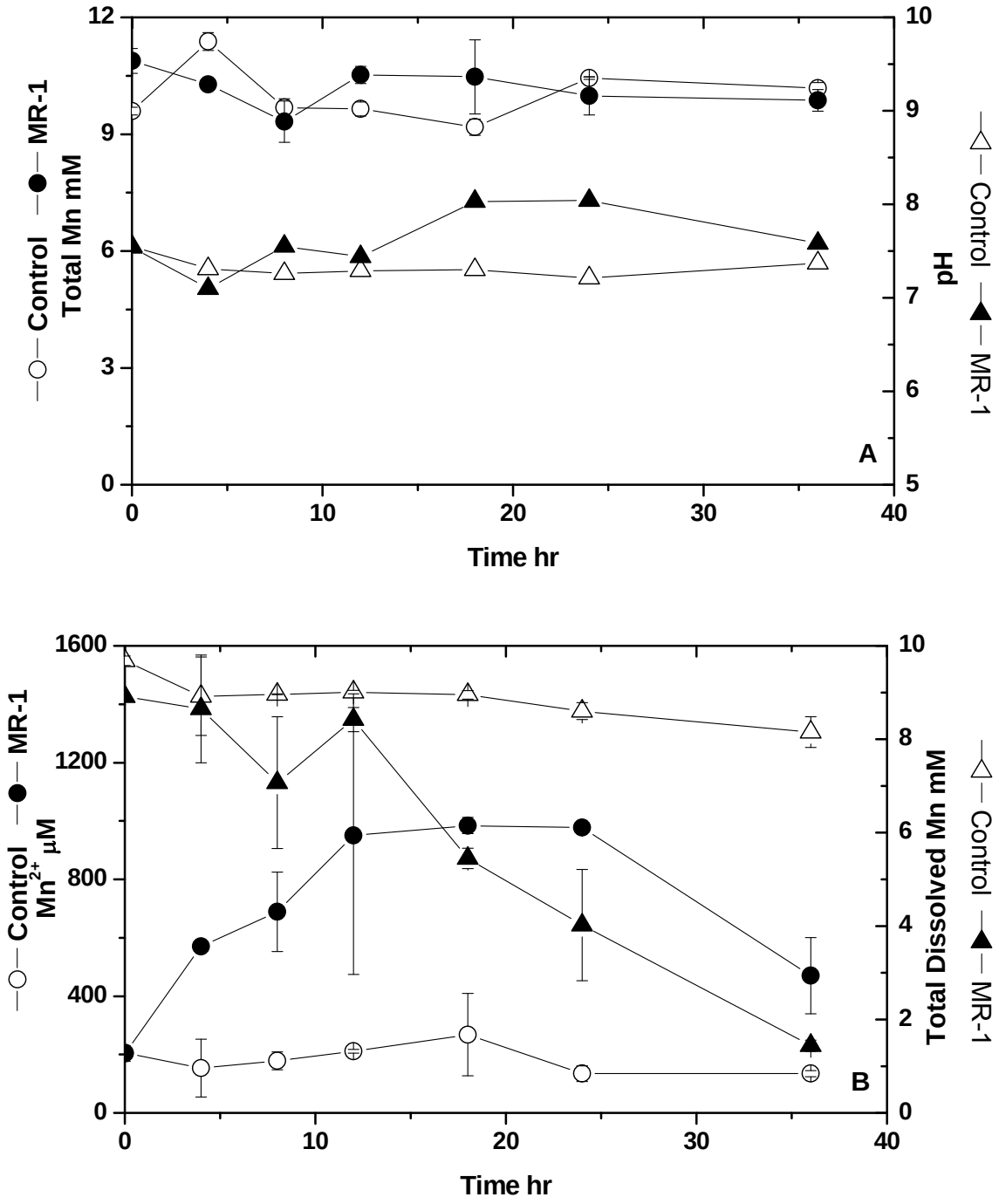

Figure A.1. (A) Concentration of total Mn (circles, left y-axis) and pH (triangles, right y-axis) as a function of time during incubations with colloidal Mn oxide. (B) Concentrations of Mn^{2+} (circles, left y-axis) and total dissolved Mn (TDM) (triangles, right y-axis) as a function of time during incubations. The incubations included both chemical control (without bacteria) (open symbols) and live reactors with 10^7 cells/ml *Shewanella oneidensis* MR-1 (solid symbols). Error bars represent standard deviations from at least duplicates.

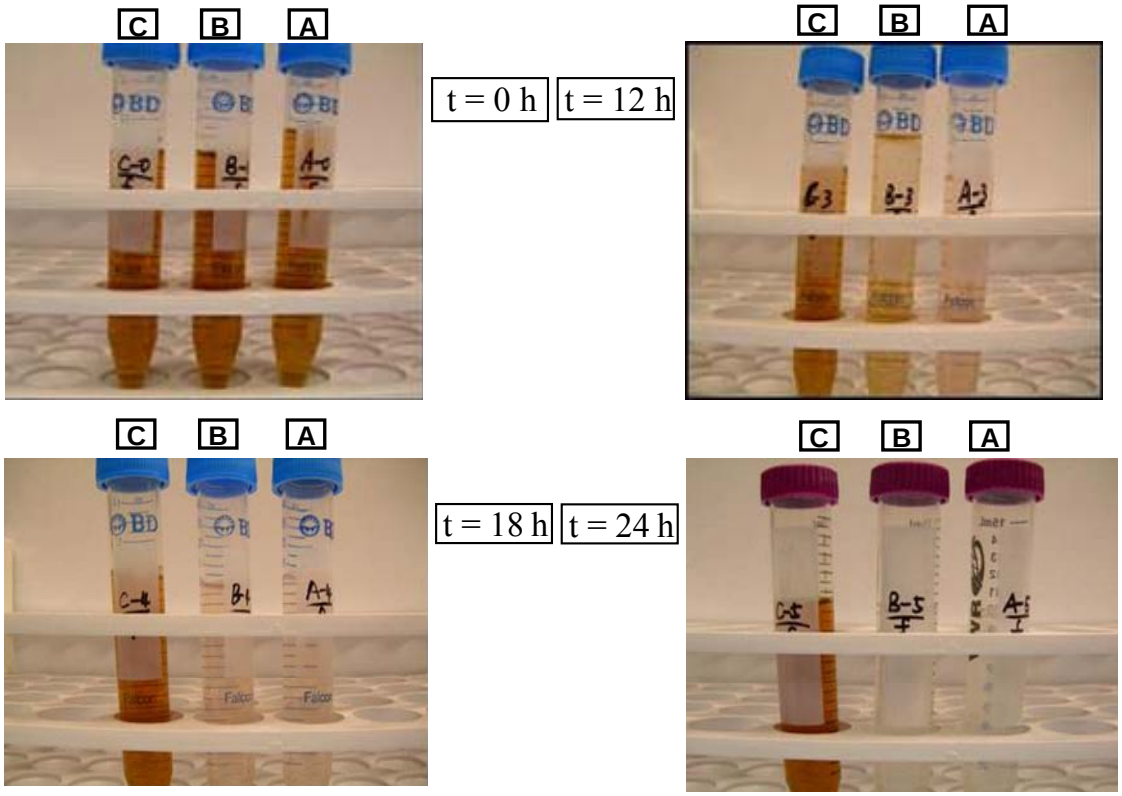

Figure A.2. Changes in color of the supernatant from incubations with colloidal Mn oxides after addition of pyrophosphate (the samples were extracted from Hungate tubes at each time point, and pyrophosphate was added after filtration with 0.2 μm filter) (C is the abiotic control, A and B are two replicates of the live incubations with wild-type strain of *Shewanella oneidensis* MR-1).

A.2. Application of XPS on determining the oxidation state of Mn in solid surface during anaerobic incubations with *S. oneidensis* MR-1.

A surface sensitive technique XPS (X-ray photoelectron spectroscopy) was used to detect the oxidation state of Mn in the surface layer (1-10 nm) of the solid phase in the anaerobic incubations with MR-1. XPS spectras were obtained in a SSX-100 X-ray photoelectron spectrometer (Surface Science centre), with a monochromatized Al Kα X-ray source (1487 eV) and a base pressure of 1×10^{-9} Torr in the analytical chamber. Survey scans were recorded using a 600 μm spot size and fixed pass energy of 160 eV to survey all elements presenting in the sample surface (Figure A.3). Each element was identified according its specific binding energy. Narrow scans were recorded subsequently for interesting elements, including C, O, and Mn. The shape and the binding energy of each peak were used to determine the chemical state of the emitting atom and the composition of chemical states (in percentage) of the element.

The XPS (Mn) ($2p_{3/2}$) spectra obtained via narrow scans (Figure A.3) were used to analyze the percentage of Mn(II), Mn(III), and Mn(IV) at the sample surface. Parameters for Mn(2p) spectrum of Mn(II), Mn(III), and Mn(IV) were listed in Table A.1 (Nesbitt and Banerjee, 1998). All peaks were fitted using 70:30 (Gaussian : Lorentzian) peak shape with fixed full width at half maximum (FWHM) (Figure A.4). Summary of the fit was listed in Table A.2. The composition of Mn in the surface of a solid sample from incubations of MR-1 at 24 hours was calculated as 12% of Mn(II), 20% of Mn(III), and 68% of Mn(IV).

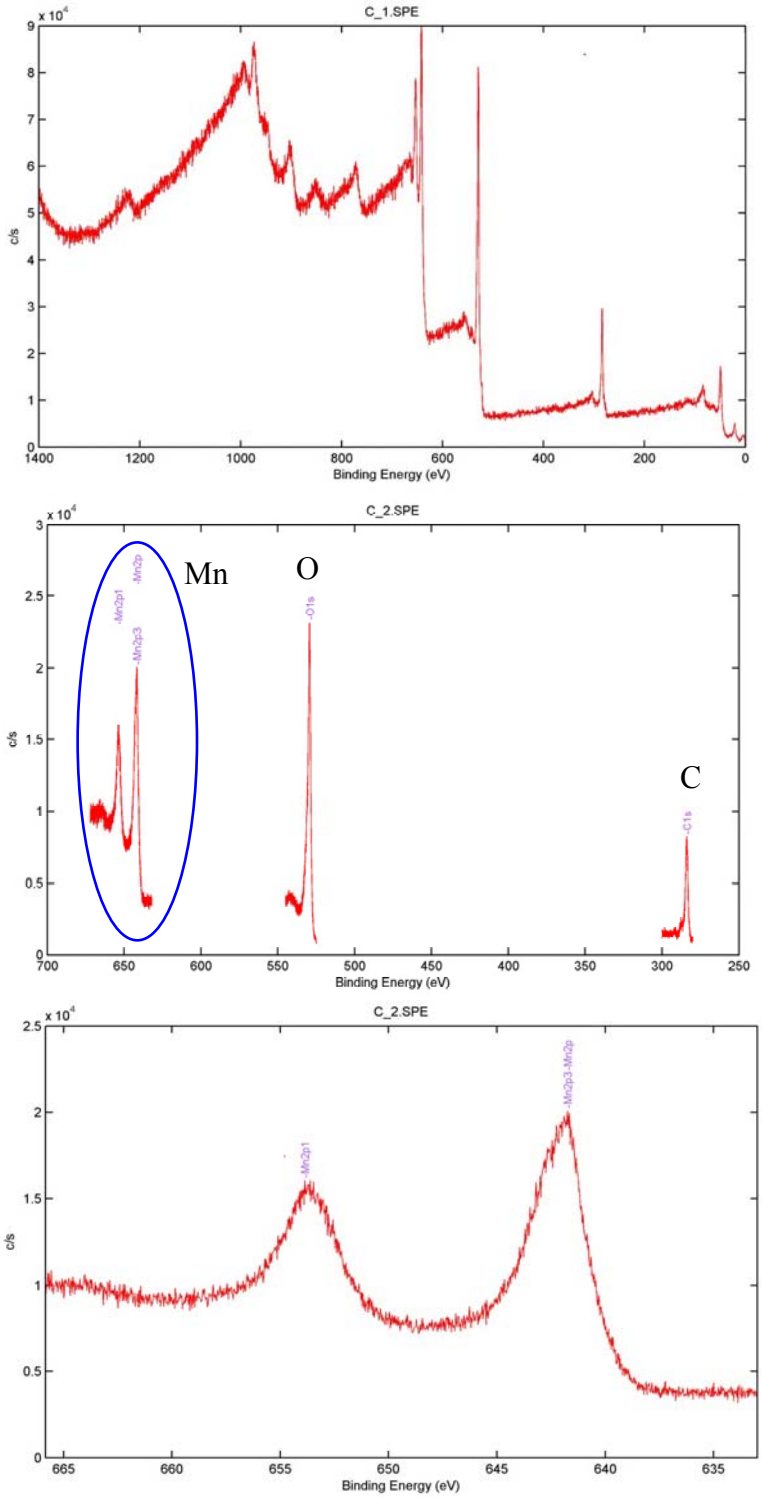

Figure A.3. Survey scan (C_1. SPE) and narrow scans of C, O, and Mn (C_2. SPE) in solid samples from incubations of amorphous MnO_2 with *Shewanella oneidensis* MR-obtained from SSX-100 X-ray photoelectron spectrometer.

Table A.1. Peak parameters for Mn free ions and Mn bound oxyhydroxides measured in XPS (*Nesbitt and Banerjee, 1998*).

Peak ID (eV)	B.E. (eV)	FWHM (percent)	Intensity*	Comments
Mn(2p) Parameters: Calculated (Gupta and Sen 1974, 1975)				
Mn^{2+}-free Ion	640.0	1.0	100.0	Multiplet no. 1
Mn^{2+}-free Ion	641.3	1.0	75.2	Multiplet no. 2
Mn^{2+}-free Ion	642.4	1.0	50.8	Mulitplet no. 3
Mn^{2+}-free Ion	643.1	1.0	25.2	Multiplet no. 4
Mn^{2+}-free Ion	647.6	1.0	15.0	Multiplet no. 5
Fitted (Fig. 2)				
Mn^{2+}-in MnO	640.0	1.7	100.0	Multiplet no. 1
Mn^{2+}-in MnO	641.2	1.7	76.0	Multiplet no. 2
Mn^{2+}-in MnO	642.0	1.7	49.0	Multiplet no. 3
Mn^{2+}-in MnO	642.9	1.7	25.0	Multiplet no. 4
Mn^{2+}-in MnO	647.5	1.7	10.2	Multiplet no. 5
Mn^{2+}-in MnO	645.0	3.5	30.3	Satellite
Calculated (Gupta and Sen 1974, 1975)				
Mn^{3+}-free Ion	640.7	1.0	100.0	Multiplet no. 1
Mn^{3+}-free Ion	641.4	1.0	100.0	Multiplet no. 2
Mn^{3+}-free Ion	642.3	1.0	135.0	Multiplet no. 3
Mn^{3+}-free Ion	643.1	1.0	70.0	Multiplet no. 4
Mn^{3+}-free Ion	644.9	1.0	30.0	Multiplet no. 5
Fitted (Fig. 3c)				
Mn^{3+}-Manganite	640.7	1.25	100.0	Multiplet no. 1
Mn^{3+}-Manganite	641.4	1.25	100.0	Multiplet no. 2
Mn^{3+}-Manganite	642.2	1.25	116.0	Multiplet no. 3
Mn^{3+}-Manganite	643.2	1.25	73.0	Multiplet no. 4
Mn^{3+}-Manganite	644.6	1.60	28.0	Multiplet no. 5
Calculated (Gupta and Sen 1974, 1975)				
Mn^{4+}-free Ion	641.9	1.0	100.0	Multiplet no. 1
Mn^{4+}-free Ion	642.9	1.0	66.7	Multiplet no. 2
Mn^{4+}-free Ion	643.8	1.0	33.3	Multiplet no. 3
Mn^{4+}-free Ion	644.8	1.0	13.5	Multiplet no. 4
Mn^{4+}-free Ion	646.8	1.0	23.3	Multiplet no. 5

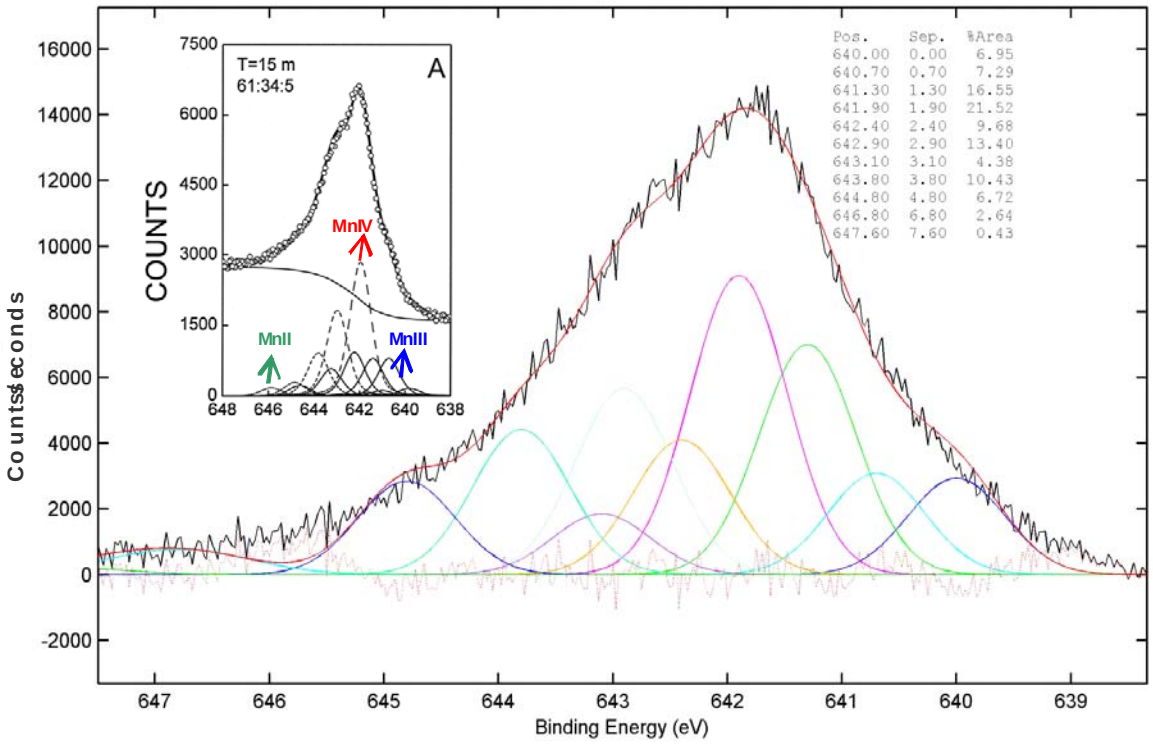

Figure A.4. Fitted Mn2p3/2 spectrum of the solid sample from incubations of amorphous MnO_2 with *S. oneidensis* MR-1. The fitting parameters were used according to the procedures described in reference (Nesbitt and Banerjee, 1998). The insect displays an example of fitting spectrum from the literature (Banerjee and Nesbitt, 2001). The red solid curve represents the best fit to the spectral data.

Table A.2. Summary of fitted binding energies and peak intensities obtained from the Mn(2p) spectrum of the samples to calculate the proportions of Mn(II), Mn(III), and Mn(IV) at the solid surface. The percentage of each species was calculated based on the summary of peak intensities (counts) for all the peaks of the specific species (Mn(II), (III), or (IV)

MnII peaks eV	**Counts**	**MnIII peaks eV**	**Counts**	**MnIV peaks eV**	**Counts**
640.00	2944.00	**640.70**	3937.00	**641.90**	12301.00
641.30	2213.89	**641.40**	3937.00	**642.90**	8204.77
642.40	1495.55	**642.30**	5314.95	**643.80**	4096.23
643.10	741.89	**643.10**	2755.90	**644.80**	1660.64
647.60	441.60	**644.90**	1181.10	**646.80**	2866.13

APPENDIX B SUPPLEMENTAL INFORMATION FOR CHAPTER 4

Electrochemical measurement of Mn(III) during the incubations with mutant strains *Sol* d29 and d64

The addition of desferrioxamine B (Def-B) that forms strong Mn(III)-Def-B complexes and out-competes natural Mn(III) complexes has been proposed for quantification of Mn(III) via the electrochemical measurement of Mn(III)-Def-B (Trouwborst et al., 2006). Desferrioxamine B is a common trihydroxamate siderophore and exists mostly in the fully protonated form of H_4Def-B at physiological pH (structure and binding constants shown in Figure B. 1) (Duckworth and Sposito, 2005b, Faulkner et al., 1994). Def-B is a linear molecule and contains three hydroxamate functions with a primary amino group at one end (Figure B. 1). During complexation, Def-B ligand wraps around Mn(III) ion to form high stability complexes of 1:1 stoichiometry (MLH) (Faulkner et al., 1994).

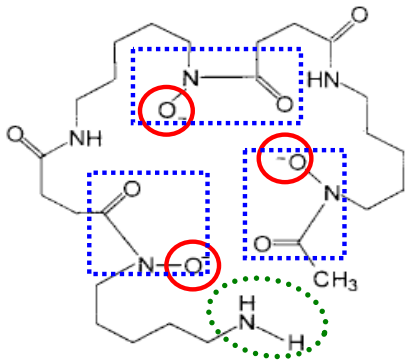

	Average[h]
K_{HL}	10.85 (4)
K_{H_2L}	9.52 (6)
K_{H_3L}	8.97 (2)
K_{H_4L}	8.32 (2)

Figure B. 1. structure and binding constants of Def-B (Faulkner et al., 1994).

An electrochemical approach was utilized to measure the Mn(III)-Def-B complex and quantify the concentration of soluble Mn(III) in natural systems (Trouwborst et al., 2006). Def-B generally presents a signal at -1.34 eV Vs SCE and Mn(III)-DEF-B complexes present a signal at -1.19 eV Vs SCE (Trouwborst et al., 2006). Voltammetric measurements were constituted with a DLK-60A electrochemical analyzer using a 0.5 mm diameter Ag/AgCl reference electrode, a mercury drop electrode as working electrode, and a Pt electrode as counter electrode. Voltammetric parameters used in the current study included: cyclic voltammetry, N_2 purged seawater as the electrolyte, scan rate of 500 mV/s, and 3 second deposition time at -0.1eV.

Difficulties associated with the Mn(III)-Def-B measurement:

1. The pH affected Def-B signals by voltammetry (Figure B.2). Def-B signals shifted to more negative voltages at higher pH. Buffered electrolyte should be used to maintained the pH around 8.
2. Def-B was able to complex with not only Mn(III) but also Mn(II) (Duckworth and Sposito, 2005a, Duckworth and Sposito, 2005b) (Figure B.3). The Mn(II)-Def-B signal (at -1.52 eV) found in the Mn(III) standards with addition of Def-B may be caused by either dispropornation of Mn(III) in seawater electrolyte or internal reaction of Mn(III) with Def-B (Duckworth and Sposito, 2005a).
3. Electrochemical signals showed bad reproducibility and the calibration of Mn(III) showed much lower sensitivities than those reported (Trouwborst et al., 2006), which may be affected by the competition between pyrophosphate (soluble Mn(III) standards used) and Def-B in complexing Mn(III).

Def-B was added into sub-samples (after filtration) for the detection of Mn(III) by voltammetry during anaerobic incubations of *S. Oneidensis* MR-1 strains (including the wild-type strain and mutant strains *Sol* d29, and *Sol* d64) with either amorphous or colloidal MnO_2, (Figure B.4 and Figure B.5). The signal at around -1.15 - 1.20 eV (Mn(III)-Def-B signal) showed significant decrease during the wild-type incubations with either amorphous or colloidal MnO_2 (Figure B.4 and Figure B.5). Besides the Mn(III)-Def-B signal, two other signals were also detected after addition of Def-B, the putative Def-B signal and Mn(II)-Def-B signal, which suggested the possibility of internal reaction of Mn(III) with Def-B (Figure B.4 and Figure B.5). In addition, the conventional Mn(III) measurement (colorimetric approach) showed different results in the evolution of Mn(III) in incubations of colloidal MnO2 in the presence of the wild-type strain, or mutant strain d29, or d64. Concentrations of Mn(III) increased in the wild-type incubations and remained at background levels in the two *Sol* incubations. Therefore, due to the uncertainty in peak shift, interference of Mn(II)-Def-B complexation, and the difficulty with the calibration of Mn(III)-Def-B, the electrochemical approach was not used for Mn(III) quantification in the other incubations.

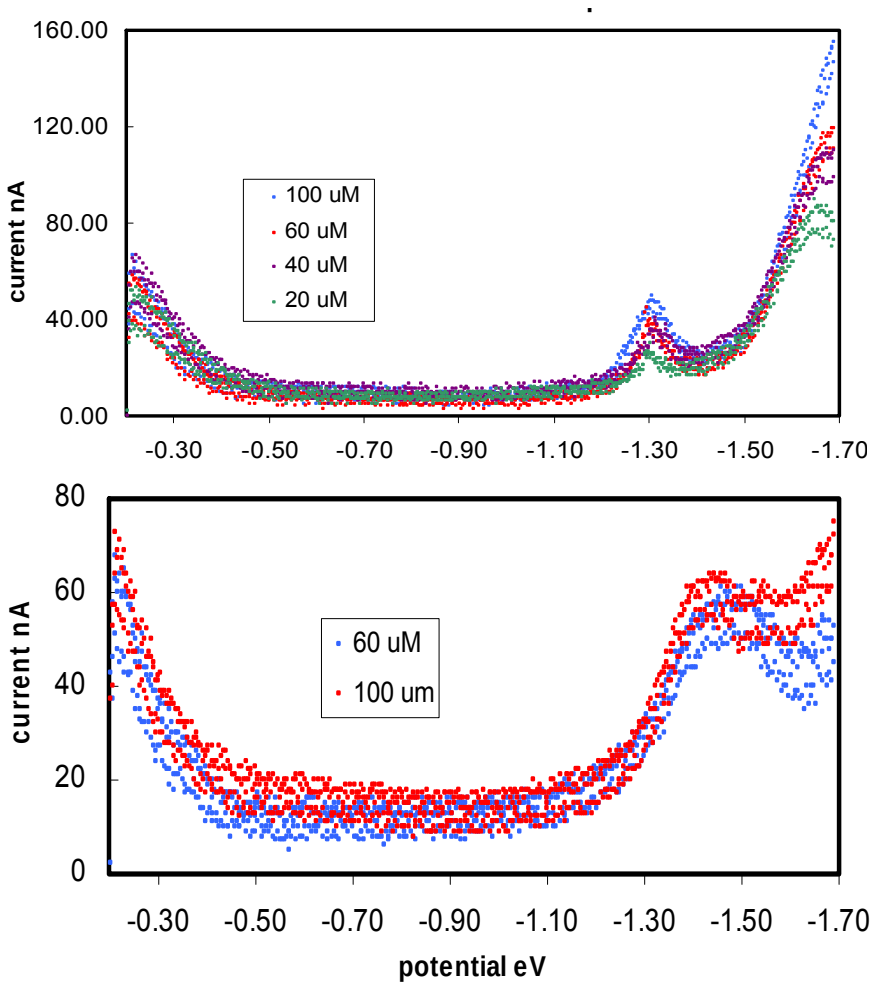

Figure B.2. Effect of pH (pH 10, the upper figure, and pH 8, the bottom figure) on the electrochemical signal of Def-B.

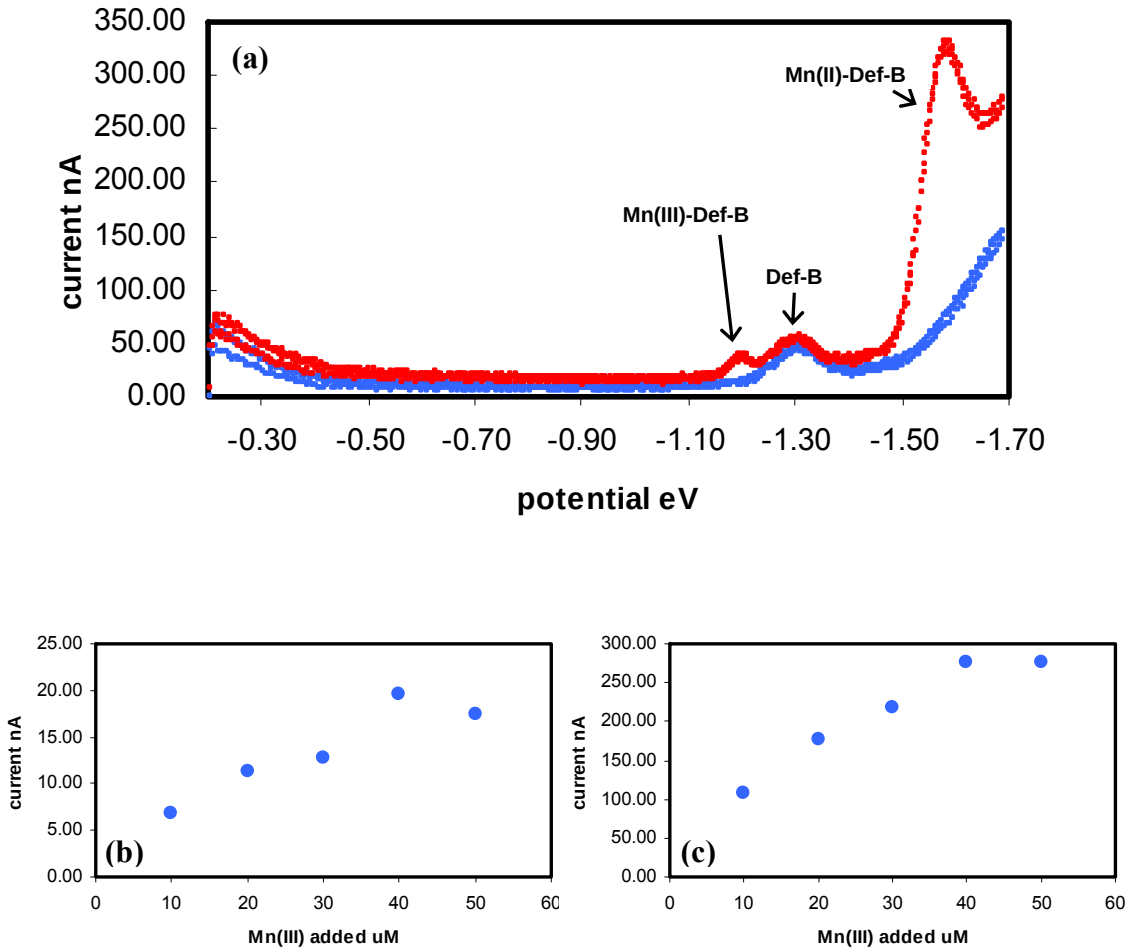

Figure B.3. (a) Voltammograph of 100 µM Def-B at pH 8 with (red) or without (blue) 50 µM Mn(III)-pyrophosphate (soluble Mn(III) standards). The calibration curves of complexes Mn(III)-Def-B (at -1.17 V, (b)) and Mn(II)-Def-B (at -1.52 V, (c)).

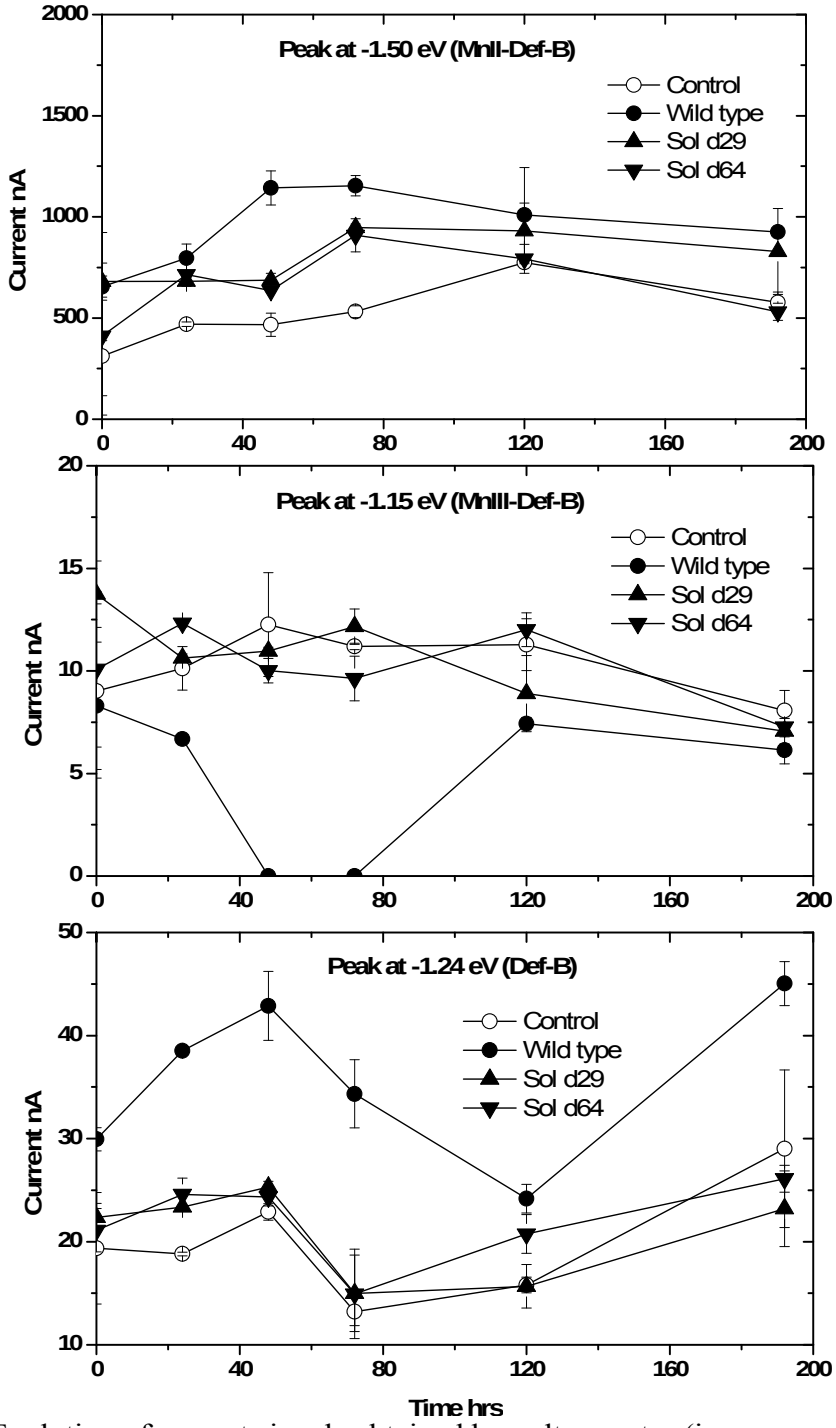

Figure B.4. Evolution of current signals obtained by voltammetry (in presence of 100 µM Def-B) as a function of time during the incubations of amorphous MnO_2 with the wild-type strain (solid circles), Sol d29 (upward triangles), Sol d64 (downward triangles), and the abiotic control (open circles). Three peaks were found in the voltammogram after addition of Def-B, including Mn(II)-Def-B peak at -1.50 eV, Mn(III)-Def-B peak at -1.15 eV, and Def-B peak at -1.24 eV).

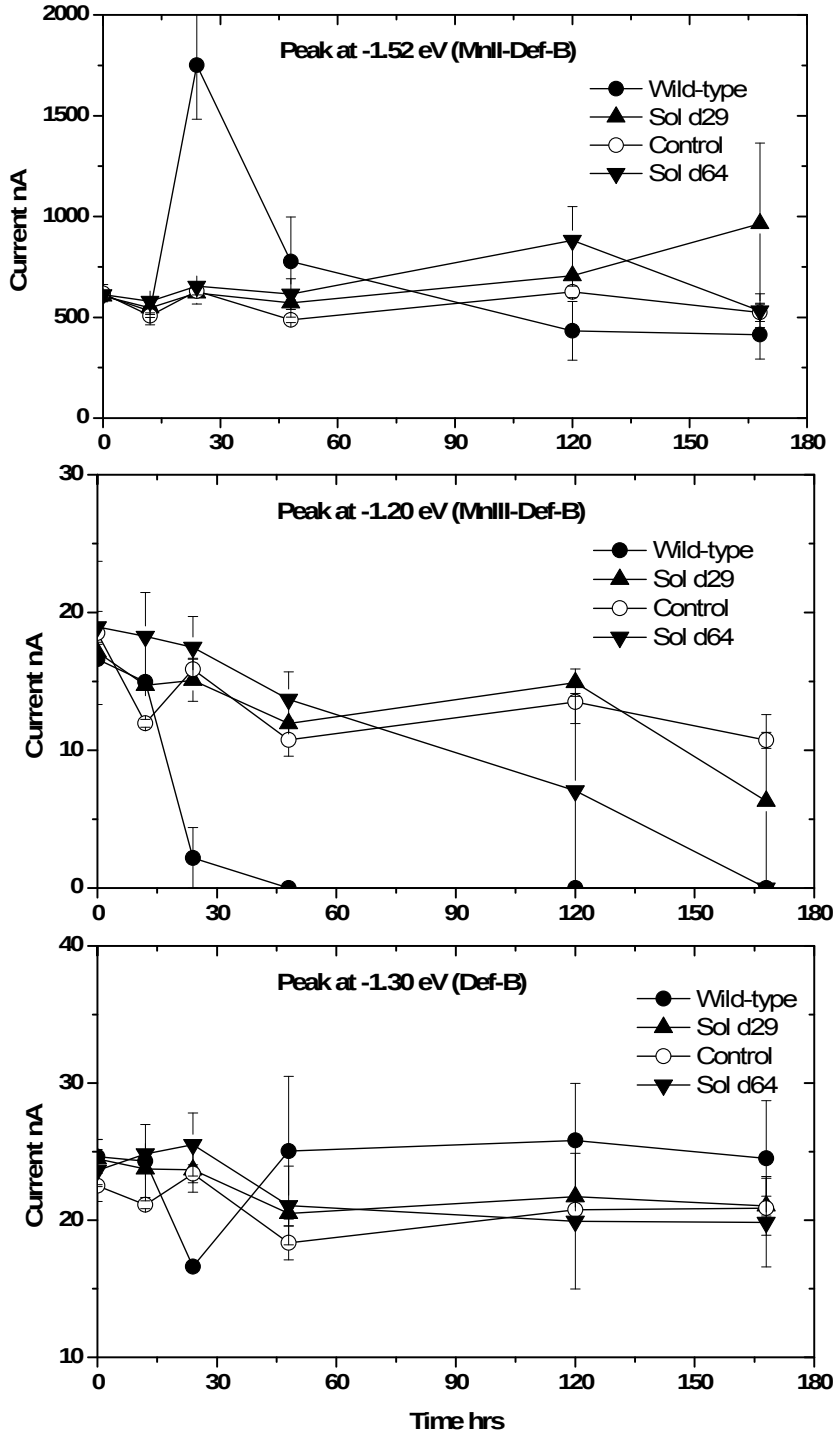

Figure B.5. Evolution of current signals obtained by voltammetry (in presence of 100 µM Def-B) as a function of time during the incubations of colloidal MnO_2 with the wild-type strain (solid circles), Sol d29 (upward triangles), Sol d64 (downward triangles), and the abiotic control (open circles). Three peaks were found in the voltammogram after addition of Def-B, including Mn(II)-Def-B peak at -1.50 eV, Mn(III)-Def-B peak at -1.15 eV, and Def-B peak at -1.24 eV).

APPENDIX C SUPPLEMENTAL INFORMATION FOR CHAPTER 5

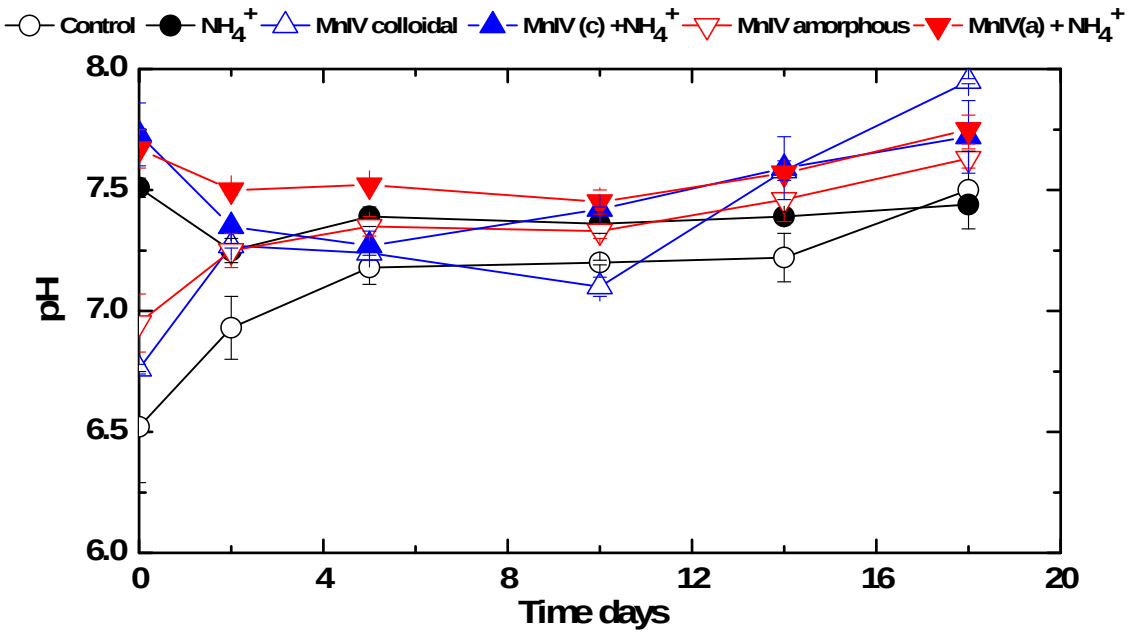

Figure C.1. Evolution of pH in solution as a function of time in anaerobic slurry incubations conducted without any amendment (T1, control, open circles) or in the presence of 800 µM $^{15}NH_4^+$ (T2, solid circles), 300 µM colloidal MnO_2 (T3, open blue upward triangles), 800 µM $^{15}NH_4^+$ and 300 µM colloidal MnO_2 (T4, solid blue upward triangles), 400 µM amorphous MnO_2 (T5, open red downward triangles), and 800 µM $^{15}NH_4^+$ and 400 µM amorphous MnO_2 (T6, solid red downward triangles). The error bars represent the standard deviations of duplicate incubations.

Enrichment culture of Mn-reducing anaerobic nitrifying microorganisms

Enrichment experiments were conducted in collaboration with Dr. DiChristina's group. For these enrichment experiments, approximately 1 g of sediment (Skidaway salt marsh, Core M) was incubated with 20 ml of artificial seawater (50% diluted in DI water) in a sealed Hungate tubes. The artificial seawater is composed of 0.5M NaCl, 10 mM $MgCl_2$, 14 mM Na_2SO_4, 9 mM KCl, 1 mM $CaCl_2$, 2 mM $NaHCO_3$, 2 mM MOPS, 2 mM

KH_2PO_4, 0.8 mM KBr, 2.5 mM $SrCl_2$, 0.4 mM H_3BO_3, 0.001 mM KF, 1 ml/L trace elements, and 2 ml/L vitamins. Different combination of Mn, NH_4^+, and acetate were amended in a total of 12 different treatments (Table C.1). Either amorphous MnO_2 or soluble Mn(III)-pyrophosphate was used as electron acceptor in these slurry incubations. Three types of control incubations were conducted simultaneously with each treatment, including (1) without sediment, (2) with heat-killed sediment, and (3) with sediment and molybdate (10 mM). Every 30 days, each reactor was transferred into fresh medium under identical conditions (with a dilution factor of 20). The enrichment strategy was to dilute sediments under controlled conditions (Mn, N, and carbon source) to purify the microbial community that are involved in reducing Mn and oxidizing NH_4^+ under anaerobic conditions

The initial 120-days of serial dilution

After 120-days of incubations (4 dilution transfers), reduction capability of Mn(IV) and Mn(III) were maintained in the enrichments (Figure C.2 and Figure C.3). Proportionally higher activity of Mn(IV/III) reduction was observed in treatments amended with 0.2 mM of Mn(IV) or Mn(III), compared to the corresponding 5 mM treatments (Figure C.2 and Figure C.3). In addition, little difference was found between treatments amended or not with acetate (Figure C.2 and Figure C.3). Therefore, in the following enrichment experiment, each of the enrichment was transferred into a 120ml-sealed serum bottle under identical conditions but without amendment of acetate.

Batch reactor incubations of the 120-day enrichment culture

A 180-days incubation of the 120-days enrichment were then conducted in serum bottles in the presence of either soluble Mn(III) or solid Mn(IV). Significant Mn(III) reduction was observed in treatments amended with 0.2 mM Mn(III)-pyrophosphate (Figure C.4). As all reactors were incubated in the absence of organic carbon, electron donor, other than organic carbon, must be coupled to Mn(III) reduction. In addition, more Mn(II) was produced in the enrichment amended with 1 mM NH_4^+ compared to the enrichment without NH_4^+ (Figure C.4). The reduction activity of Mn(III) was also visually observed in a following spiking experiment, in which an extra 0.2 mM of Mn(III)-pyrophosphate were added to the enrichment amended with both Mn(III) and NH_4^+ (Figure C.5). Reduction of Mn(III) finished in the live reactor in 5 hrs and the two types of controls (abiotic and heat-killed) maintained the brown color (the color of Mn(III)) during the 8-hr experiment (Figure C.5). Interestingly, molybodate reactors (Live + Mo) presented slower reduction rates of Mn(III), compared to the live reactors (Figure C.5), which may be due to the inhibition of sulfate reduction by molybodate. These results imply that sulfate reduction may also influence the redox cycles of Mn and N in these enrichment. The microbial community structure of these enrichments is now investigated in the microbiology lab.

Effect of different sulfur sources

The final enrichment of in the Mn(III) and NH_4^+ reactor was incubated with different sulfur sources (cysteine, cystine, methionate, and sulfate) to investigate the involvement of sulfur in the redox cycle of Mn and N. The capability of Mn(III) reduction was retained in the enrichment fed with different sulfur sources but presented

different phase lag (Figure C.6). Compared to the original incubation with high sulfate concentration (15 mM), the cysteine and cystine incubations both showed a phase lag of 15 days. The methione incubations showed a phase lag of 21 days (Figure C.6). In the incubations without any sulfur source, Mn(II) production was not detected until 29 days of the incubations (Figure C.6). The maximum production rate of Mn(II) were similar among different S sources, with 4.2 ± 1.4 μM Mn^{2+}/day (high sulfate), 5.2 ± 1.5 μM Mn^{2+}/day (no sulfur sources), 3.7 ± 0.2 μM Mn^{2+}/day (cystine), 4.9 ± 2.4 μM Mn^{2+}/day (methionine), and 5.4 ± 2.8 μM Mn^{2+}/day (cysteine). Therefore, sulfur may be involved in the redox cycle of Mn, by initially inhibit the reduction of Mn(III); but its role remains still unclear.

Table C.1. Treatments conducted for serial enrichment experiments, including with or without (1) 1 mM acetate, (2) Mn(III)/Mn(IV), and (3) NH_4^+. The ratio of Mn:NH_4^+ was set at either 0.2:1 (mM) or 5:5 (mM). Oxidized form of Mn included amorphous MnO_2 and soluble Mn(III)-pyrophosphate.

Treatments	**1**	**2**	**3**	**4**	**5**	**6**	**7**	**8**	**9**	**10**	**11**	**12**
Mn(IV) or Mn(III) (mM)	0	0	0.2	0	0.2	0.2	0.2	5	0	5	5	5
NH_4^+ (mM)	0	0	0	1	0	1	1	0	5	0	5	5
Acetate (mM)	0	1	0	0	1	0	1	0	0	1	0	1

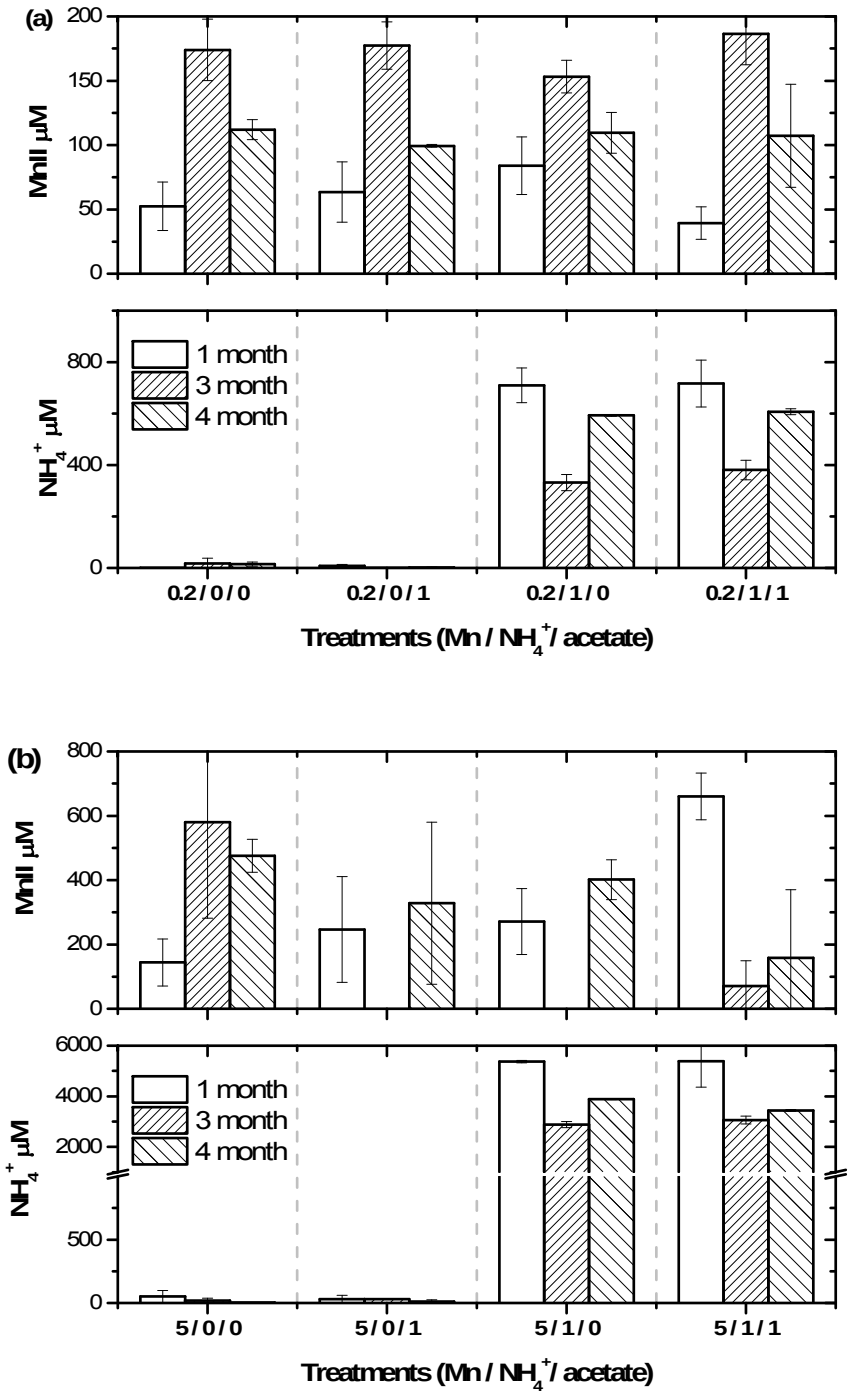

Figure C.2. Concentrations of soluble Mn(II) and NH_4^+ in each transfer (1, 3, and 4 month) during the first 120 days of enrichment, in treatments amended with (a) 0.2 mM and (b) 5 mM of amorphous MnO_2. The x-axis shows the combination of the MnO_2, NH_4^+, or acetate amendment. For example, 0.2/0/1 represents the treatment containing 0.2 mM of MnO_2, 0 mM of NH_4^+, and 1 mM of acetate.

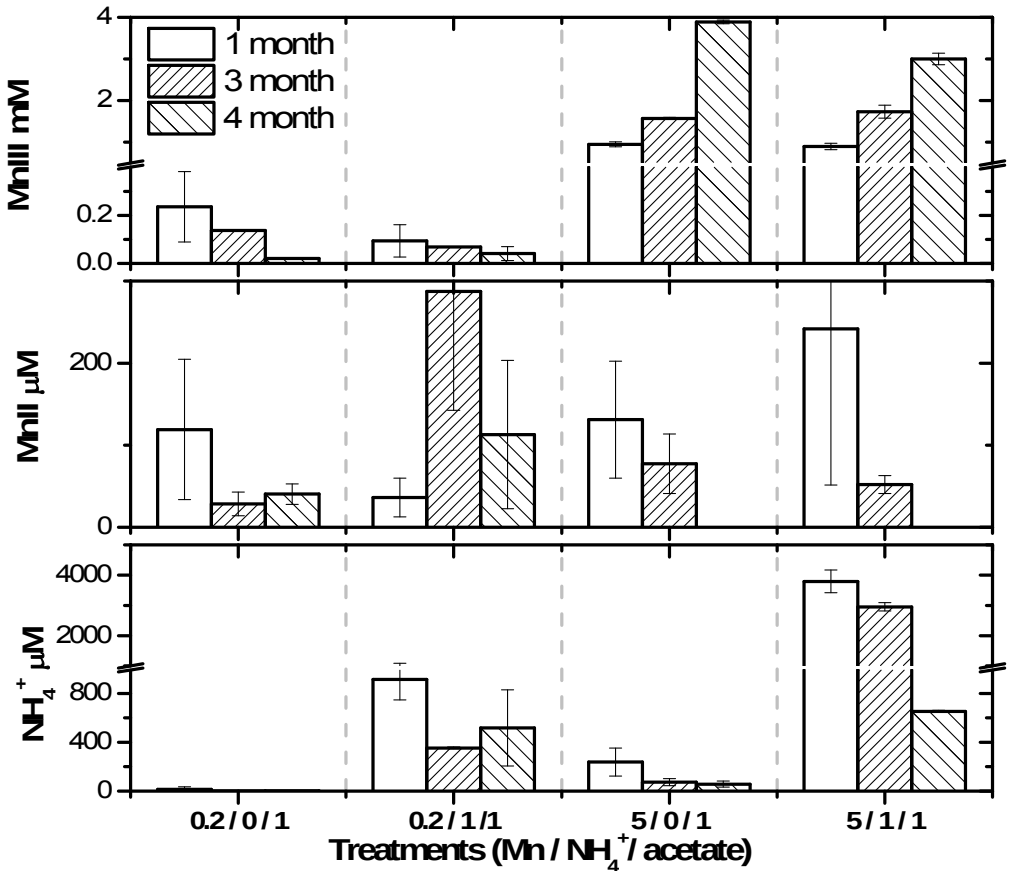

Figure C.3. Concentrations of soluble Mn(III), Mn(II), and NH_4^+ in each transfer (1, 3, and 4 month) during the first 120 days of enrichment, in treatments amended with 0.2 mM and 5 mM of soluble Mn(III)-pyrophosphate complexes. The x-axis shows the combination of the MnO_2, NH_4^+, or acetate amendment. For example, 0.2/1/1 represents the treatment containing 0.2 mM of Mn(III), 1 mM of NH_4^+, and 1 mM of acetate.

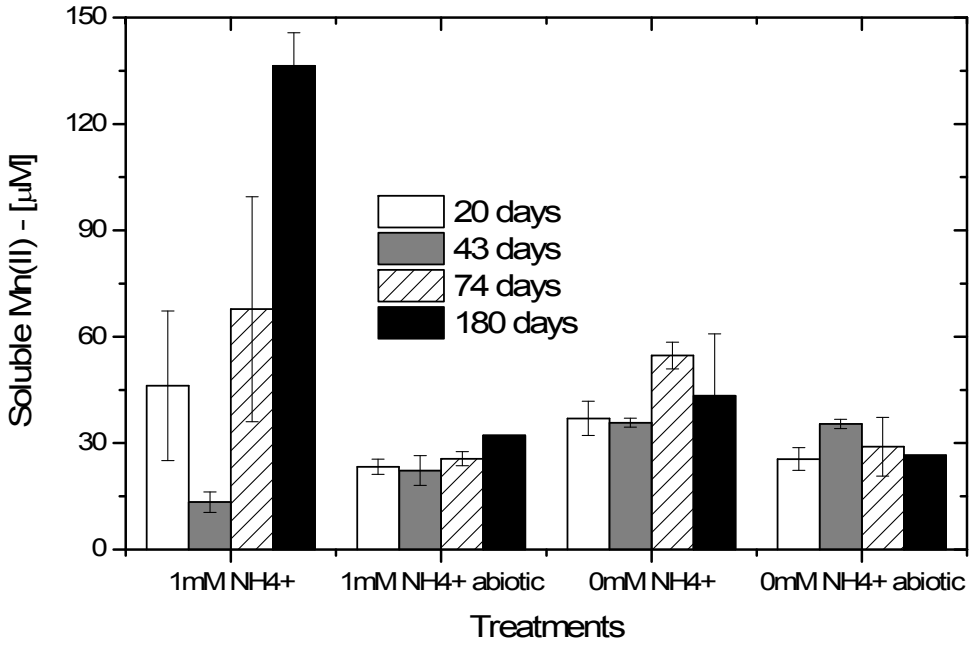

Figure C.4. The production of soluble Mn(II) over a 180 days long set of batch incubations with the enrichment treated with 0.2 mM of soluble Mn(III)-pyrophosphate. The x-axis represents different treatments, including additional amendment of 1 mM NH_4^+ and an abiotic control.

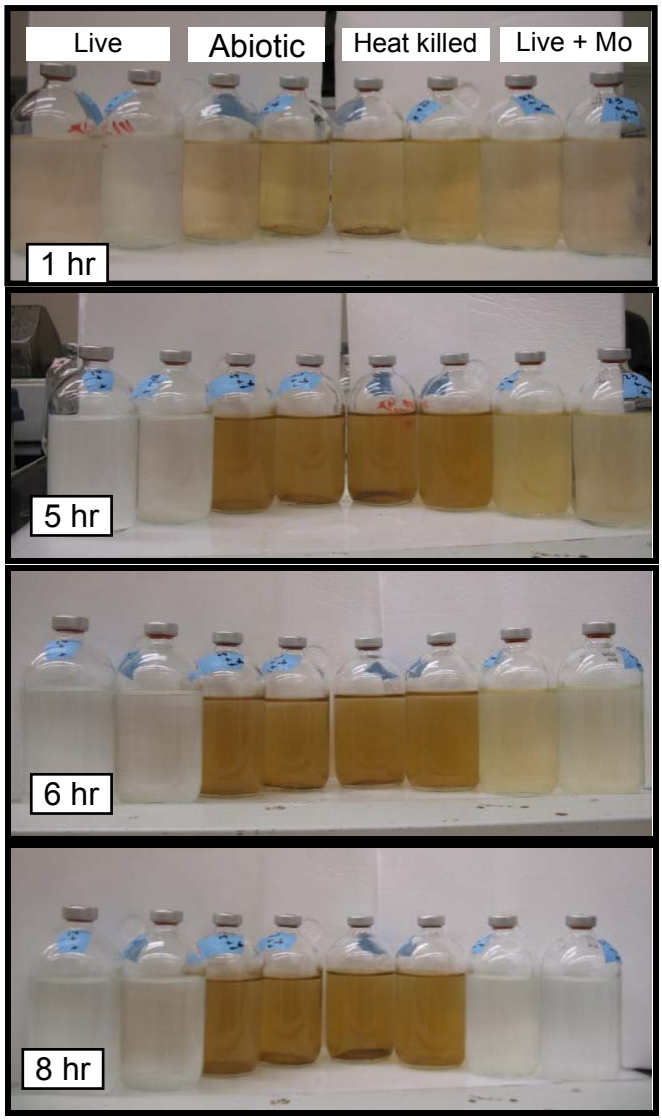

Figure C.5. A 8-hr spiking-experiment of the enrichment treated with 0.2 mM of Mn(III) and 1 mM of NH_4^+, including duplicates of live reactors, duplicates of abiotic control (no enrichment), duplicates of heat-killed control, and duplicates of live reactors with 10 mM of molybdate.

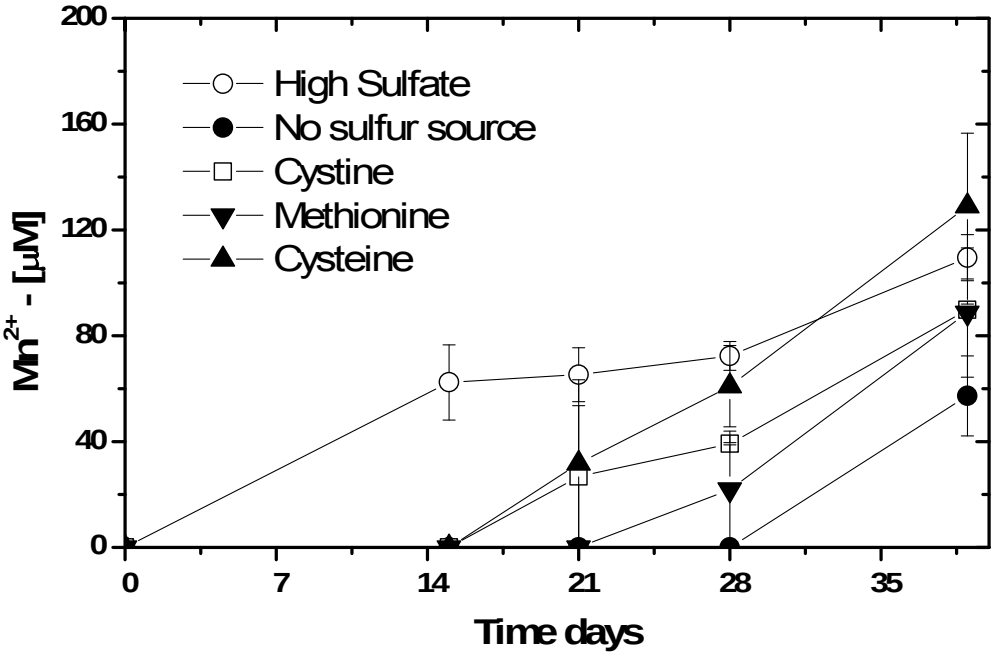

Figure C.6. The production of soluble Mn(II) during an independent set of 27-days incubations with the 120 days enrichment treated with 0.2 mM of soluble Mn(III)-pyrophosphate and 1 mM NH_4^+ but different sulfur sources, including no sulfur sources (solid circles), cystine (open squares), methionine (solid downward triangles), and cysteine (open upward triangles).

REFERENCES

ABELIOVICH, A. & VONSHAK, A. 1992. Anaerobic metabolism of *Nitrosomona Europaea*. *Archives of Microbiology,* 158**,** 267-270.

ADAMS, L. F. & GHIORSE, W. C. 1987. Characterizatoin of extracellular Mn^{2+}-oxidizing activity and siolation of an Mn^{2+}-oxidizing protein from *Leptothrix Discophora* SS-1 *Journal of Bacteriology,* 169**,** 1279-1285.

ALLER, R. C. 1990. Bioturbation and manganese cycling in hemipelagic sediments. *Philosophical Transactions of the Royal Society of London Series a-Mathematical Physical and Engineering Sciences,* 331**,** 51-68.

ALLER, R. C. 1994. The sedimentary Mn cycle in Long Island Sound - its role as intermediate oxidant and the influence of bioturbation, O_2 and C(org) flux on diagenetic reaction balances. *Journal of Marine Research,* 52**,** 259-295.

AN, S. M. & GARDNER, W. S. 2002. Dissimilatory nitrate reduction to ammonium (DNRA) as a nitrogen link, versus denitrification as a sink in a shallow estuary (Laguna Madre/Baffin Bay, Texas). *Marine Ecology-Progress Series,* 237**,** 41-50.

AN, S. M., GARDNER, W. S. & KANA, T. 2001. Simultaneous measurement of denitrification and nitrogen fixation using isotope pairing with membrane inlet mass spectrometry analysis. *Applied and Environmental Microbiology,* 67**,** 1171-1178.

ANDERSON, C. R., DICK, G. J., CHU, M. L., CHO, J. C., DAVIS, R. E., BRAUER, S. L. & TEBO, B. M. 2009. *Aurantimonas manganoxydans*, sp nov and *Aurantimonas litoralis*, sp nov.: Mn(II) Oxidizing Representatives of a Globally Distributed Clade of alpha-Proteobacteria from the Order Rhizobiales. *Geomicrobiology Journal,* 26**,** 189-198.

ANSCHUTZ, P., DEDIEU, K., DESMAZES, F. & CHAILLOU, G. 2005. Speciation, oxidation state, and reactivity of particulate manganese in marine sediments. *Chemical Geology,* 218**,** 265-279.

ANSCHUTZ, P., SUNDBY, B., LEFRANCOIS, L., LUTHER, G. W. & MUCCI, A. 2000. Interactions between metal oxides and species of nitrogen and iodine in bioturbated marine sediments. *Geochimica Et Cosmochimica Acta,* 64**,** 2751-2763.

BANERJEE, D. & NESBITT, H. W. 2001. XPS study of dissolution of birnessite by humate with constraints on reaction mechanism. *Geochimica Et Cosmochimica Acta,* 65**,** 1703-1714.

BARGAR, J. R., TEBO, B. M., BERGMANN, U., WEBB, S. M., GLATZEL, P., CHIU, V. Q. & VILLALOBOS, M. 2005. Biotic and abiotic products of Mn(II) oxidation by spores of the marine Bacillus sp. strain SG-1. *American Mineralogist,* 90**,** 143-154.

BARTLETT, R., MORTIMER, R. J. G. & MORRIS, K. 2008. Anoxic nitrification: Evidence from Humber Estuary sediments (UK). *Chemical Geology,* 250**,** 29-39.

BARTLETT, R., MORTIMER, R. J. G. & MORRIS, K. M. 2007. The biogeochemistry of a manganese-rich Scottish sea loch: Implications for the study of anoxic nitrification. *Continental Shelf Research,* 27**,** 1501-1509.

BELIAEV, A. S. & SAFFARINI, D. A. 1998. *Shewanella putrefaciens* mtrB encodes an outer membrane protein required for Fe(III) and Mn(IV) reduction. *Journal of Bacteriology,* 180**,** 6292-6297.

BENDER, M., JAHNKE, R., WEISS, R., MARTIN, W., HEGGIE, D. T., ORCHARDO, J. & SOWERS, T. 1989. Organic-carbon oxidation and benthic nitrogen and silica dynamics in San-Clemente Basin, a continental borderland site. *Geochimica Et Cosmochimica Acta,* 53**,** 685-697.

BORLOO, J., VERGAUWEN, B., DE SMET, L., BRIGE, A., MOTTE, B., DEVREESE, B. & VAN BEEUMEN, J. 2007. A kinetic approach to the dependence of dissimilatory metal reduction by *Shewanella oneidensis* MR-1 on the outer membrane cytochromes *c* OmcA and OmcB. *Febs Journal,* 274**,** 3728-3738.

BORUCKI, W. J. 1984. Lighting - estimates of the rates of energy-dissipation and nitrogen-fixation *Reviews of Geophysics,* 22**,** 363-372.

BOTHE, H., FERGUSON, S. J. & NEWTON, W. E. (eds.) 2007. *Biology of the nitrogen cycle,* Amsterdam, The Netherlands: Elsevier.

BOTHE, H., JOST, G., SCHLOTER, M., WARD, B. B. & WITZEL, K. P. 2000. Molecular analysis of ammonia oxidation and denitrification in natural environments. *Fems Microbiology Reviews,* 24**,** 673-690.

BRANDES, J. A., DEVOL, A. H. & DEUTSCH, C. 2007. New developments in the marine nitrogen cycle. *Chemical Reviews,* 107**,** 577-589.

BRENDEL, P. J. & LUTHER, G. W. 1995. Development of a gold amalgam voltammetric microelectrode for the determination of dissolved Fe, Mn, O-2, and S(-II) in porewaters of marine and fresh-water sediments. *Environmental Science & Technology,* 29**,** 751-761.

BRETSCHGER, O., OBRAZTSOVA, A., STURM, C. A., CHANG, I. S., GORBY, Y. A., REED, S. B., CULLEY, D. E., REARDON, C. L., BARUA, S., ROMINE, M. F., ZHOU, J., BELIAEV, A. S., BOUHENNI, R., SAFFARINI, D., MANSFELD, F., KIM, B. H., FREDRICKSON, J. K. & NEALSON, K. H. 2007. Current production and metal oxide reduction by *Shewanella oneidensis* MR-1 wild type and mutants. *Applied and Environmental Microbiology,* 73**,** 7003-7012.

BRISTOW, G. & TAILLEFERT, M. 2008. VOLTINT: A Matlabg (R)-based program for semi-automated processing of geochemical data acquired by voltammetry. *Computers & Geosciences,* 34**,** 153-162.

BRODA, E. 1977. 2 KINDS OF LITHOTROPHS MISSING IN NATURE. *Zeitschrift Fur Allgemeine Mikrobiologie,* 17**,** 491-493.

BROUWERS, G. J., DE VRIND, J. P. M., CORSTJENS, P., CORNELIS, P., BAYSSE, C. & DEJONG, E. 1999. cumA, a gene encoding a multicopper oxidase, is

involved in Mn2+ oxidation in Pseudomonas putida GB-1. *Applied and Environmental Microbiology,* 65**,** 1762-1768.

BRUNET, R. C. & GARCIAGIL, L. J. 1996. Sulfide-induced dissimilatory nitrate reduction to ammonia in anaerobic freshwater sediments. *Fems Microbiology Ecology,* 21**,** 131-138.

BURNES, B. S., MULBERRY, M. J. & DICHRISTINA, T. J. 1998. Design and application of two rapid screening techniques for isolation of Mn(IV) reduction-deficient mutants of *Shewanella putrefaciens*. *Applied and Environmental Microbiology,* 64**,** 2716-2720.

BURNS, J. L. 2010. *Molecular mechanism of metal respiration by Shewanella oneidensis MR-1*. Ph.D., Georgia Institute of Technology.

BURNS, J. L. & DICHRISTINA, T. 2011. Single conserved cysteine in CXXC motif or outer membrane protein MtrB is required for anaerobic metal respiration by *Shewanella oneidensis* MR-1, Manuscript under review.

BURNS, J. L. & DICHRISTINA, T. J. 2009. Anaerobic Respiration of Elemental Sulfur and Thiosulfate by Shewanella oneidensis MR-1 Requires psrA, a Homolog of the phsA Gene of Salmonella enterica Serovar Typhimurium LT2. *Applied and Environmental Microbiology,* 75**,** 5209-5217.

BURNS, J. L., GINN, B. R., BATES, D. J., DUBLIN, S. N., TAYLOR, J. V., APKARIAN, R. P., AMARO-GARCIA, S., NEAL, A. L. & DICHRISTINA, T. J. 2010. Outer Membrane-Associated Serine Protease Involved in Adhesion of Shewanella oneidensis to Fe(III) Oxides. *Environmental Science & Technology,* 44**,** 68-73.

CANFIELD, D. E., THAMDRUP, B. & HANSEN, J. W. 1993. The anaerobic degradation of organic-matter in danish coastal sediments - iron reduction, manganese reduction, and sulfate reduction. *Geochimica Et Cosmochimica Acta,* 57**,** 3867-3883.

CAPONE, D. G. & KNAPP, A. N. 2007. Oceanography - A marine nitrogen cycle fix? *Nature,* 445**,** 159-160.

CLEMENT, J. C., SHRESTHA, J., EHRENFELD, J. G. & JAFFE, P. R. 2005. Ammonium oxidation coupled to dissimilatory reduction of iron under anaerobic conditions in wetland soils. *Soil Biology & Biochemistry,* 37**,** 2323-2328.

COATES, J. D., ELLIS, D. J., GAW, C. V. & LOVLEY, D. R. 1999. *Geothrix fermentans* gen. nov., sp nov., a novel Fe(III)-reducing bacterium from a hydrocarbon-contaminated aquifer. *International Journal of Systematic Bacteriology,* 49**,** 1615-1622.

CODISPOTI, L. A., BRANDES, J. A., CHRISTENSEN, J. P., DEVOL, A. H., NAQVI, S. W. A., PAERL, H. W. & YOSHINARI, T. 2001. The oceanic fixed nitrogen and nitrous oxide budgets: Moving targets as we enter the anthropocene? *Scientia Marina,* 65**,** 85-105.

COTTON, F. A., WILKINSON, G., MURILLO, C. A. & BOCHMANN, M. (eds.) 1999. *Advanced Inorgnaic Chemistry,* New York: John Wiley & Sons Inc.

DALE, J. R., WADE, R. & DICHRISTINA, T. J. 2007. A conserved histidine in cytochrome c maturation permease CcmB of Shewanella putrefaciens is required for anaerobic growth below a threshold standard redox potential. *Journal of Bacteriology,* 189**,** 1036-1043.

DALSGAARD, T. & THAMDRUP, B. 2002. Factors controlling anaerobic ammonium oxidation with nitrite in marine sediments. *Applied and Environmental Microbiology,* 68**,** 3802-3808.

DALSGAARD, T., THAMDRUP, B. & CANFIELD, D. E. 2005. Anaerobic ammonium oxidation (anammox) in the marine environment. *Research in Microbiology,* 156**,** 457-464.

DAVISON, W. 1993. Iron and Manganese in Lakes. *Earth-Science Reviews,* 34**,** 119-163.

DE SCHAMPHELAIRE, L., RABAEY, K., BOON, N., VERSTRAETE, W. & BOECKX, P. 2007. Minireview: The potential of enhanced manganese redox cycling for sediment oxidation. *Geomicrobiology Journal,* 24**,** 547-558.

DEGRAAF, A. A. V., DEBRUIJN, P., ROBERTSON, L. A., JETTEN, M. S. M. & KUENEN, J. G. 1996. Autotrophic growth of anaerobic ammonium-oxidizing micro-organisms in a fluidized bed reactor. *Microbiology-Uk,* 142**,** 2187-2196.

DEN CAMP, H., KARTAL, B., GUVEN, D., VAN NIFTRIK, L., HAAIJER, S. C. M., VAN DER STAR, W. R. L., VAN DE PAS-SCHOONEN, K. T., CABEZAS, A., YING, Z., SCHMID, M. C., KUYPERS, M. M. M., VAN DE VOSSENBERG, J., HARHANGI, H. R., PICIOREANU, C., VAN LOOSDRECHT, M. C. M., KUENEN, J. G., STROUS, M. & JETTEN, M. S. M. 2006. Global impact and application of the anaerobic ammonium-oxidizing (anammox) bacteria. *Biochemical Society Transactions,* 34**,** 174-178.

DESVAUX, M., PARHAM, N. J., SCOTT-TUCKER, A. & HENDERSON, I. R. 2004. The general secretory pathway: a general misnomer? *Trends in Microbiology,* 12**,** 306-309.

DEUTSCH, C., SARMIENTO, J. L., SIGMAN, D. M., GRUBER, N. & DUNNE, J. P. 2007. Spatial coupling of nitrogen inputs and losses in the ocean. *Nature,* 445**,** 163-167.

DEVRIND, J. P. M., DEVRINDDEJONG, E. W., DEVOOGT, J. W. H., WESTBROEK, P., BOOGERD, F. C. & ROSSON, R. A. 1986. Manganese oxidation by spores and spore coats of a marine *Bacillus* species. *Applied and Environmental Microbiology,* 52**,** 1096-1100.

DICHRISTINA, T. J., FREDRICKSON, J. K. & ZACHARA, J. M. 2005. Enzymology of electron transport: Energy generation with geochemical consequences. *Molecular Geomicrobiology.* Chantilly: Mineralogical Soc America.

DICHRISTINA, T. J., MOORE, C. M. & HALLER, C. A. 2002. Dissimilatory Fe(III) and Mn(IV) reduction by *Shewanella putrefaciens* requires *ferE*, a homolog of the *pulE* (*gspE*) type II protein secretion gene. *Journal of Bacteriology,* 184**,** 142-151.

DISMUKES, G. C. 1986. THE METAL CENTERS OF THE PHOTOSYNTHETIC OXYGEN-EVOLVING COMPLEX. *Photochemistry and Photobiology,* 43**,** 99-115.

DOLLHOPF, M. E., NEALSON, K. H., SIMON, D. M. & LUTHER, G. W. 2000. Kinetics of Fe(III) and Mn(IV) reduction by the Black Sea strain of *Shewanella putrefaciens* using in situ solid state voltammetric Au/Hg electrodes. *Marine Chemistry,* 70**,** 171-180.

DUCKWORTH, O. W., BARGAR, J. R. & SPOSITO, G. 2009. Coupled biogeochemical cycling of iron and manganese as mediated by microbial siderophores. *Biometals,* 22**,** 605-613.

DUCKWORTH, O. W. & SPOSITO, G. 2005a. Siderophore-manganese(III) interactions II. Manganite dissolution promoted by desferrioxamine B. *Environmental Science & Technology,* 39**,** 6045-6051.

DUCKWORTH, O. W. & SPOSITO, G. 2005b. Siderophore-manganese(III) interactions. I. Air-oxidation of manganese(II) promoted by desferrioxamine B. *Environmental Science & Technology,* 39**,** 6037-6044.

DUCKWORTH, O. W. & SPOSITO, G. 2007. Siderophore-promoted dissolution of synthetic and biogenic layer-type Mn oxides. *Chemical Geology,* 242**,** 497-508.

EMELYANOV, E. M. 2001. Biogenic components and elements in sediments of the Central Baltic and their redistribution. *Marine Geology,* 172**,** 23-41.

ENGSTROM, P., DALSGAARD, T., HULTH, S. & ALLER, R. C. 2005. Anaerobic ammonium oxidation by nitrite (anammox): Implications for N-2 production in coastal marine sediments. *Geochimica Et Cosmochimica Acta,* 69**,** 2057-2065.

ETTWIG, K. F., BUTLER, M. K., LE PASLIER, D., PELLETIER, E., MANGENOT, S., KUYPERS, M. M. M., SCHREIBER, F., DUTILH, B. E., ZEDELIUS, J., DE BEER, D., GLOERICH, J., WESSELS, H., VAN ALEN, T., LUESKEN, F., WU, M. L., VAN DE PAS-SCHOONEN, K. T., DEN CAMP, H., JANSSEN-MEGENS, E. M., FRANCOIJS, K. J., STUNNENBERG, H., WEISSENBACH, J., JETTEN, M. S. M. & STROUS, M. 2010. Nitrite-driven anaerobic methane oxidation by oxygenic bacteria. *Nature,* 464**,** 543-+.

FAULKNER, K. M., STEVENS, R. D. & FRIDOVICH, I. 1994. Characterizatoin of Mn(II) complexes of linear and cyclic desferrioxamine as mimics of superoxide-dismutase activity. *Archives of Biochemistry and Biophysics,* 310**,** 341-346.

FDZ-POLANCO, F., FDZ-POLANCO, M., FERNANDEZ, N., URUENA, M. A., GARCIA, P. A. & VILLAVERDE, S. 2001. New process for simultaneous removal of nitrogen and sulphur under anaerobic conditions. *Water Research,* 35**,** 1111-1114.

FENNESSEY, C. M., JONES, M. E., TAILLEFERT, M. & DICHRISTINA, T. J. 2010. Siderophores Are Not Involved in Fe(III) Solubilization during Anaerobic Fe(III) Respiration by *Shewanella oneidensis* MR-1. *Applied and Environmental Microbiology,* 76**,** 2425-2432.

FRANCIS, C. A., ROBERTS, K. J., BEMAN, J. M., SANTORO, A. E. & OAKLEY, B. B. 2005. Ubiquity and diversity of ammonia-oxidizing archaea in water columns and sediments of the ocean. *Proceedings of the National Academy of Sciences of the United States of America,* 102**,** 14683-14688.

FROELICH, P. N., KLINKHAMMER, G. P., BENDER, M. L., LUEDTKE, N. A., HEATH, G. R., CULLEN, D., DAUPHIN, P., HAMMOND, D., HARTMAN, B. & MAYNARD, V. 1979. Early oxidation of organic-matter in pelagic sediments of the eastern equatorial Atlantic - suboxic diagenesis. *Geochimica Et Cosmochimica Acta,* 43**,** 1075-1090.

GALLOWAY, J. N. & COWLING, E. B. 2002. Reactive nitrogen and the world: 200 years of change. *Ambio,* 31**,** 64-71.

GALLOWAY, J. N., DENTENER, F. J., CAPONE, D. G., BOYER, E. W., HOWARTH, R. W., SEITZINGER, S. P., ASNER, G. P., CLEVELAND, C. C., GREEN, P. A., HOLLAND, E. A., KARL, D. M., MICHAELS, A. F., PORTER, J. H., TOWNSEND, A. R. & VOROSMARTY, C. J. 2004. Nitrogen cycles: past, present, and future. *Biogeochemistry,* 70**,** 153-226.

GALLOWAY, J. N., SCHLESINGER, W. H., LEVY, H., MICHAELS, A. & SCHNOOR, J. L. 1995. Nitrogen-fixation - anthropogenic enhancement - environmental response *Global Biogeochemical Cycles,* 9**,** 235-252.

GORBY, Y. A., YANINA, S., MCLEAN, J. S., ROSSO, K. M., MOYLES, D., DOHNALKOVA, A., BEVERIDGE, T. J., CHANG, I. S., KIM, B. H., KIM, K. S., CULLEY, D. E., REED, S. B., ROMINE, M. F., SAFFARINI, D. A., HILL, E. A., SHI, L., ELIAS, D. A., KENNEDY, D. W., PINCHUK, G., WATANABE, K., ISHII, S., LOGAN, B., NEALSON, K. H. & FREDRICKSON, J. K. 2006. Electrically conductive bacterial nanowires produced by *Shewanella oneidensis* strain MR-1 and other microorganisms. *Proceedings of the National Academy of Sciences of the United States of America,* 103**,** 11358-11363.

GRASSHOFF, K., EHRHARDT, M. & KREMLING, K. (eds.) 1983. *Methods of Seawater Analysis,* Weinheim: Verlag Chemie GmbH.

GREENE, A. C., PATEL, B. K. C. & SHEEHY, A. J. 1997. Deferribacter thermophilus gen nov, sp nov, a novel thermophilic manganese- and iron-reducing bacterium isolated from a petroleum reservoir. *International Journal of Systematic Bacteriology,* 47**,** 505-509.

GRIBSHOLT, B., KOSTKA, J. E. & KRISTENSEN, E. 2003. Impact of fiddler crabs and plant roots on sediment biogeochemistry in a Georgia saltmarsh. *Marine Ecology-Progress Series,* 259**,** 237-251.

GRUBER, N. & SARMIENTO, J. L. 1997. Global patterns of marine nitrogen fixation and denitrification. *Global Biogeochemical Cycles,* 11**,** 235-266.

GRUZINA, T. G., BALAKINA, M. N., KARAMUSHKA, V. I., STEPURA, L. G. & ULBERG, Z. R. 1997. The bacterial plasma membrane ATPase in assessment of heavy metal toxicity. *Microbiology,* 66**,** 8-11.

HAAS, J. R. & DICHRISTINA, T. J. 2002. Effects of Fe(III) chemical speciation on dissimilatory Fe(III) reduction by *Shewanella putrefaciens*. *Environmental Science & Technology,* 36**,** 373-380.

HALL, C. A. 2009. *Insights into marine nitrogen cycling in coastal sediments: Inputs, losses, and measurement techniques.* Doctor of Philosophy, Georgia Institute of Technology.

HALL, P. O. & ALLER, R. C. 1992. Rapid, small-volume, flow-injection analysis for sigma-CO_2 and NH_4^+ in marine and fresh-waters. *Limnology and Oceanography,* 37**,** 1113-1119.

HAMERSLEY, M. R., LAVIK, G., WOEBKEN, D., RATTRAY, J. E., LAM, P., HOPMANS, E. C., DAMSTE, J. S. S., KRUGER, S., GRACO, M., GUTIERREZ, D. & KUYPERS, M. M. M. 2007. Anaerobic ammonium oxidation in the Peruvian oxygen minimum zone. *Limnology and Oceanography,* 52**,** 923-933.

HARTSHORNE, R. S., REARDON, C. L., ROSS, D., NUESTER, J., CLARKE, T. A., GATES, A. J., MILLS, P. C., FREDRICKSON, J. K., ZACHARA, J. M., SHI, L., BELIAEV, A. S., MARSHALL, M. J., TIEN, M., BRANTLEY, S., BUTT, J. N. & RICHARDSON, D. J. 2009. Characterization of an electron conduit between bacteria and the extracellular environment. *Proceedings of the National Academy of Sciences of the United States of America,* 106**,** 22169-22174.

HAU, H. H. & GRALNICK, J. A. 2007. Ecology and biotechnology of the genus *Shewanella*. *Annual Review of Microbiology,* 61**,** 237-258.

HEIDELBERG, J. F., PAULSEN, I. T., NELSON, K. E., GAIDOS, E. J., NELSON, W. C., READ, T. D., EISEN, J. A., SESHADRI, R., WARD, N., METHE, B., CLAYTON, R. A., MEYER, T., TSAPIN, A., SCOTT, J., BEANAN, M., BRINKAC, L., DAUGHERTY, S., DEBOY, R. T., DODSON, R. J., DURKIN, A. S., HAFT, D. H., KOLONAY, J. F., MADUPU, R., PETERSON, J. D., UMAYAM, L. A., WHITE, O., WOLF, A. M., VAMATHEVAN, J., WEIDMAN, J., IMPRAIM, M., LEE, K., BERRY, K., LEE, C., MUELLER, J., KHOURI, H., GILL, J., UTTERBACK, T. R., MCDONALD, L. A., FELDBLYUM, T. V., SMITH, H. O., VENTER, J. C., NEALSON, K. H. & FRASER, C. M. 2002. Genome sequence of the dissimilatory metal ion-reducing bacterium Shewanella oneidensis. *Nature Biotechnology,* 20**,** 1118-1123.

HEIJNEN, J. J. & VANDIJKEN, J. P. 1992. In search of a themodynamic description of biomass yields for the chemotrophic growth of microorganisms. *Biotechnology and Bioengineering,* 39**,** 833-858.

HEINTZE, S. G. & MANN, P. J. G. 1947. Soluble complexes of manganic manganese. *Journal of Agricultural Science,* 37**,** 23-&.

HENNEKE, E., LUTHER, G. W. & DELANGE, G. J. 1991. Determination of inorganic sulfur speciation with polarographic techniques - some preliminary - results for recent hypersaline anoxic sediments. *Marine Geology,* 100**,** 115-123.

HERSZAGE, J. & AFONSO, M. D. 2003. Mechanism of hydrogen sulfide oxidation by manganese(IV) oxide in aqueous solutions. *Langmuir,* 19**,** 9684-9692.

HULTH, S., ALLER, R. C., CANFIELD, D. E., DALSGAARD, T., ENGSTROM, P., GILBERT, F., SUNDBACK, K. & THAMDRUP, B. 2005. Nitrogen removal in marine environments: recent findings and future research challenges. *Marine Chemistry,* 94**,** 125-145.

HULTH, S., ALLER, R. C. & GILBERT, F. 1999. Coupled anoxic nitrification manganese reduction in marine sediments. *Geochimica Et Cosmochimica Acta,* 63**,** 49-66.

JAVANAUD, C., MICHOTEY, V., GUASCO, S., GARCIA, N., ANSCHUTZ, P., CANTON, M. & BONIN, P. 2011. Anaerobic ammonium oxidation mediated by Mn-oxides: from sediment to strain level. *Research in Microbiology,* 162**,** 848-857.

JENSEN, K. M., JENSEN, M. H. & COX, R. P. 1996. Membrane inlet mass spectrometric analysis of N-isotope labelling for aquatic denitrification studies. *Fems Microbiology Ecology,* 20**,** 101-109.

JENSEN, M. M., KUYPERS, M. M. M., LAVIK, G. & THAMDRUP, B. 2008. Rates and regulation of anaerobic ammonium oxidation and denitrification in the Black Sea. *Limnology and Oceanography,* 53**,** 23-36.

JETTEN, M. S. M., VAN NIFTRIK, L., STROUS, M., KARTAL, B., KELTJENS, J. T. & OP DEN CAMP, H. J. M. 2009. Biochemistry and molecular biology of anammox bacteria. *Critical Reviews in Biochemistry and Molecular Biology,* 44**,** 65-84.

JONES, M. E., FENNESSEY, C. M., DICHRISTINA, T. J. & TAILLEFERT, M. 2010. *Shewanella oneidensis* MR-1 mutants selected for their inability to produce soluble organic-Fe(III) complexes are unable to respire Fe(III) as anaerobic electron acceptor. *Environmental Microbiology,* 12**,** 938-950.

KALVELAGE, T., JENSEN, M. M., CONTRERAS, S., REVSBECH, N. P., LAM, P., GUNTER, M., LAROCHE, J., LAVIK, G. & KUYPERS, M. M. M. 2011. Oxygen Sensitivity of Anammox and Coupled N-Cycle Processes in Oxygen Minimum Zones. *Plos One,* 6.

KANA, T. M., DARKANGELO, C., HUNT, M. D., OLDHAM, J. B., BENNETT, G. E. & CORNWELL, J. C. 1994. Membrane inlet mass-spectrometer for rapid high-precision determination of N-2, O-2, and Ar in environmental water samples. *Analytical Chemistry,* 66**,** 4166-4170.

KLEWICKI, J. K. & MORGAN, J. J. 1998. Kinetic behavior of Mn(III) complexes of pyrophosphate, EDTA, and citrate. *Environmental Science & Technology,* 32**,** 2916-2922.

KNOWLES, R. 1982. DENITRIFICATION. *Microbiological Reviews,* 46**,** 43-70.

KOSTKA, J. E., LUTHER, G. W. & NEALSON, K. H. 1995. Chemical and Biological Reduction of Mn(III)-pyrophosphate Complexes - Potential Importance of Dissolved Mn(III) as an Environmental Oxidant. *Geochimica Et Cosmochimica Acta,* 59**,** 885-894.

KOUZUMA, A., HASHIMOTO, K. & WATANABE, K. 2012. Roles of siderophore in manganese-oxide reduction by Shewanella oneidensis MR-1. *Fems Microbiology Letters,* 326**,** 91-98.

KRISHNAN, K. P., SINHA, R. K., KRISHNA, K., NAIR, S. & SINGH, S. M. 2009. Microbially mediated redox transformations of manganese (II) along with some other trace elements: a study from Antarctic lakes. *Polar Biology,* 32**,** 1765-1778.

KUYPERS, M. M. M., SLIEKERS, A. O., LAVIK, G., SCHMID, M., JORGENSEN, B. B., KUENEN, J. G., DAMSTE, J. S. S., STROUS, M. & JETTEN, M. S. M. 2003. Anaerobic ammonium oxidation by anammox bacteria in the Black Sea. *Nature,* 422**,** 608-611.

LAM, P., JENSEN, M. M., LAVIK, G., MCGINNIS, D. F., MULLER, B., SCHUBERT, C. J., AMANN, R., THAMDRUP, B. & KUYPERS, M. M. M. 2007. Linking crenarchaeal and bacterial nitrification to anammox in the Black Sea. *Proceedings of the National Academy of Sciences of the United States of America,* 104**,** 7104-7109.

LAM, P., LAVIK, G., JENSEN, M. M., VAN DE VOSSENBERG, J., SCHMID, M., WOEBKEN, D., DIMITRI, G., AMANN, R., JETTEN, M. S. M. & KUYPERS, M. M. M. 2009. Revising the nitrogen cycle in the Peruvian oxygen minimum zone. *Proceedings of the National Academy of Sciences of the United States of America,* 106**,** 4752-4757.

LEARMAN, D. R., VOELKER, B. M., VAZQUEZ-RODRIGUEZ, A. I. & HANSEL, C. M. 2011. Formation of manganese oxides by bacterially generated superoxide. *Nature Geoscience,* 4**,** 95-98.

LENSING, H. J., VOGT, M. & HERRLING, B. 1994. Modeling of biologically mediated redox processes in the subsurface. *Journal of Hydrology,* 159**,** 125-143.

LOVLEY, D. R. 1991. DISSIMILATORY FE(III) AND MN(IV) REDUCTION. *Microbiological Reviews,* 55**,** 259-287.

LOVLEY, D. R., GIOVANNONI, S. J., WHITE, D. C., CHAMPINE, J. E., PHILLIPS, E. J. P., GORBY, Y. A. & GOODWIN, S. 1993. Geobacter-metallireducens gen-nov, a microorganism capable of coupling the complete oxidation of organic-compounds to the reduction of iron and other metals. *Archives of Microbiology,* 159**,** 336-344.

LOVLEY, D. R., HOLMES, D. E. & NEVIN, K. P. 2004a. *Advances in Microbial Physiology*, Academic Press Ltd.

LOVLEY, D. R., HOLMES, D. E. & NEVIN, K. P. 2004b. Dissimilatory Fe(III) and Mn(IV) reduction. *Advances in Microbial Physiology, Vol. 49.* London: Academic Press Ltd.

LOVLEY, D. R. & PHILLIPS, E. J. P. 1988. Novel mode of microbial energy-metabolism-organic-carbon oxidation coupled to dissimilatory reduction of iron or manganese. *Applied and Environmental Microbiology,* 54**,** 1472-1480.

LOVLEY, D. R. & WOODWARD, J. C. 1996. Mechanisms for chelator stimulation of microbial Fe(III)-oxide reduction. *Chemical Geology,* 132**,** 19-24.

LUTHER, G. W. 2005. Manganese(II) oxidation and Mn(IV) reduction in the environment - Two one-electron transfer steps versus a single two-electron step. *Geomicrobiology Journal,* 22**,** 195-203.

LUTHER, G. W. 2010. The Role of One- and Two-Electron Transfer Reactions in Forming Thermodynamically Unstable Intermediates as Barriers in Multi-Electron Redox Reactions. *Aquatic Geochemistry,* 16**,** 395-420.

LUTHER, G. W., SUNDBY, B., LEWIS, B. L., BRENDEL, P. J. & SILVERBERG, N. 1997. Interactions of manganese with the nitrogen cycle: Alternative pathways to dinitrogen. *Geochimica Et Cosmochimica Acta,* 61**,** 4043-4052.

MACKIN, J. E. & ALLER, R. C. 1984. Ammonium adsorption in marine-sediments. *Limnology and Oceanography,* 29**,** 250-257.

MADIGAN, M. T., MARTINKO, J. M. & PARKER, J. (eds.) 2003. *Brock Biology of Microorganisms,* Upper Saddle River, NJ.: Pearson Education Inc.

.

MADISON, A. S., TEBO, B. M. & LUTHER, G. W. 2011. Simultaneous determination of soluble manganese(III), manganese(II) and total manganese in natural (pore)waters. *Talanta,* 84**,** 374-381.

MARSILI, E., BARON, D. B., SHIKHARE, I. D., COURSOLLE, D., GRALNICK, J. A. & BOND, D. R. 2008. *Shewanella* Secretes flavins that mediate extracellular electron transfer. *Proceedings of the National Academy of Sciences of the United States of America,* 105**,** 3968-3973.

MARTIN, J. M. & MEYBECK, M. 1979. Elemental mass-balance of material carried by major world rivers. *Marine Chemistry,* 7**,** 173-206.

MILLALEO, R., REYES-DIAZ, M., IVANOV, A. G., MORA, M. L. & ALBERDI, M. 2010. Manganese as essential and toxic element for plants: transport, accumulation and resistance mechanisms. *Journal of Soil Science and Plant Nutrition,* 10**,** 476-494.

MILLERO, F. J. 1986. the thermodynamics and kinetics of the hydrogen-sulfide system in natural-waters. *Marine Chemistry,* 18**,** 121-147.

MORGAN, J. J. 2000a. Manganese in natural waters and earth's crust: Its availability to organisms. *Metal Ions in Biological Systems, Vol 37.* New York: Marcel Dekker.

MORGAN, J. J. 2000b. *Metal Ions in Biological Systems*, Marcel Dekker.

MORGAN, J. J. 2005. Kinetics of reaction between O-2 and Mn(II) species in aqueous solutions. *Geochimica Et Cosmochimica Acta,* 69**,** 35-48.

MORTIMER, R. J. G., HARRIS, S. J., KROM, M. D., FREITAG, T. E., PROSSER, J. I., BARNES, J., ANSCHUTZ, P., HAYES, P. J. & DAVIES, I. M. 2004. Anoxic nitrification in marine sediments. *Marine Ecology-Progress Series,* 276**,** 37-51.

MORTIMER, R. J. G., KROM, M. D., HARRIS, S. J., HAYES, P. J., DAVIES, I. M., DAVISON, W. & ZHANG, H. 2002. Evidence for suboxic nitrification in recent marine sediments. *Marine Ecology-Progress Series,* 236**,** 31-35.

MOSIER, A. R., DORAN, J. W. & FRENEY, J. R. 2002. Managing soil denitrification. *Journal of Soil and Water Conservation,* 57**,** 505-513.

MOURET, A., ANSCHUTZ, P., LECROART, P., CHAILLOU, G., HYACINTHE, C., DEBORDE, J., JORISSEN, F. J., DEFLANDRE, B., SCHMIDT, S. & JOUANNEAU, J. M. 2009. Benthic geochemistry of manganese in the Bay of Biscay, and sediment mass accumulation rate. *Geo-Marine Letters,* 29**,** 133-149.

MULDER, A., VANDEGRAAF, A. A., ROBERTSON, L. A. & KUENEN, J. G. 1995. Anaerobic ammonium oxidation discovered in a denitrifying fluidized-bed reactor. *Fems Microbiology Ecology,* 16**,** 177-183.

MURRAY, J. W. 1974. Surface chemistry of hydrous manganese-dioxide. *Journal of Colloid and Interface Science,* 46**,** 357-371.

MURRAY, J. W., BALISTRIERI, L. S. & PAUL, B. 1984. The oxidation-state of manganese in marine-sediments and ferromanganese nodules. *Geochimica Et Cosmochimica Acta,* 48**,** 1237-1247.

MURRAY, J. W., CODISPOTI, L. A. & FRIEDERICH, G. E. 1995. Oxidation-reduction environments - the suboxic zone in the Black-sea. *In:* HUANG, C. P., OMELIA, C. R. & MORGAN, J. J. (eds.) *Aquatic Chemistry - Interfacial and Interspecies Processes.* Washington: Amer Chemical Soc.

MYERS, C. R. & MYERS, J. M. 2002. MtrB is required for proper incorporation of the cytochromes OmcA and OmcB into the outer membrane of Shewanella putrefaciens MR-1. *Applied and Environmental Microbiology,* 68**,** 5585-5594.

MYERS, C. R. & MYERS, J. M. 2003a. Cell surface exposure of the outer membrane cytochromes of *Shewanella oneidensis* MR-1. *Letters in Applied Microbiology,* 37**,** 254-258.

MYERS, C. R. & NEALSON, K. H. 1988. Bacterial manganese reduction and growth with manganese oxide as the sole electron-acceptor. *Science,* 240**,** 1319-1321.

MYERS, J. M. & MYERS, C. R. 2000. Role of the tetraheme cytochrome CymA in anaerobic electron transport in cells of *Shewanella putrefaciens* MR-1 with normal levels of menaquinone. *Journal of Bacteriology,* 182**,** 67-75.

MYERS, J. M. & MYERS, C. R. 2001. Role for outer membrane cytochromes OmcA and OmcB of *Shewanella putrefaciens* MR-1 in reduction of manganese dioxide. *Applied and Environmental Microbiology,* 67**,** 260-269.

MYERS, J. M. & MYERS, C. R. 2003b. Overlapping role of the outer membrane cytochromes of *Shewanella oneidensis* MR-1 in the reduction of manganese(IV) oxide. *Letters in Applied Microbiology,* 37**,** 21-25.

NEALSON, K. H., TEBO, B. M. & ROSSON, R. A. 1988. Occurrence and mechanisms of microbial oxidation of manganese. *Advances in Applied Microbiology,* 33**,** 279-318.

NERETIN, L. N., POHL, C., JOST, G., LEIPE, T. & POLLEHNE, F. 2003. Manganese cycling in the Gotland Deep, Baltic Sea. *Marine Chemistry,* 82**,** 125-143.

NESBITT, H. W. & BANERJEE, D. 1998. Interpretation of XPS Mn(2p) spectra of Mn oxyhydroxides and constraints on the mechanism of MnO2 precipitation. *American Mineralogist,* 83**,** 305-315.

NEUMANN, T., HEISER, U., LEOSSON, M. A. & KERSTEN, M. 2002. Early diagenetic processes during Mn-carbonate formation: Evidence from the isotopic composition of authigenic Ca-rhodochrosites of the Baltic Sea. *Geochimica Et Cosmochimica Acta,* 66**,** 867-879.

NEWMAN, D. K. & KOLTER, R. 2000. A role for excreted quinones in extracellular electron transfer. *Nature,* 405**,** 94-97.

NEWTON, J. D. 2006. *Evidence for manganese-catalyzed nitrogen cycling in salt marsh sediments.* Master of Science, Georgia Institute of Technology.

NIELSEN, L. P. 1992. Denitrification in sediment determined from nitrogen isotope pairing. *Fems Microbiology Ecology,* 86**,** 357-362.

OKAZAKI, M., SUGITA, T., SHIMIZU, M., OHODE, Y., IWAMOTO, K., DEVRINDDEJONG, E. W., DEVRIND, J. P. M. & CORSTJENS, P. 1997. Partial purification and characterization of manganese-oxidizing factors of *Pseudomonas fluorescens* GB-1. *Applied and Environmental Microbiology,* 63**,** 4793-4799.

OTERO, X. L., FERREIRA, T. O., HUERTA-DIAZ, M. A., PARTITI, C. S. M., SOUZA, V., VIDAL-TORRADO, P. & MACIAS, F. 2009. Geochemistry of iron and manganese in soils and sediments of a mangrove system, Island of Pai Matos (Cananeia - SP, Brazil). *Geoderma,* 148**,** 318-335.

PARK, W., NAM, Y. K., LEE, M. J. & KIM, T. H. 2009. Anaerobic Ammonia-oxidation Coupled with Fe(3+) Reduction by an Anaerobic Culture from a Piggery Wastewater Acclimated to NH(4)(+)/Fe(3+) Medium. *Biotechnology and Bioprocess Engineering,* 14**,** 680-685.

PARKER, D. L., MORITA, T., MOZAFARZADEH, M. L., VERITY, R., MCCARTHY, J. K. & TEBO, B. M. 2007. Inter-relationships of MnO2 precipitation, siderophore-Mn-(III) complex formation, siderophore degradation, and iron limitation in Mn-(II)-oxidizing bacterial cultures. *Geochimica Et Cosmochimica Acta,* 71**,** 5672-5683.

PARKER, D. L., SPOSITO, G. & TEBO, B. M. 2004. Manganese(III) binding to a pyoverdine siderophore produced by a manganese(II)-oxidizing bacterium. *Geochimica Et Cosmochimica Acta,* 68**,** 4809-4820.

PAVLOSTATHIS, S. G. & GIRALDOGOMEZ, E. 1991. Kinetics of anaerobic treatment. *Water Science and Technology,* 24**,** 35-59.

PEREZ-BENITO, J. F. 2002. Reduction of colloidal manganese dioxide by manganese(II). *Journal of Colloid and Interface Science,* 248**,** 130-135.

PEREZ-BENITO, J. F., ARIAS, C. & AMAT, E. 1996. A kinetic study of the reduction of colloidal manganese dioxide by oxalic acid. *Journal of Colloid and Interface Science,* 177**,** 288-297.

PEREZBENITO, J. F. & ARIAS, C. 1992. A kinetic-study of the reaction between soluble (colloidal) manganese-dioxide and formic-acid. *Journal of Colloid and Interface Science,* 149**,** 92-97.

PEREZBENITO, J. F., MATAPEREZ, F. & BRILLAS, E. 1987. PERMANGANATE OXIDATION OF GLYCINE - KINETICS, CATALYTIC EFFECTS, AND MECHANISMS. *Canadian Journal of Chemistry-Revue Canadienne De Chimie,* 65**,** 2329-2337.

PINCHUK, G. E., RODIONOV, D. A., YANG, C., LI, X. Q., OSTERMAN, A. L., DERVYN, E., GEYDEBREKHT, O. V., REED, S. B., ROMINE, M. F., COLLART, F. R., SCOTT, J. H., FREDRICKSON, J. K. & BELIAEV, A. S. 2009. Genomic reconstruction of *Shewanella oneidensis* MR-1 metabolism reveals a previously uncharacterized machinery for lactate utilization. *Proceedings of the National Academy of Sciences of the United States of America,* 106**,** 2874-2879.

PITTS, K. E., DOBBIN, P. S., REYES-RAMIREZ, F., THOMSON, A. J., RICHARDSON, D. J. & SEWARD, H. E. 2003. Characterization of the *Shewanella oneidensis* MR-1 decaheme cytochrome MtrA. *Journal of Biological Chemistry,* 278**,** 27758-27765.

POSTMA, D. 1985. Concentration of Mn and separation from Fe in sediments. 1. Kinetics and stoichiometry of the reaction between birnessite and dissolved Fe(II) at 10-degree-C. *Geochimica Et Cosmochimica Acta,* 49**,** 1023-1033.

PRADEEP, E. D. & JINNO, K. 2010. A Numerical Approach to Simulate the Biogeochemical Involvement in a Coastal Reduced Groundwater Environment. *Water Air and Soil Pollution,* 207**,** 369-389.

PRESCOTT, L. M., HARLEY, J. P. & KLEIN, D. A. (eds.) 1996. *Microbiology,* Dubuque, IA: Wm. C. Brown Publishers.

REGUERA, G., MCCARTHY, K. D., MEHTA, T., NICOLL, J. S., TUOMINEN, M. T. & LOVLEY, D. R. 2005. Extracellular electron transfer via microbial nanowires. *Nature,* 435**,** 1098-1101.

RICHARDSON, D. J., WEHRFRITZ, J. M., KEECH, A., CROSSMAN, L. C., ROLDAN, M. D., SEARS, H. J., BUTLER, C. S., REILLY, A., MOIR, J. W. B.,

BERKS, B. C., FERGUSON, S. J., THOMSON, A. J. & SPIRO, S. 1998. The diversity of redox proteins involved in bacterial heterotrophic nitrification and aerobic denitrification. *Biochemical Society Transactions,* 26**,** 401-408.

ROZAN, T. F. & LUTHER, G. W. 2002. An anion chromatography/ultraviolet detection method to determine nitrite, nitrate, and sulfide concentrations in saline (pore) waters. *Marine Chemistry,* 77**,** 1-6.

RUPPEL, D. T., DEXTER, S. C. & LUTHER, G. W. 2001. Role of manganese dioxide in corrosion in the presence of natural Biofilms. *Corrosion,* 57**,** 863-873.

SAFFARINI, D. A., DICHRISTINA, T. J., BERMUDES, D. & NEALSON, K. H. 1994. Anaerobic respiratoin of *Shewanella putrefaciens* requireds both chromosomal and plamid-borne genes. *Fems Microbiology Letters,* 119**,** 271-277.

SCHIPPERS, A. & JORGENSEN, B. B. 2001. Oxidation of pyrite and iron sulfide by manganese dioxide in marine sediments. *Geochimica Et Cosmochimica Acta,* 65**,** 915-922.

SCHMIDT, I., SLIEKERS, O., SCHMID, M., CIRPUS, I., STROUS, M., BOCK, E., KUENEN, J. G. & JETTEN, M. S. M. 2002. Aerobic and anaerobic ammonia oxidizing bacteria competitors or natural partners? *Fems Microbiology Ecology,* 39**,** 175-181.

SCHRUM, H. N., SPIVACK, A. J., KASTNER, M. & D'HONDT, S. 2009. Sulfate-reducing ammonium oxidation: A thermodynamically feasible metabolic pathway in subseafloor sediment. *Geology,* 37**,** 939-942.

SCHULZ, H. D., DAHMKE, A., SCHINZEL, U., WALLMANN, K. & ZABEL, M. 1994. Early diagenetic processes, fluxes, and reaction-rates in sediment of the south-Atlantic. *Geochimica Et Cosmochimica Acta,* 58**,** 2041-2060.

SHI, L., DENG, S., MARSHALL, M. J., WANG, Z. M., KENNEDY, D. W., DOHNALKOVA, A. C., MOTTAZ, H. M., HILL, E. A., GORBY, Y. A., BELIAEV, A. S., RICHARDSON, D. J., ZACHARA, J. M. & FREDRICKSON, J. K. 2008. Direct involvement of type II secretion system in extracellular translocation of *Shewanella oneidensis* outer membrane cytochromes MtrC and OmcA. *Journal of Bacteriology,* 190**,** 5512-5516.

SHI, L., SQUIER, T. C., ZACHARA, J. M. & FREDRICKSON, J. K. 2007. Respiration of metal (hydr)oxides by *Shewanella* and *Geobacter*: a key role for multihaem *c*-type cytochromes. *Molecular Microbiology,* 65**,** 12-20.

SORENSEN, J., JORGENSEN, K. S., COLLEY, S., HYDES, D. J., THOMSON, J. & WILSON, T. R. S. 1987. Depth localization of denitrification in a deep-sea sediment from the Madera abyssal-plain. *Limnology and Oceanography,* 32**,** 758-762.

STONE, A. T. 1987a. Microbial metabolites and the reductive dissolution of manganese oxides - oxalate and pyruvate. *Geochimica Et Cosmochimica Acta,* 51**,** 919-925.

STONE, A. T. 1987b. Reductive dissolution of manganese (III/IV) oxides by substitued phenols. *Environmental Science & Technology,* 21**,** 979-988.

STONE, A. T. & MORGAN, J. J. 1984a. Reduction and dissolution of manganese(III) and manganese(IV) oxides by organics. 1. reaction with hydroquinione. *Environmental Science & Technology,* 18**,** 450-456.

STONE, A. T. & MORGAN, J. J. 1984b. Reduction and dissolution of manganese(III) and manganese(IV) oxides by organics. 2. survey of the reactivity of organics. *Environmental Science & Technology,* 18**,** 617-624.

STOOKEY, L. L. 1970. Ferrozine - a new spectrophotometric reagent for iron. *Analytical Chemistry,* 42**,** 779-&.

STROUS, M., VANGERVEN, E., KUENEN, J. G. & JETTEN, M. 1997. Effects of aerobic and microaerobic conditions on anaerobic ammonium-oxidizing (Anammox) sludge. *Applied and Environmental Microbiology,* 63**,** 2446-2448.

STUMM, W. & MORGAN, J. J. (eds.) 1996. *Aquatic chemistry,* New York: John Wiley & Sons, Inc.

SUNDA, W. G. & HUNTSMAN, S. A. 1986. Relationships among growth-rate, cellular manganese concentrations and manganese transport kinetics in estuarine and oceanic species of the diatom thalassiosira. *Journal of Phycology,* 22**,** 259-270.

TAILLEFERT, M., BECKLER, J. S., CAREY, E., BURNS, J. L., FENNESSEY, C. M. & DICHRISTINA, T. J. 2007a. *Shewanella putrefaciens* produces an Fe(III)-solubilizing organic ligand during anaerobic respiration on insoluble Fe(III) oxides. *Journal of Inorganic Biochemistry,* 101**,** 1760-1767.

TAILLEFERT, M., BONO, A. B. & LUTHER, G. W. 2000a. Reactivity of freshly formed Fe(III) in synthetic solutions and (pore)waters: Voltammetric evidence of an aging process. *Environmental Science & Technology,* 34**,** 2169-2177.

TAILLEFERT, M., LUTHER, G. W. & NUZZIO, D. B. 2000b. The application of electrochemical tools for in situ measurements in aquatic systems. *Electroanalysis,* 12**,** 401-412.

TAILLEFERT, M., NEUHUBER, S. & BRISTOW, G. 2007b. The effect of tidal forcing on biogeochemical processes in intertidal salt marsh sediments. *Geochemical Transactions,* 8.

TEBO, B. M., BARGAR, J. R., CLEMENT, B. G., DICK, G. J., MURRAY, K. J., PARKER, D., VERITY, R. & WEBB, S. M. 2004. Biogenic manganese oxides: Properties and mechanisms of formation. *Annual Review of Earth and Planetary Sciences,* 32**,** 287-328.

TEBO, B. M., JOHNSON, H. A., MCCARTHY, J. K. & TEMPLETON, A. S. 2005. Geomicrobiology of manganese(II) oxidation. *Trends in Microbiology,* 13**,** 421-428.

TESSIER, A., CAMPBELL, P. G. C. & BISSON, M. 1979. Sequential extraction procedure for the speciation of particulate trace-metals. *Analytical Chemistry,* 51**,** 844-851.

THAMDRUP, B. 2000a. *Advances in Microbial Ecology*, Kluwer Academic / Plenum Publisher.

THAMDRUP, B. 2000b. Bacterial manganese and iron reduction in aquatic sediments. *Advances in Microbial Ecology, Vol 16.* New York: Kluwer Academic / Plenum Publ.

THAMDRUP, B. & DALSGAARD, T. 2000. The fate of ammonium in anoxic manganese oxide-rich marine sediment. *Geochimica Et Cosmochimica Acta,* 64**,** 4157-4164.

THAMDRUP, B. & DALSGAARD, T. 2002. Production of N-2 through anaerobic ammonium oxidation coupled to nitrate reduction in marine sediments. *Applied and Environmental Microbiology,* 68**,** 1312-1318.

THAMDRUP, B., DALSGAARD, T., JENSEN, M. M., ULLOA, O., FARIAS, L. & ESCRIBANO, R. 2006. Anaerobic ammonium oxidation in the oxygen-deficient waters off northern Chile. *Limnology and Oceanography,* 51**,** 2145-2156.

TROUWBORST, R. E., CLEMENT, B. G., TEBO, B. M., GLAZER, B. T. & LUTHER, G. W. 2006. Soluble Mn(III) in suboxic zones. *Science,* 313**,** 1955-1957.

VAN CAPPELLEN, P., VIOLLIER, E., ROYCHOUDHURY, A., CLARK, L., INGALL, E., LOWE, K. & DICHRISTINA, T. 1998. Biogeochemical cycles of manganese and iron at the oxic-anoxic transition of a stratified marine basin (Orca Basin, Gulf of Mexico). *Environmental Science & Technology,* 32**,** 2931-2939.

VAN DE VOSSENBERG, J., RATTRAY, J. E., GEERTS, W., KARTAL, B., VAN NIFTRIK, L., VAN DONSELAAR, E. G., DAMSTE, J. S. S., STROUS, M. & JETTEN, M. S. M. 2008. Enrichment and characterization of marine anammox bacteria associated with global nitrogen gas production. *Environmental Microbiology,* 10**,** 3120-3129.

VENKATESWARAN, K., MOSER, D. P., DOLLHOPF, M. E., LIES, D. P., SAFFARINI, D. A., MACGREGOR, B. J., RINGELBERG, D. B., WHITE, D. C., NISHIJIMA, M., SANO, H., BURGHARDT, J., STACKEBRANDT, E. & NEALSON, K. H. 1999. Polyphasic taxonomy of the genus Shewanella and description of Shewanella oneidensis sp. nov. *International Journal of Systematic Bacteriology,* 49**,** 705-724.

VILLINSKI, J. E., SAIERS, J. E. & CONKLIN, M. H. 2003. The effects of reaction-product formation on the reductive dissolution of MnO2 by Fe(II). *Environmental Science & Technology,* 37**,** 5589-5596.

VON CANSTEIN, H., OGAWA, J., SHIMIZU, S. & LLOYD, J. R. 2008. Secretion of flavins by Shewanella species and their role in extracellular electron transfer. *Applied and Environmental Microbiology,* 74**,** 615-623.

WARD, B. B., DEVOL, A. H., RICH, J. J., CHANG, B. X., BULOW, S. E., NAIK, H., PRATIHARY, A. & JAYAKUMAR, A. 2009. Denitrification as the dominant nitrogen loss process in the Arabian Sea. *Nature,* 461**,** 78-U77.

WARNKEN, K. W., SANTSCHI, P. H., ROBERTS, K. A. & GILL, G. A. 2008. The cycling and oxidation pathways of organic carbon in a shallow estuary along the Texas Gulf Coast. *Estuarine Coastal and Shelf Science,* 76**,** 69-84.

WEATHERB MW 1967. Phenol-hypochlorite reactoin for determination of ammonia. *Analytical Chemistry,* 39**,** 971-&.

WEBB, S. M., DICK, G. J., BARGAR, J. R. & TEBO, B. M. 2005. Evidence for the presence of Mn(III) intermediates in the bacterial oxidation of Mn(II). *Proceedings of the National Academy of Sciences of the United States of America,* 102**,** 5558-5563.

WEE, S., TAILLEFERT, M. & DICHRISTINA, T. 2011. *Shewanella oneidensis* MR-1 mutants selected for their inability to reduce disulfides contain mutations in outer membrane β-barrel protein MtrB, mauscript under review.

WEE, S., TAILLEFERT, M. & DICHRISTINA, T. 2012. *Shewanella oneidensis* MR-1 mutants selected for their inability to reduce disulfides contain mutations in outer membrane β-barrel protein MtrB, mauscript under review.

WEISS, R. F. 1970. Solubility of nitrogen, oxygen and argon in water and seawater. *Deep-Sea Research,* 17**,** 721-&.

WHITE, D. J., NOLL, M. R. & MAKAREWICZ, J. C. 2008. Does Manganese Influence Phosphorus Cycling under Suboxic Lake Water Conditions? *Journal of Great Lakes Research,* 34**,** 571-580.

WINKLER, L. W. 1888. Die Bestimmung des in Wasser gelosten Sauerstoffen. *Berichte der Deutschen Chemischen Gesellschaft,* 21**,** 2843-2855.

YAO, W. S. & MILLERO, F. J. 1993. The rate of sulfide oxidation by delta-MnO_2 in seawater. *Geochimica Et Cosmochimica Acta,* 57**,** 3359-3365.

ZHANG, G. S., QU, J. H., LIU, H. J., LIU, R. P. & LI, G. T. 2007. Removal mechanism of As(III) by a novel Fe-Mn binary oxide adsorbent: Oxidation and sorption. *Environmental Science & Technology,* 41**,** 4613-4619.